Synthesis of novel polymer-bound morpholine-N-oxides as possible oxidants in alkene oxidation

A dissertation submitted in fulfilment of the requirements for the degree

MAGISTER SCIENTIAE

in the

DEPARTMENT OF CHEMISTRY
FACULTY OF SCIENCE

at the

UNIVERSITY OF THE FREE STATE

by

Blenerhassitt Edward Buitendach

Supervisor: Prof. J.C. Swarts
Co-Supervisor: Prof. B.C.B Bezuidenhoudt

March 2008

CONTENTS

List of abbreviations

$(DHQD)_2PHAL$	-	hydroquinidine 1,4-phthalazinediyl diether
^1H NMR	-	proton nuclear magnetic resonance
ACE	-	active chain end
AD	-	asymmetric dihydroxylation
AKR	-	aminolytic kinetic resolution
AM	-	activated monomer
BNCT	-	boron neutron capture therapy
cm^{-1}	-	wave number
CV	-	cyclic voltammogram
DCM	-	dichloromethane
DMF	-	dimethylformamide
DMDO	-	dimethyldioxirane
DSC	-	differential scanning calorimetry
E°'	-	formal reduction potential
E_{pa}	-	anodic peak potential
E_{pc}	-	cathodic peak potential
EPO	-	styrene epoxide
eq.	-	equivalents
Fc	-	ferrocene
Fc*	-	decamethyl ferrocene
GAP	-	glycidyl azide polymer
HPMA	-	N-(2-hydroxypropyl)methacrylamide
i_{pa}	-	anodic peak current
i_{pc}	-	cathodic peak current
IR	-	infrared
LDPE	-	low-density polyethylene
LET	-	linear energy transfer
m-CPBA	-	*m*-chloroperbenzoic acid
Mn(TDCPP)Cl	-	chloro 5,10,15,20-tetrakis(2,6-dichlorophenyl) porphyrinatomanganese(III)
m.p.	-	melting point

MPc	-	metallated phthalocyanine
MW	-	molecular weight
NMO	-	N-methylmorpholine-N-oxide
PASP	-	polyaspartic acid
Pc	-	phthalocyanine
PDT	-	photodynamic therapy
PECH	-	polyepichlorohydrin
PEG	-	poly(ethylene glycol)
PLGA	-	poly(lactide-co-glycolide)
PolyGLYN	-	glycidyl nitrate polymer
ppm	-	parts per million
PS-MC-OsO_4	-	polymer supported microencapsulated osmium tetroxide
PSI	-	polysuccinimide
Salen	-	N,N'-ethylenebis(salicylidene aminato)
Salph	-	N,N'-(ophenylene)-*bis*(salicylideneimine)
SCE	-	saturated calomel electrode
$TBAPF_6$	-	tetrabutylammonium hexafluorophosphate
THF	-	tetrahydrofuran
TLC	-	thin layer chromatography
TPP	-	*meso*-tetraphenylporphyrin
UHMWPE	-	Ultra-high-molecular-weight polyethylene
UV/Vis	-	ultraviolet–visible

List of structures

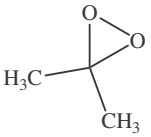

Dimethyldioxirane

[1]

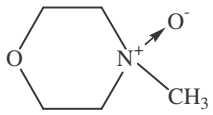

N-Methylmorpholine-N-oxide

[2]

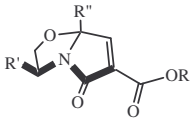

R = Me, tBu
R' = i-Pr, Ph, t-Bu
R" = Me, Ph

Unoxidized lactams

[3]

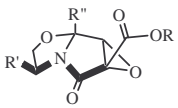

Epoxidized lactams

[4]

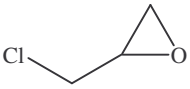

Epichlorohydrin

[5]

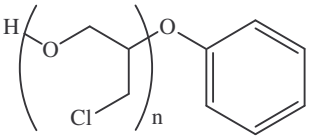

Polyepichlorohydrin

[6]

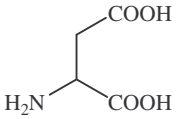

D,L-aspartic acid

[7]

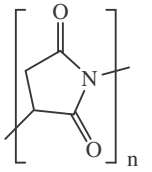

Polysuccinimide

[8]

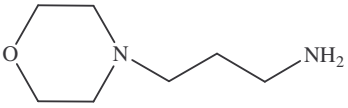

3-Aminopropyl-N-morpholine

[9]

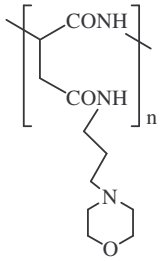

Poly[N-(3-morpholinopropyl)]aspartamide

[10]

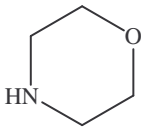

Morpholine

[11]

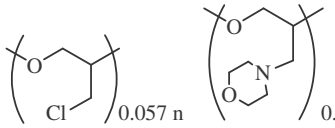

0.057 n

0.943n

n = 263

Poly[N-(morpholinomethylene)]ethylene oxide

[12]

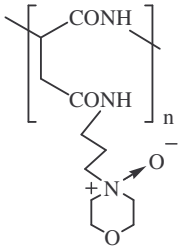

Poly[N-(3-morpholinopropyl)-N-oxide]aspartamide

[13]

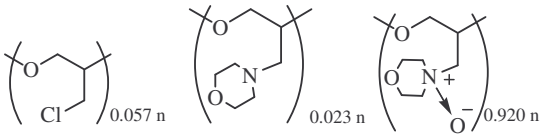

Poly[N-(morpholinomethylene)-N-oxide]ethylene oxide

[14]

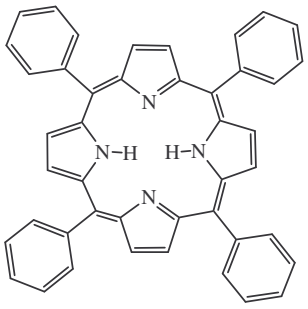

meso-Tetraphenylporphyrin

[15]

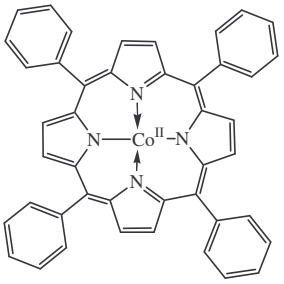

Tetraphenylporhyrinatocobalt(II)

[16]

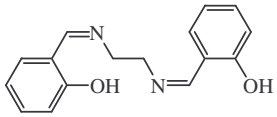

Bis(salicylidene)ethylenediamine

[17]

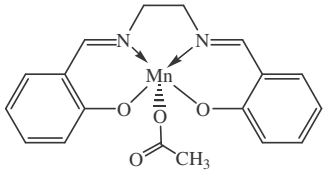

N,N'-Bis(salicylidene)ethylenediaminomanganese(III) acetate

[18]

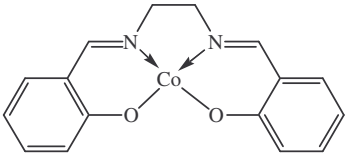

N,N'-Bis(salicylidene)ethylenediaminocobalt(II)

[19]

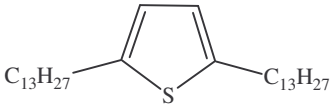

2,5-Tridecylthiophene

[20]

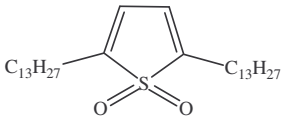

2,5-Tridecylthiophenesulfone

[21]

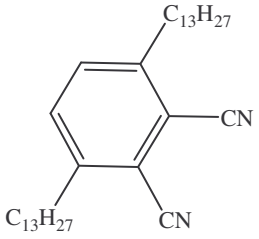

3,6-Tridecylphthalonitrile

[22]

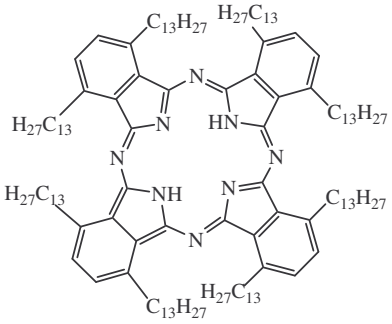

1,4,8,11,15,18,22,25-Octatridecylphthalocyanine

[23]

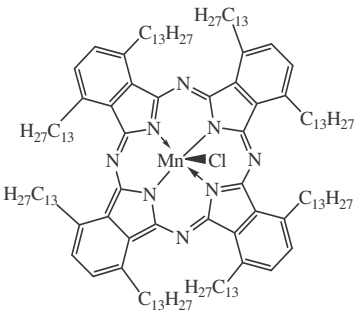

[1,4,8,11,15,18,22,25-Octatridecylphthalocyanatomanganese(III)] chloride

[24]

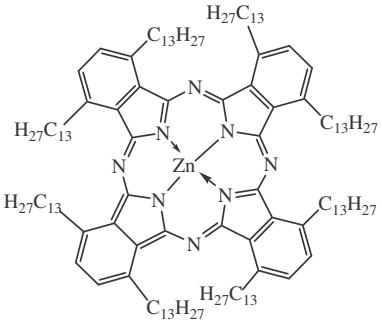

1,4,8,11,15,18,22,25-Octatridecylphthalocyanatozinc(II)

[25]

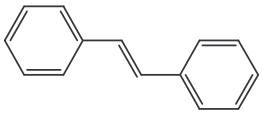

trans-Stilbene

[26]

Tridecyl-1-bromide

[27]

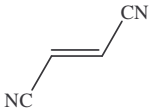

Fumaronitrile

[28]

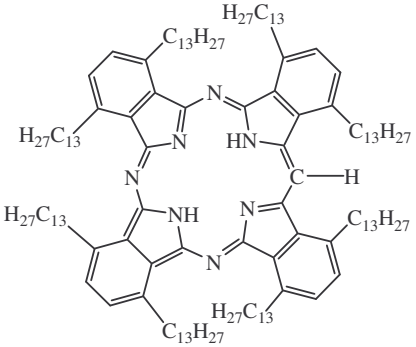

1,4,8,11,15,18,22,25-Octatridecyltetrabenzotriazaporphyrin

[29]

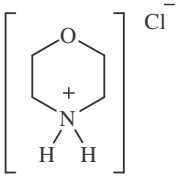

Morpholine-HCl salt

[30]

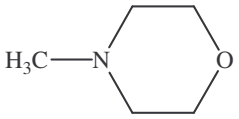

N-methylmorpholine

[31]

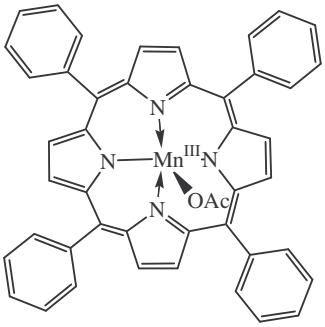

Tetraphenylporhyrinatomanganese(III) acetate

[32]

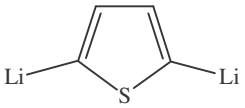

2,5-dilithiumthiophene

[33]

ACKNOWLEDGEMENTS

I hereby wish to express my gratitude towards the following people who all contributed directly or indirectly to the preparation of this thesis:

Firstly, prof. J.C. Swarts, my promoter, for his leadership and expertise during this study and for introducing me to the very interesting field of polymers and phthalocyanines. I especially appreciate the long hours he spent with me as well as various other forms of help.

Prof. B.C.B Bezuidenhoudt, my co-promoter, for his contributions and advice during this study.

Collectively, all my post-graduate colleagues for their interest in my studies, as well as their helpful advice in experimental techniques.

Dr A. Auger, Ernie Langner, Eleanor Fourie and Dr J. Conradie for the many NMR spectra they drew for me, even on very short notice.

Lastly, to my family for constant support and understanding during difficult times and for showing a keen interest in my progress.

For financial assistance during the course of my study I would like to thank NRF.

Blener Buitendach

2008

ABSTRACT

In this dissertation is reported the syntheses and characterisation of polysuccinimide- and polyepichlorohydrin-bound morpholine-N-oxide as possible polymeric oxidants. The use of ^{1}H NMR spectroscopy to determine polymer chain length and degree of fuctionalisation is described in detail. The synthesised polymers were used as potential oxidants in catalytic oxidation of alkenes. However, none of the preliminary trials on the epoxidation and dihydroxylation of trans-stilbene were successful.

Two metal-containing phthalocyanines; one coordinated to Mn(III), the other to Zn(II), were synthesized by metal insertion into the metal-free non-peripheral octa substituted phthalocyanine (2HPc-$(C_{13}H_{27})_8$). The initial complex, 2HPc-$(C_{13}H_{27})_8$, was synthesized by tetramerization of 3,6-tridecylphthalonitrile, which was prepared by a three-step synthesis from thiophene. Characterization of the phthalocyanines included electrochemical and thermal analysis. The cyclic voltammograms of the 2H and Zn phthalocyanines showed two ring-based oxidations (0.116 V; 0.487 V and 0.044 V; 0.558V respectively) as well as two ring-based reductions (-1.791 V; -1.456 V and -2.054 V; -1.663 V respectively), vs Fc/Fc^{+} at 100 mV/s. The Mn derivative showed two ring-based oxidations (0.373 V and 0.864 V) while only one ring-based reduction was observed (-1.732 V). The Mn(II) oxidation was observed at 0.641 V while Mn(III) reductions was observed at -0.742 V and -0.660 V (for Cl^{-} and CH_3O^{-} axial ligands) giving large ΔE_p values of 1.566 V and 1.484 V.

The newly synthesized tridecyl-substituted metal-free and zinc phthalocyanines exhibited liquid crystalline mesophase behavior when subjected to differential scanning calorimetric studies of between 40 ^{o}C – 120 ^{o}C and 40 ^{o}C – 280 ^{o}C respectively, giving mesophase temperature ranges of 12.4 ^{o}C and 83.0 ^{o}C respectively. The manganese phthalocyanine,

however, did not show any liquid crystal behavior. The manganese tridecyl-substituted phthalocyanine was used as catalyst in the molecular oxygen based epoxidation of *trans*-stilbene and gave low yields of the desired epoxide, *trans*-stilbene oxide. Epoxidation of *trans*-stilbene using N-methylmorpholine-N-oxide as oxidant and Mn(III)salen as co-catalyst gave *trans*-stilbene oxide in moderate yields.

OPSOMMING

In hierdie verhandeling word die sintese en karakterisering van polisuksienimied- en poliepichlorohidriengebonde morfolien-N-oksied as moontlike polimeriese oksideermiddel geraporteer. Die gebruik van ^{1}H KMR spektroskopie om polimeer kettinglengte en graad van substitusie te bepaal word deeglik beskryf. Die polimere was aanvanklik as potensiële oksidante in die katalitiese oksidasie van alkene bedoel, maar geen sukses was in die epoksidasie en dihidroksilering van *trans*-stilbeen behaal nie.

Twee metal bevattende ftalosianiene; een gekoördineerd aan Mn(III), die ander aan Zn(II), was gesintetiseer deur metaalinsersie in die metaalvrye, nie-periferale oktagesubstitueerde ftalosianien 2HPc-$(C_{13}H_{27})_8$. Die 2HPc-$(C_{13}H_{27})_8$ moederverbinding was deur die tetramerisasie van 3,6-tridesielftalonitriel berei, wat op sy beurt deur ’n drie-stap sintese vanaf tiofeen verkry is. Karakterisering van die ftalosianiene het elektrochemiese en termiese analiese ingesluit. Die sikliese voltammograme van die 2H and Zn ftalosianiene het twee ring-gebaseerde oksidasies (0.116 V; 0.487 V en 0.044 V; 0.558V onderskeidelik) asook twee ring-gebaseerde reduksies (-1.791 V; -1.456 V en -2.054 V; -1.663 V onderkeidelik) gelewer. Potensiale is ge-eik teen Fc/Fc^{+} by 100 mV/s. Die Mn derivaat het twee ring-gebaseerde oksidasies (0.373 V en 0.864 V) getoon terwyl daar net een ring-gebaseerde reduksie waargeneem is (-1.732 V). Die Mn(II) oksidasie was by 0.641 V waargeneem terwyl Mn(III) reduksies by -0.742 en -0.660 V gemeet is (vir Cl^{-} en CH_3O^{-} aksiale ligande). Hierdie potensiale gee aanleiding tot die groot ΔE_p waardes van 1.566 V en 1.484 V onderskeidelik.

Die nuwe tridesiel-gesubstitueerde 2H and Zn ftalosianiene het vloeikristal mesofase gedrag getoon in differensiëel skanderende kaleometriese studies tussen 40 ^{o}C – 120 ^{o}C (2H) en 40 ^{o}C – 280 ^{o}C (Zn), met mesofase temperatuur gebiede van 12.4 ^{o}C en 83.0 ^{o}C onderskeidelik. Die

Mn ftalosianien het egter geen vloeikristalgedrag getoon nie. Die Mn-bevattende tridesiel-gesubstitueerde ftalosianien was aangewend as katalis in die molekulêre suurstof gas gebasseerde epoksidasie van *trans*-stilbeen en het lae opbrengste van die epoksied *trans*-stilbeen oksied gelewer. Epoksidasie van trans-stilbeen met N-metielmorfolien-N-oksied as oksidant en Mn(III)salen as ko-oksidant het trans-stilbene oksied in matige opbrengste gelewer.

DECLARATION

I, Blenerhassitt Edward Buitendach, declare that the dissertation hereby submitted by me for the Magister Scientiae degree at the University of the Free State is my own independent work and has not previously been submitted by me at another university/faculty. I further more cede copyright of the dissertation in favour of the University of the Free State.

Signed:..... Date:.....

1 Introduction and aims

1.1 Introduction

Oxidations represent a very important class of chemical reactions, in nature as well as in the laboratory of the chemist. Industrially, oxidation reactions are of key importance in converting petroleum-based feedstocks, like parrafins, to useful chemicals in a highly oxidized state such as alcohols, carbonyl compounds and epoxides. Worldwide in the chemical industry millions of tons of compounds are annually produced in processes involving one or more oxidation steps.[1] These include bleaching agents, commodity chemicals, textile manufacturing, water purification chemicals, pharmaceuticals and explosives. Examples of oxidants range from simple inorganic molecules such as hydrogen peroxide and hypochlorides, to heavy metal-containing compounds such as potassium permanganate and chromium(IV) compounds, to organic oxidizers like urea hydrogen peroxide and amine oxides.

There are various obstacles that may hinder successful oxidation processes. These include high cost in industrial bulk oxidations, where several thousands of tons of oxidant, such as H_2O_2, are consumed annually. What may be cheap on small scale can amount to great costs in the manufacture of commodity chemicals in bulk. There are several needs that have to be recognised to reach the goals set by community on scientists to focus on cheaper and safer oxidation. These include the following:

a) Lower cost. To reduce cost it is often desirable for effective single-step and/or solvent-free processes.

b) The use of mild conditions, ideally involving benign reagents and benign catalysts also help to raise economic efficiency and lower the danger factor. The use of benign conditions to lower CO_2 emissions (less heating etc.) should not be overlooked.

c) Replacement of stoichiometric oxidation processes by catalytic ones lower the environmental impact of factory effluents.

d) Designing durable heterogeneous (solid) catalysts of very high activity and selectivity that are amenable to recycling is a strong research and development focus of many larger companies.

e) The use of atmospheric oxygen (preferably) or H_2O_2 (or alkyl hydroperoxides) – in order of decreasing preference – as the oxidizing agent[2] is being aggressively researched.

The use of molecular atmospheric oxygen or hydrogen peroxide as the stoichiometric oxidant instead of inorganic oxidants, notably the high oxidation state metals, goes a long way to more environmentally friendly processes.[3] O_2 or H_2O_2 are atom efficient oxidants and produce water as the only by-product.[4] The low reactivity of molecular oxygen, however, requires that it be activated to be useful in industrial oxidation processes. Some appropriate examples of activated oxygen include N-oxides such as pyridine-N-oxide and morpholine-N-oxide.[5,6] In these cases the oxygen is activated by the dentative bond formed from the lone pair of electrons on the nitrogen. At pressent, N-oxides are used in bulk quantities in various oxidation applications, but there is a strong need to recover the spent oxidant.[7] By binding the N-oxides to polymers it may be possible to augment the oxidizing properties of the polymer-bound oxidant and reclaim spent oxidants.

The activation of molecular oxygen can involve the conversion of triplet oxygen to singlet oxygen. This can be simply achieved by the use of a catalyst. Metallated porphyrins and phthalocyanines are known for there ability to produce singlet oxygen. Phthalocyanines and

porphyrins in particular have been extensively studied for their use in photodynamic therapy where they produce singlet oxygen to kill the cancer cells.[8] In industrial oxidations, mangenese porphyrins, for example, have been used as effective catalysts for the epoxidation of alkenes with various oxidants.[9,10] Phthalocyanines possess some good properties that makes them useful as catalysts for a number of industrial processes.[11] In particular their stability towards heat, acids and bases makes them prime candidates for catalytic reactions. By using porphyrins or phthalocyanines in combination with a polymer bound oxidant, it is possible that the catalytic system may be improved to give higher reaction yields, better selectivity or recyclability.

Against this background the following goals were set for this study:

1) Synthesis and evaluation of N-methylmorpholine-N-oxide (NMO) as model for the dihydroxylation of alkenes catalised by OsO_4, as well as for the epoxidation of alkenes.
2) Synthesis of poly-DL-succinimide and polyepichlorohydrin as potential polymeric carriers for morpholine.
3) Assessment of the possibility to oxidise polymer-bound morpholine to polymer-bound morpholine-N-oxide and the evaluation of these polymer derivatives for the dihydroxylation and epoxidation of *trans*-stilbene.
4) Synthesis and evaluation of porphyrin, salen and phthalocynine complexes as potential oxidation co-catalysts.

Characterisation techniques that were used for the new compounds include spectroscopic techniques (^{1}H NMR, UV/Vis and IR), electrochemical techniques (cyclic voltametry) and thermodynamic methods (DSC and variable temperature polarised light spectroscopy).

1.2 References

[1] T. Punniyamurthy, S. Velusamy and J. Iqbal, *Chem. Rev.,* **105**, 2329-2230 (2005)

[2] J. M. Thomas and R. Raja, *Catalysis Today,* **117**, 22-31 (2006)

[3] G. ten Brink, I. W. C. E. Arends and R. A. Sheldon, *Science*, **287**, 1636-1638 (2000)

[4] B. M. Trost, *Science*, **281**, 1471 (1998)

[5] Z. Zheng, J. Chen, Z. Yu and X. Han, *J. Organomet. Chem.*, **691**, 3679-3692 (2006)

[6] T. Rosenau, A. Potthast, H. Sixta and P. Kosma, *Tetrahedron*, **58**, 3073-3078 (2002)

[7] T. Rosenau, A. Hofinger, A. Potthast and P. Kosma, *Polymer*, **44**, 6153-6158 (2006)

[8] R. Bonnett, *Chem. Soc. Rev.,* **24**, 19-33 (1995)

[9] J. P. Collman, J. I. Brauman, B. Meunier, T. Hayashi and T. Kodadek, *J. Am. Chem. Soc.,* **107**, 2000 (1985)

[10] Y. Tsuda, K. Takahashi, T. Yamagushi, S. Matsui and T. Komura, *J. Mol. Cat. A: Chemical*, **130**, 285 (1998)

[11] Moser, F.H., Thomas, A.L., *The Phthalocyanines,* CRC: Boca Raton, Florida, vol. II (1983)

2 Literature survey and fundamental aspects

2.1 Introduction

This chapter provides a literature survey of topics that the author regards as pertinent to his study. It is arranged first to give background of synthetic reactions relevant to the study, followed by a discussion of the physical techniques applied to the compounds related to the present study.

There will intially be focussed on diverse oxidising agents, investigating their properties and uses, before a detailed review is given on the most important oxidising agent used in this study, namely N-morpholine oxide. This is followed by a discussion of possible co-catalysts suitable to be used with N-morpholine oxide. Next, the chemistry and applications of different polymeric carriers will be discussed. Lastly, general techniques such as electrochemistry and DSC of related compounds are discussed.

2.2 Oxidising agents

Oxidation plays a vital role in everyday life. In nature, many enzymes are present which are capable of catalysing oxidation reactions. In a number of these reactions manganese or iron containing enzymes are involved. An example of these would be chlorophyll *a*, a green pigment containing a magnesium metal centre coordinated in a porphyrin which is responsible for the absorption of light by plants to provide energy for photosynthesis. Haemoglobin, which consists of a red iron-containing porphyrin imbedded in a protein, is responsible for transporting oxygen

in the blood of vertebrates. While chlorophyll handles electrons during photosynthesis and splits oxygen from water, haemoglobin deals more directly with atomic or molecular oxygen.

Other examples of oxidation catalysts in the human body are superoxide dismutase and catalase. These two enzymes work together by using molecular oxygen to remove hydrogen from substrate molecules, thereby helping to neutralise many potentially toxic wastes.[1]

Oxidation also plays an important role in all areas of the chemical industry. The manufacturing of a great deal of chemicals involves an anoxidation step at some point. With respect to yield, chemical rate and selectivity, oxidations often proceed in an unsatisfactory manner. One way of removing such shortcomings is by means of catalysis. Catalytically improved production processes are of utmost importance to the chemical industry particularly "in a period of time of tough competition and alarming price erosion".[2]

The oxidation of organic compounds, for example, is of extreme importance in synthetic chemistry. Important oxidation reactions include the transformation of alcohols to either the corresponding carbonyl compounds or carboxylic acids, the oxidation of sulfides to sulfoxides and alkenes to epoxides and diols.

2.2.1 Hydrogen peroxide

Hydrogen peroxide (H_2O_2) is a very pale blue liquid which appears clear in a dilute solution, slightly more viscous than water. It has strong oxidizing properties and is therefore a powerful bleaching agent that has found use as a disinfectant,[3] as an oxidizer,[4,5] and in fuel-cell systems.[6,7] Hydrogen peroxide was first isolated in 1818 by Louis Jacques Thénard by reacting barium peroxide with nitric acid. An improved version of this process used hydrochloric acid, followed by sulfuric acid to precipitate the barium chloride byproduct. Biologically hydrogen peroxide is

naturally produced as a by-product of oxygen metabolism, and virtually all organisms possess enzymes known as peroxidases, which apparently harmlessly catalytically decompose low concentrations of hydrogen peroxide to water and oxygen.[8]

In 1994, about 50% of the world's production of hydrogen peroxide was used for pulp and paper-bleaching. Since H_2O_2 can decompose spontaneously into water and oxygen, it is seen as an environmentally-benign alternative to chlorine-based bleaches. H_2O_2 is one of the most powerful oxidizers known - stronger than chlorine, chlorine dioxide, and potassium permanganate (Table 2-1). Through catalysis, H_2O_2 can be converted into hydroxyl radicals (·OH) with reactivity second only to fluorine. It usually acts as an oxidizing agent, but there are many reactions where it acts as a reducing agent, releasing oxygen as a by-product.[9] It also readily forms both inorganic and organic peroxides.

Table 2-1. Standard reduction potentials of some important oxidants.[10]

Oxidant	Standard Reduction Potential, V
Fluorine	3.0
Hydroxyl radical	2.8
Ozone	2.1
Hydrogen peroxide	1.8
Potassium permanganate	1.7
Chlorine dioxide	1.5
Chlorine	1.4

Hydrogen peroxide can oxidize or reduce a variety of inorganic ions in aqueous solutions.[10] When it acts as a reducing agent, molecular oxygen is also formed. In acidic solutions Fe^{2+} is oxidized to Fe^{3+},

$$2\ Fe^{2+}{}_{(aq)} + H_2O_2 + 2\ H^+{}_{(aq)} \rightarrow 2\ Fe^{3+}{}_{(aq)} + 2\ H_2O_{(\ell)}$$

and sulfite (SO_3^{2-}) is oxidized to sulfate (SO_4^{2-}). However, potassium permanganate is reduced to Mn^{2+} by acidic H_2O_2,[9]

$$2\ MnO_4^-{}_{(aq)} + 6\ H^+{}_{(aq)} + 5\ H_2O_2 \rightarrow 2\ Mn^{2+}{}_{(aq)} + 8\ H_2O_{(\ell)} + 5\ O_{2\,(g)}$$

Under alkaline conditions, however, some of these reactions reverse; Mn^{2+} is oxidized to Mn^{4+} (as MnO_2),[10]

$$Mn^{2+}{}_{(aq)} + H_2O_2 + OH^-{}_{(aq)} \rightarrow MnO_{2\,(s)} + H^+{}_{(aq)} + H_2O_{(\ell)}$$

yet Fe^{3+} is reduced to Fe^{2+}.

$$2\ Fe^{3+}{}_{(aq)} + H_2O_2 + 2\ OH^-{}_{(aq)} \rightarrow 2\ Fe^{2+}{}_{(aq)} + 2\ H_2O_{(\ell)} + O_{2\,(g)}$$

Hydrogen peroxide is frequently used as an oxidising agent in organic chemistry. One application is for the oxidation of thioethers to sulfoxides. For example, methyl phenyl sulfide can be oxidised to methyl phenyl sulfoxide in 99% yield in methanol,[11] while further oxidation leads to the sulfone.

$$Ph\text{-}S\text{-}CH_3 + H_2O_2 \rightarrow Ph\text{-}S(O)\text{-}CH_3 + H_2O$$

Alkaline hydrogen peroxide is used for epoxidation of electron-deficient alkenes such as acrylic acids, and also for oxidation of alkylboranes to alcohols, the second step of hydroboration-oxidations.

Hydrogen peroxide's ability to oxidize amines is of particular importance regarding this study.

2.2.2 Caro's acid

Caro's acid, or peroxymonosulfuric acid (H_2SO_5), is a colorless solid melting at 45 °C. In this acid, the S(VI) center adopts its characteristic tetrahedral geometry,

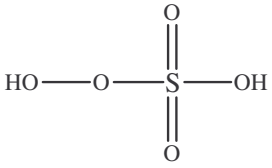

Caro's acid, as well as being a bleaching agent[12], is a powerful oxidant and is used in various oxidation reactions such as the direct oxidation of aromatic amines to nitroso compounds.[13] Due to its instability, large scale production of Caro's acid is usually done on site. The laboratory scale preparation of Caro's acid involves the combination of chlorosulfuric acid and hydrogen peroxide.

$$H_2O_2 + ClSO_2OH \rightleftharpoons H_2SO_5 + HCl_{(g)}$$

To augment the stability of the acid, the acid is neutralized. Potassium peroxymonosulfate, $KHSO_5$, is the potassium acid salt of peroxymonosulfuric acid and is the active ingredient of Oxone® (DuPont). Oxone® is a stable 2:1:1 ternary composite of K_2SO_4, $KHSO_4$ and $KHSO_5$ and its use in various oxidative[14] and deprotective transformations[15]. The oxidation potential of Oxone® is derived from its peracid chemistry as:

$$HSO_5^-{}_{(aq)} + 2\ H^+{}_{(aq)} + 2\ e^- \rightarrow HSO_4^-{}_{(aq)} + H_2O_{(l)} \qquad E^0 = 1.44\ V$$

The oxidation potential is high enough for many room temperature oxidations, making Oxone® a strong oxidant. Oxone® is used, for instance, in the direct epoxidation of D-glucal and D-galactal derivatives[16] in acetone by the *in situ* generation of dimethyldioxirane (DMDO), Scheme 2-1. Under neutral conditions, the dimethyldioxirane is a very strong yet selective oxidising agent. The DMDO goes on to oxidize the substrates double bond to the corresponding epoxide.

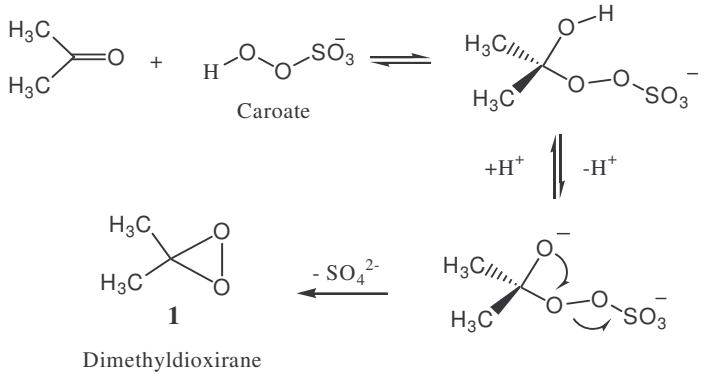

Scheme 2-1. *In situ* generation of dimethyldioxirane, **1**, in caroate/acetone mixture.

Oxone® in aqueous acetone has been extensively used in the oxidations of sulfides to sulfones or sulfoxides,[17] primary amines to nitro compounds,[18] and boronic esters or acids to alcohols.[19] It is of particular significance to this study due to its ability to oxidize substituted thiophenes to corresponding thiophene sulfones as precursors to phthalocyanines,[20] (Scheme 2-2).

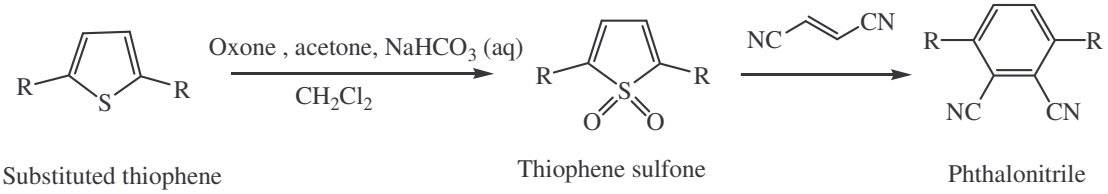

Substituted thiophene — Thiophene sulfone — Phthalonitrile

Scheme 2-2. Oxidation of a substituted thiophene by Oxone® to form the sulfone, which undergoes a Diels-Alder reaction with fumaronitrile to form the phthalonitrile as the precursor of phthalocyanines.

2.2.3 Amine oxides

An amine oxide, also known as amine-*N*-oxide or *N*-oxide, is a chemical compound that contains the functional group $R_3N^+ \rightarrow O^-$. In the strict sense the term amine oxide applies only to oxides of tertiary amines including nitrogen-containing aromatic compounds like pyridine, but is sometimes also used for the analogous derivatives of primary and secondary amines. Amine oxides are often used as protective groups for amines and as chemical intermediates.[21,22] Long-chain alkyl amine oxides are used as nonionic surfactants and foam stabilizers.[23] Amine oxides are highly polar molecules and have a polarity close to that of quaternary ammonium salts. Small amine oxides are very hydrophilic and have excellent water solubility and a very poor solubility in most organic solvents. Amine oxides are weak bases with a pK_a of around 4.5 that form R_3N^+-OH, i.e. cationic hydroxylamines, upon protonation at a pH below their pK_a.

Amine oxides can be prepared by oxidation of tertiary amines with hydrogen peroxide. Pyridine and its derivatives, however, can only be oxidized by peracids like MCPBA (*m*-chloroperoxybenzoic acid),[24] or with the aid of a catalyst.[25]

The amine oxide of interest in this study is *N*-methylmorpholine-*N*-oxide (NMO), **2**, (Figure 2-1). NMO is commercially supplied as a monohydrate $C_5H_{11}NO_2.H_2O$. It has a melting point of

70 °C, and is stable under normal conditions. Due to its high polarity, it is soluble in polar solvents, especially water. This leads to the use of a bi-phase systems in many organic oxidations.

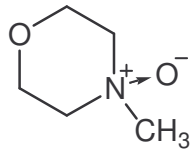

2, NMO

Figure 2-1. Structure of *N*-Methylmorpholine-*N*-oxide (NMO), **2**, showing the high polarity of the molecule.

NMO is commonly used as a single oxygen donor source and displays characteristic reactivity with various transition metals, which undergo oxidation with this reagent. Because of this, NMO is a preferred stoichiometric oxidant for transition metal-catalyzed oxidations. Other than acting as an oxidant, *N*-methylmorpholine-*N*-oxide has found major interest due to its ability to dissolve cellulose.[26] NMO is widely used as bulk sovent in industrial fiber-making processes such as the Lyocell process.[27]

NMO is used as a co-oxidant and sacrificial catalyst in oxidation reactions such as the Upjohn oxidation of olefins[28] and Sharpless *cis*-dihydroxylation of olefins.[29,30] The reaction of osmium tetroxide (OsO_4) with olefins is one of the most versatile procedures for *cis*-dihydroxylation. However, when used in stoichiometric amounts, the high cost, the high toxicity and volatility of OsO_4 hamper the large scale application. By using chlorate or hydrogen peroxide (Milas' reagent)[31] in the catalytic osmylation, OsO_4 can be regenerated, but further oxidation to an α-ketol may take place. Synthetic suitable co-oxidants are *N*-methylmorpholine *N*-oxide[32] or potassium ferricyanide ($K_3[Fe(CN)_6]$).[33] By using one mole of tertiary amine *N*-oxide as the co-oxidant, by-products can be avoided and thus improving the diol yield. During the osmium-catalysed *cis*-dihydroxylation reaction osmium(VIII) is reduced to osmium(VI) upon reaction

with the olefin. Catalytic amounts of OsO_4 can be achieved by using a co-oxidant, which oxidize osmium(VI) back to the active reagent osmium(VIII), (Scheme 2-3).

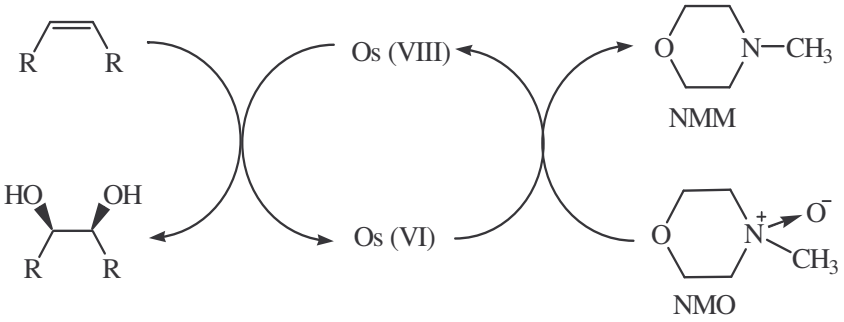

Scheme 2-3. OsO_4 catalyzed *cis*-dihydroxylation with NMO as co-oxidant.

To a lesser extent, NMO has also found application in the epoxidation of olefins through the working of metal catalysts. For example, the oxidation of enones by NMO-ruthenium trichloride is now a well known process leading to epoxy compounds, (Scheme 2-4).[34]

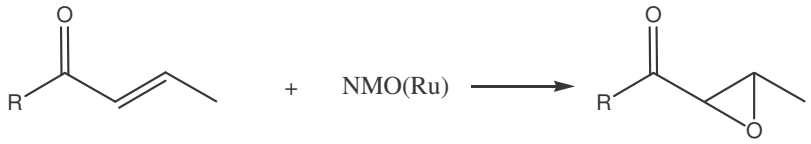

Scheme 2-4. Epoxidation of enones by NMO(Ru).

Occasionally though, NMO has been found to produce epoxides in the absence of a metal catalyst. NMO has been successfully used by Andres *et al.*[35] to stereospecifically epoxidize chiral unsaturated bicyclic lactams in high yields (90-99%) at room temperature. In an attempt to dihydroxylate various lactams, **3**, using NMO and catalytic osmium tetroxide, Andres *et al* found the epoxide products, **4**, in high yield, yet no dihydroxylated product was observed. It was determined that osmium tetroxide was not necessary for epoxidation to occur and that the

reaction of NMO by itself produced a high variety of epoxides with different unsaturated lactams, (Scheme 2-5).

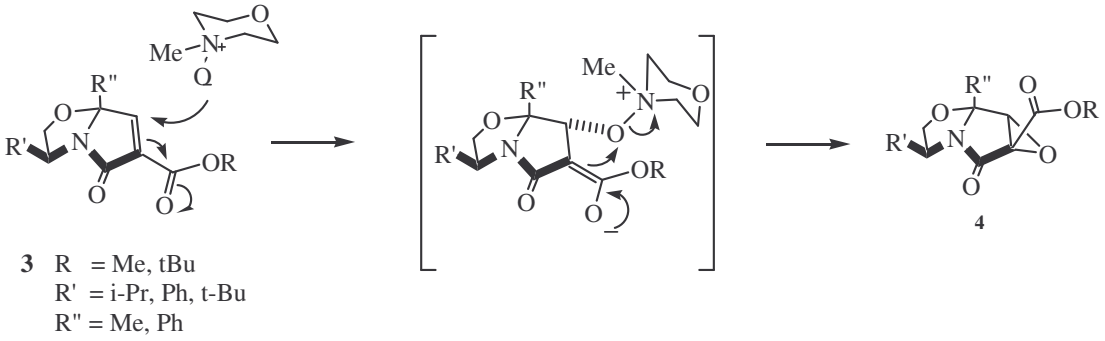

3 R = Me, tBu
R' = i-Pr, Ph, t-Bu
R" = Me, Ph

Scheme 2-5. Non-metallocatalyzed epoxidation of chiral unsaturated lactams by NMO.

2.3 Catalysts

The phrase *catalysis* was first coined by Jöns Jakob Berzelius in 1835 who was the first to note that certain chemicals speed up a reaction. Other early chemists involved in catalysis were Alexander Mitscherlich who in 1831 referred to *contact processes* and Johann Wolfgang Döbereiner who spoke of *contact action* and whose lighter based on hydrogen and a platinum sponge became a commercial success in the 1820s. Catalysis by metal complexes plays a central role in the selective, partial oxidation of both saturated and unsaturated hydrocarbons to useful products. A few catalysts were already mentioned in the previous section regarding oxidation reactions. The following section will focus on selected catalytic systems, oxidation reactions and their mechanisms of oxygen activation.

2.3.1 Osmium tetroxide

Osmium metal is lustrous, bluish white, extremely hard, and brittle even at high temperatures. It has the highest melting point and lowest vapour pressure of the platinum group. The solid metal is not affected by air at room temperature, but the powdered or spongy metal slowly gives off osmium tetroxide, which is a powerful oxidising agent and has a strong, ozone-like smell.

Osmium tetroxide, or osmium(VIII)oxide, formula OsO_4, is probably the best-known compound of osmium. Osmium tetroxide is an example of the highest oxidation state achieved by a transition element. As a d^0 metal, Os(VIII) is expected to adopt a tetrahedral geometry when bound to four ligands with the O-Os-O bond angles approximating 109.5°. OsO_4 is soluble in CCl_4 and moderately soluble in water. Osmium tetroxide is a highly toxic, very expensive compound which sublimes at room temperature. Given the care needed in handling osmium tetroxide in reactions, it is often replaced with potassium osmate dihydrate, $K_2OsO_4 \cdot 2H_2O$, which is much less volatile.[36] The use of $K_2OsO_4 \cdot 2H_2O$ as a nonvolatile Os source in combination with an inorganic co-oxidant, such as $K_3Fe(CN)_6$, led to the formulation of a *cis*-dihydroxylation premix containing all reagents and ligands. This premix is commercially available under the name of "AD-mix".[37] Furthermore, in 1998 Kobayashi *et al.* reported microencapsulated osmium tetroxide on polystyrene (PS-MC-OsO_4), with complete recovery and reuse of the osmium component in achiral oxidations.[38]

In the Sharpless *cis*-dihydroxylation of olefins depending on the co-oxidant and ligand (L) in use, more than one catalytic cycle can take place.[29] These cycles usually differ in the enantioselectivity of the formed diol products. When NMO is used as co-oxidant, for instance, there are two catalytic cycles. The primary cycle results in a high enantioselectivity output while the secondary cycle gives low selectivity, (Scheme 2-6).

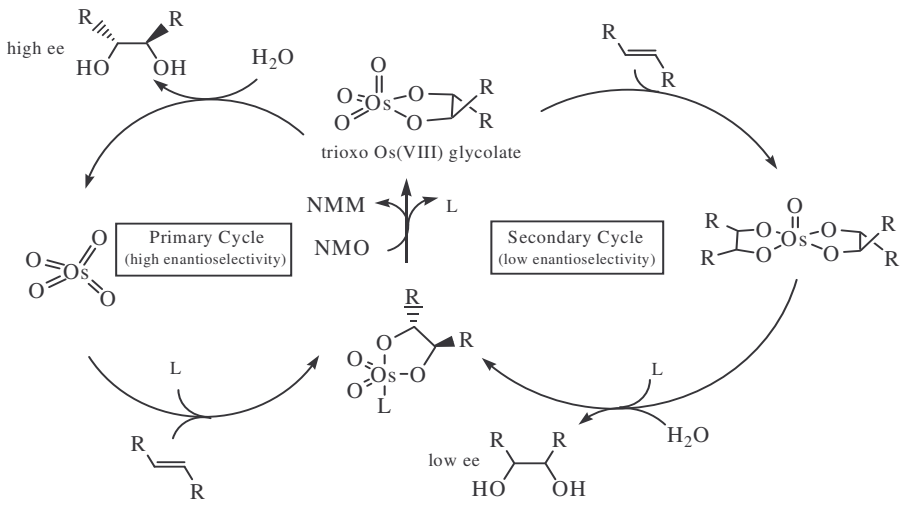

Scheme 2-6. Catalytic cycles for asymmetric dihydroxylation using NMO as co-oxidant.

However, by using $K_3Fe(CN)_6$ as the stoichiometric reoxidant under two phase conditions the secondary cycle can be virtually eliminated, (Scheme 2-7). In contrast to the homogeneous NMO conditions, there is no oxidant other than OsO_4 in the organic layer.

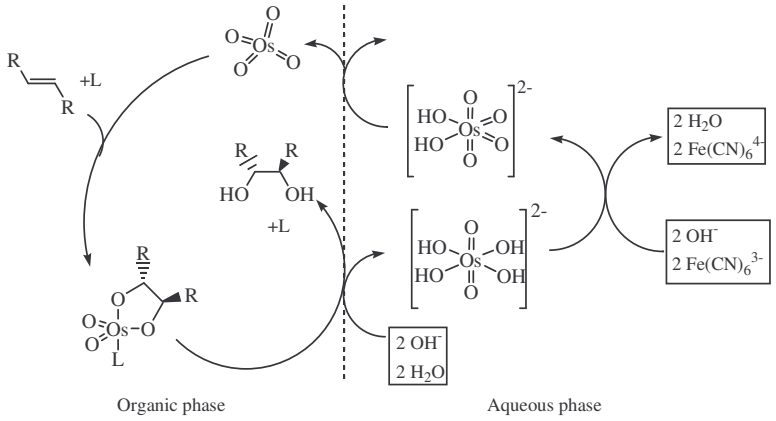

Scheme 2-7. Two phase asymmetric dihydroxylation using $K_3Fe(CN)_6$ as co-oxidant.

Through recent years, many different ligands have been tested for the Asymmetric Dihydroxylation reaction on different olefin classes to introduce enantioselectivity.[39] An in-depth discussion of the ligands role in the dihydroxylation reaction, however, does not fall within the scope of this study.

Besides dihydroxylation, OsO_4 is also used in other types of catalytic reactions. Osmium tetroxide may be used to catalyze the generation of carbonyl compounds from olefins by

promoting the catalytic oxidative cleavage of olefins with several equivalents of Oxone®, (Scheme 2-8, eq. 1).[40] The oxidative methodology can be extended to include the direct formation of lactones through oxidative cleavage of alkenols, (Scheme 2-8, eq. 2).

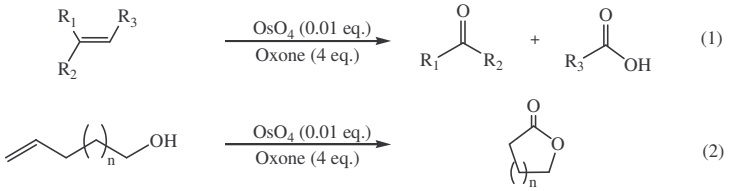

Scheme 2-8. Osmium mediated oxidative cleavage (1) and oxidative lactonization (2).

Furthermore, it has been found that generally sulfides are inert to oxidation by osmium tetroxide under stoichiometric conditions.[41,42] However, in the presence of the co-oxidant NMO and one mole percent of catalyst, a variety of sulfides can be oxidized to their corresponding sulfones in nearly quantitative yields.[43] The oxidation takes place at room temperature and is tolerant of a number of other functional groups – in some instanses chemoselective oxidation of a sulfide in the presence of an olefin is possible.

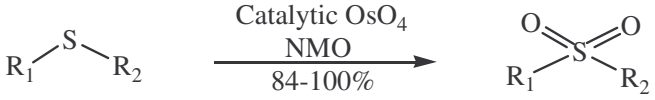

Chiral sulfoxides serve as versatile building blocks in the synthesis of pharmaceutical products and chiral ligands in asymmetric catalysis.[44] To partially oxidize sulfides to sulfoxides and not all the way to sulfones has become an area of wide research.[45] The asymmetric oxidation of sulfides to sulfoxides, for instance, can be achieved in good yields with layered double hydroxides (LDH)-supported OsO_4 catalyst using NMO as co-oxidant and $(DHQD)_2PHAL$ (hydroquinidine 1,4-phthalazinediyl diether) as a chiral ligand, although resulting in moderate enantiomeric excess (e.e's), (Scheme 2-9, p.17).[46]

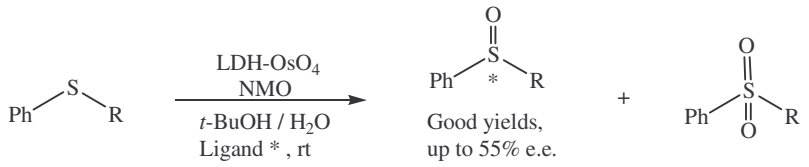

Scheme 2-9. Asymmetric oxidation of sulfides to sulfoxides

2.3.2 Metalloporphyrins and related complexes

Transition metals form good homogeneous or heterogeneous catalysts. This is because they are able to form numerous oxidation states, and as such, are able to form new compounds during a reaction providing an alternative route with a lower overall activation energy. As opposed to group 1 and group 2 metals, ions of the transition elements may have multiple stable oxidation states, since they can lose *d*-orbital electrons without a high energetic penalty. In most catalytic systems the transition metal is chelated to one or more ligands which dictate the metal's stability and reactivity. These ligands differ in their charge, size and nature of the constituent atoms. These include single atoms like chlorine (Cl^-) and sulfide (S^{2-}); to molecules such as pyridine (C_5H_5N) and ammonia (NH_3); and macrocycles such as porphyrins and phthalocyanines. Natural chelators include the porphyrin rings in haemoglobin or chlorophyll and the Fe^{3+} chelating siderophores[47] secreted by microorganisms.

(a) Porphyrins

Porphyrins (which comes from the Greek for "purple") are based on 16-atom rings containing four nitrogen atoms (Figure 2-2) making them the perfect size to bind nearly all metal ions. Heme proteins (which contain iron porphyrins) are ubiquitous in nature and serve many roles, including O_2 storage and transport (myoglobin and hemoglobin), electron transport (cytochromes b and c), and O_2 activation and utilization (cytochrome P450 and cytochrome oxidase).[48] Related macrocycles include the chlorophylls (which have a central magnesium ion) and pheophytins

(which are metal free) in the photosynthetic apparatus of plants and bacteria and vitamin B-12 (which contains cobalt) found in bacteria and animals.

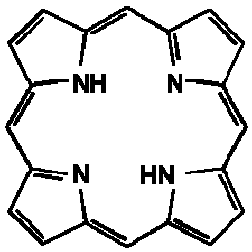

Figure 2-2. Porphine, the simplest porphyrin.

Porphyrins were originally studied for their importance in hemoglobin transfer, photosynthesis, and the disease porphyria. It was not until the late 1950's that porphyrins and metalloporphyrins were recognized and studied for their unique chemical properties. Porphyrin complexes have since been incorporated in a wide variety of catalytic reactions which includes epoxidation, hydroxylation and cyclopropanation of alkenes.[49] Other than applications as dyes, metalloporphyrins and phthalocyanines have also found application in the photodynamic therapy (PDT) of certain cancer types.

Porphyrins contain a 22 pi electron system, although only 18 electrons can be involved in any particular delocalization. All atoms are in a sp^2 configuration, giving rise to the planar structure, which conforms to Huckel's 4n + 2 rule for aromaticity. This conjugated system assumes many resonance forms and can accept substituents at a number of positions. The delocalization of the pi electrons imparts rigidity to the system, which prevents the metal-nitrogen bond's length in the complexes from varying significantly. Porphyrins can lose two protons to assume a -2 configuration, and they may also gain two protons to assume a +2 configuration. Metal insertion occurs in species that deprotonate; the lone pairs on the four nitrogens in the dinegative porphyrin readily donate to the empty d orbitals on a cationic (+2) metal acceptor. Depending on the size and oxidation state of the metal inserted, the geometry and properties of the porphyrin

may vary considerably. For instance, the geometry between the nitrogens and the metal is square planar, unless inhibited sterically. The late transition metals such as nickel are too small to fit in the cavity between the four nitrogen atoms, and the ring is forced to pucker to achieve overlap of the orbitals. If the metal is too large, such as niobium, the metal ion will be unable to fit inside the ring and will sit slightly above the ring plane. Distortions from the square planar geometry lower the stability of the complex, rendering it susceptible to demetalation by severe ring contraction or ring opening. Some metals, such as manganese, could also have an axial ligand present while bound to the porphyrin resulting in higher geometrical complexity.[50,51]

The majority of metalloporphyrins are formed by two separate and reversible one-electron oxidations to the pi-cation metal. Complexing of the metal to the porphyrin is largely dependent on the metal carrier from which the metal ion must be dissociated. Good metal carriers are large, loosely coordinated non-polar molecules soluble only in organic solvents. The optimal metal carrier is in its lowest accessible oxidation state; however, the oxidation state of the metal in its carrier often does not correspond to the oxidation state it adopts in the porphyrin. Factors other than the metal carrier that affect metal-porphyrin complexation are the solubility and the lability of the porphyrin. Strong acids reverse formation and cause demetalation. There are many methods of metal insertion in porphyrins and phthalocyanines; success of insertion can be readily determined by UV-Vis (Figure 2-3), fluorescence, and infrared spectroscopy.

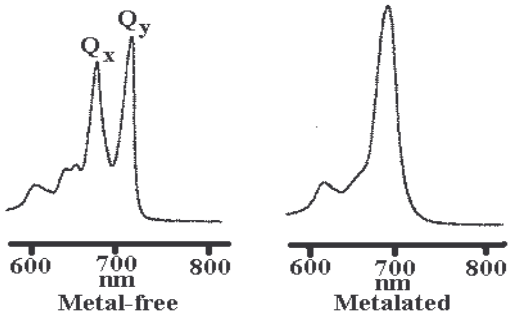

Figure 2-3. The collapse of the split Q-band of a metal free phtalocyanine into a single peak showing successful metal (Cu) insertion.[52]

Porphyrins are highly colored compounds, and often a change in color is indicative of the insertion. In addition to metalation of a porphyrin, it is also possible to transmetalate a porphyrin, wherin one metal is replaced with another of similar size and charge. Previously, iron porphyrins[53] has received much attention due to its role in hemoglobin transport, but recently ruthenium (II) and (III) porphyrins have attracted attention due to their unique role in the elucidation of electron transfer in porphyrin systems, and their usefulness in the synthesis of organic catalysts. The extent of conjugation in the porphyrin system lowers the energy necessary for inner sphere electron transfer to occur due to the pi orbital availability and their ability to participate in the transferring of the electron. It is this electron transfer that is important in activating oxygen in oxidation reactions.

There is a wide variety of catalytic reactions that may incorporate metalated porphyrins in their systems. For example, cobalt, chromium and manganese porphyrins have been used as catalysts in a variety of epoxidation of alkenes and the scope of aerobic epoxidation has been extended by ruthenium porphyrin complexes, which is converted to a dioxoruthenium(VI) porphyrin catalyst.[54] Although both oxygen atoms were used for epoxidation, long reaction times and low turnover numbers were obtained. However, by using a ruthenium substituted polyoxometalate as an inorganic dioxygenase, high yields and selectivities were obtained in 2h.[55] A chiral dioxoruthenium porphyrin complex was later synthesised resulting in epoxides with enantioselectivities in the range of 20 to 72% under aerobic conditions.[56] A variety of iron porphyrin complexes are also capable of catalysing oxidation reactions employing H_2O_2 as oxidant.[57,58] However, due to the often poor stability and difficult synthesis of these catalysts, the applicability is limited. Only a few non-heme iron complexes based on tetradentate nitrogen ligands are able to catalyse epoxidation reactions.[59]

Synthetic metalloporphyrins are known to be efficient catalysts for oxidation of hydrocarbons in the liquid phase. A variety of metal ions have been tested as central atom, among them

manganese which, when coordinated by the porphyrin ligand, shows a remarkable catalytic activity. It has been found that manganese porphyrin and its derivatives are efficient homogenous catalysts for epoxidation of olefins.[60] Manganese porphyrins and several other metal porphyrin complexes have been intensively studied as catalysts in epoxidation reactions of alkenes and the developments are summarised in several reviews.[61,62] A variety of oxidants such as iodosylarenes, alkylhydroperoxides, peracids, hypochlorites or hydrogen peroxide were employed. The early porphyrin-based catalysts often showed rapid deactivation, due to oxidative degradation. More robust catalysts for olefin epoxidation and hydroxylation of alkanes were obtained after the introduction of halogen substituents.[63] Furthermore, the additional substituents or additives like pyridine or imidazole as axial ligands improved the catalysts activity and selectivity and allowed the use of H_2O_2 for the oxidation of a wide range of substrates.[64] It has been proposed that the function of the axial coordinating additives is to favour the formation of oxomanganese(V) intermediates, which are presumed to be the actual oxidising species.[65] The catalytic epoxidation cycle of the manganese porphyrin starts with the conversion to the well established Mn(V)-oxo species (Scheme 2-10).[66] Subsequently the oxygen atom is transferred to the olefin via path **a** or **b** followed by release of the Mn(III) species and formation of the epoxide. The stepwise route **b** can give rotation around the former double bond resulting in *cis*/*trans* isomerisation leading to *trans*-epoxides starting from *cis*-alkenes as observed experimentally.

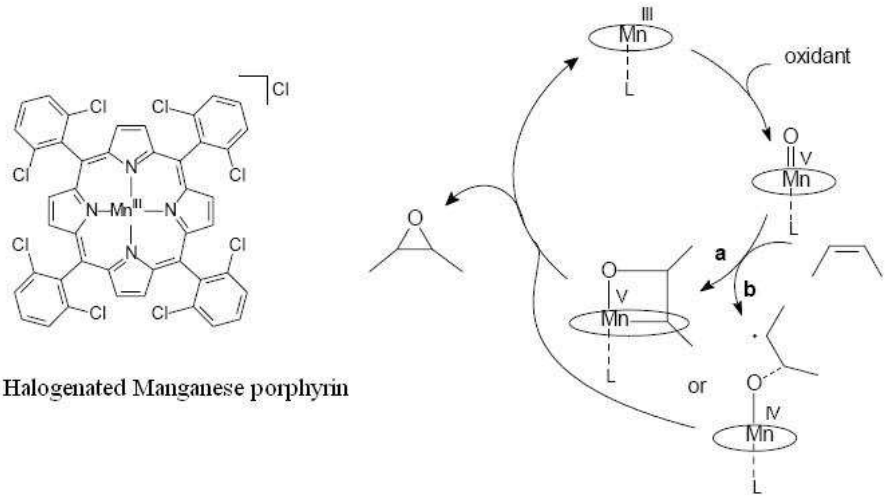

Scheme 2-10. Proposed catalytic epoxidation cycle of manganese porphyrin.

There has also been growing interest in heterogeneously-supported (eg. on Merrifield and Argogel resins) manganese porphyrins as catalysts in the epoxidation of alkenes.[67] For instance, a novel heterogeneous catalyst was developed by immobilization of the robust Mn(TDCPP)Cl (chloro 5,10,15,20-tetrakis(2,6-dichlorophenyl)porphyrinatomanganese(III)) on an inorganic support by a strong covalent bond through the β-position of the macrocycle. This catalyst was shown to be active, selective and reusable in clean epoxidation reactions using hydrogen peroxide as oxidant.[68] Also, among the various solid supports, the mesoporous silica material MCM-41, a member of the M41S family discovered by Mobil researchers, has attracted much attention due to their high surface area and well-defined hexagonal array ofuniform mesopores.[69] The mesoporous MCM-41 materials, with their ordered arrays of channels and cavities, act as suitable hosts for metalloporphyrin complexes. It has been found that these catalysts are most efficient in the epoxidation of conjugated alkene substrates (most commonly styrene and indene), followed by cyclic alkenes (cyclohexene, cyclooctene). In contrast, they are less successful in catalysing the epoxidation of less electron-rich terminal olefins such as dodec-1-ene and 1-hexene.

(b) Salen complexes

A Salen ligand (Figure 2-4, p. 23) is a dianionic and tetradendate chelating ligand in a coordination complex. Salen is a condensation for salicylic aldehyde and ethylene diamine which are the reactants for the ligand. The actual composition of the ligand depends on the various substituents. For example Salph is a salen ligand with a phenyl core group from the imine forming reaction of salicylic aldehyde with σ-diaminobenzene.

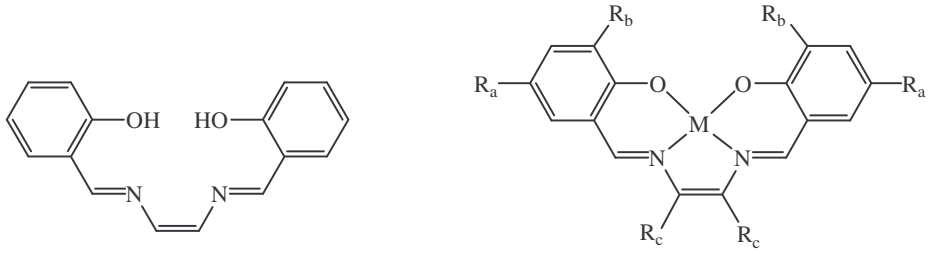

(a) **(b)**

Figure 2-4. The simple salen ligand (a) and an example of an substituted salen metal (M) complex (b).

The chiral version of this ligand has been reported using chiral 1,2-diamine. The salen derived from C2-symmetric 1,2-cyclohexyl diamine and 3,5-di-tert-butyl salicylaldehdye with different metals (Cr, Mn, Co, Al) has been used for different asymmetric transformation. Eric Jacobsen (from Harvard) is famous for using this catalyst for different reactions, for example the Jacobsen epoxidation.[70] It is complementary to the Sharpless epoxidation (used to form epoxides from the double bond in allylic alcohols). The Jacobsen epoxidation gains its stereoselectivity from a C_2 symmetric manganese(III) salen complex, which is used in catalytic amounts. After the first studies of chromium salen (*N,N*-ethylenebis(salicylidene aminato)) catalysed epoxidation of olefins,[71] Kochi *et al.* reported the use of Mn-salen complexes as epoxidation catalysts.[72] A few years after the discovery of Kochi, the groups of Jacobsen[73] and Katsuki[74] independently described a breakthrough in this olefin epoxidation by the introduction of a chiral diamine functionality in the salen ligand (Figure 2-5).

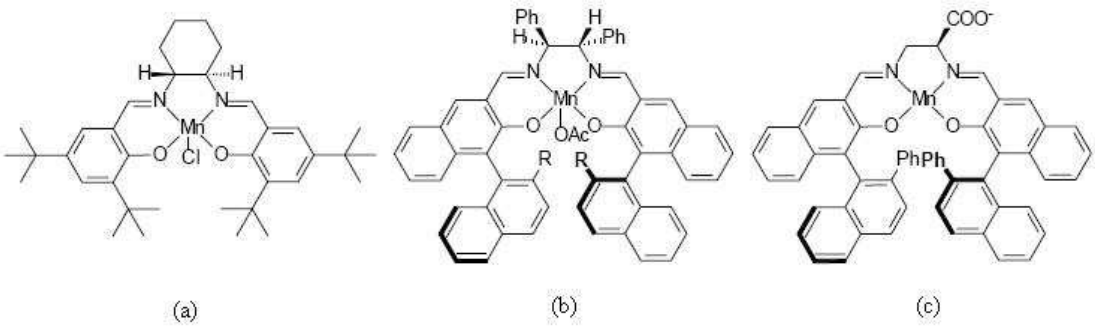

Figure 2-5. Manganese complexes studied by the groups of Jacobsen (a) and Katsuki (b and c) in epoxidation reactions.

Compared to chiral porphyrin manganese complexes, the use of the Mn-salen catalysts results generally in e.e.'s up to 90% with yields exceeding 80%. Porphyrin manganese complexes generally give e.e.'s between 50 and 90% with yields between 30% and 90%. For the conversion of *trans*-stilbene e.e.'s up to 80% were reported using these modified salen ligands.[75] A wide range of oxidants including hypochlorite, iodosylbenzene, or *m*-chloroperbenzoic acid (*m*-CPBA) can be applied.[76,77] The oxidizing species in the catalytic oxidation reaction is proposed to be a Mn(V)-oxo intermediate,[78] similar to the Mn-porphyrin catalyst (Scheme 2-10, p.22), and was confirmed by electrospray ionisation mass spectrometry.[79,80]

(c) Phthalocyanines

Phthalocyanines (Pcs) are typically purple, blue or green macrocyclic compounds similar in structure to tetraazaporphyrins, but having four additional fused benzo rings (Figure 2-6). The phthalocyanine macrocycle is also related to some other macrocyclic complexes, for example subphthalocyanines[81], superphthalocyanines[82] or hemiporphyrazines[83].

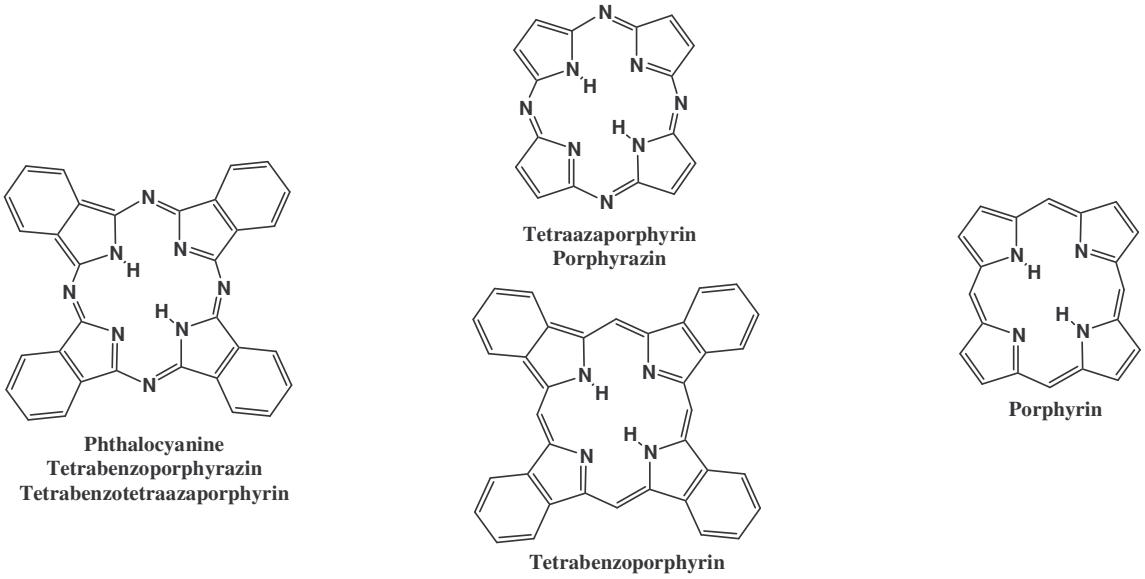

Figure 2-6. Relationship between porphyrins and phthalocyanines.

In the past Pcs have usually constituted a group of crystalline or polycrystalline compounds, whose insolubility in organic solvents is a very common characteristic. However, with the introduction of long-chain lipophilic subtituents on the periphery of the Pc ring, the solubility of the Pcs in nonpolar solvents has drastically improved and in some cases has provided these compounds with thermotropic behavior.[84]

There are various synthetic routes for making phthalocyanines imploying different starting materials (Figure 2-7), the most comon is the tetramerization of a suitable phthalonitrile precursor. Depending on how the starting materials are derivitized, the resulting phthalocyanine can have a wide range of properties even before a metal is introduced into the central cavity.

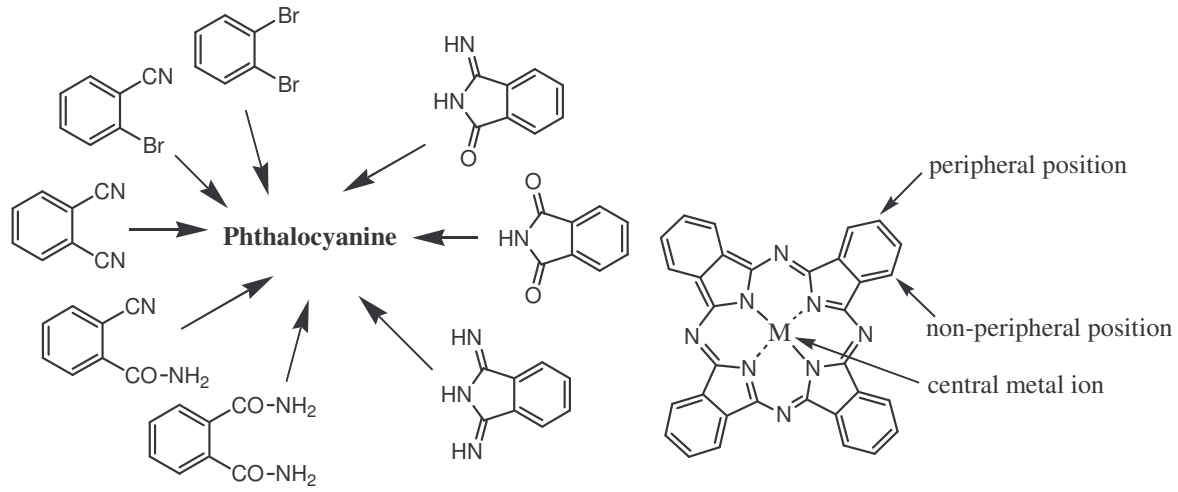

Figure 2-7. Typical starting materials for the synthesis of phthalocyanines and the different positions for derivitizing.

The remarkable properties of phthalocyanines make them important commercial commodities. In particular, their intense blue/green colours and stability towards heat, acids and bases have ensured their extensive use as pigments and dyes.[85,86] Their classical use as dyes is now being overshadowed by other applications taking advantage of the intense UV/vis absorption of the Q-band, normally between 670 and 730 nm. There is now extensive research into the applications of phthalocyanines in various other fields, for example in fuel cells[87], optical data storage systems[88], gas sensing devices[89], photovoltaic cells[90], electrophotography[91], and in electrochromic displays[92]. For example, optical limiting materials have been intensively studied owing to their potential applications in the protection of optical sensors and human eyes from high-intensity lasers. Phthalocyanines, like fullerenes[93], are materials that optically limit via a nonlinear absorption process at 532 nm laser irradiation due to the population of excited states through multi-step absorption. A novel lead phthalocyanine with the substituent group of octa-dodecaoxyl long chains has been investigated for its optical limiting performances.[94]

Phthalocyanines are also recognized as having excellent potential in the photodynamic therapy (PDT) and boron neutron capture therapy (BNCT) of certain cancer types and have been

extensively studied for possible aplications.[95] Specifically, aluminium and zinc phthalocyanine derivatives have been examined to be used as photosensitizers for PDT.[96,97] PDT treatment consists in loading the target cells with a photosensitizer that is able to generate highly reactive species (mainly singlet oxygen) upon irradiation with light of the appropriate wavelenght. The resulting oxidation of several subcellular targets, including proteins and unsaturated lipids, in the microenvironment of the photosensitizer causes cell death, via either random necrosis or apoptosis. Similarly, BNCT is based on the interaction of the non radioactive ^{10}B nucleus and a thermal neutron.[98] By administering a ^{10}B-containing sensitizer that can be selectively delivered to the target cell and subsequently irradiating the area with thermal neutrons, the ^{10}B nucleus splits into high linear energy transfer (LET) particles, namely an alpha particle and a lithium ion. Such particles deliver a relatively large amount of energy (±2.3 MeV) in a mean free path of about 10 μm, which is equivalent to the average diameter of a normal cell. As with PDT, the cytotoxic effect exerted by LET particles through the ionization processes is thus confined to the cell they are generated in.

Concerning catalysts, various examples of metalated phthalocyanines are used as catalysts for a number of industrial processes. Metal phthalocyanine (MPc) complexes have been used as catalysts in polymerization of olefins[99] and in the oxidation of sulfide to thiosulfide compounds.[100] Many different metals and phthalocyanines have been studied in various catalytic reactions. Copper phthalocyanine complexes have been investigated in epoxidation reactions, e.g. epoxidation of styrene.[101] The catalytic activities of the different CuPc complexes in the epoxidation reaction of styrene in acetonitrile have been investigated and it was found that substituted CuPc complexes yielded styrene epoxide (EPO) and benzaldehyde (–CHO) as major products. On the contrary, unsubstituted CuPc was selective for benzaldehyde. In the oxidation of various organic substrates and the epoxidation of olefins[102], iron tetrasulfophthalocyanine (FePcS) covalently grafted in the dimeric form yielded catalyst more active and selective then

those containing monomeric species but suffered from a lack of stability transforming into less selective monomer complexes during catalysis. Iron tetrasulfophthalocyanine was also immobilized on silica (FePcS–SiO2) and its activity examined on the allylic oxidation of cyclohexene using TBHP as oxidant.[103]

Phthalocyaninatomanganese(II/III) complexes are an interesting class of compounds since they have a very versatile redox chemistry.[104] This redox chemistry together with the ability of PcMn(II) to form reversibly a dioxygen complex PcMn(O_2) via Mn-O bonds[105], makes them possible catalyst for oxidations and model compounds for biological processes. Additionally, manganese phthalocyanine complexes can be imployed in fuel cells as a cathode coating film to catalize the reduction of oxygen to water.[87]

2.4 Polymeric support

Since this research program proposes the use of functionalised polymers as possible oxidants, a brief background on polymers is deemed essential. For the purpose of this study, functionalised polymers are macromolecules to wich oxidative groups are covantly bound. The following section will focus on the general properties of polymers as well as some usess for specific polymers. Lastly a background on polyepichlorohydrin (PECH) and polysuccinimide (PSI), the two polymeric carriers used in this study, will follow.

2.4.1 Introduction to polymers and their properties

A polymer is a substance composed of molecules with large molecular mass made of repeating structural units, or monomers. Polymers in which monomers are connected by covalent chemical bonds (Figure 2-8) are inert to dissociation. Well known examples of polymers include plastics, DNA and proteins. While the term polymer in popular usage suggests "plastic", polymers

comprise a large class of natural and synthetic materials with a variety of properties and purposes.

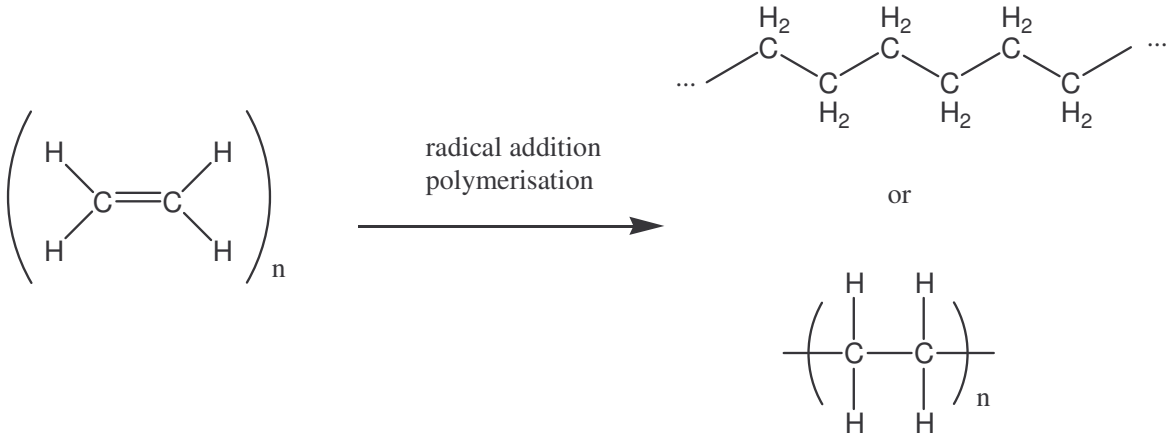

Figure 2-8. Polymerisetion of ethylene through radical addition polymerisation to polyethylene.

Natural polymer materials such as shellac and amber have been in use for centuries. Biopolymers such as proteins (for example hair, skin and part of the bone structure) and nucleic acids play crucial roles in biological processes. A variety of other natural polymers exist, such as cellulose, which is the main constituent of wood and paper. In biological processes biopolymers such as proteins (for example in hair, skin and part of the bone structure) and nucleic acids, play crucial roles. The well known natural polymer, rubber, through vulcanization, was the first popularized semi-synthetic polymer. Today many commodity polymers are in use, including polyethylene, polypropylene, polyvinyl chloride, polyethylene terephthalate, polystyrene and polycarbonate.[106] Each of these polymers has its own characteristic modes of degradation and resistances to heat, light and chemicals.

The bulk properties of polymers are strongly dependent upon their structure and mesoscopic behavior. A number of qualitative relationships between structure and properties are known.[107] The chain length, branching, chemical cross-linking, inclusion of plasticizers and the degree of crystallinity all contibute the the properties of the final polymer. For instance, increasing the

chain length of the polymer tends to decrease chain mobility, increasing strength, toughness, and the glass transition temperature (Tg). This is a result of the increase in chain interactions such as Van der Waals attractions and entanglements that come with increased chain length. These interactions tend to fix the individual chains more strongly in position and resist deformations and matrix breakup, both at higher stresses and higher temperatures. The attractive forces between polymer chains play a large part in determining a polymer's properties. Because polymer chains are so long, these interchain forces are amplified far beyond the attractions between conventional molecules. Different side groups on the polymer can lend the polymer to ionic bonding or hydrogen bonding between its own chains. These stronger forces typically result in higher tensile strength and melting points.

The intermolecular forces in polymers can be affected by dipoles in the monomer units.[108] Poly(vinylidene fluoride)'s structure and piezoelectric properties have been widely studied in terms of its dipole moment and polarizability.[109,110] Polymers containing amide or carbonyl groups can form hydrogen bonds between adjacent chains; the partially positively charged hydrogen atoms in N-H groups of one chain are strongly attracted to the partially negatively charged oxygen atoms in C=O groups on another. These strong hydrogen bonds, for example, result in the high tensile strength and melting point of polymers containing urethane or urea linkages. For example, polyesters have dipole-dipole bonding between the oxygen atoms in C=O groups and the hydrogen atoms in H-C groups. Dipole bonding is not as strong as hydrogen bonding, so a polyester's melting point and strength are lower than Kevlar's[111] (a polyamide), but polyesters have greater flexibility.

2.4.2 Polymer uses

Synthetic polymers truly are versatile materials and found a large number of aplications in everyday life. The annual production of thermosetting resins, such as phenol and epoxy resins was about 1.26 million tons in Japan in 2003.[112] For epoxy and polycarbonate resins, 195 and 409 thousand tons were produced in Japan in 2003, respectively. These crosslinked epoxy and phenol resins are manufactured for use mainly in electrical and electronic appliances and automobile industry. The following applications are only a small fraction of the large variety of uses.

Polyethylene (IUPAC name polyethene) is a thermoplastic commodity heavily used in consumer products. Over 60 million tons of the material is produced worldwide every year. Polyethylene is classified into several different categories based mostly on its density and branching. Ultra–high-molecular-weight polyethylene (UHMWPE), with a molecular weight numbering in the millions, is used in applications where high tensile strength and duribility is required.[113] These include can and bottle handling machine parts, moving parts on weaving machines, bearings, gears, edge protection on ice rinks, butchers' chopping boards, etc. It is used in bearing couples for artificial joint systems where it forms combination of the UHMWPE acetabular component joining with the metal (in particular, Co-Cr alloy) for the femoral component and still remains the most popular material for joint arthroplasty since its first application by Charnley in 1962.[114,115] At the other end of the scale is low-density polyethylene (LDPE), defined by a density range of 0.910 - 0.940 g/cm^3. LDPE has a high degree of short and long chain branching, which means that the chains do not pack well into a crystal. It has therefore less strong intermolecular forces as the instantaneous-dipole induced-dipole attraction is less. This results in a lower tensile strength and increased ductility. LDPE is created by free radical polymerization. The high degree of branches

with long side chains gives molten LDPE unique and desirable flow properties. LDPE is used for both rigid containers and plastic film applications such as plastic bags and film wrap.

Currently in pharmaceutics, many polymers are used as carriers for the delivery of drugs, proteins, targeting moieties, and imaging agents. Several polymers, poly(ethylene glycol) (PEG), N-(2-hydroxypropyl)methacrylamide (HPMA), and poly(lactide-co-glycolide) (PLGA) copolymers have been successfully utilized in clinical research.[116] These polymers are mainly used in the delivery of prodrugs. A prodrug is a form of a drug that remains inactive during its delivery to the site of action and is activated by the specific conditions in the targeted site. A conjugation of a drug with a polymer forms a so-called 'polymeric prodrug'. Polymeric conjugates of conventional polymeric prodrugs have several advantages over their low molecular weight precursors. The main advantages include: (1) an increase in water-solubility of low-soluble or insoluble drugs; (2) protection of drug from deactivation and preservation of its activity during circulation; (3) an improvement in pharmacokinetics; (4) a reduction in antigenic activity of the drug leading to a less pronounced immunological body response; (5) the ability to provide passive or active targeting of the drug specifically to the site of its action; (6) the possibility to form an advanced complex drug delivery system, which, in addition to drug and polymer carrier, may include several other active components that enhance the specific activity of the main drug.[117]

Similarly, in catalysis polymers are used as structural support by binding the catalyst and creating, depending on polymer proportions, a heterogeneous or homogeneous system.[118] Some examples have already been mentioned under the catalyst section. Chiral Mn(III) salen complexes, for example, supported on the mesoporous molecular sieve MCM-48 can be employed as catalyst in the asymmetric epoxidation of some unfunctionalized olefins. As chiral catalysts are expensive, their separation and repeated recycling is highly desirable. Compared to

the small-molecule homogeneous counterparts, the polymeric heterogeneous catalysts are more stable and can be recycled three times without loss of enantioselectivity.[119] Polymer-supported heterogeneous manganese porphyrins have been widely investigated as catalysts in the epoxidation of alkenes.[68]

There are also examples in which the polymer forms the ligand for the metal and as result becomes a polymeric catalyst. It was found that polymeric chiral Cr(III) salen complexes catalyzed regio-, diastereo-, and enantioselective aminolytic kinetic resolution (AKR) of trans-stilbene oxide, trans-b-methyl styrene oxide, and 6-CN-chromene oxide proceeded smoothly at room temperature, providing the desired anti-b-amino alcohols in high yields and enantiomeric excess (up to 100%).[120]

2.4.3 Polyepichlorohydrin (PECH)

For this study, a monohydroxy terminated polyepichlorohydrin was chosen as possible catalyst carrier in this study. Polyepichlorohydrin (PECH), **6**, is normally prepared by the cationic ring-opening polymerisation of a substituted oxirane monomer called epichlorohydrin, **5**, using diffferent types of initiators and Lewis acids as catalysts (Scheme 2-11, p. 34). For this study phenol was chosen as a co-initiator. PECH ranges from viscous liquids and rubbery amorphous materials to a crystaline polymer, depending on the stereo regularity of the final product. By using a predefined quantity of phenol as co-initiator and controlling the rate of epichlorohydrin addition, the molecular weight (MW) and polydispersity can be controlled. The polymer can then be further functionalised by subtitution reactions involving the chlorine atom.

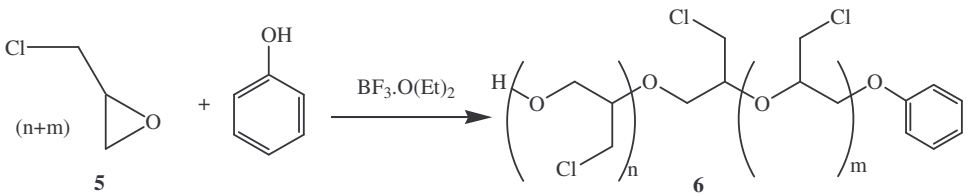

Scheme 2-11. Polymerisation of epichlorohydrin, **5**, to polyepichlorohydrin, **6**, using $BF_3.O(Et)_2$ as initiator and phenol as co-initiator.*

The preparation of polymers with hydroxyl end groups from cyclic ethers in the presence of hydroxyl-containing initiators has been studied by several groups.[121] In this reaction, two mechanisms compete (Scheme 2-12), the Active Chain End mechanism (ACE) and the Activated Monomer mechanism (AM). The ACE mechanism involves a tertiary oxonium propagation ion, and the generation of the hydroxyl group occurs by a chain transfer reaction by the hydroxyl-containing compound.

In the second mechanism, the protonated monomer is attacked by the alcohol during the initiation step and by the neutral growing species in the propagation step, generating a polymer with the same number of hydroxyl end groups as the initiator.

* In practice, the structure of PECH, **6**, consists of a random mixture of head-tail, head-head and tail-tail coupling and only one mode of coupling will be shown in the following sections.

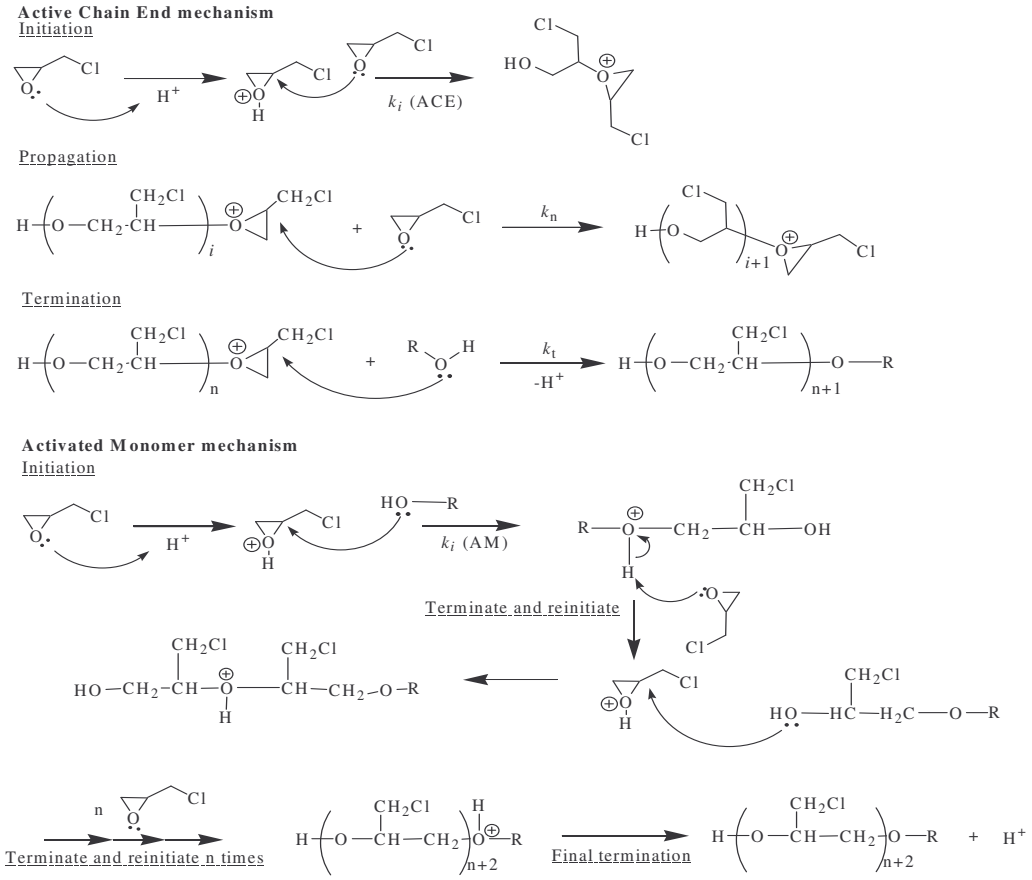

Scheme 2-12. Competing mechanisms for the polymerization of epichlorohydrin, the Active Chain End mechanism (ACE) and Activated Monomer mechanism (AM).

Cyclic structures are formed in the ACE mechanism by an intramolecular chain transfer reaction (Scheme 2-13), which reduces the MW of the end product and the yield of the reaction, but increases the polydispersity for the MW range studied[121]. Biedron et al. verified that the cyclic fraction in the final product depends on the nature of the initiator.[121a]

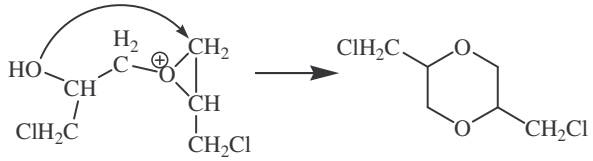

Scheme 2-13. Cyclisation reaction.

Whereas the ACE mechanism can lead to undesirable cyclization reactions, the AM forms only linear polyols, which is advantageous in order to obtain accurate target molecular weight products, as in Eq. 1:

$$M_n = \frac{n_{mon}}{n_{in}} \times M_{mon} + M_{in} \quad (1)$$

n_{mon} represents the number of moles of the monomer consumed, M_{mon} the monomer molar mass, n_{in} the number of moles of the initiator and M_{in} the initiator molar mass. Kubisa and Penczek[121b] showed that the AM mechanism dominates by maintaining a monomer's ''starving'' condition, i.e. the monomer should be slowly added to the reaction system, keeping its concentration as low as possible.

PECH is widely used as starting material for various polymer end products. One application is that of energetic polymers as binders in the formulations of solid propellants. Hydroxy terminated PECH is used as a starting material for manufacturing glycidyl azide polymer (GAP) and glycidyl nitrate polymer (PolyGLYN). GAP has been extensively investigated because it has stable energetic polymer characteristics and is compatible with the other propellant ingredients.[122] GAP, when used as an energetic binder, must have the appropriate molecular weight (between 1500 and 3000) and hydroxyl end groups to be later cured with isocyanates. As part of this study, PECH will be functionalized with morpholine groups.

2.4.4 Polysuccinimide (PSI)

Polysuccinimide (PSI), **8**, is a polymer that may be used as a starting point for the synthesis of polymeric drug carriers. Other than its drug-carrier applications, PSI and its derivatives have also found applications as hydrogels.[123] Hydrogels based on both natural and synthetic polymers have continued to be of interest for encapsulation of drugs. More recently, such hydrogels have become especially attractive to the new field of "tissue engineering" as matrices for repairing and regenerating a wide variety of biological tissues and organs. Polyaspartic acid (PASP) is hydrolised polysuccinimide with a free carboxylic acid group or amino group. PASP resin is biodegradable with high water absorbency, and it is commonly used as soil amendments, and in manufacturing of diapers, sanitary napkins, medicals, cosmetics, fabrics, metal absorbent

materials, etc.[124] PSI is a water insoluble polymer that is synthesised by acid-catalysed [125]polycondensation of aspartic acid, **7**, (Scheme 2-14).[126] Although PSI in itself isn't water soluble, it can easily be made so by converting it to various polyaspartimides.

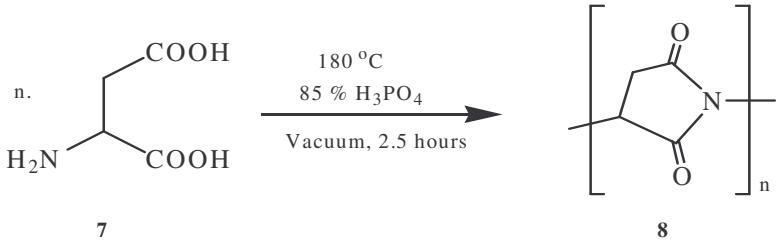

7 **8**

Scheme 2-14. Acid catalised polycondensation of L-aspartic acid, **7**, to polysuccinimide, **8**.†

Through nucleophilic attack, the imide rings of **8** can be opened by using various nucleophiles such as amines (Scheme 2-15). The nucleophile of choice for this study is N-(3-aminopropyl)-morpholine, **9**. N-(3-aminopropyl)-morpholine is classically used to impart water solublity to PSI, especially for drug carrier applications. It is doubly convenient to this study by increasing solublity and providing the morpholine functionality for the oxidation locus.

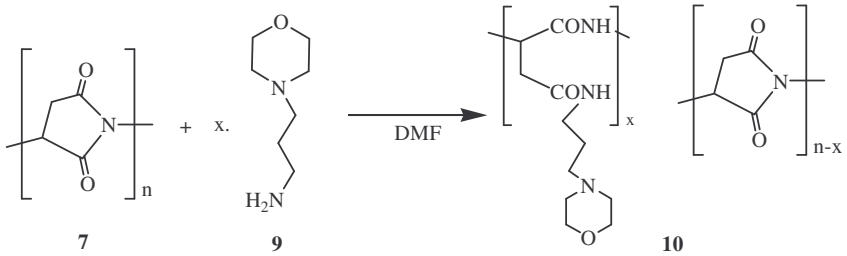

7 **9** **10**

Scheme 2-15. Nucleophilic attack on PSI, **7**, by N-(3-aminopropyl)-morpholine, **9**, resulting in the opening of the amide rings to form a polyaspartamide, **10**.

The polymers chosen for this study were selected to be hydrophobic (PECH) and hydrophylic (PSI). The solubility properties of these potential polymeric morpholine carriers will ultimately influence the catalytic reaction conditions of oxidation.

† The use of a single stereo isomer of aspartic acid is not necessary since scrambling occurs during the polymerization.

2.5 Electroanalytical chemistry

As an analytical method, cyclic voltammetry is possibly the simplest and most versatile electroanalytical technique for the study of electro-active species such as transition metal catalyst. In dealing with transition metal complexes for catalytic reactions, it is often useful to know the redox behaviour of the catalysts. Cyclic voltammetry is useful in that it can probe the redox behaviour of the analysed species over a wide potential range, in a relatively short amount of time.[127]

A redox couple can either be electrochemically reversible or irreversible. If a system is electrochemically reversible it means that the rate of electron transfer between the working electrode and substrate is fast enough to maintain the concentration of the oxidised and reduced species in equilibrium at the electrode surface. In an irreversible system, the rate of electron transfer is too slow to maintain equilibrium. For this study electrochemical experiments were performed to investigate the redox behaviour of a phthalocyanine oxidation catalyst. The basics of cyclic voltammetry and a brief description on the redox behaviour of porphyrins and phthalocyanines will be given in the following section.

2.5.1 Introduction to cyclic voltammetry

In cyclic voltammetry (CV), one measures the resulting current between a working electrode and an auxilliary electrode when the potential of the working electrode is changed. During the whole process the analysed solution remains stationary. The potential of the working electrode (usually glassy carbon, gold or platinum) is controlled relative to a reference electrode. There are various reference electrodes available, most commonly used are the saturated calomel electrode (SCE), a silver/silver chloride electrode (Ag/AgCl) or a silver/silver nitrate electrode ($Ag/AgNO_3$). The

controlled potential, applied over these two electrodes, can be viewed as an excitation signal. This signal is a linear potential scanning with a triangular waveform (Figure 2-9). Depending on the system, the experiment starts at an initial potential, E_i, where the system is redox silent, proceeding to a predetermined limit switching potential, $E_{\lambda 1}$, where the direction of the potential change is reversed.

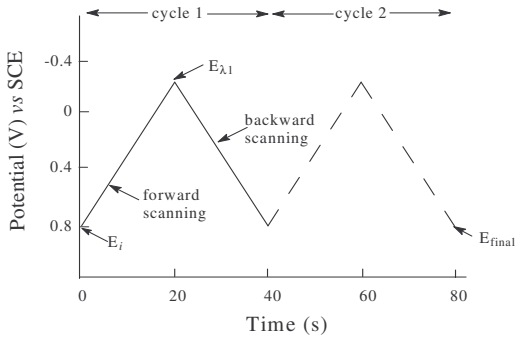

Figure 2-9. A typical excitation signal for cyclic voltammetry – a triangular potential waveform.

For a typical cyclic voltammogram, the current response (vertical axis) is plotted as a function of the applied potential (horizontal axis), (Figure 2-10 A). If the redox process is electrochemical reversible, the measured peak current is directly proportional to the scanrate as well as the concentration of the analyte.

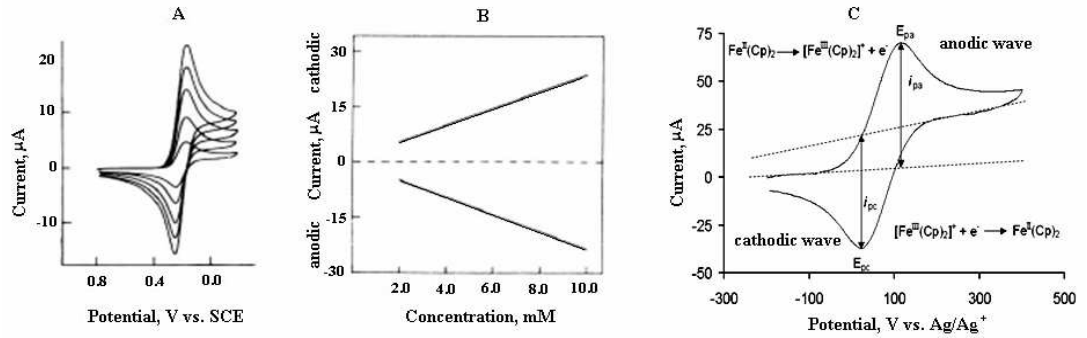

Figure 2-10. (A) Cyclic voltammograms of $K_3Fe(CN)_6$ in 1 M KNO_3. Scan rate = 20 mV/s. Pt working electrode. Concentration = 2, 4, 6, 8, and 10 mM. (B) Plot of i_{pc} versus concentration and i_{pa} versus concentration from voltammograms in (A). (C) Cyclic voltammogram of 3.0 mmol.dm^{-3} ferrocene measured in 0.1 mol.dm^{-3} tetrabutylammonium hexafluorophosphate/acetonitrile with glassy carbon working electrode at 25°C, scan rate 100mV.s^{-1}.[127]

In cyclic voltammetry there are some important parameters to consider (Figure 2-10 C). These are the peak anodic potential (E_{pa}), peak cathodic potential (E_{pc}) as well as the magnitudes of the peak anodic current (i_{pa}) and peak cathodic current (i_{pc}). The formal reduction potential (E^0) for an electrochemically reversible redox couple is midway between the two peak potentials and is calculated by: $E^{0'} = (E_{pa} + E_{pc})/2$.

Theoretically, an electrochemical couple is considered electrochemically reversible when the difference in peak potentials (ΔE_p) is 59 mV at 25˚C for a one electron transfer process (Figure 11).

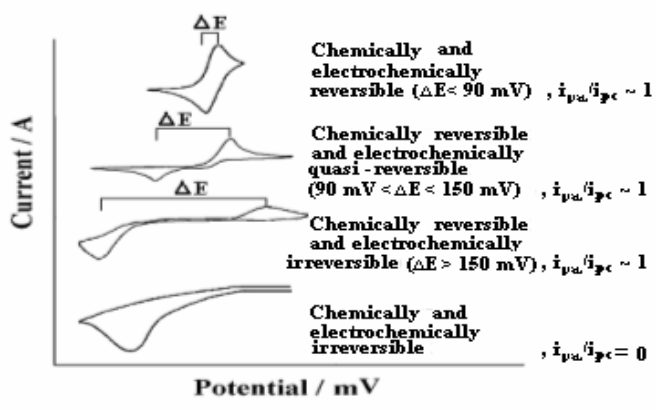

Figure 11. ΔE as a indication of electrochemical reversibility.

In practice due to electrode imperfections and other factors, a redox couple with an experimentally determined ΔE_p value up to 90 mV is often still considered to indicate electrochemical reversibility. As result of slow electron transfer kinetics at the electrode surface, peak separation increases and the electrochemical couple becomes more electrochemical irreversible. Also, the values of i_{pa} and i_{pc} should be identical for a chemically reversible redox couple, implying: $i_{pc}/i_{pa} = 1$. An electrochemically quasi-reversible couple is where both the oxidation and reduction processes takes place, but the electrochemical kinetics are slow and ΔE_p > 59 mV (usually between 90 mV and 150 mV). Any ΔE_p value greater than 150 mV designates an electrochemical irreversible couple where only oxidation or reduction takes place.

When preparing a cyclic voltammetry experiment, there are various steps to consider.[127] Firstly, a suitable medium consisting of a solvent containing a supporting electrolyte is needed for electrochemical phenomena to occur. The solubility of the species under investigation must be at least 1 x 10^{-4} mol dm^{-3} in the particular solvent and the electrolyte concentration must be at least 100 times greater than the conc. of the investigated species. An ideal solvent should possess electrochemical and chemical inertness over a wide potential range and should preferably be unable to solvate the electrochemical species. Most often used is acetonitrile (CH_3CN). Tetrahydrofuran (THF) is also commonly used but distorts results via coordination. Cathodic results are not distorted in this solvent. Dichloromethane is used when a strictly non-coordinating solvent is required. The supporting electrolyte is to increases the conductivity of the medium and evectively carries most of the current. Tetrabutylammonium hexafluorophosphate ($TBAPF_6$) is the most widely used supporting electrolyte in organic solvents although it distorts results due to ion pairing. It is also an IUPAC directive to use an internal standard in an electrochemical experiment. Due to its reversible electrochemistry, ferrocene is usually used (Figure 2-10 C). However, should the CV peak of the ferrocene overlap with one of the analytes peaks, other internal standards such as decamethyl ferrocene may be used. By IUPAC directive, potentials should be reported vs the Fc/Fc^+ couple.

2.5.2 Electrochemistry of phthalocyanines

The electrochemistry of phthalocyanines is very rich and, given the right solvent and conditions, up to four successive reversible ring reductions and two ring oxidations can be observed. To illustrate a typical ring-based redox process the cyclic voltammogram of 1,4,8,11,15,18,22,25-octadidecylphthalocyanine (a phthalocyanine substituted on the 8 non-peripheral positions with $C_{12}H_{25}$-alkyl chains) is given in Figure 2-12.[128] The potential scan starts at an initial potential where the system is redox silent (0 Volts in this case) and scans in the positive direction. Two

ring-based oxidations occur at 418mV and 929 mV (peaks I and II respectively) before the scan direction is reversed at 1000 mV and reduction of the oxidised species takes place. Further reduction of the Pc takes place at -1265 mV and -1619 mV (peaks III and IV respectively) before the scan direction is reversed again at -1800 mV, oxidising the reduced species. Each peak represents a one electron process.

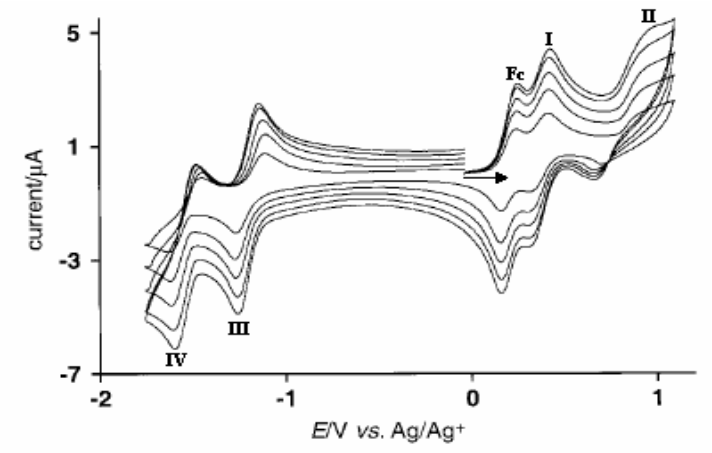

Figure 2-12. Cyclic voltammogram (CV) of 1,4,8,11,15,18,22,25-octadidecylphthalocyanine in 1,2-dichloroethane (1 mmol dm^{-3}) containing 0.1 mol dm^{-3} tetrabutylammonium hexafluorophosphate at scan rates of 50 (smallest i_p values), 100, 150, 200 and 250 mV s^{-1} on a platinum working electrode at 25 ^oC. The CV shows two ring-centered reversible oxidation peaks (III and IV) and two reversible reduction peaks (I and II). Two more reduction peaks lie outside the solvent window. The peak labelled Fc is that of ferrocene that has been added as an internal reference.

The electrochemical process of the various peaks in Figure 2-12 can be represented by the following scheme:

$$2HPc^{2-} \underset{+e^-}{\overset{IV\ -e^-}{\rightleftharpoons}} 2HPc^{-} \underset{+e^-}{\overset{III\ -e^-}{\rightleftharpoons}} 2HPc \underset{+e^-}{\overset{I\ -e^-}{\rightleftharpoons}} 2HPc^{+} \underset{+e^-}{\overset{II\ -e^-}{\rightleftharpoons}} 2HPc^{2+}$$

The electrochemical properties of metallated phthalocyanines (MPcs) have been intensively studied and remain a field of wide interest.[129] Incorporation of different metals into the core of the phthalocyanine ring and variations in the substituents on the periphery of the ring can help to activate or deactivate redox processes. Redox processes occurring in phthalocyanine complexes may be centered at the phthalocyanine ring or at the central metal and are affected by various factors. These include: 1) the nature of the substituents on the phthaolcyanine ring, 2) the type

and oxidation state of the central metal, 3) the presence and nature of the axial ligands co-ordinated to the central metal.

2.6 Liquid crystals

2.6.1 Introduction

For many compounds that have rod-like or disc-like shapes (like the phthalocyanines), the melting process occurs by way of one or more intermediate phases (known as mesophases) as the temperature is increased. The phthalocyanine complex investigated in this study as catalyst is that of a non-peripherally substituted octatridecylphthalocyanine metal complex. Long chain alkyl and alkoxy substituted phthalocynines are intensively studied for their liquid crystal properties.[130] However, in the context of this study the long chains improve the solubility of the phthalocyanine complex by disrupting the π-stacking of the phthalocyanine cycles. As mentioned before, phthalocyaninatomanganese complexes show a versatile redox chemistry which has been intensively investigated in the past.[104] However, there are only a few studies concerning the thermal behaviour behaviour of substituted manganese phthalocyanines.[131]

This intermediate state between the solid state and isotropic liquid state is a mesomorphic state often referred to as the liquid crystal state. Compounds exhibiting mesophases are called mesogens. Mesophases have properties that are intermediate between those of the fully ordered crystalline solid and the isotropic liquid. There are various methods used in studying mesophases, including the cryo-TEM method,[132] differential scanning calorimetry (DSC),[133] polarizing optical microscopy[134] and X-ray diffraction.[135] The techniques applicable to this stydy are DSC and polarizing optical microscopy.

2.6.2 Differential scanning calorimetry (DSC)

Differential scanning calorimetry (DSC) is a thermoanalytical technique in which the difference in the amount of heat required to increase the temperature of a sample relative to reference are measured. The measured quality is “heat flow difference”. These measurements can provide quantitative and qualitative information about physical and chemical changes that involve endothermic or exothermic processes, or changes in heat capacity.

During a DSC experiment, both the sample and reference are maintained at the same temperature throughout the experiment. Normally, the temperature program for a DSC analysis is designed such that the sample holder temperature increases linearly as a function of time. The reference sample should have a well-defined heat capacity over the range of temperatures to be scanned. The basic principle underlying this technique is that, when the sample undergoes a physical transformation such as phase transitions, more (or less) heat will need to flow to it than the reference to maintain the reference and sample at the same temperature. These phase changes are observed as thermal events. Whether more or less heat must flow to the sample depends on whether the process is exothermic or endothermic. For example, as a solid sample melts to a liquid it will require more heat flowing to the sample to increase its temperature at the same rate as the reference. This is due to the absorption of heat by the sample as it undergoes the endothermic phase transition from solid to liquid. Similarly, as the sample undergoes exothermic processes (such as crystallization or melting) less heat is required to raise the sample temperature at the same rate as the reference temp. By observing the difference in heat flow between the sample and reference, differential scanning calorimeters are able to measure the amount of heat absorbed or released during such transitions. DSC may also be used to observe more subtle phase changes, such as glass transitions. DSC is widely used in industrial settings as a quality control instrument due to its applicability in evaluating sample purity and for studying polymer

curing. DSC is also used in the study of liquid crystals. Using DSC, it is possible to observe the small energy changes that occur as matter converts from a solid to a liquid crystal and from a liquid crystal to an isotropic liquid.

The result of a DSC experiment is plotted on a thermogram which is a curve of heat flux versus temperature or versus time (Figure 2-13). There are two different conventions: exothermic reactions in the sample are shown either with a positive or negative peak. The ICTAC convention assigns all exothermic thermal events (such as crystallisation) as being positive.

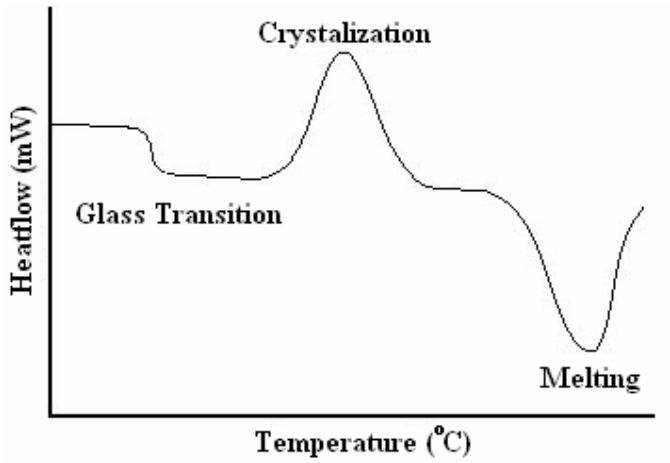

Figure 2-13. Features of a DSC curve.

Thermograms can be used to calculate enthalpies of transitions. This is done by integrating the peak corresponding to a given transition. It can be shown that the enthalpy of transition can be expressed using the following equation:

$$\Delta H = KA,$$

where ΔH is the enthalpy of transition, K is the calorimetric constant, and A is the area under the curve. The calometric constant will vary from instrument to instrument, and can be determined by analyzing a well-characterized sample with known enthalpies of transition.

Some of the properties of a sample that can be measured by DSC include: glass transitions; melting and boiling points; crystallisation time and temperature (percent crystallinity); heats of

fusion and reactions (specific heat capacity and oxidative/thermal stability); rate and degree of curing in polymers (reaction kinetics); and purity.

2.7 References

[1] C. Starr and R. Taggart, *Biology: The Unity and Diversity of Life (9th Ed.),* Brookes/Cole, pp 108–109, 116–117 (2001)

[2] J.J. Dannacher, *J. Mol. Cat. A: Chem.*, **251**, 159–176 (2006)

[3] M.J. O'Donnell, A.C. Shore, R.J. Russell and D.C. Coleman, *Journal of Dentistry*, **35**, 438–451 (2007)

[4] J.K. Joseph, S.L. Jain and B. Sain, *Catalysis Communications*, **8**, 83–87 (2007)

[5] N.I. Kuznetsova, N.V. Kirillova, L.I. Kuznetsova, M.Yu. Smirnova and V.A. Likholobov, *Journal of Hazardous Materials*, **146**, 569–576 (2007)

[6] D.N. Prater and J.J. Rusek, *Applied Energy*, **74**, 135–140 (2003)

[7] G.H. Miley et al, *Journal of Power Sources*, **165**, 509–516 (2007)

[8] G. Zhao and N.D. Chasteen, *Analytical Biochemistry*, **349**, 262–267 (2006)

[9] M.N. El Hazek, T.A. Lasheen and A.S. Helal, *Hydrometallurgy*, **84**, 187–191 (2006)

[10] D.A. Skoog, D.M. West and F.J. Holler, *Fundamentals of Analytical Chemistry (7th Ed.),* Brookes/Cole, pp 303–410, A12–A15 (1996)

[11] N.N. Mahamuni, P.R. Gogate and A.B. Pandit, *Ultrason. Sonochem.*, **14**, 135–142 (2007)

[12] E.L. Springer and J.D. McSweeny, *Tappi J.*, **76**, 194–199 (1993)

[13] B. Holmes, *Journal of the American Chemical Society*, **82**, 3454 (1960)

[14] K.S. Webb and S.J. Ruszkay, *Tetrahedron*, **54**, 401–410 (1998)

[15] P. Ceccherelli, M. Curini, M.C. Marcrotullio, F. Epifano and O. Rosati, *Synthetic Letters*, 767–768 (1996)

[16] P. Cheshev, A Marra and A Dondoni, *Carbohydrate Research*, **341**, 2714–2716 (2006)

[17] K.S. Webb, *Tetrahedron Lett.*, **55**, 3457 (1994)

[18] K.S. Webb and V. Seneviratne, *Tetrahedron Lett.*, **36**, 2377 (1995)

[19] K.S. Webb and D. Levy, *Tetrahedron Lett.*, **36**, 5117 (1995)

[20] Y. Miyahara and T. Inazu, *Tetrahedron Lett.,* **31,** 5955 (1990)

[21] S.K. Singh, M.S. Reddy, M. Mangle and K.R. Ganesh, *Tetrahedron*, **63**, 126–130 (2007)

[22] B.W. Yoo, J.W. Choi and C.M. Yoon, *Tetrahedron Let.*, **47**, 125–126 (2006)

[23] R. Kakehashi, S. Yamamura, N. Tokai, T. Takeda, K. Kaneda, K. Yoshinaga and H. Maeda, *Journal of Colloid and Interface Science*, **243**, 233–240 (2001)

[24] J. March, *Advanced Organic Chemistry: Reactions, Mechanisms and Structure (4th Ed.)*, John Wiley & Sons, Inc., pp 1200–1201 (1992)

[25] F.F. Bamoharrama, M.M. Heravi, M. Roshani and N. Tavakoli, *Journal of Molecular Catalysis A: Chemical*, **252**, 219–225 (2006)

[26] T. Rosenau, A. Hofinger, A. Potthast and P. Kosma, *Polymer*, **44**, 6153–6158 (2003)

[27] T. Rosenau, A. Hofinger, A. Potthast and P. Kosma, *Prog. Polym. Sci.*, **26**, 1763–1837 (2001)

[28] M. Gomes Jr. and O.A.C. Antunes, *Catalysis Communications*, **2**, 255 (2001)

[29] H.C. Kolb, M.S. VanNieuwenhze and K.B. Sharpless, *Chem. Rev.*, **94**, 2483–2547 (1994)

[30] M. Schröder, *Chem. Rev.*, **80**, 187–213 (1980)

[31] N.A. Milas *et al.*, *J. Am. Chem. Soc.*, **58**, 1302 (1936)

[32] V. VanRheenen, R.C. Kelly and D.Y. Cha, *Tetrahedron Lett*., **23**, 1973–1976 (1976)

[33] M. Minato, K. Yamamoto, J. Tsuji, *J. Org. Chem.*, **55**, 766–768 (1990)

[34] G. Caroling, J. Rajaram and J.C. Kuriacose, *Ind. J. Chem.*, **27A**, 873 (1988)

[35] C.J. Andres, N. Spetseris, J.R. Norton and A.I. Meyers, *Tetrahedron Lett.*, **36**, 1613 (1995)

[36] S. Torii, P. Liu, N. Bhuvaneswari, C. Amatore and A. Jutand, *J. Org. Chem.*, **61**, 3055–3060 (1996)

[37] T. Yokomatsu, T. Yamagishi, T. Sada, K. Suemune and S. Shibuya, *Tetrahedron*, **54**, 781–790 (1998)

[38] S. Nagayama, M. Endo and S. Kobayashi, *J. Org. Chem.*, **63**, 6094 (1998)

[39] Q. Liua, Z. Zhanga, F. Van Rantwijkb and R.A. Sheldonb, *Journal of Molecular Catalysis A: Chemical*, **224**, 213–216 (2004)

[40] D.C. Whitehead, B.R. Travis and B. Borhan, *Tetrahedron Lett.*, **47**, 3797–3800 (2006)

[41] C. Djerassi and A.A. Engle, *J. Am. Chem. Soc*., **75**, 3838 (1953)

[42] E. Vadejs and C.K. McClure, *J. Am. Chem. Soc*., **108**, 1094 (1986)

[43] S.W. Kaldor and M. Hammond, *Tetrahedron Lett.*, **32**, 5043 (1991)

[44] I. Fernandez and N. Khiar, *Chem. Rev.,* **103**, 3651 (2003)

[45] P.Kowalski, K. Mitka, K. Ossowska and Z. Kolarska, *Tetrahedron*, **61**, 1933–1953 (2005)

[46] M.L. Kantam, B.V. Prakash, B. Bharathi and Ch.V. Reddy, *Journal of Molecular Catalysis A: Chemical*, **226**, 119–122 (2005)

[47] H. Liu, K. Håkansson, J.Y. Lee and D.H. Sherman, *J. Am. Soc. Mass Spectrom.*, **18**, 842–849 (2007)

[48] F. Hannemann, A. Bichet, K.M. Ewen and R. Bernhardt, *Biochimica et Biophysica Acta*, **1770**, 330–344 (2007)

[49] K.C. Brown and T. Kodadek, *J. Am. Chem. Soc*., **114**, 8336 (1992)

[50] K.M. Smith, *Porphyrins and Metalloporphyrins: A New Edition Based on the Original Volume by J.E. Falk*, Elseview Scientific Publishing Company; New York, Ch.1 (1975)

[51] J. Huheey, E. Keiter, R. Keiter and C. Harper, *Inorganic Chemistry: Principles of Structure and Reactivity (4th Ed)*, New York, pp 891 (1993)

[52] E.H.G. Langner, M.Sc. thesis, University of the Free State, Bloemfontein, South Africa, p47 (2000)

[53] T. Yoshihiro, T. Kohshin, Y. Takahiro, M. Syuichi and K. Teruhisa, *J. Mol. Cat. A: Chem.*, **130**, 285–295 (1998)

[54] J.T. Groves and R. Quinn, *J. Am. Chem. Soc.*, **107**, 5790 (1985)

[55] R. Neumann and M. Dahan, *Nature*, **388**, 353 (1997)

[56] T.S. Lai, R. Zhang, K.K. Cheung, H.L. Kwong and C.M. Che, *Chem. Commun.* 1583–1584 (1998)

[57] B. Meunier, *Chem. Rev.*, **92**, 1411–1456 (1992)

[58] T.G. Traylor, S. Tsuchiya, Y.S. Byun, and C. Kim, *J. Am. Chem. Soc.*, **115**, 2775–2781 (1993)

[59] C. Kim, K. Chen, J. Kim, and L. Que, Jr., *J. Am. Chem. Soc.*, **119**, 5964–5965 (1997)

[60] J. Haber, J. Iwanejko, J. Poltowicz, P. Battioni and R. Mansuy, *J. Mol. Cat. A: Chem.*, **152**, 111 (2000)

[61] T. Katsuki, *Coord. Chem. Rev.*, **140**, 189–214 (1995)

[62] B. Meunier, *Chem. Rev.*, **92**, 1411–1456 (1992)

[63] D. Mansuy, *Coord. Chem. Rev.*, **125**, 129–141 (1993)

[64] E. Baciocchi, T. Boschi, C. Galli, A. Lapi and P. Tagliatesta, *Tetrahedron*, **53**, 4497–4502 (1997)

[65] J.T. Groves, Y. Watanabe and T.J. McMurry, *J. Am. Chem. Soc*., **105**, 4489–4490 (1983)

[66] R.D. Arasasingham, G.X. He and T.C. Bruice, *J. Am. Chem. Soc*., **115**, 7985–7991 (1993)

[67] E. Brulé, Y.R. de Miguel and K.K. Hiic, *Tetrahedron*, **60**, 5913–5918 (2004)

[68] S.L.H. Rebelo, A.R. Goncalves, M.M. Pereira, M.M.Q. Simoes, M.G.P.M.S. Neves and J.A.S. Cavaleiro, *J. Mol. Cat. A: Chem.*, **256**, 321–323 (2006)

[69] A.K. Rahiman, K. Rajesh, K.S. Bharathi, S. Sreedaran and V. Narayanan, *Applied Catalysis A: General*, **314**, 216–225 (2006)

[70] a) W. Zhang, J.L. Loebach, S.R. Wilson and E.N. Jacobsen, *J. Am. Chem. Soc.*, **112**, 2801–2803 (1990);
b) E.N. Jacobsen, W. Zhang, A.R. Muci, J.R. Ecker, and L. Deng, *J. Am. Chem. Soc.*, **113**, 7063–7064 (1991);
c) B.D. Brandes and E.N. Jacobsen, *J. Org. Chem.*, **59**, 4378–4380 (1994)

[71] E.G. Samsel, K. Srinivasan and J.K. Kochi, *J. Am. Chem. Soc.*, **107**, 7606–7617 (1985)

[72] K. Scrinivasan, P. Michaud, and J.K. Kochi, *J. Am. Chem. Soc.*, **108**, 2309–2320 (1986)

[73] W. Zhang, J.L. Loebach, S.R. Wilson, and E.N. Jacobsen, *J. Am. Chem. Soc*., **112**, 2801–2803 (1990)

[74] R. Irie, K. Nodda, Y. Ito and T. Katsuki, *Tetrahedron Lett.*, **31**, 7345–7348 (1990)

[75] T. Katsuki, *J. Mol. Cal. A: Chem*., **113**, 87–107 (1996)

[76] T. Katsuki, *Coord. Chem. Rev*., **140,** 189–214 (1995)

[77] D.L. Hughes, G.B. Smith, J. Liu, G.C. Dezeny, C.H. Senanayake, R.D. Larsen, T.R. Verhoeven, and P.J. Reider, *J. Org. Chem.*, **62**, 2222–2229 (1997)

[78] E.N. Jacobsen, L. Deng, Y. Furukawa, and L.E. Martinez, *Tetrahedron,* **50**, 4323–4334 (1994)

[79] D. Feichtinger, D.A. Plattner, *Angew. Chem., Int. Ed*., **36**, 1718–1719 (1997)

[80] D. Feichtinger and D.A. Plattner, *J. Chem. Soc*., *Perkin Trans.*, **2**, 1023–1028 (2000)

[81] E. Ohno-Okumura, K. Sakamoto, T. Kato, T. Hatano, K. Fukui, T. Karatsu, A. Kitamura and T. Urano, *Dyes and Pigments*, **53**, 57–65 (2002)

[82] J. Silver and Q.A.A. Jassim, *Inorganica Chimica Acta*, **144**, 281–288 (1988)

[83] S. Rodriguez-Morgade and T. Torres, *Inorganica Chimica Acta*, **230**, 153–157 (1995)

[84] J. Simon, J.J. André and A. Skoulios, *New J. Chem.*, **10**, 295 (1986)

[85] K.R.V. Reddy and J. Keshavayya, *Dyes and Pigments*, **53** 187–194 (2002)

[86] D.M. Grim and J. Allison, *International Journal of Mass Spectrometry*, **222**, 85–99 (2003)

[87] N. Sehlotho and T. Nyokong, *Journal of Electroanalytical Chemistry*, **595** , 161–167 (2006)

[88] R. Ao, L. Kümmert and D. Haarer, *Adv. Mater*., **5,** 495 (1995)

[89] Y. Lee, C. Hsiao, C. Chang and Y. Yang, *Sensors and Actuators B*, **94**, 169–175 (2003)

[90] J. Ma, J. Wang and Y. Liu, *Journal of Power Sources*, **172**, 220–224 (2007)

[91] A. Lux, G.G. Rozenberg, K. Petritsch, S.C. Moratti, A.B. Holmes and R.H. Friend, *Synthetic Metals*, **102**, 1527–1528 (1999)

[92] R.J. Mortimer, A.L. Dyer and J.R. Reynolds, *Displays*, **27**, 2–18 (2006)

[93] L.W. Tutt and A. Kost, *Nature*, **356**, 225 (1992)

[94] S. Qu, Y. Chen, Y. Wang, Y. Song, S. Liu, X. Zhao and D. Wang, *Materials Letters*, **51**, 534–538 (2001)

[95] F. Giuntini, Y. Raoul, D. Dei, M. Municchi, G. Chiti, C. Fabris, P. Colautti, G. Joria and G. Roncucci, Tetrahedron Lett., **46**, 2979–2982 (2005)

[96] D.A. Fernandez, J. Awruch and L.E. Dicello, *Photochem. Photobiol.*, **63**, 784 (1996)

[97] E.I. Yslas, V. Rivarola and E.N. Durantini, *Bioorganic & Medicinal Chemistry*, **13**, 39–46 (2005)

[98] A.H. Soloway, W. Tjarks, B.A. Barnum, F.G. Rong, R.F. Barth, I.M. Codogni, J.G. Wilson, *Chem. Rev.*, **98**, 1515–1562 (1998)

[99] S.G. Long, B. Snedeker, K. Bartosh, M.L. Werner and A. Sen, *Polym. Prep.*, **40**, 843 (1999)

[100] V. Iliev, L. Prahov, L. Bilyarska, H. Fischer, G. Schulz-Ekloff, D. Wohrle and L. Petrov, *J. Mol. Catal. A: Chem.*, **151**, 161 (2000)

[101] S. Seelan, M.S. Agashe, D. Srinivas and S. Sivasanker, *J. Mol. Cat. A: Chem.*, **168**, 61–68 (2001)

[102] A.B. Sorokin, S. Mangematin and C. Pergrale, *J. Mol. Cat. A: Chem.*, **182–183**, 267–281 (2002)

[103] L.M. González, A.L. Villa de P., C. Montes de C. and A. Sorokin, *Tetrahedron Lett.*, **47**, 6465–6468 (2006)

[104] A.B.P. Lever, P.C. Minor and J.P. Wilshire, *Inorg. Chem.*, **20**, 2550 (1981)

[105] a) A.B.P. Lever, J.P. Wilshire and S.K. Quan, *J. Am. Chem. Soc.*, **101**, 3668 (1979);

b) A.B.P. Lever, J.P. Wilshire and S.K. Quan, *Inorg. Chem.*, **20**, 761 (1981)

[106] a) M.V.S. Murty, P. Rangarajan, E.A. Grulke and D. Bhattacharyya, *Fuel Processing Technology*, **49**, 75–90 (1996);

b) M.J. Shenton and G.C. Stevens, *Thermochimica Acta*, **332**, 151–160 (1999);

c) Y. Sato, Y. Kondo, K. Tsujita and N. Kawai, *Polymer Degradation and Stability*, **89**, 317–326 (2005);

d) L.F. Al-Saidi, K. Mortensen and K. Almdal, *Polymer Degradation and Stability*, **82**, 451–461 (2003)

[107] J. Brandrup, E.H. Immergut and E.A. Grulke, *Polymer Handbook (4th Ed.)*, New York, Wiley-Interscience, (1999)

[108] S. Kovshik, M. Mikhailova, G. Polushina, E. Rjumtsev, A. Kovshik and A. Lezov, *Journal of Non-Crystalline Solids*, **351**, 2723–2727 (2005)

[109] H.M.G. Correia and M.M.D. Ramos, *Computational Materials Science*, **33**, 224–229 (2005)

[110] Z. Wang, H. Fan, K. Su and Z. Wen, *Polymer*, **47**, 7988–7996 (2006)

[111] D. Bhattacharyya and D.P.W. Horrigan, *Composites* Science *and Technology*, **58**, 267-283 (1998)

[112] Y. Sato, Y. Kondo, K. Tsujita and N. Kawai, *Polymer Degradation and Stability*, **89**, 317–326 (2005)

[113] S. Ge et al., Wear behavior and wear debris distribution of UHMWPE against Si_3N_4 ball in bi-directional sliding, *Wear* (2007), doi:10.1016/j.wear.2007.05.001

[114] Oonishi et al, *The Journal of Arthroplasty*, **21**(**7**), 944 (2006)

[115] D.H. Sochart, *Clin. Orthop*., **363**, 135 (1999)

[116] J. Khandare and T. Minko, *Prog. Polym. Sci.*, **31**, 359–397 (2006)

[117] a) A.N. Lukyanov and V.P. Torchilin, *Advanced Drug Delivery Reviews*, **56**, 1273–1289 (2004);

b) D.E. Meyer, B.C. Shin, G.A. Kong, M.W. Dewhirst and A. Chilkoti, *Journal of Controlled Release*, **74**, 213–224 (2001);

c) G. Pasut and F.M. Veronese, *Prog. Polym. Sci.*, **32**, 933–961 (2007)

[118] R.I. Kureshy, I. Ahmad, N.H. Khan, S.H.R. Abdi, S. Singh, P.H. Pandia and R.V. Jasra, *Journal of Catalysis*, **235**, 28–34 (2005)

[119] K. Yu, L. Lou, C. Lai, S. Wang, F. Ding and S. Liu, *Catalysis Communications,* **7**, 1057–1060 (2006)

[120] R.I. Kureshy, S. Singh, N.H. Khan, S.H.R. Abdi, S. Agrawal and R.V. Jasra, *Tetrahedron: Asymmetry*, **17**, 1638–1643 (2006)

[121] a) T. Biedron, P. Kubisa and S. Penczek, *J. Pol. Sci. A*, **29**, 619 (1991);

b) P. Kubisa and S. Penczek, *Prog. Polym. Sci.*, **24**, 1409 (1999);

c) A.U. Francis, S. Venkatachalam, M. Kanakavel, P.V. Ravindran and K.N. Ninan, *Eur. Polym. J.*, **39**, 831 (2003)

[122] M.B Frankel, L.R. Grant and J.E. Flanagan, *J. Propul. Power*, **8(3)**, 560 (1992)

[123] a) Y. Zhao, H. Su, L. Fang and T. Tan, *Polymer*, **46**, 5368–5376 (2005)

b) T. Gyenes et al., Swelling properties of aspartic acid-based hydrogels, *Colloids Surf. A: Physicochem. Eng. Aspects* (2007), doi:10.1016/j.colsurfa.2007.06.016

[124] a) J. Yang, F. Wang, L. Fang and T. Tan, *Composites Science and Technology*, 67, 2160–2164 (2007)

b) C.Y. Chen, et al., Recovery of Cu(II) and Cd(II) by a chelating resin containing aspartate groups, *J. Hazard. Mater.* (2007), doi:10.1016/j.jhazmat.2007.07.074

[125] P. Caliceti et al., *Biochimica et Biophysica Acta*, **1528**, 177–186 (2001)

[126] M. Tomida, T. Nakato, S. Matsunami and T. Kakuchi, *Polymer*, **38(18)**, 4733–4736 (1997)

[127] J.J. Van Benschoten, J.Y. Lewis, W.R. Heineman, D.A. Roston and P.T. Kissinger, *J. Chem. Educ.*, **60(9)**, 772 (1983)

[128] J.C. Swarts, E.H.G. Langner, N. Krokeide-Hove and M.J. Cook, *J. Mater. Chem.*, **11**, 434–443 (2001)

[129] a) C.M. Lieber and N.S. Lewis, *J. Am. Chem. Soc.*, **106**, 5033 (1984);

b) P. Ka-Wo, Y. Yan, L. Xi-You and K.P.N. Dennis, *Organometallics*, **18**, 3528 (1999)

[130] F. Yakuphanoglu, M. Durmus, M. Okutan, O. Köysal and V. Ahsen, *Physica B*, **373**, 262 (2006)

[131] a) A.B.P. Lever, S. Licoccia, B.S. Ramaswamy, S.A. Kandil and D.V. Stynes, *Inorg. Chim. Acta*, **51**, 169 (1981);

b) S .Knecht, K. Dürr, G. Schmid, L.R. Subramanian and M. Hanack, *J. Porphyrins Phthalocyanines*, **3**, 292 (1999)

[132] L. Sagalowicz, R. Mezzenga and M.E. Leser, *Current Opinion in Colloid & Interface Science*, **11**, 224–229 (2006)

[133] Z. Bashir and N. Khan, *Thermochimica Acta*, **276**, 145–160 (1996)

[134] G. Kickelbick, J. Bauer, N. Hüsing, M. Andersson and K. Holmberg, *Colloids and Surfaces A: Physicochem. Eng. Aspects*, **254**, 37–48 (2005)

[135] P. Davidson, *Prog. Polym. Sci.*, **21**, 893-950 (1996)

3 Results and Discussion

3.1 Introduction

The synthesis and characterisation of new morpholine-N-oxide derivatised polymers, namely poly-α,β- D,L-[N-(3-morpholinopropyl)-N-oxide]aspartamide **[13]** and poly-[N-(morpholinomethylene)-N-oxide]-ethylene oxide **[14]**, in accordance with goals 2 and 3 of this study are described in this chapter. This is followed by the synthesis and characterisation of co-catalysts during catalytic reactions involving the polymers. These included metal-salen, porphyrin and phthalocyanin complexes. Characterisation methods of these compounds were performed using techniques such as proton nuclear magnetic resonance (^{1}H NMR), cyclic voltammetry as well as differential scanning calorimetry (DSC). The electron transfer behaviour of phthalocyanines was especially highlighted by cyclic voltammetry and the liquid crystal behaviour of the phthalocyanines was investigated by DSC and variable temperature polarized light investigations. Lastly, trial catalytic oxidation reactions with compounds **[13]** and **[14]**, as well as epoxidations with new metallo phthalocyanines, and known salen complexes are discussed.

3.2 Synthesis and characterization of target polymers

In light of the first goals of this study, namely the synthesis of derivatised polymers as oxidants, two target polymers were chosen. N-morpholine-N-oxide derivatised polysuccinimide was chosen as a hydrophilic oxidizing polymer and N-morpholine-N-oxide derivatised polyepichlorohydrin was chosen as a hydrophobic oxidizing polymer. These polymers were

chosen for their different expected solubility properties and in the following section a detailed account of their synthesis and characterisation will be given.

3.2.1 Synthesis of polymer backbones

3.2.1.1 Polyepichlorohydrin, PECH, [6]

The polymerisation of epichlorohydrin **[5]** was achieved through a cationic ring-opening reaction (Scheme 3-1) in the pressance of BF_3 as an initiator and phenol as a co-initiator. The active monomer method of polymerization made it possible to controle the polymer's average molecular mass.

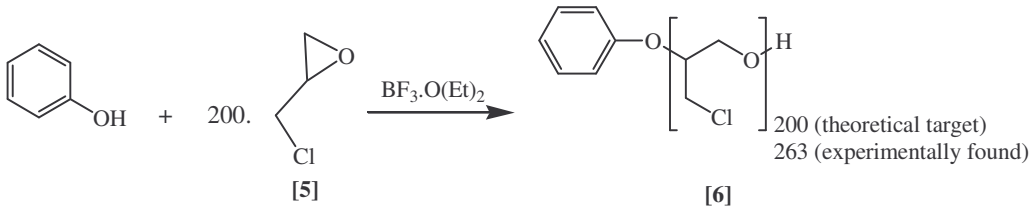

Scheme 3-1. Polymerisation of epichlorohyrin, **[5]**, using $BF_3.O(Et)_2$ as initiator and phenol as co-initiator.

The product polymer, PECH **[6],** had a target molecular mass of approximately 20 000 g $mole^{-1}$ which was calculated through the phenol-epichlorohydrin ratio. By using a phenol-epichlorohydrin ratio of 1:200 and using slow addition of monomer, PECH polymer with roughly 200 repeating units was expected in the final polymer. After 24 hours of reaction, PECH **[6]** was obtained as a nearly colourless and highly viscous liquid which was soluble in CH_2Cl_2 and $CHCl_3$. The molecular mass of PECH **[6]** was determined by using ^1H NMR spectroscopy, (Figure 3-1).

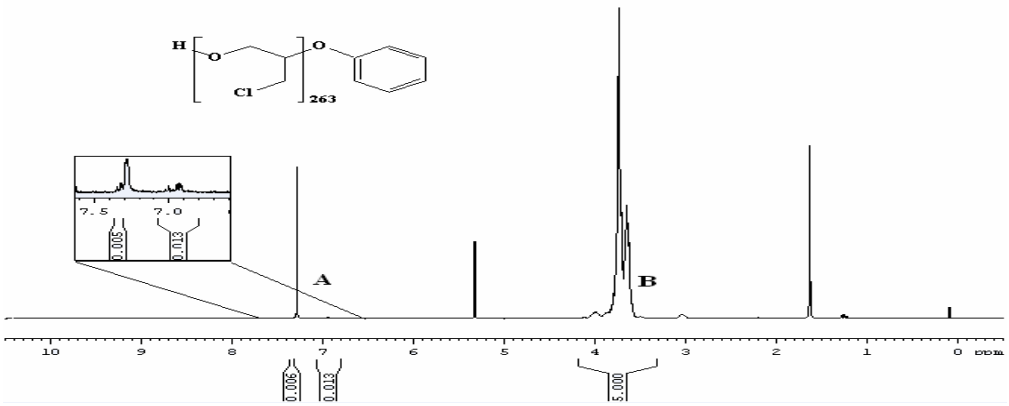

Figure 3-1. ^{1}H NMR spectrum of PECH, **[6]**, in $CDCl_3$.

Utilizing the ^{1}H NMR spectrum of PECH, the following method was used to calculate the number average molecular mass of PECH: in the region 6.90 – 7.03 ppm and 7.30 – 7.36 ppm (A), the signals represent the aromatic protons of the terminal phenyl ring. The integrated value of 0.019 (0.006 + 0.013) must therefore be corresponding to the five phenyl protons. The signals observed at 3.55 – 3.84 ppm (B) corresponds to the five protons adjacent to the ether linkage and adjacent to the chloride atom and as such, represents the five protons of the epichlorohydrin repeating units in polymer **[6]**. The signals at (B) were calibrated to a value of 5.000. When the integral value of (A) is adjusted to 5.000, the value of (B) becomes 1316 for the 5 protons per repeating unit of the polymer. Finally, by dividing 1315.790 by the 5 protons, the number of repeating units works out as 263, i.e. n = 263. The total number average molar mass of polymer **[6]**, containing 263 epichlorohydrin units and 1 phenyl unit and 1 hydroxide unit in the backbone, correspond to (263 x 92.5245 g mol^{-1}) + 94.11 + 17.007 = 24 000 g mol^{-1}, which is slightly higher than the target molar mass of 20 000 g $mole^{-1}$. The discrepancy is attributed to the workup procedure. Low molecular mass fractions are not expected to precipitate from the solvent of the reaction, and were thus discarded during the workup. The remaining precipitated polymer consequently will thus be enriched in higher molecular mass fractions and account for the M_r = 24 000 over the expected 20 000.

3.2.1.2 Polysuccinimide, PSI, [8]

Through the acid-catalysed thermal polymerization of aspartic acid **[7]** at 185 ^{o}C and under reduced pressure, polysuccinimide (PSI), **[8]**, was synthesised as a white solid (Scheme 3-2). The crude polymer was purified by fractional reprecipitation from DMF with water to give a final yield of 78 % PSI. This type of polymerization is an example of poly-condensation and as the reaction proceeds, water is formed as byproduct. By proceeding under reduced pressure and high temperature, the polymerization is forced to completion, liberating a high molecular mass PSI.

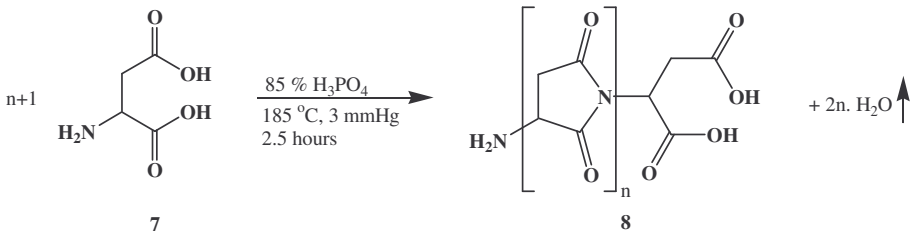

Scheme 3-2. Thermal polymerization of D,L-aspartic acid **[7].**

This method of polymerization of aspartic acid typically leads to a polymer with an average molar mass of 57 000 g mole^{-1}, though higher molar masses have also been reported.[1] PSI is highly hydrophobic and is not soluble in most aprotic organic solvents except DMF and DMSO. Thus, all further reactions and characterization involving PSI were performed in DMF or DMSO. The ^{1}H NMR (Spectrum A1) of PSI performed in DMSO-d_6 showed signals at 5.28 ppm (1H, CH), 3.13 ppm (1H, CH_2) and 2.70 ppm (1H, CH_2), (Figure 3-2, p. 55).

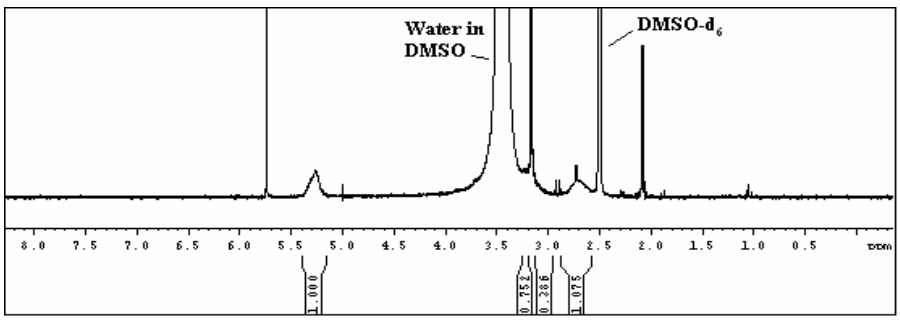

Figure 3-2. ^{1}H NMR spectrum of polysuccinimide, **[8]**, in DMSO-d_6.

There were no observable uncyclized aspartic acid units in the polymer backbone evident from the absence of a proton signal at about 4.80 ppm. Using lower temperatures and shorter times (120 ^{o}C and 1 hour), it was found that some of the monomers remained in the uncyclized state (Scheme 3-3, p. 56).

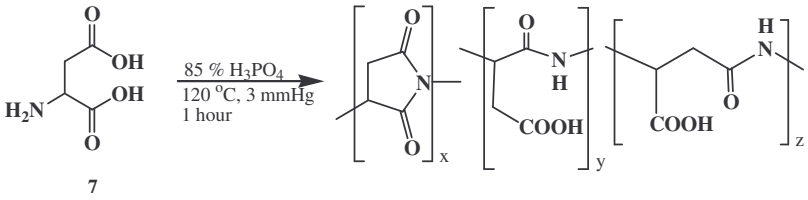

Scheme 3-3. Incomplete cyclization of aspartic acid is observed at 120 ^{o}C.

3.2.2 Anchoring of morpholine substituents to polymer backbones

In light of goal 3 of this study, polymers **[6]** and **[8]** were derivatised with morpholine functionalities. Since the desired properties of the final polymers were expected to be different, the functionalisation of the polymers proceeded through different routes. Polymer **[6]** was derivatised with morpholine while polymer **[8]** was derivatised with 3-aminopropyl-N-morpholine, **[9]**.

3.2.2.1 Anchoring of 3-aminopropyl-N-morpholine to PSI

The fact that the imide rings of PSI can easily be opened by a nucleophilic attack of a wide range of amines was used to functionalise the polymer with morpholine groups. As such a nucleophile, 3-aminopropyl-N-morpholine, **[9],** was anchored to PSI by slowly adding 1.1 equivalents of it to a solution of PSI in DMF at 0 ^{o}C while initially stirring for 20 minutes at 0 ^{o}C (Scheme 3-4). After stirring at room temperature for 6.5 hours, the reaction mixture was diluted with water and put through dialysis to remove any low molecular weight polymers and starting materials. The

product was then freeze dried to give the product poly-α,β-D,L-[N-(3-morpholinopropyl)]aspartamide, **[10]**, as a spongy white solid in 79 % yield.

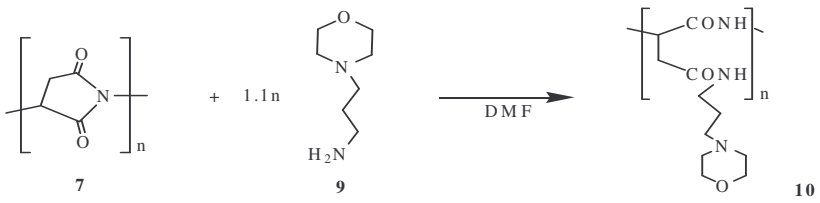

Scheme 3-4. Nucleophilic attack on PSI, **7**, by N-(3-aminopropyl)-morpholine, **9**.

In polymer chemistry, 3-aminopropyl-N-morpholine is usually used as a functionality that imparts water solubility to a polymer. Used as a co-polymer in conjuction with other functionalities, it makes otherwise hydrophobic polymers water soluble, depending on the ratio of the 3-aminopropyl-N-morpholine to the other substituents. For this particular study, 3-aminopropyl-N-morpholine was used to form a homo-polymer. Polymer **[10]** was, as expected, a highly water-soluble polymer in contrast to the water-insoluble PSI. The extent of substitution was confirmed through the ^{1}H NMR of polymer **[10]** in D_2O, (Figure 3-3), as100%.

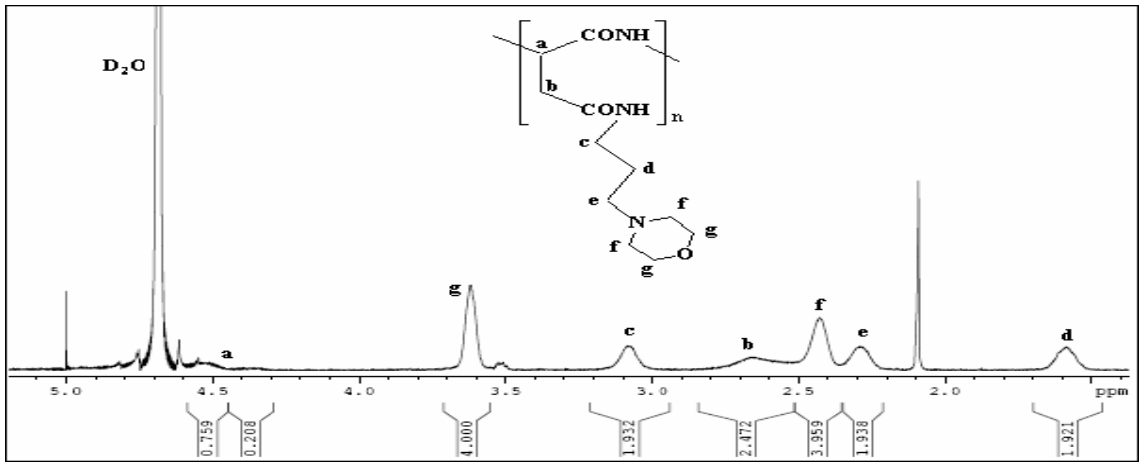

Figure 3-3. Assignment of proton signals in the ^{1}H NMR of polymer **[10]**: 4.35-4.55 (1H, s, a-CH), 3.62 (4H, s, g-CH_2), 3.07 (2H, s, c-CH_2), 2.66 (2H, s, b-CH_2), 2.43 (4H, s, f-CH_2), 2.29 (2H, s, e-CH_2), 1.58 (2H, s, d-CH_2).

The absence of PSI peaks at 5.28 ppm showed that 3-aminopropylmorpholine quantitatively reacted with PSI to give **[10]**. By setting the integral of peak *g* to integrate for 4 protons (2 x

CH_2), all the peaks were assigned to their proton groups, Figure 3-3. Peak *a* is split into two components and peak *b* is broad because **[9]** (3-aminopropylmorpholine) can open the succinimide ring of **[7]** at either of the two oxygen atoms giving rise to both α and β isomers of **[10]**.

3.2.2.2 Anchoring of morpholine to PECH

PECH **[6]** is a polymer that contains alkyl side chains with a terminal chlorine atom attached to them. These chlorine atoms make it possible to functionalise the polymer with a wide range of substituents. A different approach for the functionalisation of PECH was required to that of PSI. Rather than a ring opening nucleophylic attack as was used to generate **[10]**, morpholine was anchored onto PECH by quaternization of the amine group of morpholine. After neutralization, the Cl-atom of PECH was effectively substituted by the morpholine group, (Scheme 3-5).

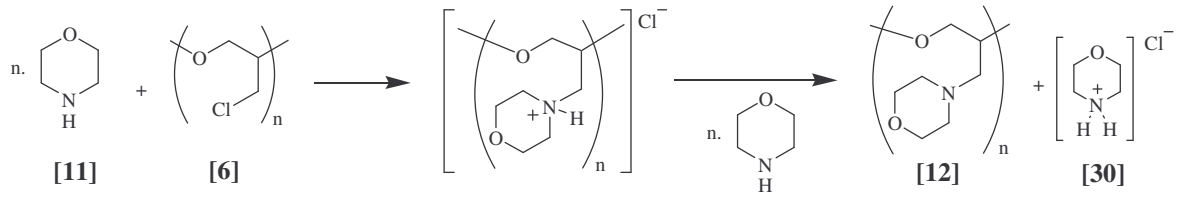

[11] **[6]** **[12]** **[30]**

Scheme 3-5. Functionalization of PECH, **[6]**, with morpholine, **[11]**.

Initially, PECH was refluxed with 2 eq. of morpholine in benzene under inert atmosphere for 24 hours. As the reaction proceeded, a white precipitate formed which was highly water soluble. The precipitate was later identified from its ^{1}H NMR spectrum as the morpholine-HCl salt **[30]**, (Figure 3-4, p. 59). The reason for using at least 2 eq. of morpholine in the reaction was that for every morpholine molecule that reacted with the polymer, one molecule of HCl formed and was subsequently captured by the second unreacted morpholine molecule.

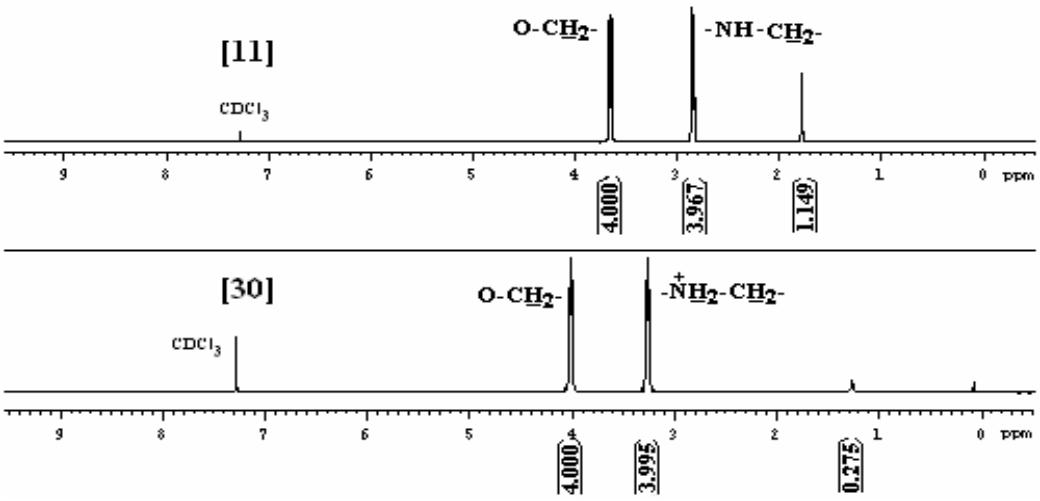

Figure 3-4. Effect of quaternization of the amine group in morpholine on the -CH_2- chemical shifts in the ^{1}H NMR spectra of **[11]** and **[30]**.

The anchoring of morpholine to PECH determined by ^{1}H NMR (see below) were not quantitative. Only ca. 50 % of Cl atoms on **[6]** was displaced, and the method was slightly altered to increase the amount of substitution on the polymer. 2.8 eq. of morpholine was used while toluene was used as a higher boiling solvent. This will from this point onward be known as attachment method 1. After refluxing PECH and morpholine in toluene under inert atmosphere for 72 hours the solution turned from colourless to light yellow. The fine morpholine-HCl salt was removed by means of centrifuge and the liquid phase washed with a saturated $NaOH_{(aq)}$ solution. Drying over $MgSO_4$ and evaporating the toluene gave a dark yellow polymer in 80 % yield. By repeating this method several times, morpholine attachments of between 65 and 80 % were achieved on PECH (see next paragraph and Figure 3-5 below). To attempt greater attachment, reducing the solvent volume was considered. By using the polymer **[6]** itself as solvent, it is possible to increace the attachment efficiency of morpholine. PECH **[6]**, however, is a highly viscous material and effective mixing would have been troublesome. The polymer was therefore dissolved in a minimum of DMSO (1 ml per gram of polymer) before adding morpholine and heating the mixture under argon atmosphere to no more than 110 ^oC for 3 days. This will from this point onward be known as attachment method 2. The morpholine-HCl formed

was in this case removed by filtration. This method required considerable aqueous work-up and evaporation to remove the DMSO. The final product was a dark, very viscous polymer at 45 % yield.

The effectiveness of the morpholine attachment was determined from the ^{1}H NMR of the product polymer. As an example, the morpholino-derivative **[12]** obtained from attachment method 1 (toluene as solvent) was used in the calculations. To calculate the percentage of morpholine units on polymer **[12]**, its spectrum was compared with that of morpholine **[11]**, N-methylmorpholine **[31]** and PECH **[6]**, (Figure 3-5, p. 60).

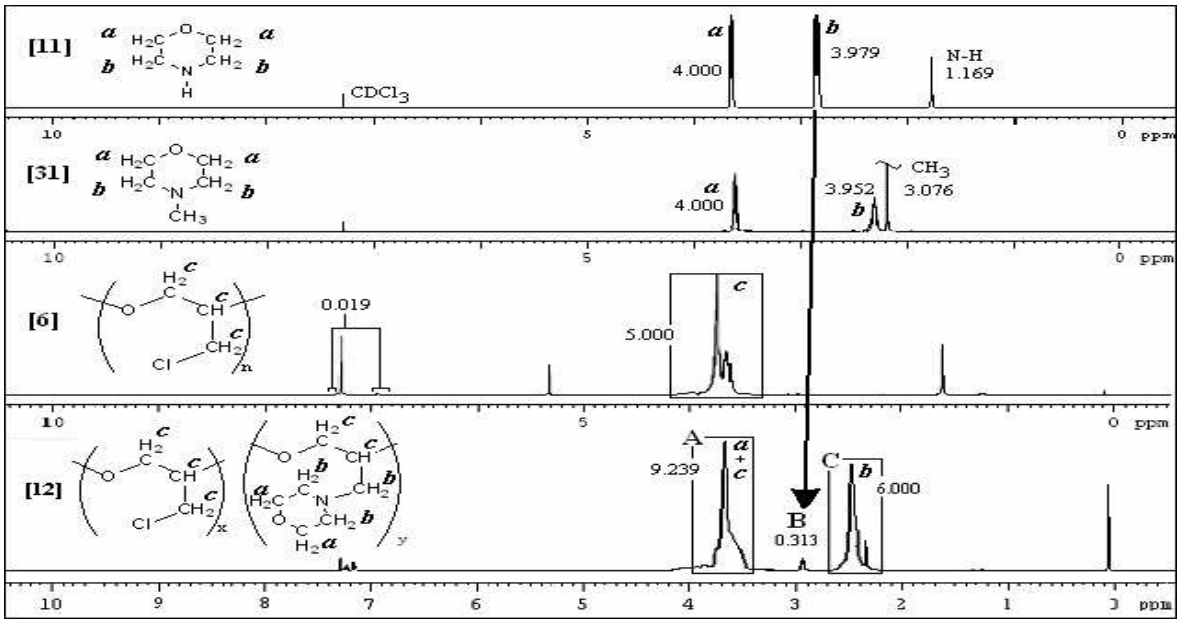

Figure 3-5. ^{1}H NMR spectra of morpholine **[11]**, N-methylmorpholine **[31]**, PECH **[6]** and morpholino derivative **[12]** in $CDCl_3$. Numbers are integral values.

For the morpholino-derivative **[12]** obtained from method 1, peak **C** was set to integrate for 6 protons representing the 3 methylene groups directly next to the nitrogen atom. The spectrum of N-methylmorpholine showed a peak at 3.60 and 2.30 ppm, integrating for the N-methylene protons, ***b***, and the ether-methylene protons, ***a***, respectively. This gave a good estimate to the positions of the polymer-bound morpholine group's methylene peaks. Also, the polymer bound

morpholine's ether-methylene protons, ***a***, were found to overlap with the backbone protons, ***c***, of PECH **[6]**. From the spectrum of morpholine **[11]** it was determined that peak **B** of **[12]** originates from the unreacted morpholine's N-methylene protons, ***b***. The ether-methylene protons, ***a***, of **[11]** overlaps with peak A of **[12]** and the integral must be subtracted from that of peak **A**. Since integrals of ***a*** and ***b*** in **[11]** should be the same, it follows that for peak **A** the corrected integration value is 9.239 – 0.313 = 8.926. If 100 % coupling were achieved an integral value of 7 for peak **A** would be obtained. Using the calculated value of **A,** the actual percentage coupling was determined as: (7 x 100) / 8.926 = 78.4 %. This implies that 78.4 % of the repeating units of polymer **[12]** contain the morpholine functionality, while 21.6 % contain the unreacted chlorine functionality. By assigning n = average number of repeating units, and x and y representing the fraction of unsubstituted and substituted units respectively, it follows that [12] is a copolymer with composition:

[12]
(method 1)

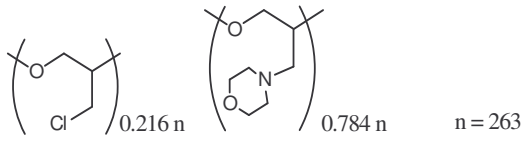

n = 263

Employing the same calculations to the morpholino derivative obtained from attachment method 2 (DMSO reaction), the percentage coupling was found to be 94 %. This is a considerably higher attachment success rate than that of method 1, but it requires more effort to purify and dry the resulting polymer. For all following reactions polymer **[12]** obtained from method 2 was used due to its higher morpholine content.

3.2.3 Oxidation of polymers to form N-oxide substituted polymers

3.2.3.1 Oxidation of N-methylmorpholine

Before attempting to oxidize the morpholine-substituted polymers, a suitable oxidation procedure had to be established. The oxidation of N-methylmorpholine, **[31]**, to N-

methylmorpholine-N-oxide, **[2]**, was chosen as a model reaction for amine oxidation since it closely represents the morpholino functionalities in the polymers. The synthesis of N-methylmorpholine-N-oxide from N-methylmorpholine was achieved by stirring a solution of N-methylmorpholine in ethanol and an excess of 30 % H_2O_2 for 16 hours at room temperature. Excess H_2O_2 was destroyed with powdered MnO_2 during workup. N-methylmorpholine-N-oxide was recovered quantitatively and confirmed by means of ^{1}H NMR analysis, (Figure 3-6, p. 62).

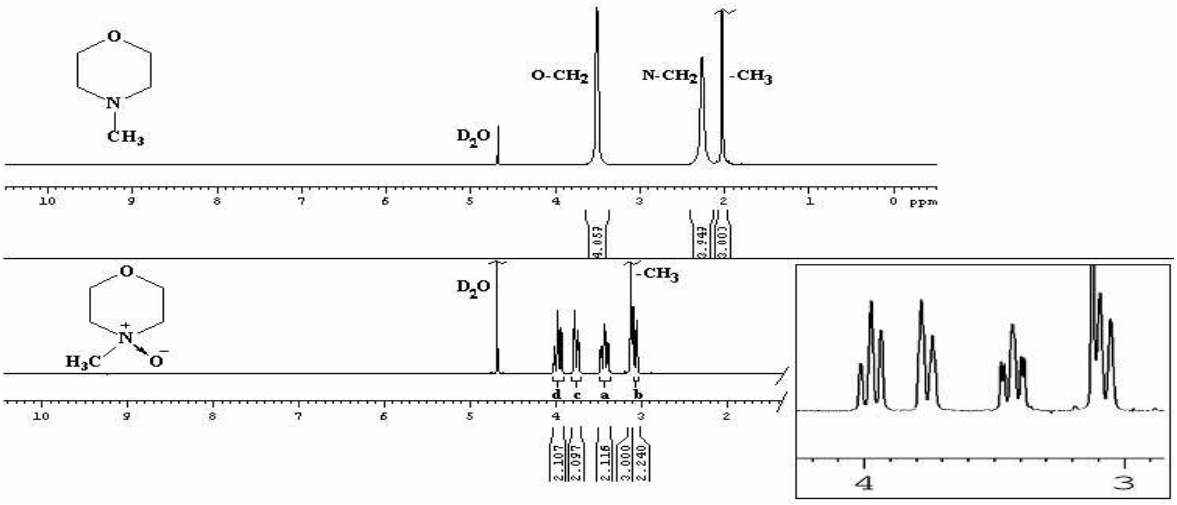

Figure 3-6. ^{1}H NMR spectra of N-methylmorpholine, **[31]**, (bottom) and N-methylmorpholine-N-oxide, **[2]**, (top) in D_2O, showing the effect of oxidation of the nitrogen atom on the proton signals. Assignment of the N-methylmorpholine-N-oxide protons involves axial and equatorial protons and is dicussed below.

The ^{1}H NMR spectrum of N-methylmorpholine-N-oxide can be explained by comparing the structures of N-methylmorpholine and N-methylmorpholine-N-oxide, (Figure 3-7, p. 63). Firstly, both the structures of N-methylmorpholine and N-methylmorpholine-N-oxide are not planar; they have the same conformation as that of cyclohexane. Each of the $-CH_2$ protons in the ring can adopt an equatorial or axial conformation (one equatorial and one axial per $-CH_2$). In N-methylmorpholine, the two methylene groups nearest to the nitrogen atom are equivalent and those nearest to the ether oxygen are equivalent, leading to the peaks integrating for 4 protons at 3.48 ppm (-O-C<u>H</u>$_2$-CH$_2$-N-) and 2.25 ppm (-O-CH$_2$-C<u>H</u>$_2$-N-). The singlet at 2.02 ppm is assigned to the 3 protons of the methyl group.

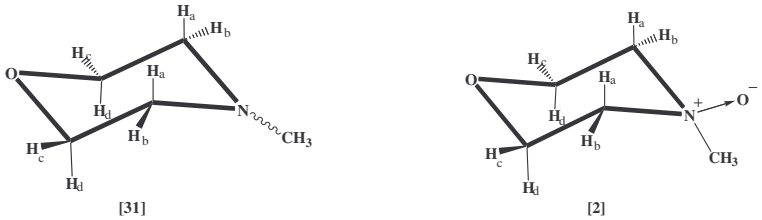

Figure 3-7. Structure of N-methylmorpholine, **[31]**, and N-methylmorpholine-N-oxide, **[2]**.

Secondly, upon oxidation of the nitrogen atom, the methylene protons are no longer equivalent, the axial and equatorial protons experience different environments. The protons closest to the nitrogen atom are most effected by the presence of the oxygen and are shifted more down-field than the ether-methylene protons. Also, the tetrahedral geometry of the nitrogen atom forces the oxygen atom to be closer in space to the axial protons than the equatorial protons. The result is that the axial protons closest to the N-oxygen atom experience a greater influence of the electron density around the oxygen atom and results the NMR signal being shifted down-field. As result of the difference in the environments of the protons, each methylene peak in the spectrum of N-methylmorpholine splits into 2 multiplets in N-methylmorpholine-N-oxide's spectrum. This splitting and shifting of the peaks was also apparent in the spectra of the oxidized polymers **[13]** and **[14]**, and provided a convenient method of estimating the extent of oxidation.

3.2.3.2 Oxidation of Poly-α,β-D,L-[N-(3-morpholinopropyl)]aspartamide, [10]

Having proved successful in oxidizing N-methylmorpholine to N-methylmorpholine-N-oxide, hydrogen peroxide was imployed in the oxidation of the morpholino polymers. To oxidize morpholino derivative **[10]**, the polymer was dissolved in ethanol and stirred with 30 % H_2O_2 over 16 hours, (Scheme 3-6).

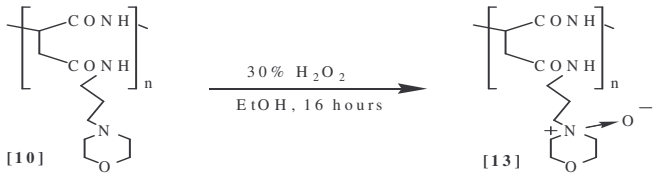

Scheme 3-6. Complete oxidation of morpholino derivative **[10]** with hydrogen peroxide.

As the reaction proceeded a white precipitate formed. The precipitate was identified as the oxidised polymer, Poly-α,β-D,L-[N-(3-morpholinopropyl)-N-oxide]aspartamide **[13]**, and was filtered off and dried at 80 ^{o}C for 30 minutes before drying at reduced pressure for 2 hours. The highly water soluble polymer **[13]** was isolated in 72 % yield. From the ^{1}H NMR spectrum (Figure 3-2, p. 55) of **[13]** it was determined that the oxidation proceded nearly quantitively. Since the product precipitates out of the reaction mixture as result of its increasing ionic character, the polymer units with a low percentage of oxidized repeating units remains in the filtrate while the highly oxidized product is filtered of. This explains the non-quantitive yield of 72 %.

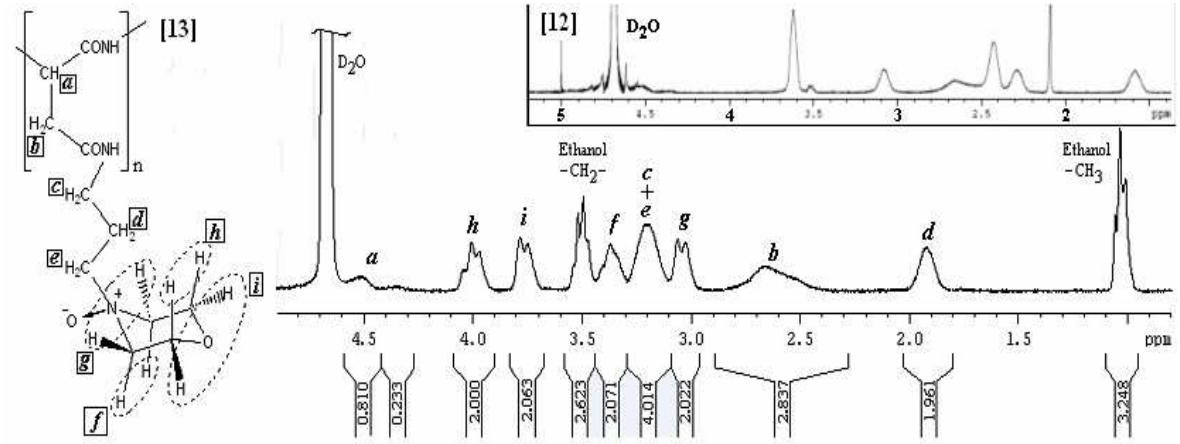

Figure 3-8. ^{1}H NMR Proton assignments of polymer **[13]** in D_2O. Insert top right is polymer **[12]** in D_2O. The ethanol peaks comes from residue of solvent that is trapped in **[13]** and is very difficult to remove.

By comparing the spectra of polymers **[10]** and **[13]** the extent of oxidation was determined. The peak at 1.58 ppm of the un-oxidized polymer **[10]**, which integrated for the central –CH_2 of the alkyl link *d*, shifted upon oxidation of the morpholino-nitrogen to 1.93 ppm. There were no sign of a peak remaining at 1.58 in the spectrum of the oxidized polymer, **[13]**, indicating that **[10]** was quantitatively oxidized to **[13]**. The peaks of **[10]** at 3.62 ppm and 2.43 ppm for the morpholino –CH_2 groups were also split upon oxidation, as was the case with N-methylmorpholine-N-oxide. The –CH_2 protons of the alkyl link next to the morpholino-nitrogen

was not split in the same way as the morpholino -CH_2 groups since free rotation can occur around the C-N bond of the alkyl link, as with the methyl group in N-methylmorpholine-N-oxide.

3.2.3.3 Oxidation of Poly[N-(morpholinomethylene)]ethylene oxide, [12]

After the successful oxidations of N-methylmorpholine and polymer **[10]**, the same procedure was attempted on polymer **[12]**, (Scheme 3-7, p. 65). Polymer **[12]** derived from morpholine attachment method 2 was used as it has a higher morpholine group concentration and thus more nitrogen atoms to be oxidized.

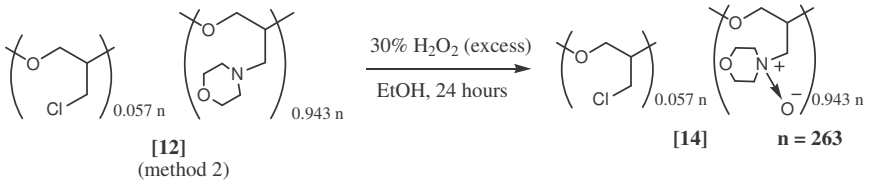

[12] (method 2) **[14]** **n = 263**

Scheme 3-7. Complete oxidation of polymer **[12]** using a large excess of H_2O_2 as oxidant

The workup yielded a highly viscous, CH_2Cl_2 soluble polymer. Though the properties of the polymer were inline with the targeted properties, it was revealed through ^1H NMR that the polymer was only partially oxidized, (Figure 3-9). The reaction was optimized by using a greater excess of H_2O_2 and resulted in the fully oxidized polymer **[14]**. Though the polymer was no longer soluble in aprotic organic solvents, the fully oxidized polymer **[14]** was chosen as oxygen source in the oxidation of alkenes due to its higher oxygen content.

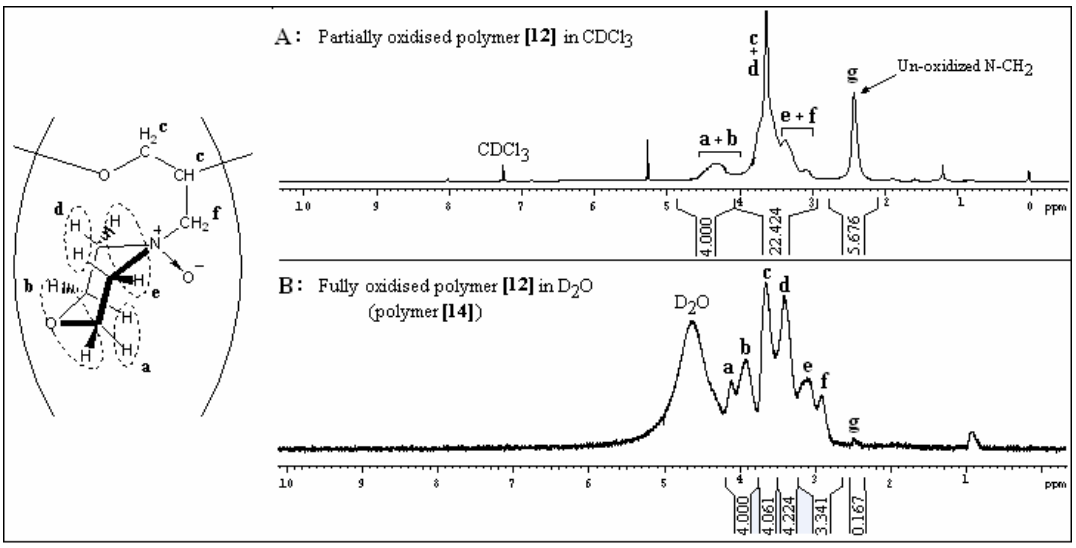

Figure 3-9. ^{1}H NMR spectra of partially oxidized polymer **[12]**, A, and fully oxidized polymer **[12]**, B.

The same splitting of proton signals that were observed upon oxidation of N-methylmorpholine and polymer **[10]** can be seen in the oxidation of polymer **[12]**. Due to the overlap of proton signals of polymer **[14]** (Figure 3-9B), as well as the presence of un-oxidised morpholino units, the integrals used are only used as an estimate of the oxidation extent. The NMR peak labeled **g** in Figure 3-9 integrates for the 6 methylene protons next to the un-oxidised nitrogen atom. Peaks **a** and **b** integrates for axial and equatorial methylene protons next to the ether oxygen of the morpholine units while peaks **d** and **e** includes the methelene protons next to the nitrogen atom of the morpholine units. Peaks **e** and **f** incorporates the rest of the polymer backbone's protons. As result of the splitting and shifting of proton signals upon oxidation of polymer **[12]**, the intensities of peaks **a**, **b**, **e** and **f** increases while peak **g**'s intensity decreases as more and more N-oxides form. By setting the integral of peak **g** in Figure 3-9B to 6.00 the other peaks' values changes accordingly to: **a** + **b** = 143.71, **c** = 145.90, **d** = 151.76 and **e** + **f** = 120.04. This gives a total of 561 protons in the region of 2.70 – 4.10 ppm versus the six protons of the un-oxidized nitrogen at 2.48 ppm. Subtracting the 7 remaining protons of the un-oxidized repeating units leaves 554 protons for the rest of the polymer, giving a ratio of 554:13 → 42.7:1 for [oxidized

morpholino and unsubstituted repeating units] / [unoxidized morpholino repeating units]. Applying this ratio to polymer **[12]** results in the following composition for polymer **[14]**:

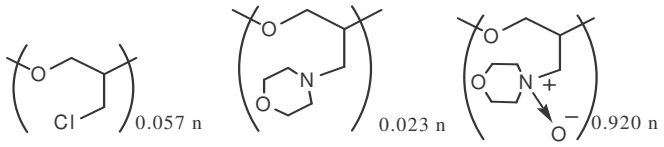

[14] **n = 263**

The oxidation of polymer **[12]** therefore proceeded nearly quantitively with 97.5 % of the morpholine substituted units being oxidized. By applying the same calculations to the partially oxidized polymer, (Figure 3-9A), it was found that the polymer contained 37.9 % unoxidized morpholine units, resulting in a repeating unit ratio of:

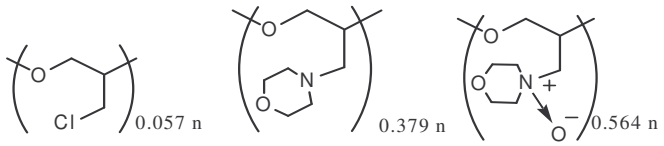

[14] **n = 263**

The difference in oxidation percentage of the partially- and fully oxidized polymer was also observed in the infra red spectra of the compounds (Spectra B7 and B8 respectively). The stretching frequency for aliphatic N-O bonds is observed at 960±20 cm^{-1}. The partially oxidized polymer did not show a clear peak in the 960±20 cm^{-1} region while the fully oxidized polymer showed a strong peak at 975 cm^{-1}, indicating successful amine oxidation.

3.3 Synthesis and characterization of metal catalysts

Having synthesized morpholino-N-oxide derivatised polymers **[13]** and **[14]**, the focus was shifted to the synthesis of suitable co-catalysts to evaluate the possible oxidation properties of the polymers. Manganese and cobalt complexes were chosen as possible oxidation catalysts for the trials. The simple salen and porphyrin complexes were synthesized for this goal. As an

extension on oxidation co-catalysts, a novel new manganese phthalocyanine was also synthesized as possible catalyst in air oxidations.

3.3.1 Salen complexes

It is apparent from the literature survey (2.3.2.a., p. 23) that metal-salen complexes, especially those of manganese, are highly effective epoxidation catalysts. Chiral Mn(III) salen complexes, as in Jacobsen's asymmetric olefin epoxidation[2], have proven activity and selectivity for enantioselective epoxidation of unfunctionalized olefins under homogeneous as well as heterogeneous conditions. Therefore, manganese complexes were an obvious choice to evaluate polymers **[13]** and **[14]**'s oxidation performance. The simplest salen ligand, 2HSalen **[17]**, was chosen as basis for the epoxidation catalysts due to its ease of synthesis, (Scheme 3-8). For comparison with [Mn(III)Salen]OAc **[18]**, the cobalt(II) **[19]** derivative was also synthesized.

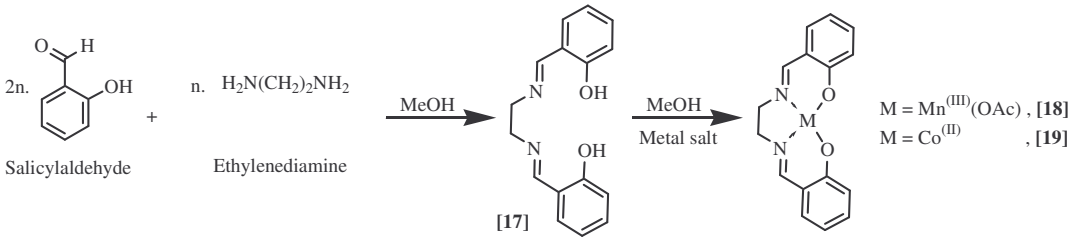

Scheme 3-8. Synthesis of catalysts [Mn(III)Salen]OAc ,**[18]**, and Co(II)Salen, **[19]**.

The synthesis of the metal-free ligand was surprisingly simple and proceeded nearly quantitatively. By using methanol as solvent in a variation of the original synthesis, the reaction was driven to completion because of the poor solubility of **[17]** in methanol. Only a few seconds after adding a solution of 1 eq. of ethylenediamine in methanol to a stirred solution of 2 eq. of salicylaldehyde in methanol, 2HSalen formed as a bright yellow precipitate. The precipitate was filtered off and washed with cold MeOH after stirring for 30 minutes. Recrystallization from chloroform / methanol gave ligand **[17]** in 75 % yield and the ^{1}H NMR spectrum (Spectrum

A11) gave the following peaks: 8.37 (2H, s, 2 x benzylidenimin-H), 6.85-7.32 (8H, m, 2 x C_6H_4), 3.96 (4H, s, 2 x -CH_2-).

The metallation of **[17]** proved just as straightforward as the ligands synthesis. For the synthesis of complex **[18]**, 2HSalen was dissolved in boiling methanol before a solution of $Mn(OAc)_2$ ($CoCl_2$ for complex **[19]**) in minimal methanol was added. In both cases the reaction was instantaneous. The ligand solution changed from yellow to a dark greenish-brown colour upon addition of the metal salt. After refluxing for a further 10 minutes the reaction mixture was cooled to room temperature and the greenish-brown precipitate collected by filtration. Recrystalization from chloroform / methanol yielded complexes **[18]** and **[19]** in 84 % and 94 % respectively. The metal-complexation was confirmed by UV/Vis (Figure 3-10, p.69) and ^1H NMR.

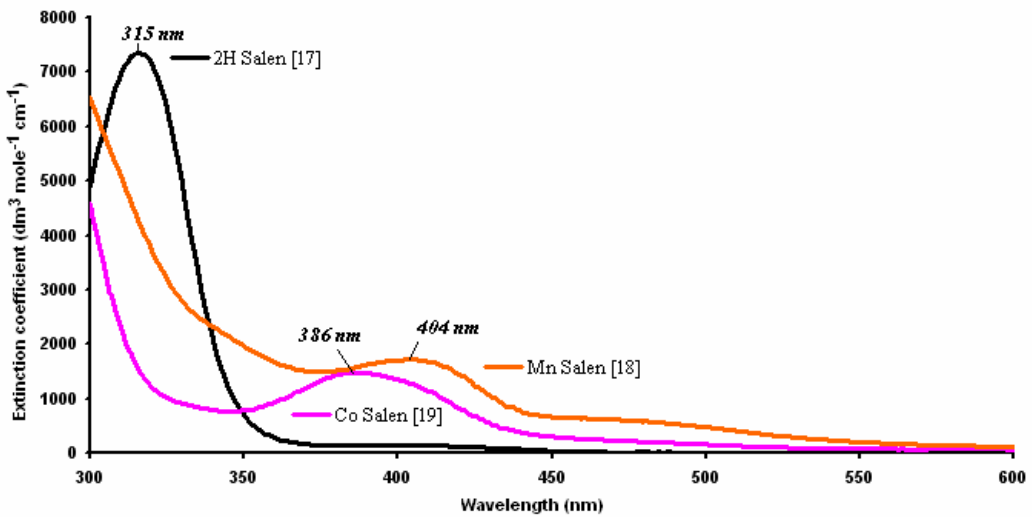

Figure 3-10. UV/VIS absorption spectra of extinction coefficient ($dm^3mol^{-1}cm^{-1}$) *vs.* wavelength of the Salen compounds **[17]**, **[18]** and **[19]** in acetonitrile.

The UV/Vis spectrum of complex **[18]** showed the formation of an absorbtion peak at 404 nm and the disappearance of the metal-free ligand's absorbtion peak at 315 nm upon metalation with manganese. The red-shifting in the absorption wavelenght is caused by the presence of the electron poor Mn(III) metal center. The red shift observed in compound **[19]**'s spectrum was not

so pronounced as that of **[18]** since Co(II) is not as electron poor as Mn(III), resulting in the absorption peak at 386 nm.

Both the ^{1}H NMR spectra of **[18]** and **[19]** were subject to the paramagnetic character of the respective metal centers, (Spectra A12 and A13). A paramagnetic species influence a magnetic field due to the presence of one or more unpaired electrons, thus influencing the NMR spectra. The metal center of complex **[19]** is Co(II) with a configuration of [Ar]3d^{7}, making it paramagnetic with one unpaired electron. The electron configuration of Mn(III) in complex **[18]** is [Ar]3d^{4}, also making it paramagnetic. The presence of paramagnetic metals in metallo-organic compounds can cause large proton chemical shifts which may be positive or negative, depending on the electron distribution, as well as peak broadening. While diamagnetic metals do influence their organic surroundings, the influence is very small.

Complexes **[18]** and **[19]** had melting points greater than 250 ^{o}C while the free ligand melted at 127 ^{o}C. Interestingly, upon heating the manganese(III) salen complex's melting point varied with different heating rates. Viewed under polarized light, changes in the colour of the Mn(III) salen crystals were observed at around 230 ^{o}C, (Figure 3-11). The colour gradually changed from yellowish-brown to deep red, remaining solid up to 350 ^{o}C.

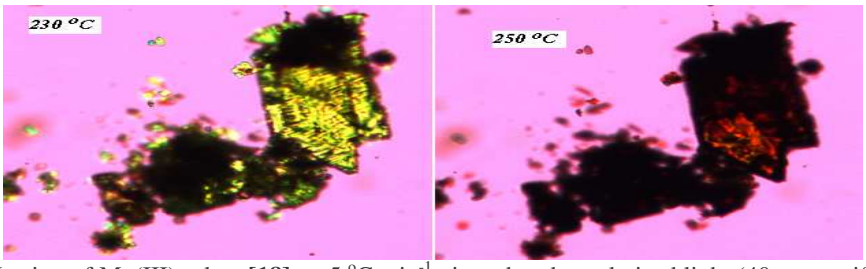

Figure 3-11. Heating of Mn(III) salen, **[18]**, at 5 ^{o}C min^{-1} viewed under polarized light (40 x magnification) clearly showed colour transitions.

Upon further heating the crystals seemed to decompose at 380 ^{o}C. The changes observed can be attributed to the formation of [O=Mn^{V}(salen)]OAc as result of the air oxidation of complex **[18]**. It is also possible that through disproportionation, μ-oxo bridged dimers could form[3]:

$$[O{=}Mn^{V}(salen)]^{+} + [Mn^{III}(salen)]^{+} \rightleftharpoons [(salen)Mn^{IV}{-}O{-}Mn^{IV}(salen)]^{2+}$$

However, such dimers were not confirmed in this study. By applying a faster heating rate of 15 $^{o}C\ min^{-1}$ on another sample, the complex was molten at 300 ^{o}C before it could be fully oxidized. The molten material eventually also turned deep red in colour. This observation indicates effective oxygen transfer (binding) to the Mn(III) complex. The complex Co(II)(salen), **[19]**, also reversibly binds O_2, but was not observed during heating in the same manner as **[18]**.

3.3.2 Porphyrins

Based on the various catalytic applications of metallated porphyrins (see 2.3.2a, p. 18), it was regarded as appropriate to evaluate the oxidative polymers with a metaloporphyrin as catalyst. Tetraphenyl-porphyrinatocobalt(II), Co(II)TPP **[16]**, was synthesised according to Scheme 3-9.[4] Originally, manganese was chosen as the central metal following the generally successful epoxidation applications of Mn(III)Salen catalysts as well as manganese porphyrins[5]. However, due to difficulties in purifying the manganes derivative, the cobalt derivative was chosen (see Chapter 4). Since a wide variety of cobalt porphyrin derivatives have been found to have catalytic oxidation potential, especially in the epoxidation of alkenes, Co(II)TPP was chosen as a candidate for possible catalyst in the epoxidation of alkenes by N-oxides.[6,7]

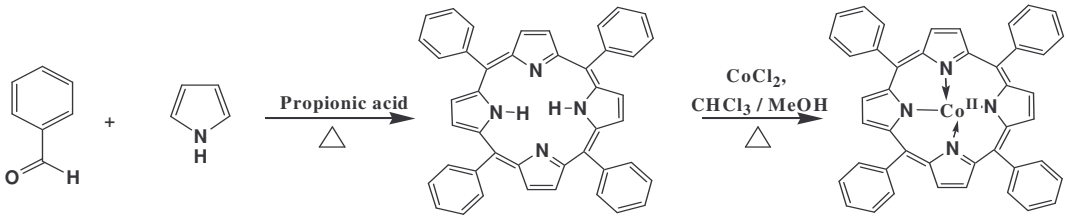

Scheme 3-9. Synthesis of Tetraphenylporphyrinatocobalt(II), **[16]**.

Tetraphenylporhyrin **[15]** was synthesized by refluxing equivalent amounts of benzaldehyde and pyrrole in propionic acid for 1 hour. After cooling the precipitate was filtered off and washed with methanol and water, giving meso-tetraphenylporphyrin, **[15]**, in 19.6 % yield. The ^{1}H NMR

of **[15]** in $CDCl_3$ (Spectrum A9) showed the β-pyrrole protons at 8.88 ppm as well as the phenylic protons at 8.26 and 7.79 ppm.

The metallation of porphyrin **[15]** with cobalt proceeded more easily than with manganese. Since all attempts to purify the manganese porphyrin derivative were unsuccessful, research on it was discontinued in favour of a manganese phthalocyanine. Purification of porphyrin **[16]** by column chromatography proceeded without problems since the cobalt porphyrin did not stick to the column and was recovered in 70 % yield. The UV-Vis spectroscopy of **[15]** and **[16]** (Figure 3-12, p. 72) did not show a great difference in the absorbsion maxima of the two compounds other than an increase in the extinction coefficient upon metallation. The ^{1}H NMR of **[16]**, on the other hand, (Spectrum A10) showed the influence of the paramagnetic Co^{II} center clearly. The phenylic protons shifted down-field from 8.26 and 7.79 ppm in **[15]** to 9.95 ppm in **[16]**. The β-pyrrole protons were affected most due to their position on the macrocycle and shifted down-field from 8.88 ppm in **[15]** to 13.15 ppm in **[16]**.

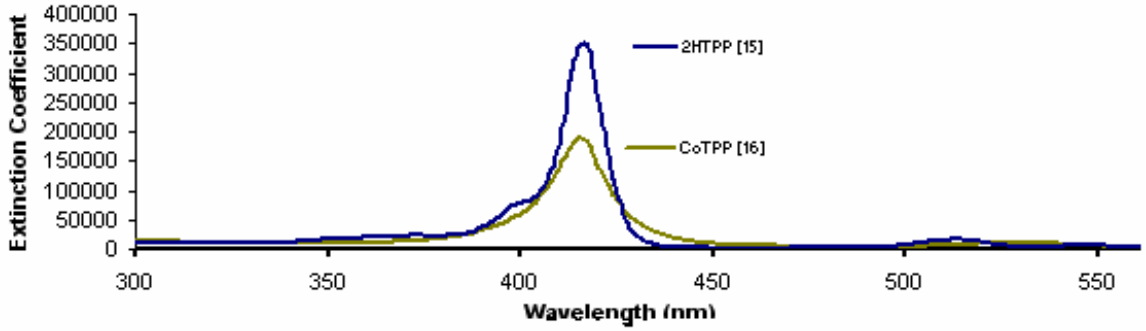

Figure 3-12. UV/VIS absorption spectra of extinction coefficient ($dm^3mol^{-1}cm^{-1}$) *vs.* wavelength of porphyrins **[15]** and **[16]** in THF.

While the UV/Vis spectrum of the cobalt porphyrin was inconclusive, the IR spectrum did support successful metalation of the free ligand. The spectrum of **[15]** (Spectrum B9) showed the secondary amine N-H stretching frequency at 3 312 cm^{-1}. This peak disappeared upon insertion of cobalt in the synthesis of **[16]** (Spectrum B10). These observations, as well as the shifts in ^{1}H

NMR frequencies, support the successful synthesis of tetraphenylporhyrinatocobalt(II), **[16]**. The IR spectrum of the attempted manganese derivative **[32]** (Spectrum B20) showed a weak broad peak at 3 433 cm^{-1}, which is likely due to incomplete metalation since purification of this coumpound was not successful.

3.3.3 Phthalocyanines

As mentioned in chapter 2, there are various ways to synthesise phthalocyanines. The method incorporated in this study is that of the tetramerization of substituted phthalonitriles. 3,6-Tridecylphthalonitrile **[22]** was used as a precursor for the synthesis of the $C_{13}H_{27}$* non-peripherally substituted phthalocyanines. This new phthalonitrile was synthesized according to Scheme 3-10, following the general method McKeown [8] developed to dialkylate thiophene.

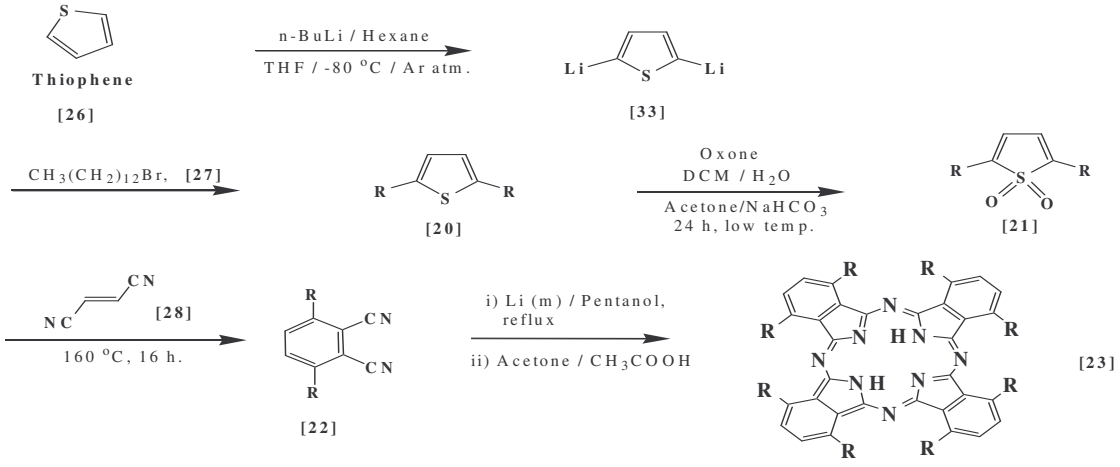

Scheme 3-10. Stepwise synthesis of octa-alkyl non-peripheral substituted phthalocyanine ligand, **[23]**. R=-$(CH_2)_{12}CH_3$.

3.3.3.1 2,5-Tridecylthiophene, [20]

Lithiation of thiophene **[26]**, to give the di-lithiated intermediate, followed by its di-tridecylation are high yielding (>80%) reactions for linear alkyl chains containing up to 8 carbon atoms, provided lithiated reactants are mixed with thiophene or tridecylbromide at –80°C under an inert

* Throughout this document $C_{13}H_{27}$ represents the linear tridecyl chain, n-$(CH_2)_{12}$-CH_3.

atmosphere.[8] A yield of 78 % (an exellent yield considering the linear alkyl chain contained 13 carbon atoms) was achieved for 2,5-tridecylthiophene **[20]**, using 24h reaction times for both the lithiation and alkylation step. The obtained crude product, a light greenish-brown oil, was purified by distilling impurities off from the crude material. The pure 2,5-tridecylthiophene was obtained by distilling of impurities at 185°C and pressure of between 2 and 5 mmHg. The residue was then run through a silica column (petroleum ether) to yield a white wax after solvent removal. The strong, sharp transmission peaks on the infrared spectrum (Figure 3-13) of **[20]** at 2849 and 1471 cm^{-1} showed the presence of the alkyl chains on the thiophene ring. Di-alkylation was confirmed by ^{1}H NMR (Spectrum A14: see appendix at the end of this thesis), where a peak at 6.63 ppm indicated 2 aromatic protons and a triplet at 0.95 ppm represents the six protons of the two methyl groups.

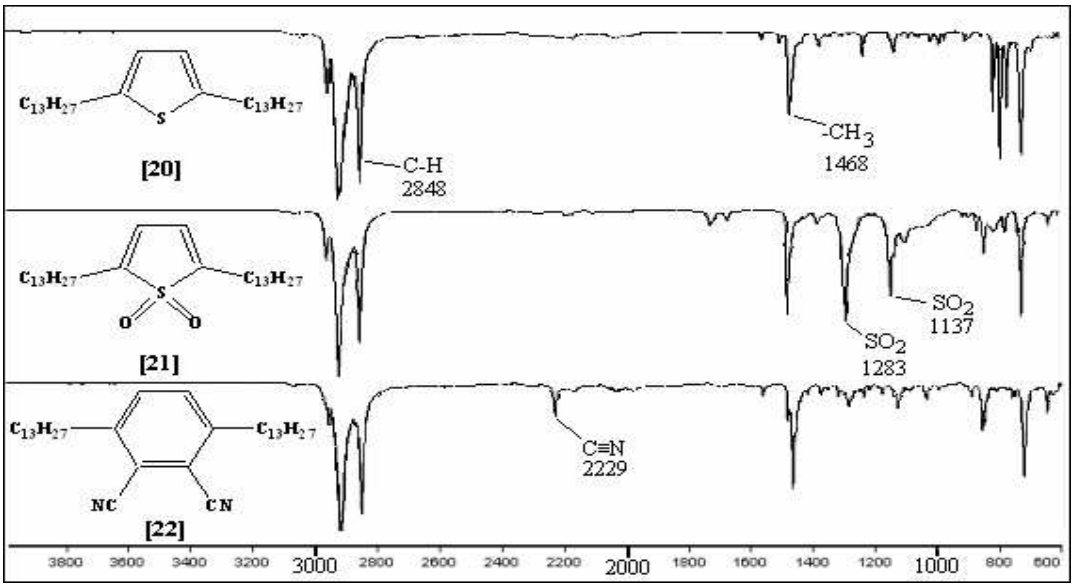

Figure 3-13. Infrared spectra with assignments (cm^{-1}) and structures of 2,5-tridecylthiophene **[20]**, 2,5-tridecylthiophenesulfone **[21]** and 3,6-tridecylphthalonitrile **[22]**.

3.3.3.2 2,5-Tridecylated thiophenesulfone, [21]

The oxidation of the 2,5-dialkylthiophene derivatives to the corresponding 2,5-dialkylthiophenesulfone generally becomes more difficult on increasing the length of alkyl chains. There are also various methods to oxidise thiophenes to thiophenesulfones, including

oxidation by potassium permanganate, sodium perborate[9] or *m*-chloroperoxybenzoic acid[10]. However, using these oxidants to oxidise long-chain (> C_{10}) substituted thiophene generally results in low yields (0 - 40 %, decreasing with increasing chain-length). The oxidant of choice for this study was dimethyldioxirane[11], **[1]** (see 2.2.2, p. 10), as it gives higher yields of long-chain substituted thiophenesulphones. Dimethyldioxirane did not need to be isolated by distillation prior to thiophene oxidation and was generated *in situ* in the reaction mixture already containing the thiophene by reacting acetone with Oxone® ($2KHSO_5.KHSO_4.K_2SO_4$, an Aldrich product) in the presence of potassium hydrogen carbonate, (Scheme 2-1, p. 10). Since dimethyldioxirane had a boiling point of 8 °C, it was trapped in the reaction vessel by using a dry ice-acetone condenser. Through efficient stirring over 24 hours, 7.00 g of 2,5-tridecylthiophene **[20]** was efficiently oxidized to the sulphone **[21]** in a yield of 65 % after recrystalization from ethanol. Two strong sharp peaks at 1233 and 1134 cm^{-1} on the IR-spectrum (Figure 3-13, p. 74) confirmed the presence of the SO_2-group in the thiophenesulphone **[21]**. The ^1H NMR (Spectrum A15) revealed that the position of the thiophenesulphone protons ($C_4\underline{H}_2SO_2$) **[21]** shifted upfield to 6.28 ppm in contrast to those of the thiophene **[20]** at 6.63 ppm. The shift of 0.35 ppm up-field is due to the fact that **[20]** is aromatic, while **[21]** is not.

3.3.3.3 3,6-Tridecylated phthalonitrile, [22]

To obtain the phthalocyanine precursor, 3,6-tridecylated phthalonitrile **[22]**, a Diels-Alder condensation[8] between fumaronitrile **[28]** and 2,5-tridecylthiophenesulfone **[21]** was carried out (Scheme 3-10, p. 73). This was achieved by heating fumaronitrile and **[21]** in the presence of a minimal quantity of chloroform (used to wash reagents into tube) in a sealed glass tube over 18 hours at 160 °C. As little chloroform as possible was used since its presence can decrease the yield of the desired phthalonitrile dramatically. As the reaction proceeds, SO_2 and H_2 gas are eliminated and, together with the heating process, results in a pressure increase. To protect the oven from possible explosion damage, the sealed glass tubes were inserted into steel pipes filled

with sand. After purification by column chromatography (toluene) and recrystallisation from ethanol, 3,6-Tridecylphthalonitrile **[22]** was obtained in 58.79 % which is a very good yield for this type of reaction. Yields of 30-45 % are usually associated with this particular reaction and many factors, such as reaction time, temperature, chloroform content, chromatographic technique and recrystallization can influence the yield.[8] The IR transmission peak at 2229 cm^{-1} (Figure 3-13, p. 74), as well as the dissepearence of the SO_2 peaks, confirmed the presence of the nitrile groups (C≡N).

3.3.3.4 1,4,8,11,15,18,22,25-Octatridecylphthalocyanines, [23], [24] and [25]

While it is possible to synthesise the metalated phthalocyanines **[24]** (manganese) and **[25]** (zinc) directly by cyclotetramerization of the nitrile **[22]** in the presence of the respective metal salts in refluxing butanol, in this stydy they were obtained from the metal-free derivative **[23]**, (Scheme 3-11).

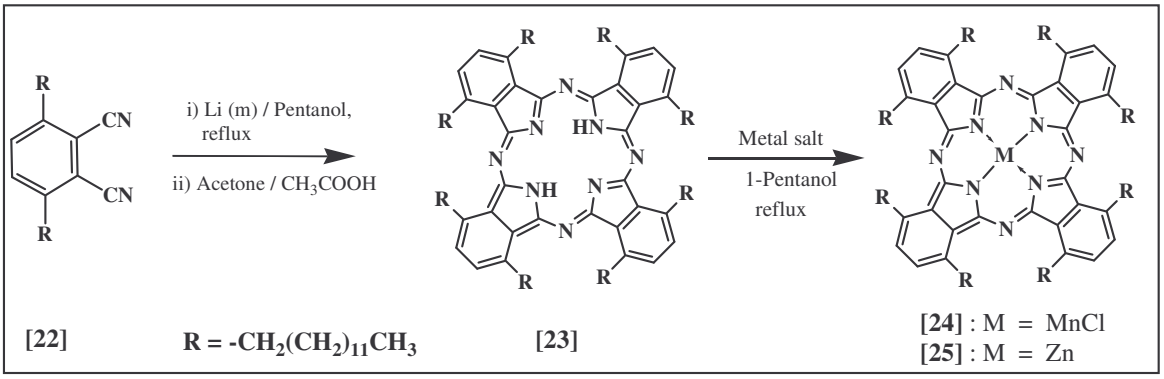

Scheme 3-11. Synthesis of octa non-peripheral $C_{13}H_{27}$ Pcs†: 2HPc **[23]**, MnPc **[24]** and ZnPc **[25]**, $C_{13}H_{27}$ = $-(CH_2)_{12}CH_3$. Metal salts: $MnCl_2 \cdot 4H_2O$ and $ZnCl_2$ respectively.

3,6-Tridecylphthalonitrile, **[22],** was refluxed for 18 hours in 1-pentanol under inert atmosphere in the presence of a small excess of lithium metal (5 eq.) to cyclotetramerise the phthalonitrile

† From this point on 2HPc, MnPc and ZnPc will refer to the respective metal-free, manganese and zinc octa non-peripheral $C_{13}H_{27}$-substituted phthalocyanines.

into the lithiated phthalocyanine. The lithiated phthalocyanine was then converted into the metal-free derivative, **[23]**, by acid work-up. Initially a large excess of lithium metal (50 eq.) and 1-pentanol was used in the synthesis, however, this proved unsuccessful since the isolated products physical appearance was not satisfactory (pale-blue, waxy substance versus a darker blue crystalline appearance for the correct subtance) and it did not give a favourable ^{1}H NMR spectrum. Column chromatography on silica with hexane did not yield the desired product and seemed to deteriorate the phthalocyanine as judged from its ^{1}H NMR spectra. After changing the solvent, decreasing the lithium metal and doing away with column chromatography, the desired phthalocyanine was obtained as a dark blue/grey waxy solid after recrystallisation from THF with methanol in 23 % yield. The metal-free phthalocyanine, **[23]**, was characterized by ^{1}H NMR (Spectrum A17) spectroscopy and UV-Vis spectroscopy (Figure 3-14). The ^{1}H NMR peaks obtained were assigned as follows (in ppm): 7.87 (8H, s, Ar-H), 4.46 (16H, s, 8 x Ar-CH_2-), 2.10 (16H, m, 8 x –CH_2-), 1.25 (160H, m, 8 x –(CH_2)$_{10}$-), 0.85 (24H, t, 8 x –CH_3).

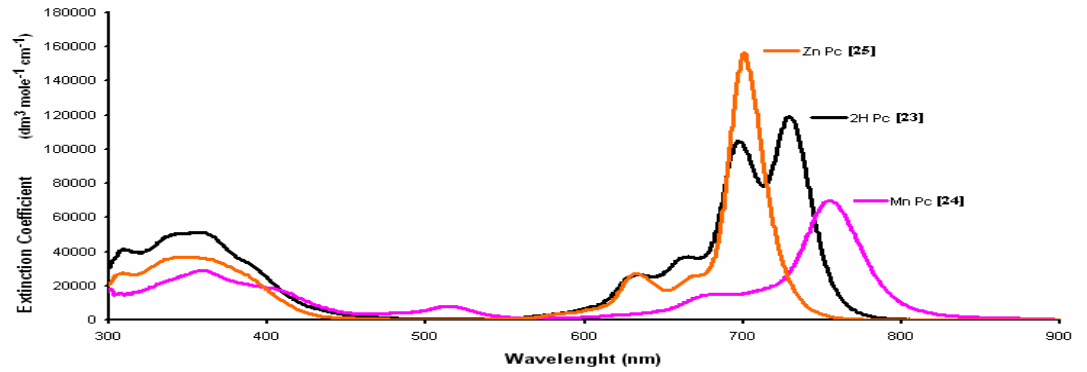

Figure 3-14. UV/VIS absorption spectra of extinction coefficient ($dm^3mol^{-1}cm^{-1}$) *vs.* wavelength of phthalocyanines **[23]**, **[24]** and **[25]** in THF.

The successful insertion of transition-metals in the metal-free phthalocyanine **[23]** was evident from the UV-Vis spectra of the various phthalocyanines, (Figure 3-14). The metal-free phthalocyanine is turquoise green while the zinc derivative **[25]** is bright blue in the crystalline state. The manganese derivative **[24]** is a reddish-brown colour in the solid state. In solution, however, both the metal-free and zinc compounds appear to have a turquoise green colour while

the manganese compound has a red colour. The UV-Vis spectum of Pc **[23]** showed two strong absorbtions of the Q-band at 696 and 727 nm. These two peaks are characteristic of metal-free phthalocyanine, their position determined by the range and characteristics of substituents on the phthalocyanine ring, as well as the characteristics of the metal coordinated in the central cavity. By inserting a metal into the sentral cavity of the phthalocyanine, the two Q-band peaks collapses into a single Q-band peak which position is usually shifted by a few nm, depending on the metal inserted. This is due to the fact that metal-free and metal-containing phthalocyanines differ in having D_{2h} and D_{4h} symmetry respectively and is especially manifested in the Q-band region. Degeneracy of the lowest energy singlet state of the metallated derivatives is lifted in the metal-free derivatives. This leads to the observed splitting of the Q-band of the metal free phthalocyanine into a Qx and Qy component at about 727 and 696 nm in **[23]**'s spectrum while metallated phthalocyanines have only a singlet Q-band. A red-shift of the Q-band is frequently observed when inserting a stronger electron-withdrawing metal into a metal free phthalocyanine. In the case of the manganese derivative, **[24]**, the peak red-shifted by 41 nm to 753 nm due to the electron withdrawing effect of the Mn(III) center. When inserting a Zn(II) metal center (derivative **[25]**) into the metal-free derivative the Q-bands collapsed into a single Q-band at 700 nm, blue-shifted by 12 nm. The Mn(III) metal center is more electron-negative then the Zn(II), resulting in the 53 nm difference in the maximum absorbance of the two metalated phthalocyanines.

The manganese(III) phthalocyanine, **[24]**, was synthesized by refluxing 2H phthalocyanine, **[23]**, in 1-butanol under an inert atmosphere with $MnCl_2 \cdot 4H_2O$ as the metal source, (Scheme 3-11, p. 76). The reaction was checked by TLC and after 24 hours of refluxing the reaction was still incomplete. Additional Mn-salt was added and refluxed for a further 24 hours, after which the metallation was deemed complete. The product was precipitated out with water, filtered and air dried. An attempt was made to purify the Mn phthalocyanine **[24]** through column

chromatography over silca, however, the Mn phthalocyanine stuck to the baseline (CH_2Cl_2/CH_3OH 4:1 in various ratios). After the first fraction (2H phthalocyanine) was eluted, the methanol was increased to 1:1 and eventually the Mn phthalocyanine **[24]** was obtained (69 %). The product did nonetheless spend a great deal of time on the column and it was decided that, in all the future synthesis of **[24],** 2.5 eq. excess of Mn salt is used for the metallation, eliminating the need for column chromatography. This was done to minimalise any derogation of the product as well as possible axial-ligand displacement on the central manganese atom while on the column. Due to the peak broadening paramagnetic effect of the Mn(III) ion, proper integrals for the 1H NMR of **[24]** could not be obtained (see spectrum A18). Mn phthalocyanine **[24]** was thus characterized through UV-Vis spectroscopy (Figure 3-14, p. 77) and elemental analysis.

The expected elemental analysis of the pure compound ($C_{136}H_{224}N_8ClMn$ **[24])** required: C, 79.23 %; H, 10.95 %; N, 5.44 %; Cl, 1.72 % and Mn, 2.66 %. The experimental elemental analysis found was C, 76.70 %; H, 10.93 %; N, 4.69 %; Cl, 0.94 % and Mn, 2.20 %. The oxygen content was not analysed. The carbon and chlorine content was notable lower than expected and a possible explaination is that some of the axial chlorine ligands underwent ligand exchange during the workup process, lowering the chlorine content. A possible ligand that could replace a chlorine atom during workup is methoxide, CH_3O^{1-}. As the workup included water to extract inorganics, it is possible that water molecules could become trapped in between the long alkyl chains of the phthalocyanine in the form of crystal waters. By calculating different ratio's of ligand exchange and crystal waters, the following combination of phthalocyanine were obtained that explains the observed results: 0.55 : 0.45 [$C_{136}H_{224}N_8ClMn{\cdot}5H_2O$] / [$C_{136}H_{224}N_8(CH_3O)Mn{\cdot}5H_2O$] – with an expected elemental analysis of C, 76.23; H, 11.03: N, 5.21; O, 4.06; Mn, 2.55; Cl, 0.91 %. Apart from trapped solvent molecules, it should also be

noted that many phthalocyanines are difficult to combust and incomplete combustion may lead to deviations from the expected elemental analysis values.[12]

From a scientific point of view it was also considered relevant to compare the electrochemical behaviour of the phthalocyanines when a redox silent, non-axial binding metal is inserted in the phthalocyanine cavity. For this purpose, the zinc phthalocyanine comlex was synthesised. The Zn(II) phthalocyanine, **[25]**, was synthesized in the same maner as for Mn(III) phthalocyanine, **[24]**. However, the reaction mixture was only refluxed for 2 hours and no additional metal salt ($ZnCl_2$) was added, resulting in a yield of 98 %. The metallation of **[23]** with zinc was achieved considerably faster than that by manganese and no further purification was required.

In addition, during the initial attemted chromatographical purification of the phthalocyanine, there was one band on the TLC of the reaction mixture after acidic workup riding close to that of the metal-free phthalocyanine. The isolated substance (~4 %) was a green, waxy solid which was presumably the crude tetrabenzotriazaporphyrin **[29]** derivative (Figure 3-15); however, the ^1H NMR obtained was not satisfactory and did not show the methine proton. The replacement of a nitrogen atom with a carbon atom during tetramerisation of the nitrile depends on the reaction conditions. Usually the occurance of the tetrabenzotriazaporphyrin derivative increases when using higher alcohols, and thus higher reaction temperatures, since the carbon atom of the methine group originates from the solvent.

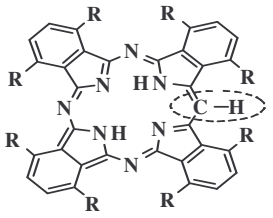

$R = -CH_2(CH_2)_{11}CH_3$

[29]

Figure 3-15. Structure of the tetrabenzotriazaporphyrin derivative **[29]**, showing the replacement of one nitrogen atom with a methine group.

3.4 Electrochemistry of new phthalocyanine complexes

For the electrochemical stydy of the phthalocyanine derivatives measurements were made on *ca.* 1 mmol dm^{-3} solutions of the compounds in CH_2Cl_2 under argon. The solutions also contained *ca.* 1 mmol dm^{-3} of an internal reference (ferrocene or decamethyl ferrocene) with 0.1 mol dm^{-3} tetrabutylammonium hexafluorophosphate (Fluka, electrochemical grade) as supporting electrolyte. The electrochemical experiment employed a three-electrode cell, which utilised a Pt auxiliary electrode, a glassy carbon working electrode with surface area 0.565 cm^2, and a Ag/Ag^+ (0.0100 M, $AgNO_3$ in acetonitrile) reference electrode constructed from a capillary tube sealed with a Vycor tip.

Cyclic voltammetry of the phthalocyanine derivatives **[23]** (Figure 3-16, p. 82) and **[24]** (Figure 3-17, p. 82) in this study was done in CH_2Cl_2 as solvent at room temperature and at 35 °C for the zinc-containing derivative, **[25]** (Figure 3-19, p. 83). The choice of temperature was determined by the solubility of the compound under investigation. Peak potential and peak current-values are summerised in Table 3-2 on p. 87 at the end of this section.

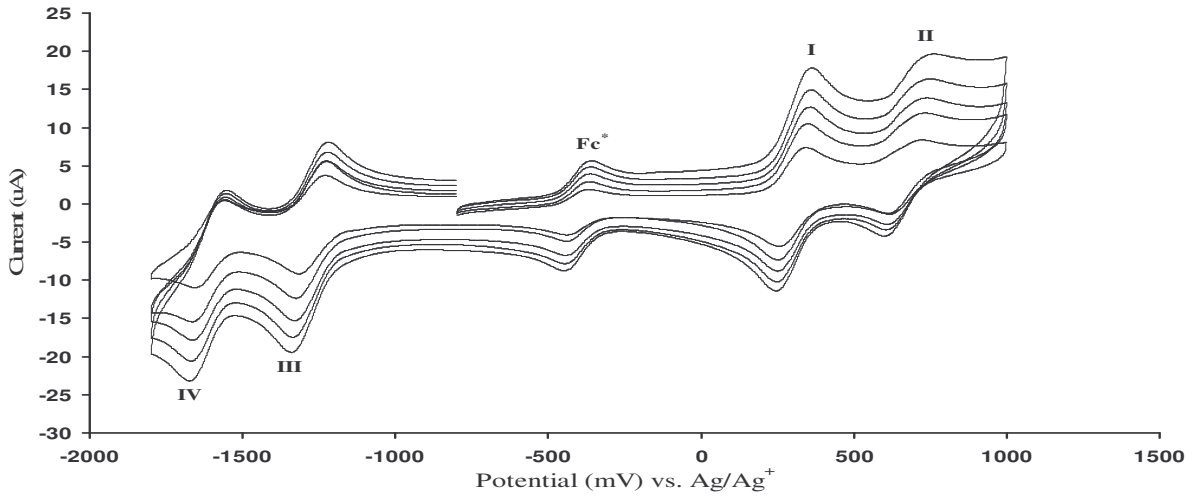

Figure 3-16. Cyclic voltammogram of 1 mmol dm^{-3} $2HPc(C_{13}H_{27})_8$ **[23]** in dichloromethane at 25 °C on a glassy carbon working electrode, at scan rates of 100 (smallest currents), 200, 300, 400 and 500 mV s^{-1}. Four well-defined ring-centered redox processes were observed (I, II, III and IV). Fc^* designates decamethyl ferrocene as the internal reference.

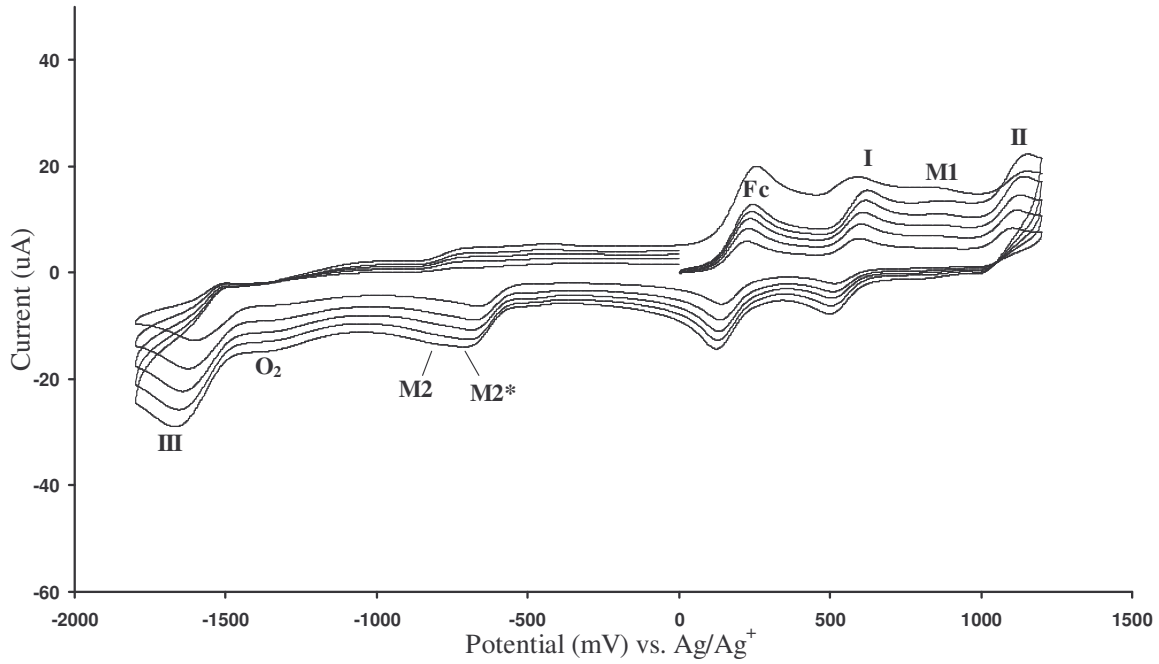

Figure 3-17. Cyclic voltammogram of 1 mmol dm^{-3} $Mn(Cl)Pc(C_{13}H_{27})_8$ / $Mn(OMe)Pc(C_{13}H_{27})_8$ **[24]** in dichloromethane at 25 °C on a glassy carbon working electrode, at scan rates of 100 (smallest currents), 200, 300, 400 and 500 mV s^{-1}. One well-defined ring-centered redox process was observed (I) while two other poorly-defined ring-centered redox processes were also observed (II and III). M1, M2 and M2* designate Mn-centered oxidation and reduction processes respectively. M2* and M2 is associated with Mn^{III}-Cl and Mn^{III}-OMe reductions to Mn^{II} respectively; while M1 is associated with Mn^{II} oxidation. Fc designates ferrocene as the internal reference.

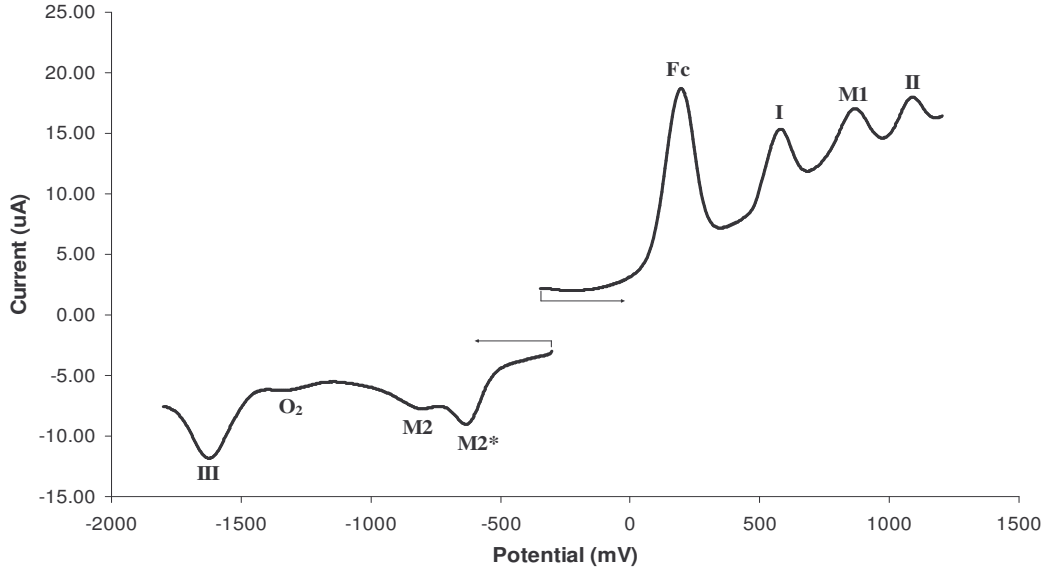

Figure 3-18. Squarewave voltammogram of 1 mmol dm^{-3} $Mn(Cl)Pc(C_{13}H_{27})_8$ / $Mn(OMe)Pc(C_{13}H_{27})_8$ **[24]** in dichloromethane at 25 °C on a glassy carbon working electrode, at a scan frequency of 50 Hz.

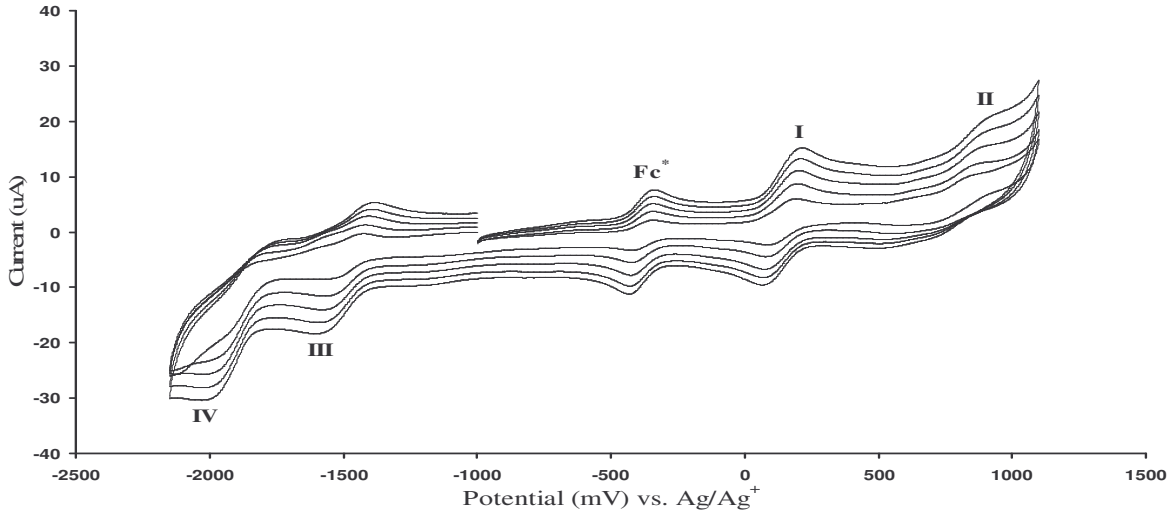

Figure 3-19. Cyclic voltammogram of 1 mmol dm^{-3} $ZnPc(C_{13}H_{27})_8$ **[25]** in dichloromethane at 35 °C on a glassy carbon working electrode, at scan rates of 100 (smallest currents), 200, 300, 400 and 500 mV s^{-1}. Two well-defined ring-centered redox processes were observed (I and III) while two other poorly-defined ring-centered redox processes were also observed (II and IV). Fc^* designates decamethyl ferrocene as the internal reference.

Although the four ring-based observed redox signals in the potential range -1 800 mV to 1 200 mV vs. Ag/Ag^+ were more ideal for the metal free phthalocyanine (2HPc), **[23]**, than for the manganese and zinc derivatives, **[24]** and **[25]**, none of them exhibited ideal reversible behaviour

(Table 3-2). Of the phthalocyanines of this study, only the zinc derivative showed CH_2Cl_2 solubility problems. To accomplish solution phase electrochemistry of **[25]** the solvent was heated to 35 ^oC to obtain a saturated solution. In contrast, the manganese derivative **[24]** was highly soluble in CH_2Cl_2 at room temperature, able to dissolve in the minimum of solvent. Electrochemical reversibility for one electron processes at 25 ^oC is characterised by peak potential differences of 59 mV and is independent of scan rate.[13] The metal-free phthalocyanine **[23]** derivative showed good, well defined, CV's in dichloromethane at 25 ^oC (Figure 3-16). The four observed redox processes that are associated with the ring-based electron transfer couples are assigned in equation1. $E^{o/}$ values vs Fc/Fc^+ are those for scan rate of 100 mV/s.

$$\underset{\text{M = 2H}}{\underset{\text{M = Mn(III)Cl}}{\underset{\text{M = Zn(II)}}{}}} \quad \overset{\text{wave IV}}{\underset{E^{o'} = -2.054\text{ V}}{\underset{E^{o'} = \text{not observed}}{\underset{E^{o'} = -1.791\text{ V}}{MPc^{2-} \overset{-e^-}{\underset{+e^-}{\rightleftharpoons}}}}}} \quad \overset{\text{wave III}}{\underset{E^{o'} = -1.663\text{ V}}{\underset{E^{o'} = -1.732\text{ V}}{\underset{E^{o'} = -1.456\text{ V}}{MPc^{-\bullet} \overset{-e^-}{\underset{+e^-}{\rightleftharpoons}}}}}} \quad \overset{\text{wave I}}{\underset{E^{o'} = -0.044\text{ V}}{\underset{E^{o'} = 0.373\text{ V}}{\underset{E^{o'} = 0.116\text{ V}}{MPc \overset{-e^-}{\underset{+e^-}{\rightleftharpoons}}}}}} \quad \overset{\text{wave II}}{\underset{E^{o'} = 0.558\text{ V}}{\underset{E^{o'} = 0.864\text{ V}}{\underset{E^{o'} = 0.487\text{ V}}{MPc^{+\bullet} \overset{-e^-}{\underset{+e^-}{\rightleftharpoons}}}}}} \quad MPc^{2+} \tag{1}$$

As expected, the redox processes of the manganese and zinc complexes were not as well defined as those of the metal-free phthalocyanine. The peak cathodic and peak anodic current ratio, i_{pc}/i_{pa}, for wave II of the metal free phthalocyanine, approached unity which indicated this electrochemical process was not accompanied by any other physical or chemical process (Table 3-2, p. 87). All the other 2H-, Mn- and ZnPc's waves investigated here deviated substantially from unity, and is acknowledged that aggregation and poor solubility may contribute to this observation. The Mn phthalocyanine contains a redox active metal center and it is the manganese's redox activity that is nicely detected in the two reduction waves M2 and M2* at -783 mV and -684 mV respectively; and in the single oxidation wave M1 at 850 mV (vs Ag/Ag^+). Waves M2 and M2* was observed as two peaks because **[24]** exists as a mixture of complexes $[(Mn\text{-}Cl)Pc(C_{13}H_{27})_8 \cdot 5H_2O] : [(Mn\text{-}OMe)Pc(C_{13}H_{27})_8 \cdot 5H_2O] = 0.55 : 0.45$. Wave M2 is assigned to the chlorine derivative, and M2* to the methoxide derivative. The oxidation wave, M1, has only one peak as manganese(II) complexes normally are not associated with axial ligands and

hence M1 manifests as a single peak. The redox couples M1-M2 and M1-M2* showed very large ΔE_p values of 1 633 mV and 1 535 mV respectively. The large ΔE_p and i_{pc}/i_{pa} values showes that these redox processes are electrochemical irreversible not in the least because the coordinationsphere of Mn(II) and Mn(III) are not the same. The reduction wave IV of the manganese derivative was not observed since it falls outside the solvent window of this experiment. The presence of the Mn(III) center shifted wave IV to a more negative potential, Figure 3-20.

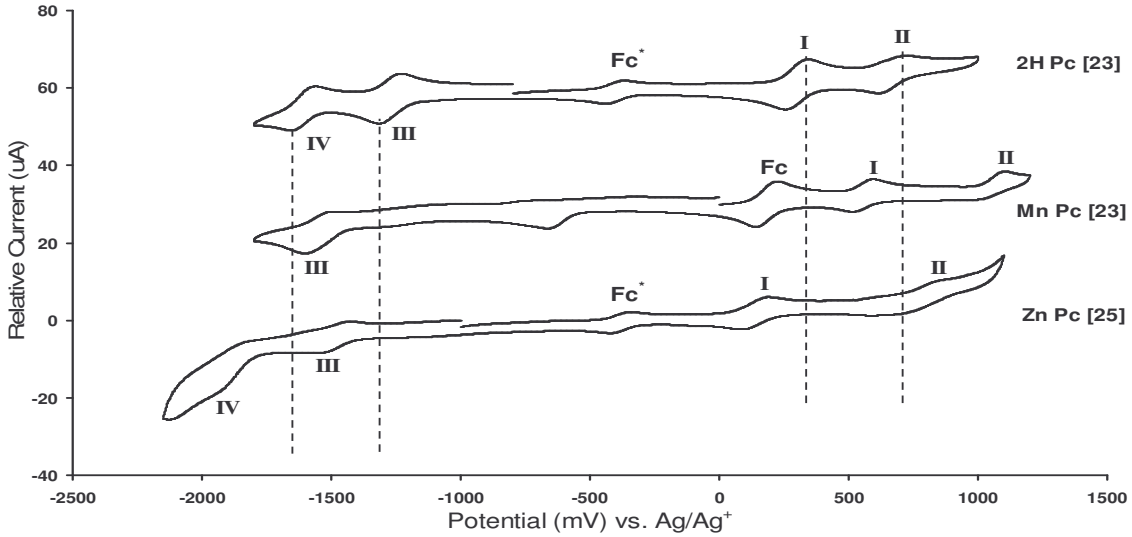

Figure 3-20. Cyclic voltammograms showing the four ring centered redox processes I, II, III and IV of the series of octa-alkylated Pc derivatives **[23]**, **[24]** and **[25]** on a glassy carbon working electrode in CH_2Cl_2, at a scan rate of 100 mV s^{-1}. The dashed lines indicate the changes in oxidation potentials of the ring centered redox processes upon metalation of **[23]**. Fc and Fc^* designates internal references ferrocene and decamethyl ferrocene respectively.

Table 3-1. Comparison of the formal reduction potentials, $E^{o/} = (E_{pa} + E_{pc})/2$ where E_{pa} and E_{pc} are the peak anodic and peak cathodic potentials respectively, of phthalocyanines **[23]**, **[24]** and **[25]** (bold) with related long-chain phthalocyanines obtained from *J. Mater. Chem.*, **11**, 434–443 (2001).[a]

Phthalocyanine, scan rate / mV s^{-1}	**$E^{o/}$ Wave IV (V)**	**$E^{o/}$ Wave III (V)**	**$E^{o/}$ Wave I (V)**	**$E^{o/}$ Wave II (V)**
2H C_{10}, 100[b]	-1.575	-1.175	0.359	0.732
2H C_{12}, 50[b]	-1.541	-1.188	0.380	0.813
2H C_{13} [23], 100[a]	**-1.608**	**-1.273**	**0.299**	**0.670**
2H C_{15}, 50[c]	-1.563	-1.180	0.390	0.982
2H C_{18}, 50[c]	–	-1.220	0.413	0.896
Mn C_{13} [24], 100[b]	**–**	**-1.549**	**0.556**	**1.047**
Zn C_{10}, 100[c]	-1.569	-1.340	0.218	0.873
Zn C_{12}, 50[c]	–	-1.330	0.277	0.894
Zn C_{13} [25], 100[d]	**-1.871**	**-1.480**	**0.139**	**0.741**
Zn C_{15}, 50[c]	–	-1.439	0.294	0.891
Zn C_{18}, 50[c]	–	–	0.292	–

[a] These authers used a Pt working electrode and, except for the 2H C_{10} and 2H C_{12} derivatives, studied the electrochemistry at 75 °C in dichloroethane. The present study used CH_2Cl_2 as solvent, 35 °C and a glassy carbon working electrode. [b] Experiment done in dichloromethane at 25 °C. [c] Experiment done in 1,2-dichloroethane at 75 °C. [d] Experiment done in dichloromethane at 35 °C.

From Table 3-1 one can clearly see the difference in the formal reduction potentials of the C_{13} phthalocyanines's ring-centered redox processes compared to related long-chain phthalocyanines. The shift in potential is mainly due to the different experimental conditions used for the longer chain phthalocyanines. However, when comparing the $E^{o/}$ values at identical conditions of the C_{10} and C_{13} phthalocyanines, the effect of chainlength is evident. Reduction wave IV is 33 mV more negative in the metal-free C_{13} phthalocyanine than in the corresponding C_{10} phthalocyanine. Similarly, wave III is 98 mV more negative; while oxidation waves I and II are 60 mV and 143 mV more negative respectively. This trend is also visible in the rest of the long-chain metalfree phthalocyanines and indicates at least for waves IV and III that with increased substituent chainlenght, the phthalocyanine macrocycle becomes easier to oxidise. For Waves I and II the trend appears to be the opposite. These contrasting sets of results cannot be explained with confidence with the present available knowledge concerning the redox behaviour of these complexes.

Table 3-2. Peak anodic potentials, E_{pa}, or peak cathodic potentials, P_{pc}, difference in peak anodic and peak cathodic potentials, ΔE_p, formal reduction potentials, $E^{\circ\prime}$, peak anodic currents, i_{pa}, or peak cathodic currents, i_{pc} and peak cathodic / peak anodic current ratios, i_{pc}/i_{pa}, for the indicated phthalocyanines. Values designated by a dash, "-", indicates values that are either not observed, distorted or to small to be measured accurately. Wave number I through IV designates ring-centered redox couples of the phthalocyanines while M1, M2 and M2* designates redox couples associated with the central metal complex in **[24]**.

Compound	*v*/ mV s^{-1}	Wave **I**					Wave **II**				
		E_{pa}/mV	ΔE_p/mV	$E^{\circ\prime}$/mV	i_{pa}/μA	i_{pc}/i_{pa}	E_{pa}/mV	ΔE_p/mV	$E^{\circ\prime}$/mV	i_{pa}/μA	i_{pc}/i_{pa}
2HPc **[23]**	100	344	90	299	5.94	0.83	724	108	670	3.00	1.06
	200	350	100	300	7.58	0.95	734	124	672	3.62	1.10
	300	358	108	304	9.71	0.77	740	130	675	3.85	1.01
	400	360	110	305	11.16	0.71	750	146	677	4.87	0.90
	500	362	118	303	12.40	0.69	758	156	680	5.57	0.95
Average		**355**		**302**		**0.79**	**741**		**675**		**1.00**
MnPc **[24]**	100	596	80	556	2.89	0.86	1104	114	1047	3.75	-
	200	602	94	555	3.99	0.87	1120	124	1058	4.89	-
	300	608	100	558	5.26	0.78	1126	136	1058	6.18	-
	400	618	116	560	6.44	0.81	1140	144	1068	8.00	-
	500	622	122	561	7.10	0.85	1152	166	1069	9.48	-
Average		**609**		**558**		**0.84**	**1128**		**1060**		
ZnPc **[25]**	100	188	98	139	4.08	0.73	836	190	741	1.71	0.93
	200	196	116	138	5.63	0.88	870	264	738	2.44	-
	300	206	130	141	6.52	0.89	902	364	720	2.85	-
	400	208	138	139	7.99	0.84	936	408	732	2.91	-
	500	212	146	139	9.57	0.77	946	446	723	3.93	-
Average		**202**		**139**		**0.82**	**898**		**731**		

Compound	*v*/ mV s^{-1}	Wave **IV**					Wave **III**				
		E_{pc}/mV	ΔE_p/mV	$E^{\circ\prime}$/mV	i_{pc}/μA	i_{pc}/i_{pa}	E_{pc}/mV	ΔE_p/mV	$E^{\circ\prime}$/mV	i_{pc}/μA	i_{pc}/i_{pa}
2HPc **[23]**	100	-1656	96	-1608	4.60	1.57	-1316	86	-1273	3.75	0.90
	200	-1664	108	-1610	7.22	1.54	-1326	98	-1277	6.33	1.04
	300	-1662	106	-1609	6.92	1.50	-1330	104	-1278	8.27	1.33
	400	-1670	116	-1612	7.36	1.66	-1336	114	-1279	11.01	1.52
	500	-1674	120	-1614	7.46	1.56	-1340	120	-1280	11.28	1.52
Average		**-1665**	**109**	**-1611**		**1.57**	**-1330**		**-1277**		
MnPc **[24]**	100	-	-	-	-	-	-1602	106	-1549	5.11	3.04
	200	-	-	-	-	-	-1622	126	-1559	6.88	3.17
	300	-	-	-	-	-	-1646	146	-1570	9.75	4.43
	400	-	-	-	-	-	-1652	160	-1572	11.66	5.35
	500	-	-	-	-	-	-1666	170	-1581	13.49	5.55
Average							**-1638**		**-1566**		
ZnPc **[25]**	100	-1930	118	-1871	-	-	-1534	108	-1480	3.28	4.37*
	200	-1976	166	-1893	-	-	-1570	152	-1494	4.78	1.69
	300	-2004	234	-1887	-	-	-1580	174	-1493	6.19	1.66
	400	-2024	284	-1882	-	-	-1588	194	-1491	7.31	1.59
	500	-2012	284	-1870	-	-	-1600	214	-1493	8.23	1.67
Average		**-1989**		**-1881**			**-1574**		**-1480**		**1.65**

Table 3-2. (*cont.*)

Compound	*v*/ mV s^{-1}	Internal reference (Fc^*)					Internal reference (Fc)				
		E_{pa}/mV	ΔE_p/mV	E°'/mV	i_{pa}/μA	i_{pc}/i_{pa}	E_{pa}/mV	ΔE_p/mV	E°'/mV	i_{pa}/μA	i_{pc}/i_{pa}
2HPc **[23]**	100	-368	74	-405	1.70	1.42	-	-	-	-	-
	200	-366	76	-404	2.39	1.43	-	-	-	-	-
	300	-364	80	-404	2.90	1.36	-	-	-	-	-
	400	-362	84	-404	3.68	1.14	-	-	-	-	-
	500	-356	94	-403	3.95	1.25	-	-	-	-	-
Average		**-363**		**-404**		**1.32**					
MnPc **[24]**	100	-	-	-	-	-	224	82	183	4.41	1.06
	200	-	-	-	-	-	230	94	183	6.55	0.96
	300	-	-	-	-	-	236	104	184	7.26	1.01
	400	-	-	-	-	-	238	110	183	8.86	0.94
	500	-	-	-	-	-	244	120	184	9.19	0.87
Average							**234**		**183**		**0.97**
ZnPc **[25]**	100	-344	78	-383	2.48	0.81*	-	-	-	-	-
	200	-344	80	-384	2.66	1.12	-	-	-	-	-
	300	-342	82	-383	3.51	1.15	-	-	-	-	-
	400	-340	90	-385	4.33	1.12	-	-	-	-	-
	500	-340	88	-384	4.73	1.03	-	-	-	-	-
Average		**-342**	**84**	**-384**		**1.11**					

Compound	*v*/ mV.s^{-1}	M1 – M2[a] couple[b]					M1 – M2* couple				
		E_{pa}/mV	ΔE_p/mV	E°'/mV	i_{pa}/μA	i_{pc}/i_{pa}	E_{pa}/mV	ΔE_p/mV	E°'/mV	i_{pa}/μA	i_{pc}/i_{pa}
Mn Pc **[24]**	100	824	1566	41	-	-	824	1484	82	3.96[c]	-
	200	836	1618	27	0.21	-	836	1516	78	0.21	23.3
	300	850	1642	29	0.30	-	850	1536	82	0.30	18.7
	400	868	1666	70	0.49	-	868	1560	88	0.49	12.7
	500	874	1674	74	0.96	-	874	1578	85	0.96	6.86
Average		**850**	**1633**	**48**			**850**	**1535**	**83**		

[a] The redox couples of M1, M2 and $M2^*$ could not be fully resolved due to poor peak separation of M2 and M2*; and the undetected reduction peak of M1. [b] E_{pc} values are given as a best estimate since the M2 reduction peak occurs as a shoulder on the M2* reduction peak. [c] i_{pc} of M2*.

3.5 Thermal study of new phthalocynine complexes

3.5.1 DSC study

Structure-thermal behaviour relationships have previously been established particularly in the area of columnar mesophase formation of 1,4,8,11,15,18,22,25-octakisalkylphthalocyanines.[14] The relationship of alkyl chain length and metal ion on the phase transition temperatures and mesophase range has been established. In each series liquid crystallinity is exhibited by compounds with C_6-C_{10} chains. Upon metalalion with zinc it was found that C_5 chain proved to be the limiting chain length which supports mesophase behaviour. In a series of long chain (C_{10}, C_{12}, C_{15} and C_{18}) metal-free and zinc phthalocyanines, it was found that the metal-free and zinc derivatives with C_{12} chains had the lowest crystalline to discotic liquid crystal mesophase transition temperatures.[15] For comparison with the previous phthalocyanine series the C_{13} chain length phthalocynine derivatives of this study were examined by DSC.

The observations of the phase transitions made during the differential scanning calorimetry study were confirmed through polarized light microscopy. Values of the phase transitions were obtained from the third heating and cooling cycles, (Figure 3-21, p. 90 and Figure 3-22, p. 92). Measurements for phthtalocynines **[23]**, **[24]** and **[25]** are summarised in Table 3-3, p. 94

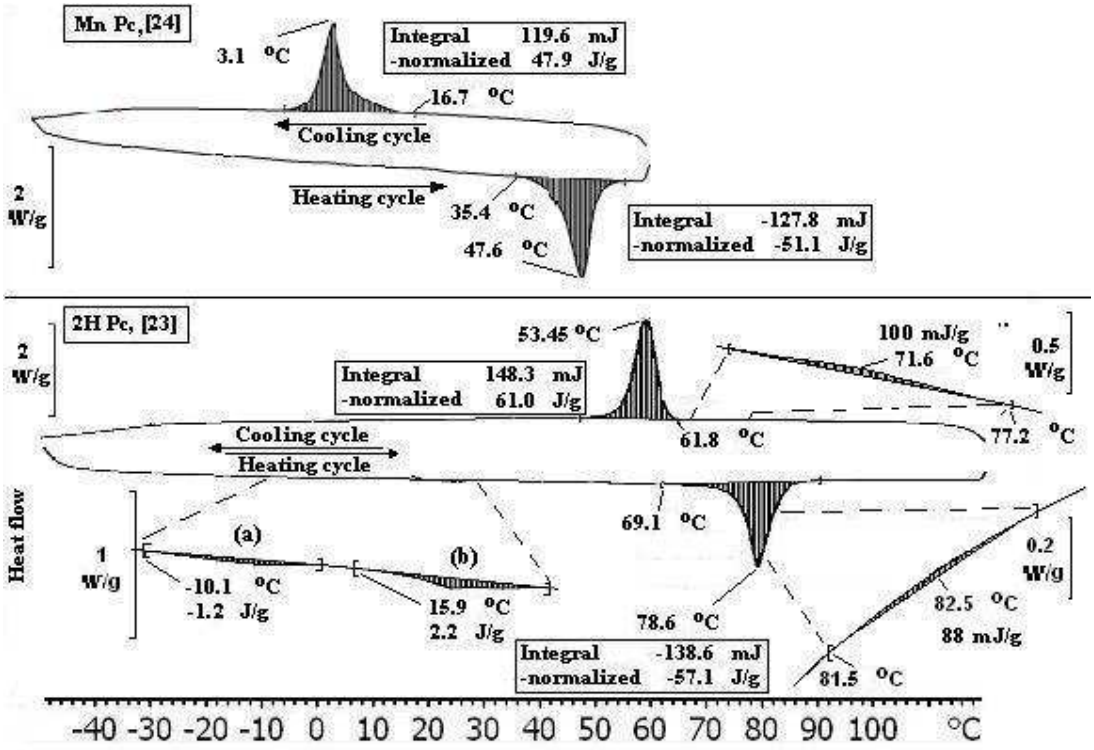

Figure 3-21. Differential scanning calorimetry (DSC) thermograms of heat flow ($W.g^{-1}$) *vs.* temperature (^oC), for the manganese containing octa-tridecylphthalocyanine derivative, **[24]**, and the metal-free octa-tridecylphthalocyanine derivative, **[23]**. A heating and cooling rate of 10°C min^{-1} was used.

The zinc derivative **[25]** showed liquid crystalline behaviour over a much larger temperature range than the metal-free **[23]** compound while the manganese derivative **[24]** showed no liquid crystalline behaviour. The DSC plot of the metal-free phthalocyanine **[23]** showed only the transition from crystalline solid phase (K) to a discotic mesophase (D) at 69.1 ^oC. No transition peak was clearly observed for the transition from the discotic mesophase to the isotropic liquid phase (I), heating past the observed clearing point of **[23]**. The D→I transition was just detectable as a small shoulder on the K→D transition peak at 81.5 ^oC and as such the value of ΔH is given as a best estimate (174 J $mole^{-1}$). The I→D transition (237 J $mole^{-1}$) on the cooling cycle was more clearly visible due to supercooling which shifts the D→K transition to lower temperatures and separating the peaks. The presence of a mesophase is confirmed from the polarized optical microscopy of the phthalocyanines (p. 95). The energy barrier to overcome in the transition from D to I may in this case be too small to be detected by DSC. Transitions from

crystalline solid to isotropic liquid or a mesophase requires relatively large amounts of energy (due to the physical differences and degrees of freedom of the phases) and is usually manifested on a DSC curve as a large exothermic peak on the cooling cycle; endothermic on the heating cycle. Transitions of a mesophase to isotropic liquid and *vice versa* requires far less energy and results in small peaks and are not always observed. The position of the peaks on the heating and cooling cycles is also an indication of the types of phase changes taking place. The D→C or I→C transition's corresponding peak on the cooling cycle is usually, depending on cooling rate, tens of degrees lower than the heating cycle's due to super cooling. The transition of I→D on the other hand, only differs by a few degrees due to the similarity of the liquid crystal and liquid phases. The transition energies, ΔH, of the corresponding peaks should be the same for the heating and cooling cycles, unless changes like decomposition or secondary reactions occurred upon heating. The observed changes in enthalpy on the heating cycle (112.5 $kJ.mol^{-1}$) is close to that of the transition energies on the cooling cycle (120.4 $kJ.mol^{-1}$), showing almost no changes occurred. Additionally two solid state crystalline transitions, Figure 3-21 (a) and (b), were observed at -10.1 ^{o}C and 15.9 ^{o}C with ΔH values of 2.3 kJ $mole^{-1}$ and 4.3 kJ $mole^{-1}$ respectively. While the clearing point was not observed in the DSC graph of **[23]**, the liquid crystal range of 15 ^{o}C was obtained by using the clearing point obtained from the polarized light microscopy.

The DSC plot of the manganese derivative, **[24]**, only showed the melting (C→I) transition at 35.4 ^{o}C and the corresponding recrystallization (I→C) transition as observed from the polarized optical microscopy study, confirming the absence of a mesophase. The presence of an axial ligand on the manganese center disrupts the packing of the macrocycle and thus lowers the melting point as well as reducing any possibility of mesophase occurance. The observed changes in enthalpy on the heating cycle (105.4 $kJ.mol^{-1}$) is also close to that of cooling cycle (98.7

kJ.mol^{-1}), showing that the compound is relatively stable and that almost no chemical changes occurred.

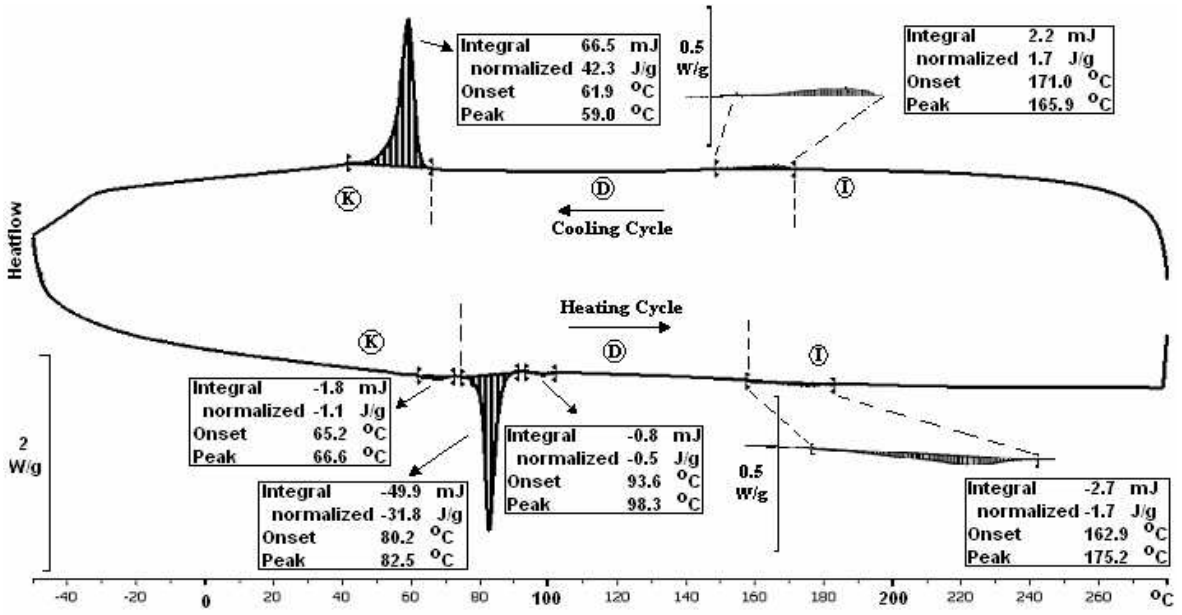

Figure 3-22. Differential scanning calorimetry (DSC) graph of heat flow (w.g^{-1}) *vs.* temperature (C^{o}), for zinc-containing phthalocyanine derivative, **[25]**, showing mesophase transition peaks. A heating and cooling rate of 10°C min^{-1} was used. K: crystalline phase, D: discotic mesophase and I: isotropic liquid.

In contrast to the DSC plots of **[23]** and **[24]**, the plot of the zinc derivative **[25]** (Figure 3-22) showed the transition of D→I at 163.0 ^{o}C (ΔH = 3.5 kJ mole^{-1}) in addition to the K→D transition at 80.0 ^{o}C (ΔH = 64.6 kJ mole^{-1}), confirming the presence of a mesophase. The change in enthalpy on the heating cycle of the D→I transition is almost identical to that of the cooling cycle (3.5 kJ.mol^{-1}), while the proximity of the peaks confirms the D→I transition of a clearing point. In addition a mesophase-transition was also observed at 94.6 ^{o}C with a change in enthalpy of 1.1 kJ mole^{-1}. No further transitions were observed in the mesophase as well as past the observed clearing point. One would expect that the properties of the C_{13} phthalocyanine to lay somewere in between that of the C_{12} and C_{15} phthalocyanine, however, this was not the case. As with the metal free phthalocyanine **[23]**, the liquid cystal range of phthalocyanine **[25]** is considerably smaller than that of related long-chain phthalocyanines with 83 ^{o}C *vs* 145.6 ^{o}C for C_{12} and 110.9 ^{o}C for C_{15}, (see Table 3-3). This is the consequence of uneven numbered chain

substituent length for C_{13} versus C_{12}, and for the more wax like behaviour of C_{15}. The same derivation was also made for C_9 substituent. To emphasise the influence of odd versus even chain lengths, note the phase change temperatures in Figure 3-23 below. The crystalline to mesophase transition temperature is also higher than expected compared to the other phthalocyanines in the series, (80 ^oC *vs* 59 ^oC for C_{12} and 66 ^oC for C_{15}).

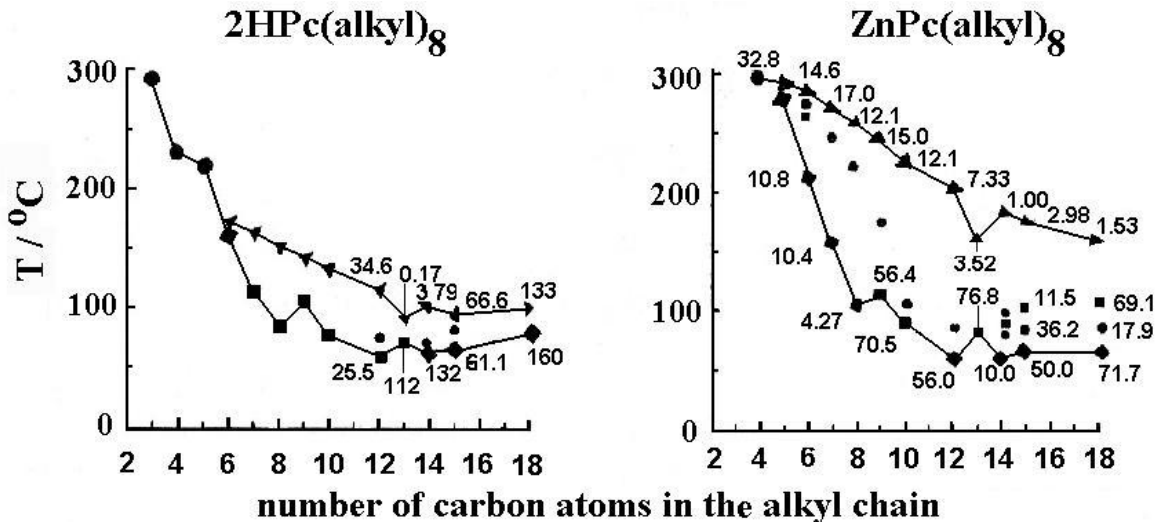

Figure 3-23. Comparison of the effect alkyl substituent chain length has on temperature range in which metal-free and zinc phthalocyanines exhibit mesophase behaviour. The bottom line represents the temperature at which the crystalline solid to mesophase transition occurs, while the top line shows the temperature at which the mesophase converts into an isotropic liquid. The dots show someof the transitions of one mesophase to another. The numbers represent molar phase transition enthalpies (kJ $mole^{-1}$). The above diagrams are adapted from E.H.G. Langner, W.L. Davis, R.F. Shago and J.C. Swarts in "Metal-containing and metallo Supramolecular polymers and materials", Ed.: U.S. Schubert, C.R. Neurcarne and I. Manners, JACS symposium series 928, American Chemical Society, Washington DC, 2006 (pp 443 – 456), to incorporate the C_{13} complexes.

Table 3-3. Observed phase transition temperatures (°C) and transition energies (ΔH) for phthalocyanine derivatives having 8 non-peripherally substituded alkyl chains (C_{10}, C_{12}, C_{13}, C_{15} and C_{18}).

Compound, formula	Transition temp./ °C[b]	Liquid crystal range/ °C
$2HC_{10}$[a], $C_{112}H_{178}N_8$	77.5 (K→D_1; 80) 133 (D_1→I; 8.8)	55.5
$2HC_{12}$[a], $C_{128}H_{210}N_8$	59.2 (K→D_3; 35) 77.8 (D_3→D_1; –) 115.5 (D_1→I; 26)	56.3
[23] ($2HC_{13}$), $C_{136}H_{226}N_8$	-10.1 (K_3→K_2; 2.3) 15.9 (K_2→K_1; 4.3) 69.1 (K_1→D_1; 112.5) 81.5 (D_1→I; 0.2)	12.4
$2HC_{15}$[a], $C_{152}H_{258}N_8$	66.2 (K→D_3; 67) 84 (D_3→D_1; 7.1) 94 (D_1→I; 61)	27.8
$2HC_{18}$[a], $C_{176}H_{306}N_8$	79.3 (K→D_1; 160) 98.2 (D_1→I; 130)	18.9
[24] (MnC_{13}), 0.55:0.45 [$C_{136}H_{234}N_8O_5ClMn$] / [$C_{137}H_{237}N_8O_6Mn$][c]	35 (K→I; 105.4)	not liquid crystalline
ZnC_{10}[a], $C_{112}H_{176}N_8Zn$	89 (K→D_3; 71) 106.6 (D_3→D_1; –) 225.1 (D_1→I; 12)	136.1
ZnC_{12}[a], $C_{128}H_{208}N_8Zn$	60 (K→D_3; 54) 88.5 (D_3→D_1; 50) 205.6 (D_1→I; 7.1)	145.6
[25] (ZnC_{13}), $C_{136}H_{224}N_8Zn$	65.2 (K_2→K_1; 2.3) 80 (K_1→D_1; 76.8) 93.6 (D_2→D_1; 1.1) 163 (D_1→I; 3.5)	83.0
ZnC_{15}[a], $C_{154}H_{258}N_8ZnCl_6$[c]	65.3 (K→D_3; 49) 88.1 (D_3→D_2; 35) 103.6 (D_2→D_1; 11) 176.2 (D_1→I; 2.9)	110.9
ZnC_{18}[a], $C_{177}H_{305}N_8ZnCl_3$[c]	65.9 (K→D_3; 70) 91 (D_3→D_2; 18) 108.1 (D_2→D_1; 67) 160.5 (D_1→I; 1.5)	94.6

[a] Transitions of these phthalocyanines were obtained from *J. Mater. Chem.*, **11**, 434–443 (2001). [b] Mp or transition temperature for change from the crystalline state to a discotic mesophase (K→D_i), from one mesophase to another (D_i→D_{i+1}) or from a mesophase to an isotropic liquid (D_i→I), i = 1, 2 or 3 with D_1 being the highest temperature mesophase. The number that follows each indicated transition represents the enthalpy (ΔH) for that phase change as measured by DSC in kJ mol^{-1}. Where no value is given, ΔH was too small to measure. For 2H C_{12}, the transition D_1→I at 115.5 °C represents the combined energy for two phase changes due to the fact that two partially overlapping peaks could not be resolved. [c] Contains solvent impurities: ZnC_{15}•$2CHCl_3$ or ZnC_{18}•$CHCl_3$. These solvent molecules, or impurities, may imply that transition temperatures data for these compounds may not be precise.

3.5.2 Microscopy Study

The thermal phase transitions of phthalocynines **[23]**, **[24]** and **[24]** are shown in Figure 3-24.

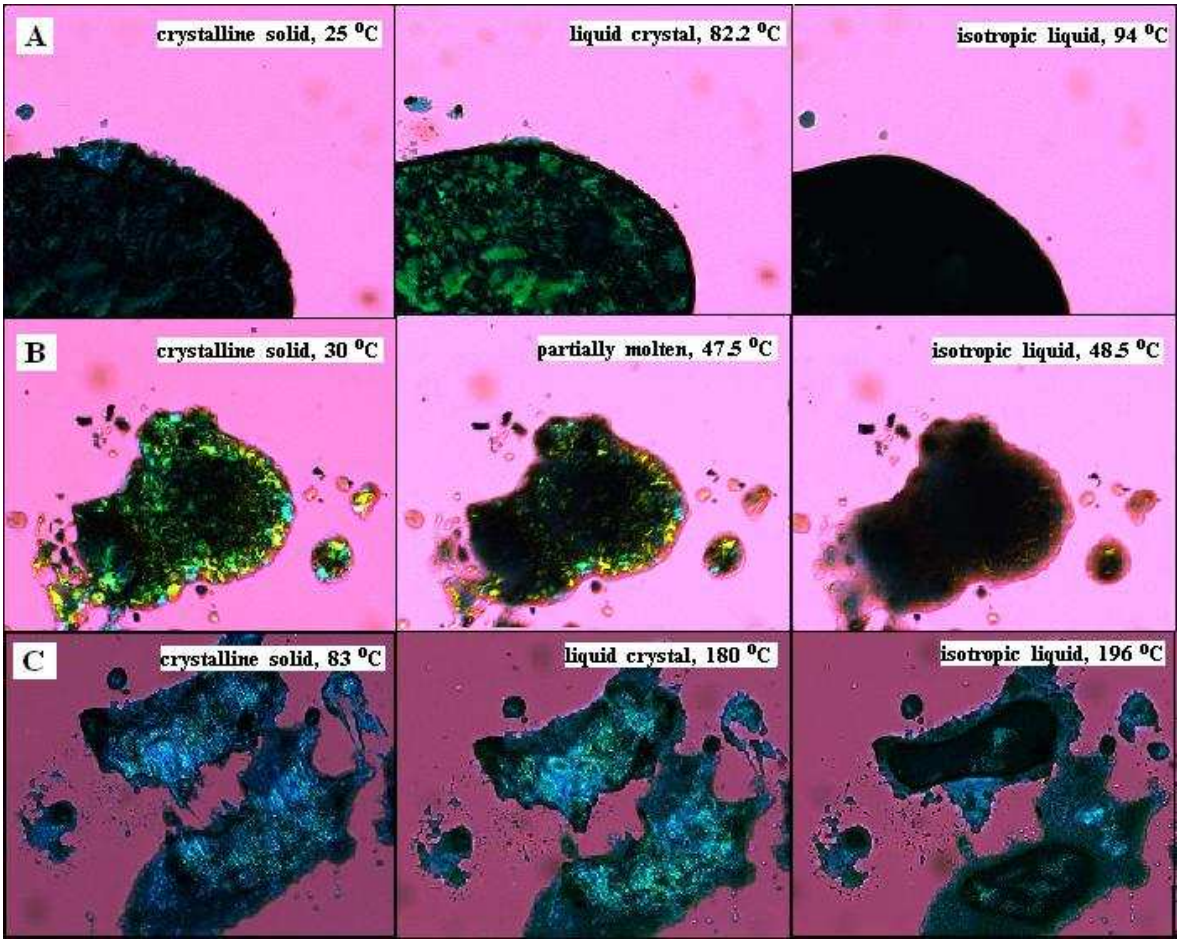

Figure 3-24. Micrographs of octa-alkyl phthalocynines **[23]** (A), **[24]** (B) and **[25]** (C) at different temperatures (°C, see right hand top corner of each slide) under polarized light. Magnification: 40x (A and B) and 100x (C).

The micrographs in Figure 3-24(A) shows the different phases of the metal-free phthalocyanine **[23]** during heating. The large dark spot is a larger portion of phthalocyanine and thus appear different to the smaller areas. Starting from a solid at 25 °C the phthalocyanine was slowly heated. At 72.6 °C the optical texture of the sample started to change, indicating a liquid crystal discotic mesophase. The metal free phthalocyanine started to melt at 84 °C, going into an isotropic liquid phase. The temperature, at which a liquid crystal completely melts to form an isotropic liquid, is known as the clearing point. The slide at 94 °C shows the large patch partially molten while the smaller patches are allready in the isotropic liquid phase. The presence of a

mesophase was even more apparent through the rapid cooling (-20 ^{o}C min^{-1}) of the isotropic liquid (Figure 3-25), showing areas of solid crystaline phthalocyanine (darker bluish areas) forming from the liquid crystal mesophase (lighter greenish areas) as it cools (D→K transition).

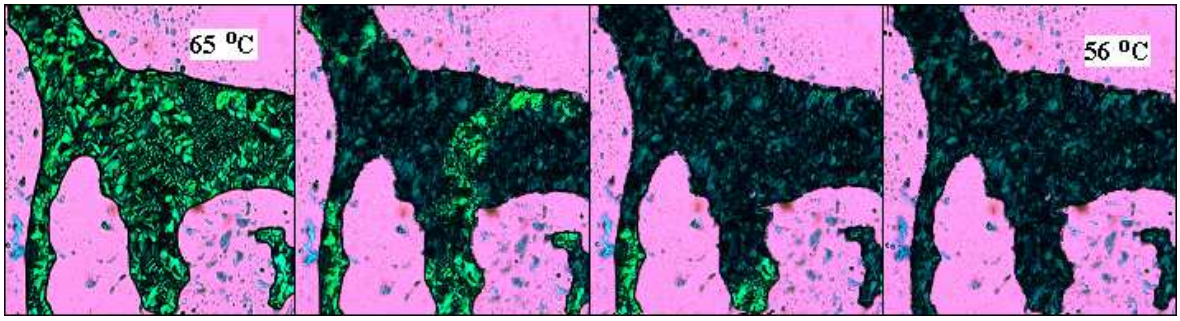

Figure 3-25. Rapid cooling (20 ^{o}C min^{-1}) of phthalocyanine **[23]** showing the change in optical texture as the sample solidifies from the liquid crystal phase (left) to the solid phase (right). Magnification: 40x under polarized light.

The micrographs in Figure 3-24(B) shows the phase changes of phthalocyanine **[24]**, the manganese(III) phthalocyanine. The micrographs show no change in optical texture from the solid phthalocyanine as it is heated. The manganese phthalocyanine starts to melt at 45 ^{o}C, much lower than that of phthalocyanines **[24]** and **[25]**. The lack of a mesophase and the low melting point of the manganese phthalocyanine is attributed to the presence of an axial ligand (Cl or methoxide) on the Mn(III) central atom. The axial ligand disrupts the π-stacking of the phthalocynine macrocycle, preventing the efficient columnar stacking of the phthalocyanine. As the phthalocyanine is heated, the intermolecular forces (Van der Waals, dipole forces) are not sufficient to hold the phthalocyanine molecules together in a columner mesophase (liquid crystal) as the side chains begin to melt. Thus this compound converts from a crystalline solid to an isotropic liquid without passing through the liquid crystal mesophase. The purpose of the tridecyl alkyl chains was to improve solubility of the Pc catalylst in organic solvents and is clearly manifested in the high solubility of the manganese derivative. The presence of an axial ligand not only lowered the melting point, but also contributed to the increased solubility of the complex.

For comparison to the manganese phthalocyanine **[24]**, the zinc phthalocyanine **[25]** was chosen as a potential liquid crystal candidate. The absence of an axial ligand would increase the columnar stacking of the phthalocyanine rings, thus increasing the meting point and lowering the solubility. This was indeed the case with **[25]** having a considerably higher melting point than the metal-free phthalocyanine as well as lower solubility. The micrographs in Figure 3-24(C) shows the phase changes of the zinc(II) phthalocyanine, **[25]**. After heating the zinc phthalocyanine to 83 ^{o}C, a change in the optical texture started to occur, indicating the presence of a mesophase. The onset of the observed phase change is only 7 ^{o}C higher than that of the metal-free phthalocyanine, **[23]**, but the temperature range of the mesophase is considerably greater. The zinc phthalocyanine's clearing point was found to be at 186 ^{o}C, giving a liquid crystal range of 101 ^{o}C vs. 12 ^{o}C for the metal free phthalocyanine.

The observed transitions and liquid crystal ranges obtained from the optical microscopy study are largely subjected to human subjectiveness on the visual changes observed. This influences the onset and end temperatuses of the transitions and could account for the differences between the values obtained from the DSC and microscopy studies.

3.6 Catalytic oxidation trials

After successfully synthesising morpholino-N-oxide derivitized polymers **[13]** and **[14],** as well as transition metal catalysts for oxidation reactions, the focus shifted to the application of these polymers in the oxidation of alkenes in light of goals 3 and 4 of this study. The objective of these trials was to find a suitable catalytic oxidation reaction using N-oxides as oxidant, as a model reaction for the evaluation of polymers **[13]** and **[14]**. The asymmetric dihydroxylation of alkenes as well as the epoxidation of alkenes were chosen as possible model reactions in the evaluation of the oxidising properties of polymers **[13]** and **[14]**. To evaluate the polymers, all reaction conditions were kept constant, changing only the oxidants. As an additional goal, the new manganese phthalocyanine, **[24]**, was investigated as possible catalyst for the epoxidation of alkenes using molecular oxygen as oxidant.

trans-Stilbene (also known as (E)-stilbene or *trans*-1,2-diphenylethylene) was chosen as representative alkene for the oxidation trials. Stilbene is chiefly used in the manufacture of dyes and optical brighteners, as well as one of the gain mediums used in dye lasers. Many stilbene derivates (stilbenoids) are present naturally in plants like resveratrol and pterostilbene. Other alkenes were also considered, but due to purification problems only *trans*-stilbene was chosen. Unlike its less common, sterically hindered *cis*-isomer (melting point of 5 – 6 ^{o}C), *trans*-stilbene is a white, crystaline solid with a melting point of 122 – 125 °C. This makes it easy to identify and isolate through column chromatography. Interestingly, *trans*-stilbene isomerizes to *cis*-stilbene under the influence of light. The reverse reaction can be induced by heat.

3.6.1 Asymmetric Dihydroxylation of alkenes with N-oxides

The Sharpless *cis*-dihydroxylation of alkenes was initially chosen as a possible model reaction for evaluating the effectiveness of polymers **[13]** and **[14]** as oxidizing agents. For the trial run with N-methylmorpholine-N-oxide as oxygen scource the following procedure was attempted. The substrate (*trans*-stilbene, 0.56 mmole) and oxidant (N-methylmorpholine-N-oxide, 0.83 mmole; 1.5 eq.) were mixed and dissolved in a two-phase mixture of *t*-butanol and water. $K_2OsO_2(OH)_4$ (1 mole %) was then added to the mixture and was stirred for 24 hours. The reaction was checked by TLC and after no product formation was visible after 24 hours, stirring continued for a further 24 hours. Although no product was detected on TLC, it was decided to isolate any possible products through column chromatography. However, the only isolated-fraction was that of the starting material, trans-stilbene as confirmed by ^{1}H NMR.

Although dihydroxylation of stilbene using N-methylmorpholine-N-oxide as oxidant was fruitless, attempts with polymers **[13]** and **[14]** in place of N-methylmorpholine-N-oxide were carried out. Using the same mole ratios as for the N-methylmorpholine-N-oxide reaction, the N-oxide polymer (**[13]** or **[14]**) was mixed with the dry catalyst and substrate before adding the solvents (first water and then *t*-BuOH). As with N-methylmorpholine-N-oxide, no product formation was detectable by TLC, even after stirring for 5 days. Changing the $K_2OsO_2(OH)_4$ ratio to 5 mole % also did not result in product formation. Other changes included using 2,6-dichloropyridine-N-oxide as oxidant; using 1:1 CH_2Cl_2 / H_2O as solvent system; only CH_2Cl_2 as solvent; and only *t*-BuOH as solvent. None of the changes resulted in any product. Considerable swelling of the polymers to form a gel was observed in the CH_2Cl_2 / water solvent system using polymer **[14]** as oxidant.

It was concluded that further research is required for this reaction to work successfully, but it was considered outside the borders of the present MSc study by the candidate.

3.6.2 Epoxidation of alkenes with N-oxides

Since no positive results were obtained from the dihydroxylation trials, attention shifted to epoxidation of alkenes. For the epoxidation trials, *trans*-stilbene was again used as representative substrate. *trans*-Stilbene can be easily distinguished from its epoxide, *trans*-stilbene oxide. From their respective ^{1}H NMR spectra (Figure 3-26) the difference between them is obvious. Upon epoxidation, the peak at 7.15 ppm integrating for the 2 ethylenic protons shifts upfield by 3.25 ppm to 3.90 ppm due to the influence of oxygen's electron density. Physically the epoxide differs from the alkene as it has a considerably lower melting point of 69 ^{o}C. The only other substance in this study with a similar melting point was N-methylmorpholine-N-oxide. However, N-methylmorpholine-N-oxide is highly water-soluble while the epoxide is not.

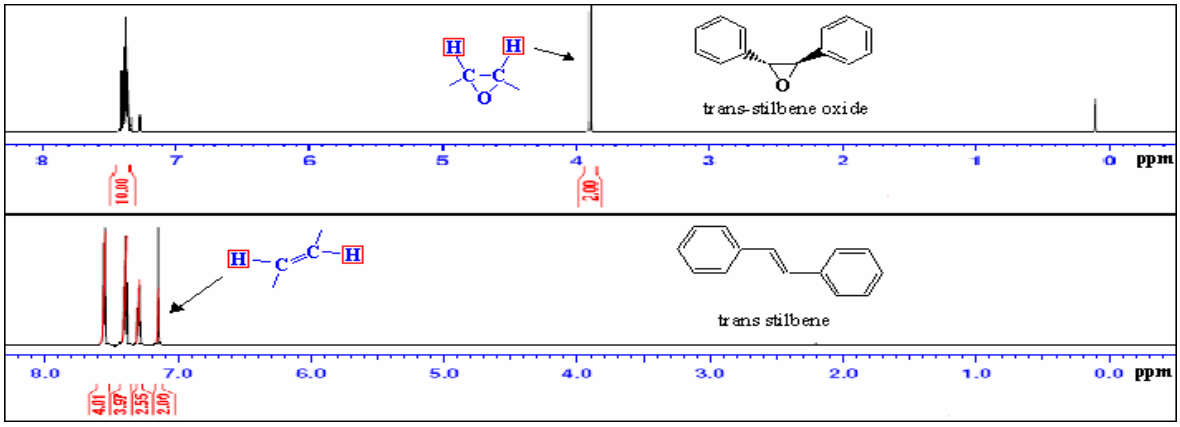

Figure 3-26. ^{1}H NMR of trans-stilbene and *trans*-stilbene oxide in $CDCl_3$.

(i) *Salen-complexes as catalyst*

Using salen complexes **[18]** and **[19]**, a method was devised for the epoxidation of trans-stilbene using N-oxides as oxidants, (Scheme 3-12, p. 101). As a model reaction [Mn(III)Salen]OAc **[18]** was used as catalyst (5 mole %), trans-stilbene as substrate and dichloromethane as solvent. N-methylmorpholine-N-oxide (1.5 eq.) was then added to the solution as oxidant and stirred for 48 hours, checking the reaction progress with TLC.

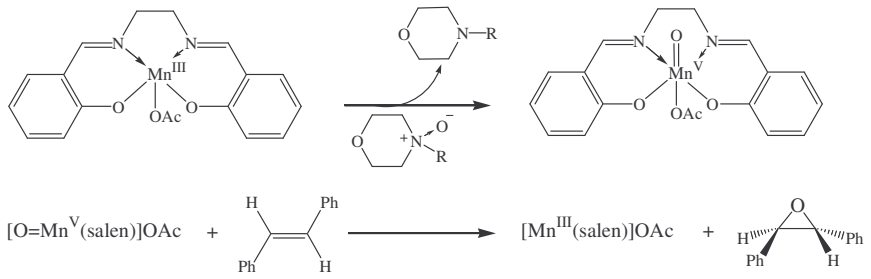

Scheme 3-12. Representation of *trans*-stilbene epoxidation catalysed by the manganese(III) salen complex, **[18]**. R = CH_3, PSI polymer or PECH polymer.

After stirring for 48 hours, TLC monitoring with 5% ethyl acetate in n-hexane as eluent revealed *trans*-stilbene at a R_f of 0.77 as well as a slower moving fraction at R_f : 0.50. The product was isolated in 30.7 % yield by column chromatography with 5% ethyl acetate in n-hexane as eluent. The product was confirmed by ^1H NMR to be trans-stilbene oxide. The reaction using [Co(II)Salen] **[19]** as catalyst in place of **[18]** resulted in no product formation, as judged from TLC analysis.

For the the epoxidation reactions using polymers **[13]** and **[14]** as oxidants in place of N-methylmorpholine-N-oxide, the method was altered slightly. Initially the procedure was identical; however, both polymers **[13]** and **[14]** did not dissolve in CH_2Cl_2 due to their ionic character, even after 48 hours of stirring. The polymers did show some swelling in the solvent, but not to the extent of those observed in the dihydroxylation trials. No epoxide formation was detected from TLC. In the second run, the polymers were dissolved in H_2O before mixing it with the CH_2Cl_2 catalyst (**[18]** and **[19]**) / substrate solution to form a two phase system. The two phase system was then vigourously stirred over 48 hours.

For this specific method an assumption was made that as polymer **[14]** (PECH derivative) oxidise the substrate at the border between the organic and hydro phase, the loss of ionic character on the polymer would result in increased solubility in CH_2Cl_2. Eventually as all the N-

oxides are consumed, the de-oxygenated polymer would move to the organic phase and be recovered essentially as polymer **[12]** (PECH-morpholino derivative). Unfortunately, this was not observed and even after 4 days of stirring no product was observed for both polymers **[13]** and **[14]**. It was expected that at least some epoxide would form with MnSalen as catalyst, judging from the N-methylmorpholine-N-oxide reactions, but it seems the polymer bound morpholine-N-oxides are not accessible enough to oxidise the catalysts.

(ii) *Tetraphenylporphyrinatocobalt(II), **[16]**, as catalyst*

Using the same procedure as for the salen catalized reactions; CoTPP **[16]** was imployed as catalyst in the epoxydation of stilbene involving N-methylmorpholine-N-oxide, **[13]** and polymer **[14]**. However, none of the reactions produced any products, with trans-stilbene as the only visible fraction on TLC.

3.6.3 Epoxidation of alkenes with molecular oxygen

As an extension to this study in the line of "greener" oxidation reactions, the manganese phthalocyanine derivative, **[24]**, was synthesised as a possible catalyst in oxidations using molecular oxygen as oxidant. Ethylene oxide, for example, is manufactured by oxidizing ethylene with air or oxygen in the presence of a silver catalyst. Alkenes furnish hydroperoxides when oxidized by oxygen in the presence of catalysts like salts of cobalt and manganese; the hydroperoxides are transformed to a number of products, including epoxides.[16]

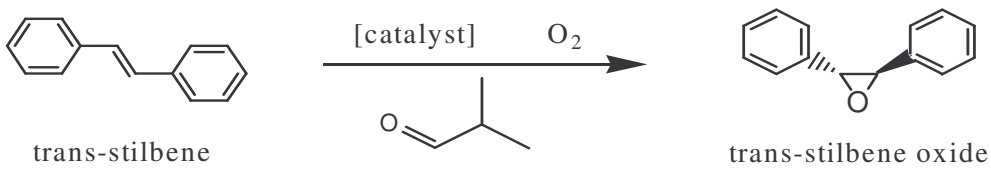

Scheme 3-13. Catalytic epoxidation of stilbene using molecular oxygen as oxidant and CH_2Cl_2 as solvent

CoTPP, **[16]**, was first employed as catalyst to determine the protocol of the reaction. In light of previous successes with other Co(II) porphyrin derivatives as catalysts, near quantitative epoxidation of *trans*-stilbene with O_2 as oxidant was deemed possible, (Scheme 3-13).[6] For the initial oxidation reactions 1.57 mole % of **[16]** was used as catalyst for the oxidation of stilbene, dissolved in CH_2Cl_2. Isobutylaldehyde (1.4 mmole; 1 : 2.5 substrate-aldehyde ratio) was added to the reaction mixture which was then vigorously stirred under an oxygen balloon at ambient conditions. The reaction was monitored by TLC and after 72 hours no product was detected. Even after 7 days and further addition of aldehyde no product was visible. Focus then shifted to the manganese phthalocyanine derivative, **[24]**.

For the epoxidation reaction using manganese phthalocyanine **[24]** as catalyst, the same procedure was used as for **[16]**. 0.25 mole % of phthalocyanine was used as catalyst for the epoxidation of stilbene while the substrate-aldehyde ratio was raised to 1:5. After 48 hours of vigorous stirring an epoxidation product was visible on TLC (R_f = 0.50 vs. trans-stilbene at 0.77 with 5% ethyl acetate in n-hexane as eluent). At 72 hours of stirring no further product formation was visible and the product was isolated in the same manner as for the epoxidation of alkenes with the Salen complexes. The epoxidation product was positively identified as *trans*-stilbene oxide through ^{1}H NMR, and was isolated in 17 % yield. The low yield of epoxide compared to similar systems using cobalt porphyrins as catalysts[6] may be attributed to the manganese phthalocyanines structure. Though the purpose of the long alkyl chains was to impart increased solubility to the catalyst, it is also possible that the long alkyl chains may hinder the catalytic reaction. It is possible that the phthalocynines core becomes encapsulated by the compounds' own side chains and may hinder access of the substrate or oxidant to the central manganese ion.

The author envisage that in a follow up study, techniques may be developed to also use the compounds of this study successfully in epoxidation and hydroxylation reactions.

3.7 References

[1] M. Tomida, T. Nakato, S. Matsunami and T. Kakuchi, *Polymer*, **38 (18)**, 4733 (1997)

[2] W. Zhang and E.N. Jacobsen*., J. Org. Chem.,* **56**, 2296 (1991)

[3] D. Feichtinger and D.A. Plattner, *J. Chem. Soc*., *Perkin Trans.* **2**, 1023–1028 (2000)

[4] a) A.D. Adler, *J. Org. Chem.*, **32**, 476 (1967)

b) A.D. Adler, F.R. Longo, F. Kampas and J. Kim, *J. Inorg. Nucl. Chem.,* **32**, 2443–2445 (1970)

[5] a) K.S. Suslick and B.R. Cook, *J. Chem. Soc., Chem. Commun.,* 200 (1987)

b) S. Tangestaninejad and V. Mirkhani, *J. Chem. Research (S),* 788–789 (1998);

c) Z. Li and C. Xia, *Tetrahedron Lett.*, **44**, 2069–2071 (2003)

[6] a) A.K. Mandal and J. Iqbal, *Tetrahedron*, **33 (22)**, 7641–7648 (1997);

b) X. Zhou, H. Ji, J. Xu, Li. Pei, L. Wang and X. Yao, Tetrahedron Letters, 48, 2691–2695 (2007)

[7] a) H. Kameyama, F. Narumi, T. Hattori and H. Kameyama*, J. Mol. Cat. A: Chem.*, **258**, 172–177 (2006)

b) S. Bhatia, T. Punniyamurthy, B. Bhatia and J. Iqbal, *Tetrahedron Lett.,* **27**, 6101–6122 (1993)

[8] N.B. McKeown, I. Chambrier and M.J. Cook, *J. Chem. Soc., Perkin Trans.*, **1**, 1169 (1990)

[9] A. McKillop and J.A. Tarbin, *Tetrahedron,* **31,** 5955 (1990)

[10] R. Curci, A. Giovine and G. Modena, *Tetrahedron,* **22,** 1235 (1966)

[11] a) R.W. Murray and R. Jeyaraman, *J. Org. Chem.,* **50,** 2847 (1985);

b) R.W. Murray, R. Jeyaraman and M.K. Pillay, *J. Org. Chem.,* **52,** 746 (1987)

c) K.S. Webb, *Tetrahedron Lett.*, **55**, 3457 (1994)

[12] K. Poon, Y. Yan, X. Li and D.P. Ng, *Organometallics*, **18**, 3528 (1999)

[13] D.H. Evans, K.M. O' Connell, R.A. Peterson and M.J. Kelly, *J. Chem. Educ*., **60**, 291 (1983)

[14] A.S. Cherodian, A.N. Davies, R.M. Richardson, M.J. Cook, N.B. McKeown, A.J. Thomson, J. Feijoo, G. Ungar and K.J. Harrison, *Mol. Cryst. Liq. Cryst*., **196**, 103 (1991)

[15] J.C. Swarts, E.H.G. Langner, N. Krokeide-Hove and M.J. Cook, *J. Mater. Chem.*, **11**, 434–443 (2001)

[16] E.G. Lewars, in 'Comprehensive Heterocyclic Chemistry', ed. A.R. Katritzky, Pergamon Press, Oxford, **7**, 95 (1984)

4 Experimental

4.1 Introduction

This chapter describes the chemicals, apparatus as well as experimental procedures and reaction conditions utilised to obtain data for chapter 3. The recorded ^{1}H NMR and IR spectra of the synthesised compounds are given in Appendix A and B respectively.

4.2 Materials and Techniques

4.2.1 Chemicals

Solid reagents (Merck, Aldrich and Fluka Chemicals) were employed directly without further purification. Liquid reagents and solvents were distilled prior to use unless stated otherwise. Doubly distilled water was used. THF was dried by refluxing over sodium. Dichloromethane, chloroform, methanol and ethanol (Aldrich) were used without further drying and purification. Reactions requiring an inert atmosphere were performed under a positive pressure of either nitrogen or argon. Column chromatography was performed on Kieselgel 60 (Merck, grain size 0.063-0.2 mm). Dialyses were performed against running tap water in 12 000 molecular mass cut-off cellulose membrane tubing. Product recovery after dialyse were by freeze drying on an EZ-DRY 550Q instrument at – 40 °C and 63 mTorr.

4.2.2 Instrumentaion

All ^{1}H NMR spectra were recorded in deuterated solvents on a Bruker Advance DPX 300 NMR spectrometer at 289 K. Chemical shifts were presented as δ-values, referenced to $SiMe_4$ at 0.00 parts per million (ppm). UV-VIS spectra were obtained on a Varian Cary-50 computer controlled UV-VIS Spectrometer. IR spectra (cm^{-1}) were recorded on a Bruker Tensor 27 spectrophotometer with a Bruker ATR accessory (Diamond crystal). Elemental analysis was performed by the Canadian Microanalytical Service Ltd.

Visual measurements (for the determination of melting points and phase transition temperatures) were performed on an Olympus BX-51 polarising microscope in conjuction with a Linkam TMS 92 thermal analyser with a Linkam THM 600 cell. DSC measurements were made on a Metler Toledo DSC 822^{e} instrument with heating and cooling rates of 10 ^{o}C min^{-1}.

Electrochemical measurements were made under an argon atmosphere with a computer controlled BAS voltammograph, model CV-27 using a Ag/Ag^{+} reference electrode (0.01 M solution of $AgNO_3$ in acetonitrile as Ag^{+} source), a glassy carbon working electrode, a platinum auxiliary electrode and 0.2 M tetra-n-buthylammonium hexafluorophosphate as supporting electrolyte. The concentration of the analytes was ca. 1 mM in dichloromethane. Characterizations were carried out at room temperature (20 ^{o}C) unless otherwise indicated.

4.2.3 Microscope measurements

The following protocol was followed for all microscopic determinations of melting points and phase-changes: a small amount of the compound (a few grains) was placed on a microscope slide and covered with a cover slip. Before the actual melting point determination, the sample was heated past it until molten. It was then cooled to room temperature to solidify (heating and cooling rates of 20 ^{o}C min^{-1}). This was done to remove crystal tension in the sample and to get uniform heating contact. For the determination of physical phase changes, the sample was

rapidly heated to near the first phase change, as observed from the first heating cycle. A slower heating rate (2 to 5 ^{o}C min^{-1}) was used around the phase change temperatures, halting the heating at visual changes to increase accuracy. All observations were made with polarized light.

4.2.4 DSC measurements

All DSC measurements were made by heating approximately 2 mg of material in a 40 µl Al crucible. DSC calibration was performed using standard Mettler procedures with metals Zn and In as calibration standards, having an onset melting temperature of 419.6 and 156.6 ^{o}C respectively as well as heatflow values of 107.5 and 28.45 J/g respectively. Each sample went through several heating and cooling cycles, firstly heating the sample to just past its melting point as observed in the microscopy study. This was done to insure that the sample was spread evenly over the crucible floor's surface and to negate crystal packing energies.

4.2.5 Electochemical measurements

Cyclic voltammetry, square wave voltammetry and linear sweep voltammetry experiments were performed on *ca.* 1.0 mM solutions of **[23]**, **[24]** and **[25]** in dry CH_2Cl_2 / 0.100 M $[N(^{n}Bu)_4][PF_6]$ utilising a standard three-electrode cell with circular glassy carbon electrodes of surface area 3.14 mm^2 (pre-treated by polishing on a Buehler microcloth first with 1 micron and then ¼ micron diamond paste), a Pt-wire counter electrode and a Ag/Ag$^+$ reference electrode. Because the working electrode was quickly contaminated, it was never used for more than six successive potential cycles before it was recleaned and polished. The Ag/Ag$^+$ reference electrode was constructed by immersing a Ag wire in an acetonitrile solution containing 0.010 M $AgNO_3$ and 0.100 M $[N(^{n}Bu)_4][PF_6]$ in a thin inner Luggin capillary with vycor tip. Ferrocene and/or decamethylferrocene (Fc*) was at the end of each experiment added as internal standard to the bulk solution to enable data reporting versus the Fc/Fc$^+$ couple as recommended by IUPAC.[1] Under our conditions, the Fc/Fc$^+$ couple exhibited i_{pc}/i_{pa} = 1.06, ΔE_p = 82 mV and $E^{o/}$ = 0.183 V

versus Ag/Ag^+ in CH_2Cl_2, while the Fc^*/Fc^{*+} couple exhibited i_{pc}/i_{pa} = 1.42, ΔE_p = 74 mV and $E^{o/}$ = -0.405 V versus Ag/Ag^+ in CH_2Cl_2. The Fc^*/Fc^{*+} couple was at -0.592 vs Fc/Fc^+ in CH_2Cl_2. Based on the Fc^*/Fc^{*+} ΔE_p values, with respect to this study, all processes having $\Delta E_p <$ ca. 90 mV were considered as electrochemical reversible. Processes having ΔE_p values in the range $90 < \Delta E_p < 150$ mV were considered electrochemical quasi reversible, and those that exhibited $\Delta E_p > 150$ mV were considered electrochemical irreversible.[2] An ideal one-electron electrochemical reversible process are characterised by ΔE_p = 59 mV.[3] All measurements were conducted under a blanket of argon thermostatted at 25.0 $\pm$ 0.2 ^oC in a Faraday cage connected to a BAS 100 B/W electrochemical workstation interfaced with a personal computer. Data, uncorrected for junction potentials, were collected with standard BAS 100 software and exported to Excel for manipulation and analyses. Successive experiments under the same experimental conditions showed that all formal reduction and oxidation potentials were reproducible within 5 mV. Blank experiments using solvent containing electrolyte but no phthalocyanines were performed to determine the usable potential window of each solvent and to confirm purity of each solvent / supporting electrolyte system.

4.3 Synthesis of Oxidative Polymers

4.3.1 Hydrophylic Oxidative Polymers

4.3.1.1 Polysuccinimide, PSI [8]

Powdered D,L-aspartic acid (5.0008 g, 37.6 mmole) and ortho-phophoric acid (4.9864 g, 50.9 mmole) were thoroughly mixed in a round-bottomed flask which was then connected to a rotary evaporator and vacuum pump. The flask was then submerged in an oilbath preheated to 200 ^{o}C with slow rotation at atmospheric pressure. After 5 minutes, the temperature of the oilbath was lowered to 180 – 190 ^{o}C, the pressure was reduced to below 4 mmHg and maintained for 2.5 hours. The flask was then removed from the oil and allowed to cool to 50 ^{o}C. DMF (30 mL) was then added to the reaction mixture and rotated overnight to dissolve the frothy solid product. The resulting light brown solution was then slowly poured into 3 liters of water while stirring vigorously to minimize the precipitating particle size of the solid polymer. The precipitate was filtered and washed with several portions of water before air drying overnight at room temperature. The polymer was ground to a fine powder under liquid nitrogen and briefly dried at 80 ^{o}C for 15 minutes. Finally the polymer was dried completely by drying it over P_2O_5 in an Abderhalden drying tube for 24 hours, using boiling toluene (T_B = 110 ^{o}C) as temperature control source. Yield: 2.8487 g, (29.3 mmole; 78.1%); δ_H(DMSO-d_6, Spectrum A1) 5.25 (1H, -C<u>H</u>-), 3.18 (1H, -C<u>H</u>$_2$-), 2.67 (1H, -C<u>H</u>$_2$-); ν_{max}/cm^{-1} (Spectrum B1) 1706 (C=O), 1388 (C-N).

4.3.1.2 Poly-α,β-D,L-[N-(3-morpholinopropyl)]aspartamide [10] *

PSI, **[8],** (1.0000 g, 10.3 mmole) was dissolved in DMF (8.5 mL) and kept at 0 ^{o}C on an ice-bath. N-(3-aminopropyl)morpholine **[9]** (1.6330 g, 11.3 mmole) dissolved in DMF (4.5 mL) was then

slowly added over 5 minutes to the solution of PSI after which the solution was stirred at 0 ^{o}C for 20 minutes. The mixture was then stirred a room temperature for 6.5 hours before diluting it with water (70 mL) and transferring it to a 12 000 molecular mass cut-off membrane. The solution underwent 48 hours of dialysis before being freeze-dried for 48 hours, resulting in a light, white polymeric solid.

Yield **[10]**: 1.9696 g, (8.16 mmole; 79.3 %); δ_H(D2O, Spectrum A2) 4.35-4.55 (1H, s, a-C<u>H</u>), 3.62 (4H, s, g-C<u>H$_2$</u>), 3.07 (2H, s, c-C<u>H$_2$</u>), 2.66 (2H, s, b-C<u>H$_2$</u>), 2.43 (4H, s, f-C<u>H$_2$</u>), 2.29 (2H, s, e-C<u>H$_2$</u>), 1.58 (2H, s, d-C<u>H$_2$</u>); ν_{max}/cm^{-1} (Spectrum B2) 1642 (N-H, amide I), 1530 (N-H, amide II).

4.3.1.3 Poly-α,β-D,L-[N-(3-morpholinopropyl)-N-oxide]aspartamide [13]

Polymer **[10]** (0.4000 g; 1.65 mmole) was dissolved in ethanol (30 mL) before adding 30 % H_2O_2 and stirring overnight. The resulting white precipitate was filtered off and dried at 80 ^{o}C for 30 minutes before drying under vacuum for 2 hours at 25 ^{o}C. Yield **[13]**: 0.3070 g, (1.2 mmole; 72 %); δ_H(D_2O, Spectrum A3) 4.52 (1H, s, a – C<u>H</u>), 4.00 (2H, t, 2 x axial h – OC<u>H</u>H), 3.77 (2H, d, 2 x equatorial i – OCH<u>H</u>), 3.37 (2H, t, 2 x axial f – NC<u>H</u>H), 3.20 (4H, s, c & e – NC<u>H$_2$</u>-), 3.05 (2H, d, 2 x equatorial g – NCH<u>H</u>), 2.15 (2H, s, b – C<u>H$_2$</u>), 1.92 (2H, s, d – C<u>H$_2$</u>); ν_{max}/cm^{-1} (Spectrum B3) 1644 (NH, amide I), 1535 (NH, amide II), 971 (N-O).

4.3.2 Hydrophobic Oxidative Polymers

4.3.2.1 Polyepichlorohydrin, PECH [6]

Phenol (0.0940 g, 1.0 mmole) was dissolved in a mixture of hexane (10 ml) and pentane (10 ml) in a 500 ml three-neck round-bottom flask, equipped with an overhead stirrer. Epichlorohydrin (18.84 g, 0.2036 mole) was mixed with hexane (40 ml) and approximately 0.5 ml of this mixture

* Henceforth the full IUPAC name of the polymers will not be used. Rather, derivatives will be refered to as

was added to the phenol solution via a dropping funnel. The internal temperature of the reaction was set to 25 ^{o}C with a water bath and the reaction flask flushed with nitrogen. Freshly distilled $BF_3 \cdot O(Et)_2$ complex (0.08ml) was then added to the stirring phenol mixture. The remainder of the epichlorohydrin solution was then added dropwise to the mixture over a period of 21 hours while keeping the temperature between 24-27 ^{o}C and maintaining the nitrogen atmosphere. An offwhite precipitate quickly formed. The mixture was stirred for an additional 30 minutes after the final addition of epichlorohydrin. The hexane phase was then decanted and water (100 ml) was added to the thick precipitated polymer. After stirring the polymer in water for 30 minutes, the water was decanted and the polymer dissolved in dichloromethane (100 ml). The solution was then thoroughly washed with water (6 x 100 ml) and dried over $MgSO_4$ before removing the solvents under reduced pressure to yield polyepichlorohydrin (PECH), **[6], as** a highly viscous, nearly colourless liquid. Yield **[6]**: 16.42 g, (0.1775 mole; 87.2 %); Mr = 24 445 g mol^{-1}; δ_H($CDCl_3$, Spectrum A4) 6.90–7.03 and 7.30–7.36 (5H, m, Ar-H), 3.55–3.84 (5H, -CH and 2 x -CH_2 of polymer backbone); ν_{max}/cm^{-1} (Spectrum B4) 2958, 2916 and 2875 (CH_2, CH, alkane), 1100 (O-C, ester).

4.3.2.2 Poly[N-(morpholinomethylene)]ethylene oxide [12]

Method 1

PECH, **[6]**, (0.9802 g, 10.6 mmole) was dissolved in toluene (10 ml) before morpholine (2.6076 g, 29.9 mmole) was slowly added over 5 minutes. The system was then flushed with argon before refluxing under argon for 3 days. The solution turned from colourless to light yellow and a white precipitate, morpholine-HCl salt, formed. The mixture was cooled to room temperature

---

"polymer **[10]**" or the "morpholino derivative **[10]**".

before it was centrifuged at 9 000 rpm for 10 minutes. The liquid phase was decanted, washing the liquid phase with a saturated NaOH solution. After drying the liquid phase over $MgSO_4$ and evaporating the solvents under reduced pressure, the product polymer was then dissolved in dichloromethane before removing solvents under reduced pressure, yielding a dark yellow polymer. Yield **[12]**: 1.2157 g (8.5 mmole; 80.2 %) $\delta_H(CDCl_3$, Spectrum A5) 3.65 (7H, m, 2 x -O-C$\underline{H}_2$-; -C$\underline{H}$ and -C$\underline{H}_2$ of polymer backbone), 2.45 (6H, m, 3 x N-C$\underline{H}_2$-); ν_{max}/cm^{-1} (Spectrum B5) 1113 (C-O, backbone), 1070 (C-O, morpholino), 1009 (C-N).

Method 2

PECH, **[6]**, (1.1744 g, 12.7 mmole) and morpholine (2.3221 g, 26.7 mmole) was directly mixed in a flask. DMSO (1.2 ml) was then added to the mixture before heating the mixture under argon atmosphere to no more than 110 ^oC for 3 days. After the mixture cooled to room temperature the morpholine-HCl salt was filtered of and washed with CH_2Cl_2 (3 x 10 ml), collecting the filtrate. The dark filtrate solution was then diluted with 40 ml of CH_2Cl_2 before washing it with water (3 x 200 ml) to remove the DMSO. The solution was dried over $MgSO_4$ and the solvents removed under reduced pressure with heating, yielding a dark viscous polymer.[†] Yield **[12]**: 0.8210 g (5.7 mmole; 44.8 %); $\delta_H(CDCl_3$, Spectrum A6) 3.65 (7H, m, 2 x -O-C$\underline{H}_2$-; -C$\underline{H}$ and -C$\underline{H}_2$ of polymer backbone), 2.45 (6H, m, 3 x N-C$\underline{H}_2$-); ν_{max}/cm^{-1} (Spectrum B6) 1113 (C-O, backbone), 1069 (C-O, morpholino), 1009 (C-N).

4.3.2.3 Poly[N-(morpholinomethylene)-N-oxide]ethylene oxide [14]

Polymer **[12]** (0.2670 g, 1.87 mmole) was dissolved in ethanol (20 ml) before adding 30 % H_2O_2 (10 ml, excess) to the solution. The reaction mixture was then stirred at room temperature for 24

[†] The second method was repeated and refluxed for only 24 hours and made no difference in the colour or morpholine content of the polymer, see Chapter 3.

hours. Powdered MnO_2 was then slowly added by spatula to the mixture and stirred for 45 minutes to neutralize the excess H_2O_2. After filtering off the MnO_2, the mixture was evaporated to dryness under reduced pressure. The product polymer was no longer soluble in most organic solvents such as dichloromethane. However it is highly soluble in water. Yield **[14]**: 0.2860 g (1.8 mmole; 96.0 %); δ_H(D_2O, Spectrum A8) 4.10 (2H, s, 2 x axial a – OC<u>H</u>H), 3.90 (2H, s, 2 x equatorial b – OCH<u>H</u>), 3.60 (3H, s, backbone c – C<u>H</u>$_2$-C<u>H</u>), 3.40 (2H, s, 2 x axial d – NC<u>H</u>H), 3.10, (2H, s, 2 x equatorial e – NCH<u>H</u>) 2.90 (2H, s, f – N-C<u>H2</u>); ν_{max}/cm^{-1} (Spectrum B8) 975 (N-O).

4.4 Synthesis of transition-metal catalysts

4.4.1 Metallo-porhyrins

4.4.1.1 *meso*-Tetraphenylporphyrin, 2HTPP [15][4]

Pyrrole (6.74 g, 100 mmole) and benzaldehyde (10.60 g, 100 mmole) was mixed into a flask and propionic acid (25 ml) was added as solvent. The solution was refluxed in absence of light for 1 hour and changed colour from a dark brown to black-green. The reaction mixture was then left to cool to room temperature over night. The precipitate was filtered off and washed with cold methanol (150 ml); water (200 ml) and again with methanol (150 ml) to yield the metal-free tetraphenylporphyrin, (2HTPP), as a purple crystalline powder. Yield **[15]**: 3.0055 g (4.89 mmole; 19.56 %); mp. 447-450 ^oC; λ_{max}/nm (CH_2Cl_2) 412 and 418; δ_H($CDCl_3$, Spectrum A9).8.88 (8H, s, β-pyrrole-<u>H</u>), 8.26 (4H, m, 4 x *o*-C_6<u>H</u>$_5$), 7.79 (16H, m, 4 x *m*,*p*-C_6<u>H</u>$_5$); ν_{max}/cm^{-1} (Spectrum B9) 3312 (N-H), 3055 + 3025 (=C-H stretching), 1071 (C-N), 965 (=C-H bending).

4.4.1.2 Tetraphenylporhyrinatocobalt(II), Co(II)TPP [16][5]

A solution of anhydrous $CoCl_2$ (0.04 g; 0.3 mmole) in methanol (10 ml) was added to a refluxing solution of 2HTPP **[15]** (0.1850 g; 0.3 mmole) in chloroform (40 ml). The solution was refluxed for 30 minutes before checking the reaction progress with TLC. A further portion of $CoCl_2$ (0.02 g; 0.15 mmole) was added to the refluxing solution, refluxing continued for a furter 3 hours. The reaction mixture was cooled to room temperature and solvents were removed under reduced pressure. The residue was then purified by column chromatography ($CHCl_3$/n-Hexane 1:1), collecting the first red fraction. After the evaporation of solvents, the product was recrystalised from dichloromethane–methanol. Yield **[16]**: 0.0416 g (0.062 mmole; 70.7 %); mp. 396-398 ^oC; λ_{max}/nm (CH_2Cl_2) 410; δ_H($CDCl_3$, Spectrum A10) 13.15 (8H, s, β-pyrrole-H), 9.95 (16H, m, 4 x *m*,*p*-C_6H_5), 9.70 (4H, m, 4 x *o*-C_6H_5); ν_{max}/cm^{-1} (Spectrum B10) 2962 (=C-H stretching), 1067 (C-N), 997 (=C-H bending)

4.4.1.3 Attempted synthesis of Tetraphenylporhyrinatomanganese(III) acetate, [Mn(II)TPP]OAc [32]

0.50 g of 2H TPP, **[15],** was dissolved in a mixture of chloroform (10 ml), methanol (3 ml) and distilled water (0.5 ml). 5 eq. (4.6 mmole, 0.80 g) of $Mn(OAc)_2$ was added to the porphyrin solution and refluxed for 24 hours. The reaction mixture was cooled to room temperature and cold water was added to it. The organics were extracted with chloroform, the organic layer dried over $MgSO_4$ and the solvents removed under reduced pressure. Purification of the residue was attempted through column chromatography over silica with CH_2Cl_2 / CH_3OH (4:1) as eluent. After eluating the first green fraction (metal-free tetraphenyl porphyrin) the methanol ratio was increased. The [Mn(III)TPP]OAc fraction (red band) stuck to the baseline and started to move with an increased methanol ratio of 1:1. Yield **[32]**: 0.2225 g (0.306 mmole; 37.6 %); (Found: C, 64.71; H, 4.48; N, 6.03; Mn, 6.11 %. $C_{46}H_{31}N_4O_2Mn$ requires: C, 76.03; H, 4.30; N, 7.71; Mn, 7.56 %); λ_{max}/nm (CH_2Cl_2) 478; δ_H($CDCl_3$) No satisfactory spectra were obtained due to the

peak broadening effect of the paramagnetic Mn(III) metal center.; ν_{max}/cm^{-1} (Spectrum B20) 2961 + 2923 (=C-H stretching), 1596 +1487 (=C-H arene), 1071 (C-N), 1006 (=C-H bending). All attempts to purify this compound was met with failure, hence research on this compound was discontinued in favour of a manganese phthalocyanine.

4.4.2 Metallo-Salen complexes

4.4.2.1 Bis(salicylidene)ethylenediamine, 2HSalen [17][6]

Salicylaldehyde (2.4424 g; 20 mmole) was dissolved in methanol (20 ml) and added to a mixture of ethylenediamine (0.6010 g; 10 mmole) in methanol and stirred for 30 min. A yellow precipitate formed almost immediately after combining the two solutions (the reaction is driven to completion to completion as result of the poor solubility of the product in methanol). The mixture was chilled on an ice bath before filtering of the precipitate and washing it with a small amount of cold methanol. The precipitate was then recrystalised from chloroform-methanol. Yield **[17]**: 2.0034 g (7.5 mmole; 75 %) mp. 126.2-126.9 ^{o}C; λ_{max}/nm (CH_3CN) 253 and 315; δ_H($CDCl_3$, Spectrum A11) 8.37 (2H, s, 2 x benzylidenimin-H), 6.85-7.32 (8H, m, 2 x C_6H_4), 3.96 (4H, s, 2 x -CH_2-); ν_{max}/cm^{-1} (Spectrum B11) 1678 (N=C).

4.4.2.2 *N*,*N*'-Bis(salicylidene)ethylenediaminomanganese(III) acetate, [Mn(III)Salen]OAc [18][7,8]

Anhydrous $Mn(OAc)_2$ (0.1281 g; 0.74 mmole) was dissolved in a minimum of methanol (5 ml) and added to a refluxing solution of 2HSalen, **[17]** (0.1833 g; 0.69 mmole), in methanol (25 ml). The ligand solution immediately changed colour from yellow to a dark greenish-brown colour. The solution was refluxed for 10 minutes before allowing the raction mixture to cool down to room temperature. The precipitate was filtered of and recrystalised from chloroform/methanol. Yield **[18]**: 0.2192 g (0.58 mmole; 84 %) mp. > 250 ^{o}C (see 4.3.1.); λ_{max}/nm (CH_3CN) 404; δ_H($CDCl_3$, Spectrum A12) No satisfactory integrals were obtained due to the peak broadening effect of the paramagnetic Mn(III) metal center. ν_{max}/cm^{-1} (Spectrum B12) 1696 (N=C).

4.4.2.3 *N*,*N*'-Bis(salicylidene)ethylenediaminocobalt(II), Co(II)Salen [19][7,9]

$CoCl_2 \cdot 6H_2O$ (0.1713 g; 0.72 mmole) was dissolved in a minimum of methanol (5 ml) and added to a refluxing solution of 2HSalen, **[17]** (0.1833 g; 0.69 mmole), in methanol (25 ml). The ligand solution immediately changed colour from yellow to a dark greenish-brown colour. The solution was refluxed for 10 minutes before allowing the raction mixture to cool down to room temperature. The precipitate was filtered of and recrystalised from chloroform/methanol. Yield **[19]**: 0.2036 g (0.63 mmole; 94 %) mp. 251-253 ^{o}C; λ_{max}/nm (CH_3CN) 386.1; δ_H($CDCl_3$, Spectrum A13) No satisfactory integrals were obtained due to the peak broadening effect of the paramagnetic Co(II) metal center; ν_{max}/cm^{-1} (Spectrum B13) 1631 (N=C).

4.4.3 Metallo-phthalocyanines

4.4.3.1 2,5-Tridecylthiophene [20]

Thiophene (1.8176 g; 21.6 mmole) in dry THF was treated with 25 ml of a 2.5 M of n-butyl lithium in hexane between -75 ^{o}C and -60 ^{o}C under inert atmosphere. The reaction was immediately after addition allowed to reach room temperature while stirring continuously for 24 hours. The reaction was then cooled to approximately -70 ^{o}C before adding a slight excess of 1-tridecylbromide (12.52 g; 47.6 mmole). The mixture was allowed to reach room temperature while stirring for a further 24 hours. The mixture was then poured over ice and extracted with diethyl ether (4 x 100 ml). The combined ether extracts was dried over $MgSO_4$ and solvents removed under reduced pressure at 80 ^{o}C. The crude light brown oil was then fractionally distilled under reduced pressure (< 3 mmHg) at 180 ^{o}C. The residue that did not distill was then ran through a short silica column using petroleum ether as eluent to remove impurities to yield pure 2,5-tridecylthiophene as a white wax after solvent evaporation. Yield **[20]**: 7.5706 g (16.86 mmole; 78.08 %); mp. 37.8-39.3 ^{o}C; δ_H($CDCl_3$, Spectrum A14) 6.63 (2H, s, $C_4\underline{H}_2S$), 2.80 (4H, t, 2 x -C$\underline{H}_2$-), 1.73 (4H, m, 2 x -C$\underline{H}_2$-), 1.37 (40H, s, 2 x -(C$\underline{H}_2$)$_{10}$-), 0.95 (6H, t, 2 x -C$\underline{H}_3$). ν_{max}/cm^{-1} (Spectrum B14) 2849 (C-H), 1471 (-CH_3).

4.4.3.2 2,5-Tridecylthiophenesulfone [21]

2,5-Tridecylthiophene **[20]** (7.00 g; 15.6 mmole) was dissolved in dichloromethane (250 ml) and added to a mixture of water (340 ml), acetone (250 ml) and $NaHCO_3$ (185 g) in a 2 L three-neck flask. The flask was then equipped with an effective stirrer and a large CO_2/Acetone condenser. The srirrng heterogeneous mixture was then cooled on an ice/NaCl bath before slowly adding Oxone® (315 g) in portions over a period of 30 minutes. After the final addition, the mixture was stirred for a further 24 hours, maintaining the condensing activity. Water (1 L) was then added to dissolve the inorganic salts, and the aqueous layer was decanted and extracted with

dichloromethane. The remaining solids of the reaction mixture were then dissolved in dichloromethane and washed with water. The combined aqueous layers were then extracted with dichloromethane (3 x 100 ml). Finally, all dichloromethane layers were combined, washed with water and dried over $MgSO_4$. The solvents were removed under reduced pressure and the crude product was recrystalised from ethanol. Yield **[21]**: 4.8688 g (10.13 mmole; 64.9 %); mp. 61.7-64.4 ^oC; δ_H($CDCl_3$, Spectrum A15) 6.28 (2H, s, $C_4\underline{H}_2SO_2$), 2.48 (4H, t, 2 x -C$\underline{H}_2$-), 1.65 (4H, m, 2 x -C$\underline{H}_2$-), 1.28 (40H, s, 2 x -(C$\underline{H}_2$)$_{10}$-), 0.90 (6H, t, 2 x -C$\underline{H}_3$). ν_{max}/cm^{-1} (Spectrum B15) 1233 and 1134 (-SO_2).

4.4.3.3 3,6-Tridecylphthalonitrile [22]

2,5-Tridecylthiophenesulfone **[21]** (4.6960 g; 9.8 mmole) and fumaronitrile (0.7651 g; 9.8 mmole) was washed into a glass tube with minimal $CHCl_3$. The tube was then sealed and heated at 160 ^oC for 18 hours.‡ After the tube cooled to room temperature, the contents of the tube were flushed out with a minimum of $CHCl_3$. The solvents were removed under reduced pressure at 90 ^oC until no further gas evolution (SO_2 and H_2) was observed in the melt. The residue was then purified by column chromatography, eluent toluene, collecting the second fraction. The solvent was evaporated and the product was recrystallised from ethanol. Yield **[22]**: 2.8392 g (5.76 mmole: 58.79 %) mp. 77.8-79.2 ^oC; δ_H($CDCl_3$, Spectrum A16) 7.48 (2H, s, $C_6\underline{H}_2$), 2.87 (4H, t, 2 x -C$\underline{H}_2$-), 1.67 (4H, m, 2 x -C$\underline{H}_2$-), 1.37 (40H, s, 2 x -(C$\underline{H}_2$)$_{10}$-), 0.89 (6H, t, 2 x -C$\underline{H}_3$); ν_{max}/cm^{-1} (Spectrum B16) 2229 (C≡N).

‡ The sealed glass tube is put into a sand-filled steel tube to protect the oven against any damage should the tube explode as result of the pressure build-up.

4.4.3.4 1,4,8,11,15,18,22,25-Octatridecylphthalocyanine [23]

3,6-Tridecylphthalonitrile, **[22],** (395 mg; 0.8 mmole) was dissolved in hot 1-pentanol (4 ml), at 100 ^{o}C under inert atmosphere. The solution was then brought to reflux and a *slight* excess of clean lithium metal (0.0278 g; 4 mmole) was added in small portions. The mixture was then refluxed for 18 hours while stirring under inert atmosphere. The deep green suspension was then cooled to room temperature before stirring for 15 minutes with acetone (40 ml). The solids were filtered of and washed with acetone. Acetic acid (70 ml) was then added to the combined filtrate and stirred for 30 minutes. The resulting precipitate was then filtered of and washed first with acetone and then methanol. The product was recrystallised[§] by dissolving the precipitate in a minimum of THF and filtering of any undissolved substances. The filtrate was then divided in several portions. To each portion methanol was added dropwise until the product just started to precipitate. The precipitate was filtered off and washed with diethyl ether. The filtrate was collected and methanol was again added to repeat the process until filtrate was nearly clear. The precipitate was then air dried over night before dissolving it in DCM and removing solvents under reduced pressure. Yield **[23]**: 0.0916 g (0.046 mmole; 23.0 %) mp. 84-88 ^{o}C; λ_{max}/nm (THF) 696.5 and 727.5; δ_H($CDCl_3$, Spectrum A17) 7.87 (8H, s, Ar-H), 4.46 (16H, s, 8 x Ar-CH_2-), 2.10 (16H, m, 8 x –CH_2-), 1.25 (160H, m, 8 x –$(CH_2)_{10}$-), 0.85 (24H, t, 8 x –CH_3); ν_{max}/cm^{-1} (KBr, Spectrum B17) 3428 and 3295 (N-H).

4.4.3.5 [1,4,8,11,15,18,22,25-Octatridecylphthalocyanatomanganese(III)] chloride, Mn(Cl)Pc($C_{13}H_{27}$)$_8$ / Mn(OMe)Pc($C_{13}H_{27}$)$_8$ [24]

1-Butanol (2 ml) was brought to reflux under inert atmosphere before adding **[23]** (50.5 mg; 0.026 mmole) and stirring for 10 minutes to dissolve. $MnCl_2 \cdot 4H_2O$ (0.16 g; 0.81 mmole) was

then added to the reaction mixture and refluxed for 30 minutes. The reaction was checked with TLC and another 0.03 g of the manganese salt was added. The mixture was then refluxed for 48 hours after which it was cooled on an ice-bath. 20 ml of chilled H_2O was added to the mixture and stirred for15 minutes. The precipitate was filtered off and washed firstly with water and then methanol before air drying the product. Yield **[24]**: 0.0360 g (0.018 mmole; 69 %) mp. 45-47 ^oC; (Found: C, 76.70; H, 10.93; N, 4.69; O, not tested: Cl, 0.94; Mn, 2.20 %. [0.55 $Mn(Cl)Pc(C_{13}H_{27})_8 \cdot 5H_2O$: 0.45 $Mn(OMe)Pc(C_{13}H_{27})_8 \cdot 5H_2O$] ** requires: C, 76.23; H, 11.03; N, 5.21; O, 4.06; Cl, 0.91; Mn, 2.55 %); λ_{max}/nm (THF) 753; δ_H($CDCl_3$, Spectrum A18) No satisfactory integrals were obtained due to the peak broadening effect of the paramagnetic Mn(III) metal center.

4.4.3.6 1,4,8,11,15,18,22,25-Octatridecylphthalocyanatozinc(II), $ZnPc(C_{13}H_{27})_8$ [25]

1-Butanol (2 ml) was brought to reflux under inert atmosphere before adding **[23]** (18 mg; 0.009 mmole) and stirring for 10 minutes to dissolve. Anhydrous $ZnCl_2$ (0.12 g; 0.88 mmole) was then added to the reaction mixture and refluxed for 30 minutes. The mixture was then refluxed for 2 hours after which it was cooled on an ice-bath. 20 ml of chilled H_2O was added to the mixture and stirred for15 minutes. The precipitate was filtered off and washed firstly with water and then methanol before air drying the product. Yield **[25]**: 0.0183 g (8.99×10^{-3} mmole; 98 %); mp. 191-195 ^oC; λ_{max}/nm (THF) 700; δ_H($CDCl_3$, Spectrum A19) No satisfactory NMR integrals were obtained.

---

§ Due to difficulties that arose in the purification of the product on a silica column, the Pc was only recrystallised. It proved to be sufficient purification as theUV-VIS and proton NMR spectra showed **[23]** to be clean.

4.5 General catalysis procedures

For most catalytic oxidation reactions *trans*-stilbene was chosen as the model substrate. *trans*-Stilbene **[26]** is a white crystalline solid at room temperature and is therefore easy to handle. The oxidation products of *trans*-stilbene are also solids at room temperature and the presence of phenyl rings makes it easy to identify products by means of TLC. Other substrates that were also considered were 1-octene and 4-phenyl-1-butene. However, due to problems in isolating products and substrate impurities, they were used infrequently.

4.5.1 Asymmetric dihydroxylation with OsO_4 and N-oxides

Asymmetric dihydroxylation of alkenes were carried out under normal atmospheric conditions. NMO, polymer **[13]** and polymer **[14]** was used as oxidants. The substrate (0.56 mmole) and oxidant (0.83 mmole; 1.5 eq.) was mixed and dissolved in a two-phase mixture of *t*-butanol (15 ml) and water (15 ml). $K_2OsO_2(OH)_4$ (1 mole %, relative to substrate) was the added to the mixture and was stirred for 24 hours. The reaction mixture was quenched with a saturated $NaHSO_3$ solution (15 ml) by stirring for 15 minutes. The reaction mixture was then extracted with DCM (2 x 15 ml) and the organic phase washed with sat. $NaHSO_3$ (2 x 15 ml) and sat. NaCl (2 x 15 ml). After drying over $MgSO_4$, any products were purified by column chromatography.

** Due to possible axial ligand exchange and trapped solvents the expected elemental analysis for the pure compound, (C, 79.23; H, 10.95; N, 5.44; O, 0; Cl, 1.72; Mn, 2.66 %), had to be adjusted to explain the observed values, (see Chapter 3 section 3.3.3.4).

4.5.2 Epoxidation of alkenes with salen complexes and N-oxides

Epoxidation of alkenes were carried out under normal atmospheric conditions. The dry reagents were mixed in a flask before addition of solvents. 100 mg (0.56 mmole) of *trans*-stilbene was used as substrate, while 0.83 mmole (1.5 eq.) of oxidant was used; (a) NMO, (b) polymer **[13]** and (c) polymer **[14]**. The metal catalyst ([Mn(III)Salen]OAc **[18]** – 10.6 mg; or Co(II)Salen **[19]** – 9.1 mg) were used in catalytic amounts of 5 mole % relative to the substrate. After addition of solvent (dichloromethane, 10 ml) the reaction mixture was stirred for an initial 24 hours, checking reaction progress with TLC. An additional 0.40 mmole of oxidant was added after 24 hours to the reaction mixtures and the reaction mixtures was stirred for a further 24 hours. Any epoxides formed were identified by TLC and isolated. To isolate the products, the solvent was removed from the reaction mixture under reduced pressure. The residue was dissolved in ethyl acetate (30 ml) and washed with a saturated $NaHCO_3$ solution (3 x 15 ml). The organic phase was then washed with a saturated NaCl solution before drying over $MgSO_4$. The product epoxide, stilbene oxide, was then purified by column chromatography using 5 % ethyl acetate in n-hexane as eluent (R_f = 0.50 vs. 0.77 for *trans*-stilbene). Only the reaction involving [Mn(III)Salen]OAc **[18]** as catalyst and N-methylmorpholine-N-oxide as oxidant gave the epoxide in identifiable quantities. Yield *trans*-stilbene oxide: 0.0338 g (0.172 mmole; 30.7 %); mp. 68–69 ^{o}C; δ_H($CDCl_3$, Spectrum A20) 7.45-7.35 (10H, m, Ar-H), 3.88 (2H, m, 2 x -(CH)-O-); ν_{max}/cm^{-1} (Spectrum B21) 3063 + 3035 (C-H alkane), 2990 (C-H arene), 1501 (C=C), 696 (C-H bending).

4.5.3 Epoxidation of alkenes with metallo-porphyrins and N-oxides

Epoxidation of alkenes were carried out under normal atmospheric conditions. The dry reagents were mixed in a flask before addition of solvents. 100 mg (0.56 mmole) of *trans*-stilbene was used as substrate, while 0.83 mmole (1.5 eq.) of oxidant (NMO, polymer **[13]** or polymer **[14]**)

was used. Co(II)TPP, **[16]**, were used in catalytic amounts of 1.57 mole % (5.9 mg) relative to the substrate. After addition of solvent (dichloromethane, 10 ml) the reaction mixture was stirred for an initial 24 hours, checking reaction progress with TLC. An additional 0.40 mmole of oxidant was added after 24 hours to the reaction mixtures and the reaction mixtures was stirred for a further 24 hours. No identifiable product formation was evident on TLC for neither the reactions with NMO nor the reactions with polymers **[13]** and **[14]**.

In addition, reactions using molecular oxygen as oxidant[10] were also carried out using 100 mg (0.56 mmole) substrate, isobutylaldehyde (2.8 mmole) and 5.9 mg (1.57 mole %) of catalyst dissolved in dichloromethane (10 ml). The reaction mixture was vigourously stirred under O_2 atmosphere for 3 days at room temperature, checking progress with TLC. However, again no other fraction except that of the substrate was visible on TLC (5 % ethyl acetate in hexane).

4.5.4 Epoxidation of alkenes with phthalocyanine-complexes using molecular oxygen as oxidant

Trans-stilbene (100 mg, 0.56 mmole), isobutylaldehyde (2.8 mmole; 1:5 substrate-aldehyde ratio) and phthalocyanine catalysts **[24]** (2.8 mg; 0.25 mole %) dissolved in dichloromethane was vigorously stirred under O_2 atmosphere at room temperature for 48 hours, checking reaction progress with TLC. After 72 hours of reaction, TLC showed no increase in product formation. The solvent was removed from the reaction mixture under reduced pressure. The residue was dissolved in ethyl acetate (30 ml) and washed with a saturated $NaHCO_3$ solution (3 x 15 ml). The organic phase was then washed with a saturated NaCl solution before drying over $MgSO_4$. The product, stilbene oxide, was then purified by column chromatography using 5 % ethyl acetate in n-hexane as eluent (R_f = 0.50 vs. 0.77 for *trans*-stilbene). Yield *trans*-stilbene oxide: 0.0186 g (0.095 mmole; 17 %); mp. 68–69 ^oC; δ_H($CDCl_3$, Spectrum A20) 7.45-7.35 (10H, m, Ar-H), 3.88

(2H, m, 2 x -(C<u>H</u>)-O-); ν_{max}/cm^{-1} (Spectrum B21) 3063 + 3035 (C-H alkane), 2990 (C-H arene), 1501 (C=C), 696 (C-H bending).

4.6 References

[1] G. Gritzner and J. Kuta, *J. Pure Appl. Chem.*, **56**, 461 (1984)

[2] A. Auger, A.J Muller and J.C. Swarts, *Dalton Transactions*, 3623 (2007)

[3] a) D.H. Evans, K.M. O'Connell, R.A. Peterson and M.J. Kelly, *J. Chem. Educ.*, **60**, 291(1983);

b) P.T. Kissinger and W.R. Heineman, *J. Chem. Educ.*, **60**, 702 (1983);

c) J.J. Van Benshoten, J. Y. Lewis and W. R. Heineman, *J. Chem. Educ.*, **60**, 772 (1983);

d) G.A. Mobbot, *J. Chem. Educ.*, **60**, 697 (1983).

[4] A.D. Adler, *J. Org. Chem.*, **32**, 476 (1967)

[5] A.D. Adler, F.R. Longo, F. Kampas and J. Kim, *J. Inorg. Nucl. Chem.*, **32**, 2443 (1970)

[6] A. Dhakshinamoorthy and K. Pitchumani, *Tetrahedron*, **62**, 9911 (2006)

[7] P.G. Cozzi, *Chem. Soc. Rev.*, **33**, 410–421 (2004)

[8] O. Pouralimardan, A. Chamayou, C. Janiak and H. Hosseini-Monfered, *Inorganica Chimica Acta,* **360**, 1599–1608 (2007)

[9] S.E Schaus, B.S. Brandes, J.F. Larrow, M. Tokunaga, K.B. Hansen, A.E Gould, M.E. Furrow and E.N. Jacobsen, *J. Am. Chem. Soc.*, **124**, 1307–1315, (2002)

[10] X. Zhou, H. Ji, J. Xu, Li. Pei, L. Wang and X. Yao, Tetrahedron Letters, **48**, 2691–2695 (2007)

5 CONCLUSIONS AND FUTURE PERSPECTIVES

In this study, the morpholine-containing homo-polymers poly-α,β-D,L-[N-(3-morpholinopropyl)] aspartamide and poly[N-(morpholinomethylene)]ethylene oxide were successfully synthesised by nucleophilic attack with 3-amminopropyl-N-morpholine on polysuccinimide, and by substitution of chlorine with morpholine in polyepichlorohydrin respectively. These polymers were then both successfully oxidized by hydrogen peroxide to form the new polymers poly[N-(morpholinomethylene)-N-oxide]ethylene oxide and poly-α,β-D,L-[N-(3-morpholinopropyl)-N-oxide]aspartamide. Though originally the polysuccinimide derivative and polyepichlorohydrin derivative were intended for use in polar and non-polar media respectively, both polymers were eventually soluble and used in aqueous media. The polar character of the N-oxide functionality overwhelmed the non-polar character of the polyepichlorohydrin polymer backbone with increased N-oxide content. By lowering the amount of hydrogen peroxide used in the oxidation of poly[N-(morpholinomethylene)]ethylene oxide, as well as reducing the reaction time, it is possible to control the N-oxide content of poly[N-(morpholinomethylene)-N-oxide]ethylene oxide. Although this decreases the amount of N-oxide funtionalities in the polymer as oxygen scource in alkene oxidation reactions, it did lead to polymers that were soluble mainly in organic media. It was also shown that ^{1}H NMR proved a useful method in the characterization of the synthesised polymers.

1,4,8,11,15,18,22,25-Octatridecylphthalocyanine (2HPc-$(C_{13}H_{27})_8$) was successfully synthesized through tetramerization of 3,6-tridecylphthalonitrile. To prepare the 3,6-tridecylphthalonitrile precursor, thiophene was first dialkylated by tridecylbromide to give 2,5-tridecylthiophene. The oxidation of 2,5-tridecylthiophene was achieved using *in situ* prepared dimethyldioxirane as the

preferred oxidant. The oxidants $NaBO_3$ or *m*-chloroperbenzoic acid were not considered for this chemical oxidation because their effectiveness were previously shown to decrease on the oxidation of longer-chain substituted thiophenes.

The complexation of manganese with the C_{13} phthalocyanine was achieved succsessfully after optimization of reaction conditions. Elemental analysis of the manganese phthalocyanine showed that axial chloride ligand exchange with solvent molecules (MeOH) took place. Complexation of zinc with the synthesized C_{13} phthalocyanine was achieved relatively easy and in good yields. Both the manganese and zinc phthalocynines showed characteristic metalated phthalocyanine UV/Vis spectra. The Q-band peak maximum of the manganese complex was substantialy red shifted while that of the zinc complex was blue shifted compared to that of the metal-free phthalocyanine.

Although the metal-free and zinc C_{13} phthalocyanines did possess mesophases, the temperature range of the mesophases were lower than the related C_{12} and C_{15} phthalocyanines. 2HPc-$(C_{13}H_{27})_8$ had a liquid crystal temperature range of 12.4 ^oC while ZnPc-$(C_{13}H_{27})_8$ had a range of 83 ^oC. The manganese C_{13} derivative did not show any mesophases. Electrochemistry of the metal-free and zinc C_{13} phthalocyanines in CH_2Cl_2 showed similar behaviour to related long-chain phthalocynines. Two ring-based oxidations were observed in the metal-free phthalocyanine's CV at 0.344 V and 0.724 V versus Ag/Ag^+ at 100 mV/s. Two ring-based reductions were also observed at -1.316 V and -1.656 V. The zinc derivative also showed two ring-based oxidations at 0.188 V and 0.836 V; and two ring-based reductions at -1.534 V and -1.930 V. Only one ring-based reduction at -1.602 V was observed for the manganese derivative while two ring-based oxidations at 0.596 V and 1.104 V were observed. The Mn derivative also showed one metal centered oxidation at 0.824 V and two metal centered reductions at -0.660 V

and 0.742 V. The two reductions were present because a mixture of chloride and methoxide was present as axial ligands on the central manganese atom.

The oxidation capability of the novel homo-polymers poly-α,β-D,L-[N-(3-morpholinopropyl)] aspartamide and poly[N-(morpholinomethylene)]ethylene oxide were tested by reacting them with trans-stilbene using potassium osmate, cobalt tetraphenylporphyrin, cobalt salen and manganese salen as co-catalysts. None of the reactions imploying the polymers showed any sign of substrate oxidation, while epoxidation using N-methylmorpholine-N-oxide as oxidant and the manganese salen catalyst showed moderate success. MnPc-$(C_{13}H_{27})_8$ was also used as catalyst in the O_2 induced epoxidation of trans-stilbene and successfully produced the epoxide in low yields.

Perspectives for future studies are varied. Further investigation into the availability of the N-oxide oxygen for substrate oxidation is required as well as the determination of optimum solvent systems for use with the polymers. Since both polymers are water soluble, investigation into heterogeneous oxidation systems might prove fruitfull. The use of more rigid polymeric support or ceramics could improve stability and substrate accessibility.

By replacing manganese in the phthalocyanine with metals such as cobalt or ruthenium, which have proven catalytic oxidation abilities, the catalytic performance of the phthalocyanine complex could be influenced. Other metals such as iridium, rhodium, or aluminium, might prove usefull in different types of catalytic reactions other than oxidation, for example C-C bond formation or hydroformylation. Investigation into the influence of the alkyl substituents on oxidation is also a possibilty. Alternatively, electron-rich porphyrins could be investigated in alkene oxidation reactions.

The electrochemistry of manganese phthalocyanines may be tuned by varying the chain length, as well as the group electronegativity of the phthalocyanines subtituents as well as the type of axial ligand. For example, by replacing the long-chain alkyl substituents of the phthalocyanine with more electronegative groups, like pentafluoro phenyl, the central metal may become more activated towards catalysts and become more difficult to oxidize. Also, the effect of substituting different metallocenes on the phthalocyanine could open up other applications for these hetero-metal complexes and may greatly influence the electrochemical-, liquid crystal- and photochemical behaviour of the metalated phthalocyanines.

Appendix A

^{1}H NMR Spectra

Spectrum A1: Polysuccinimide, (PSI), [8]

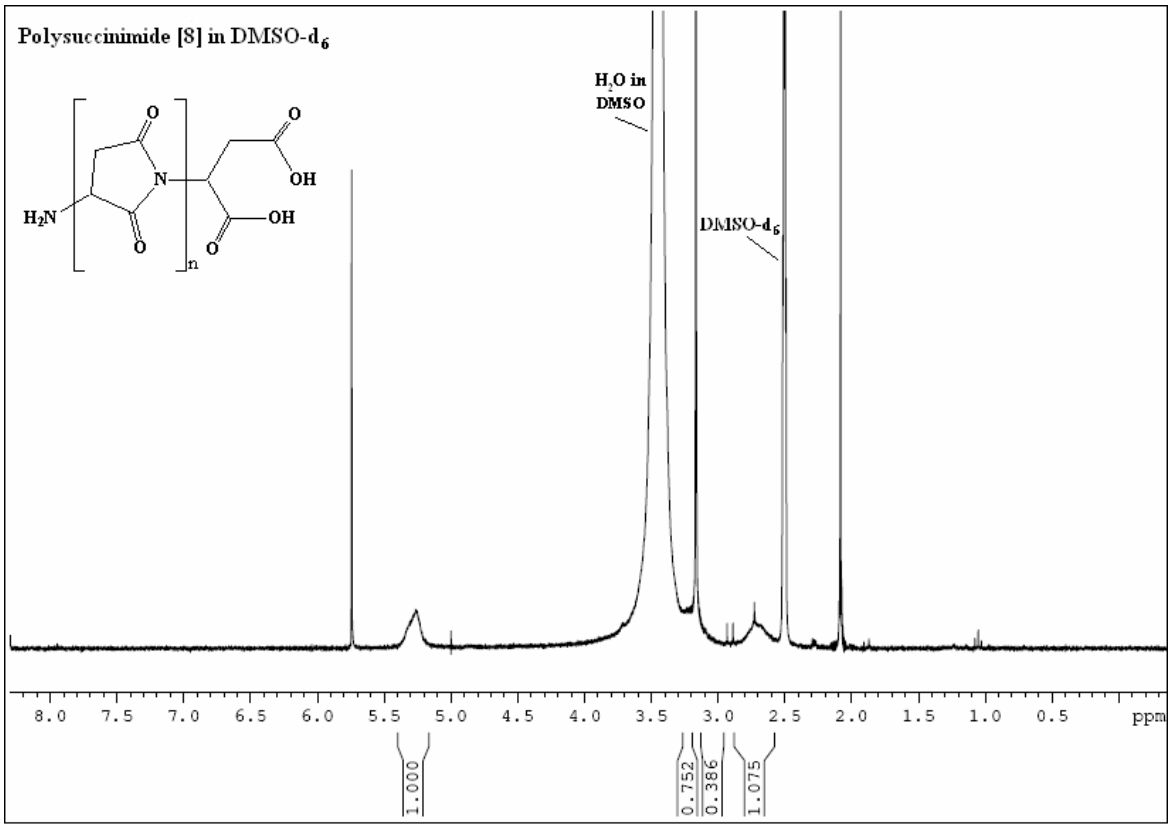

Spectrum A2: Poly-α,β-D,L-[N-(3-morpholinopropyl)]aspartamide, [10]

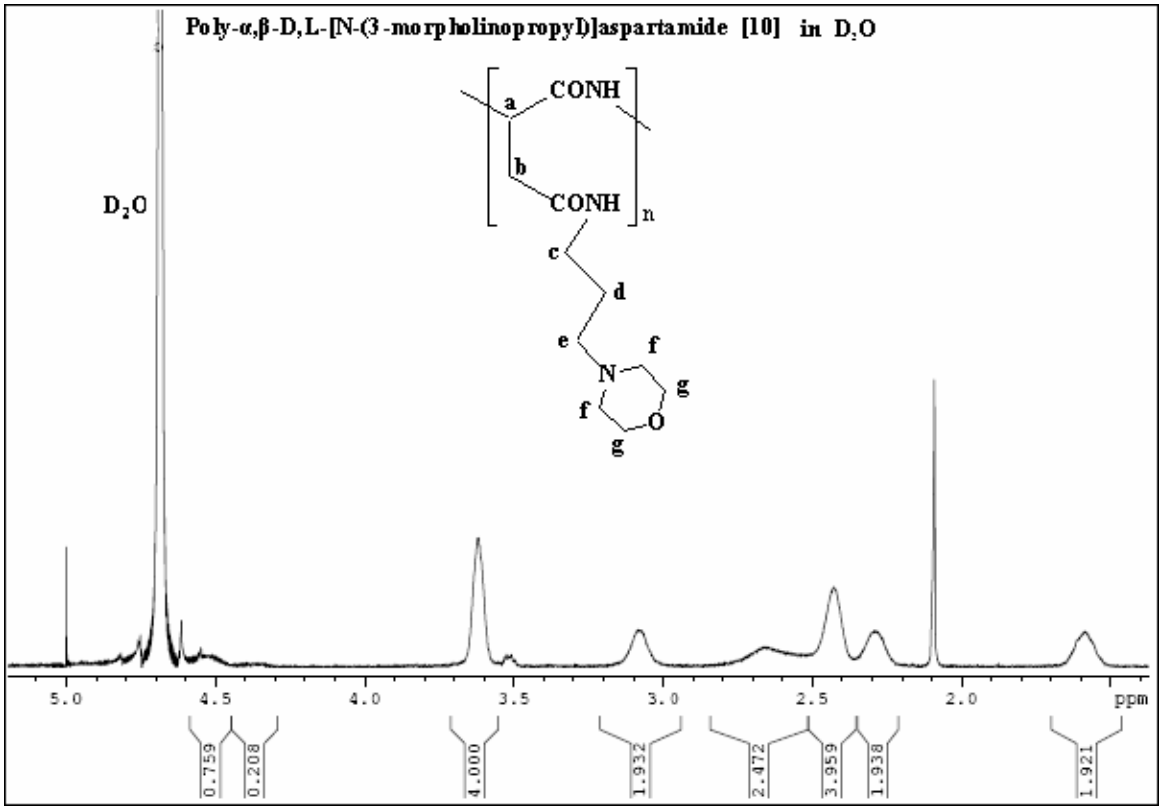

Spectrum A3: Poly-α,β-D,L-[N-(3-morpholinopropyl)-N-oxide]aspartamide, [13]

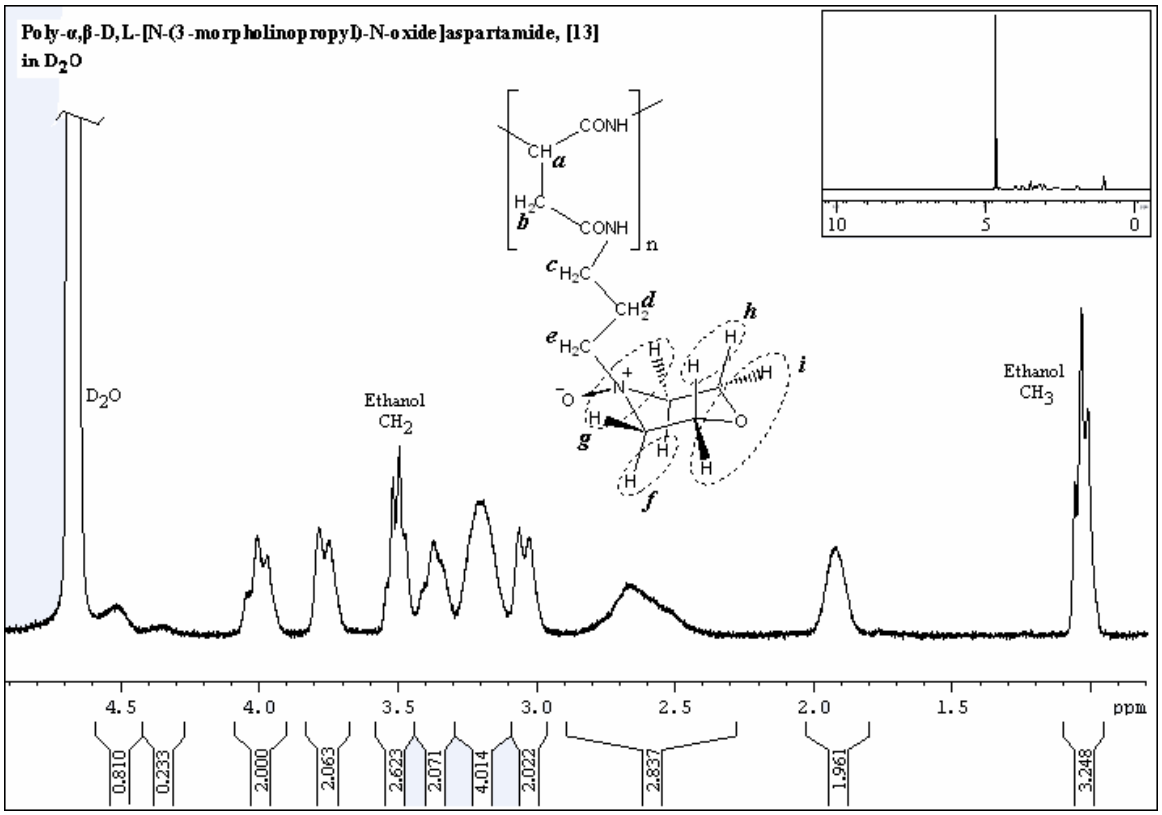

Spectrum A4: Polyepichlorohydrin, PECH [6]

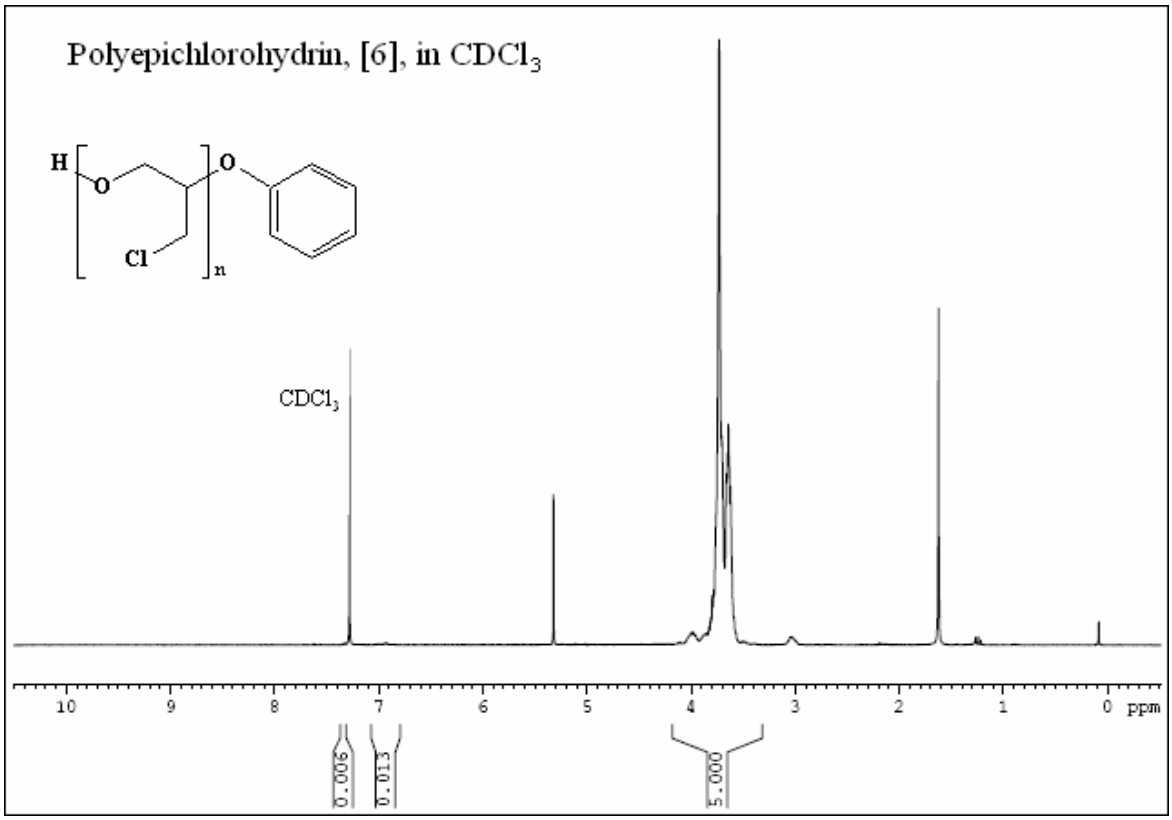

Spectrum A5: Poly[N-(morpholinomethylene)]ethylene oxide, [12] – Method 1

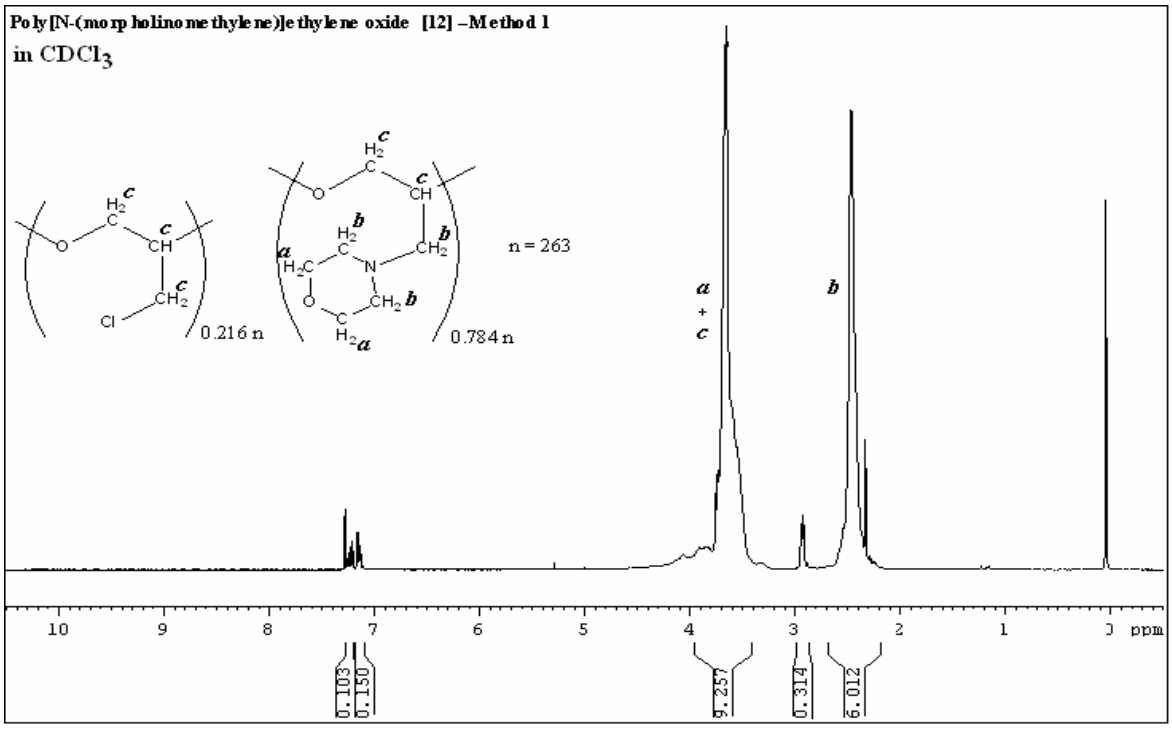

Spectrum A6: Poly[N-(morpholinomethylene)]ethylene oxide, [12] – Method 2

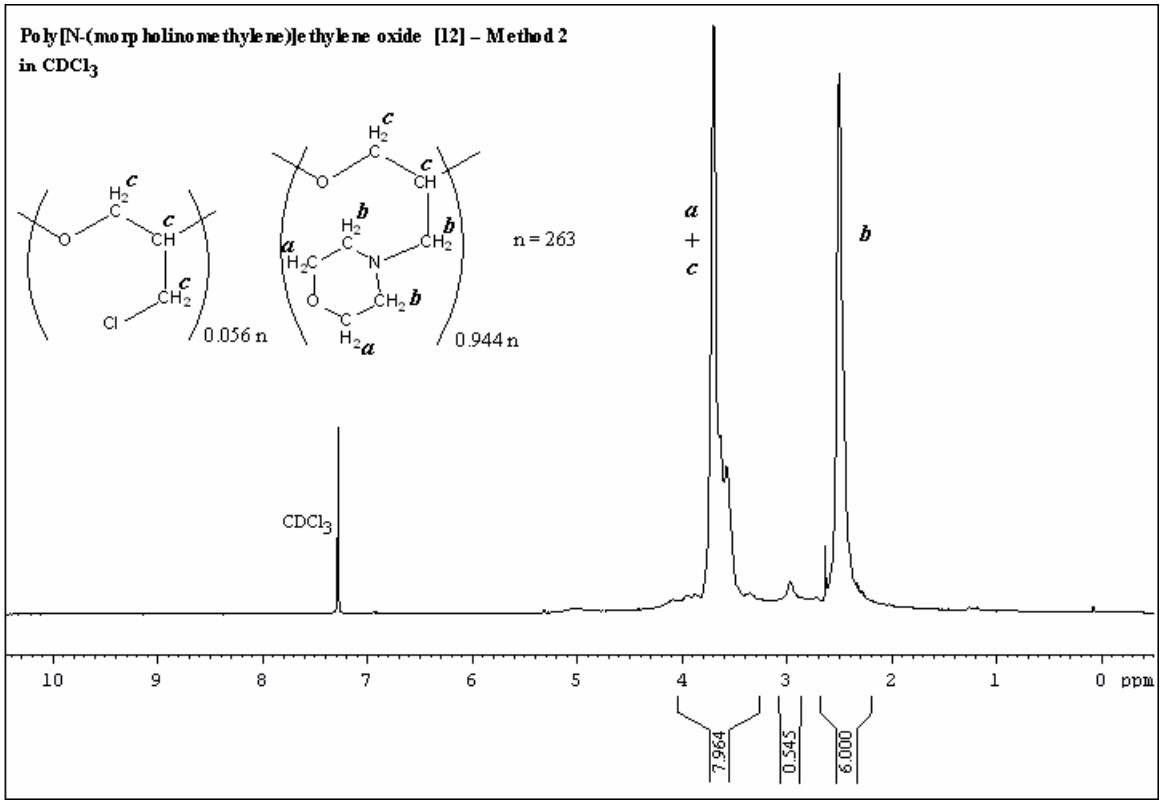

Spectrum A7: Poly[N-(morpholinomethylene)-N-oxide]ethylene oxide, [14], (incomplete oxidation).

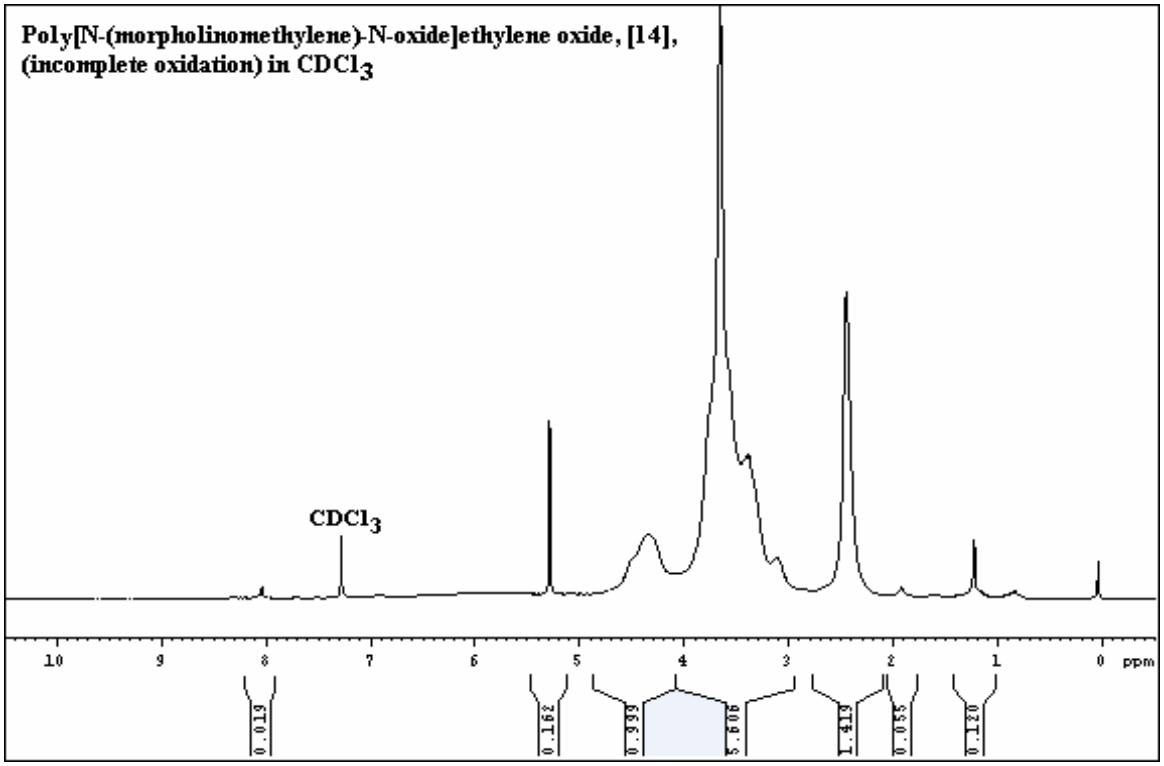

Spectrum A8: Poly[N-(morpholinomethylene)-N-oxide]ethylene oxide, [14], (complete oxidation).

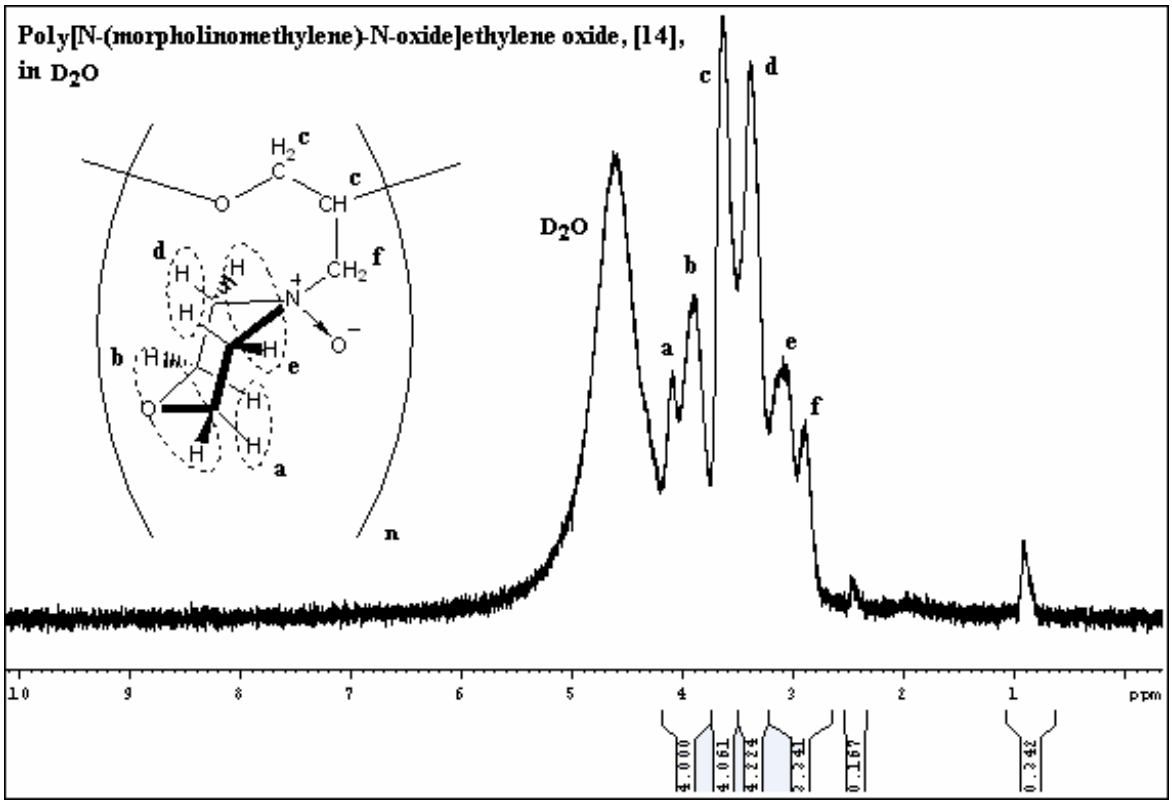

Spectrum A9: *meso*-Tetraphenylporphyrin, $C_{44}H_{30}N_4$, [15]

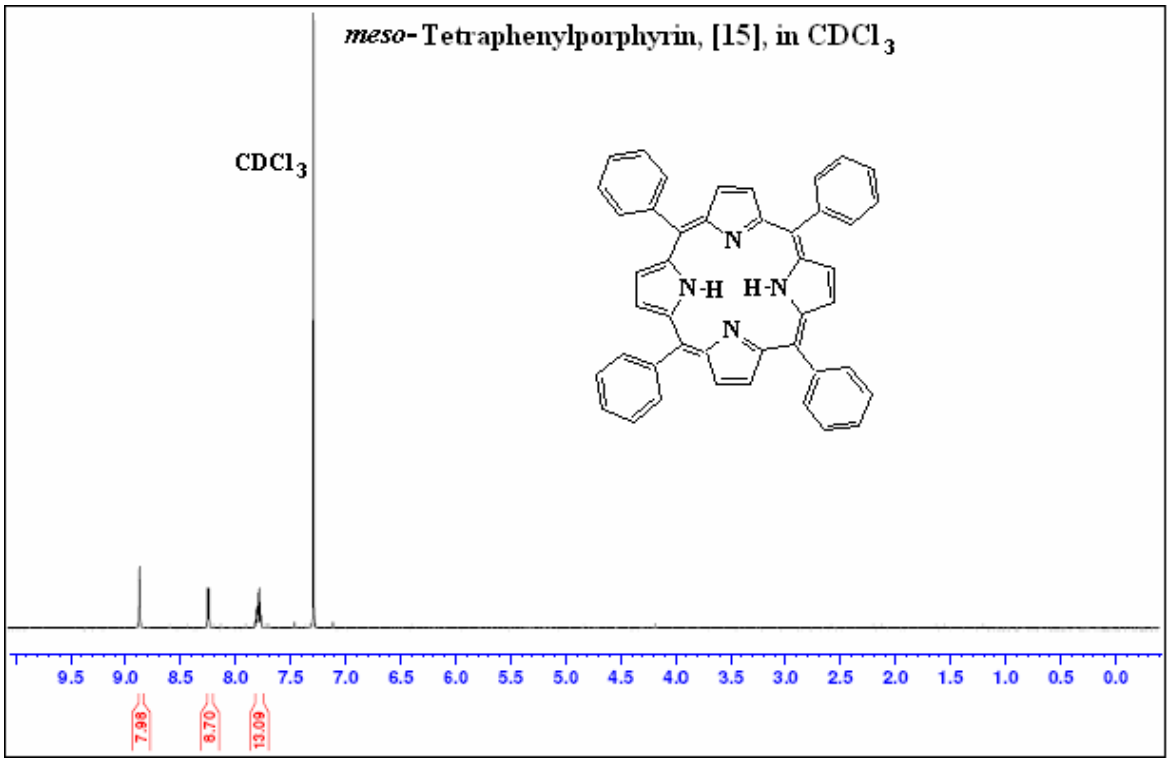

Spectrum A10: Tetraphenylporhyrinatocobalt(II), $C_{44}H_{28}N_4Co$, [16]

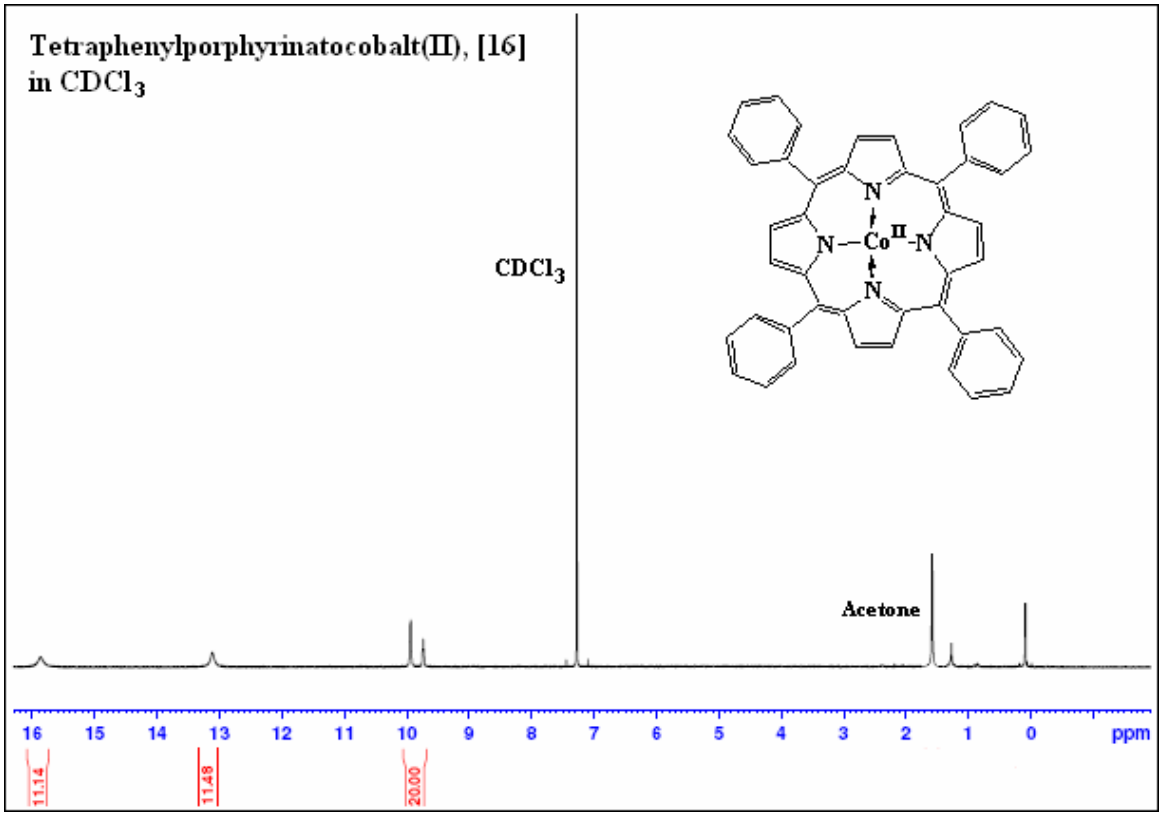

Spectrum A11: Bis(salicylidene)ethylenediamine, $C_{16}H_{16}N_2O_2$, [17]

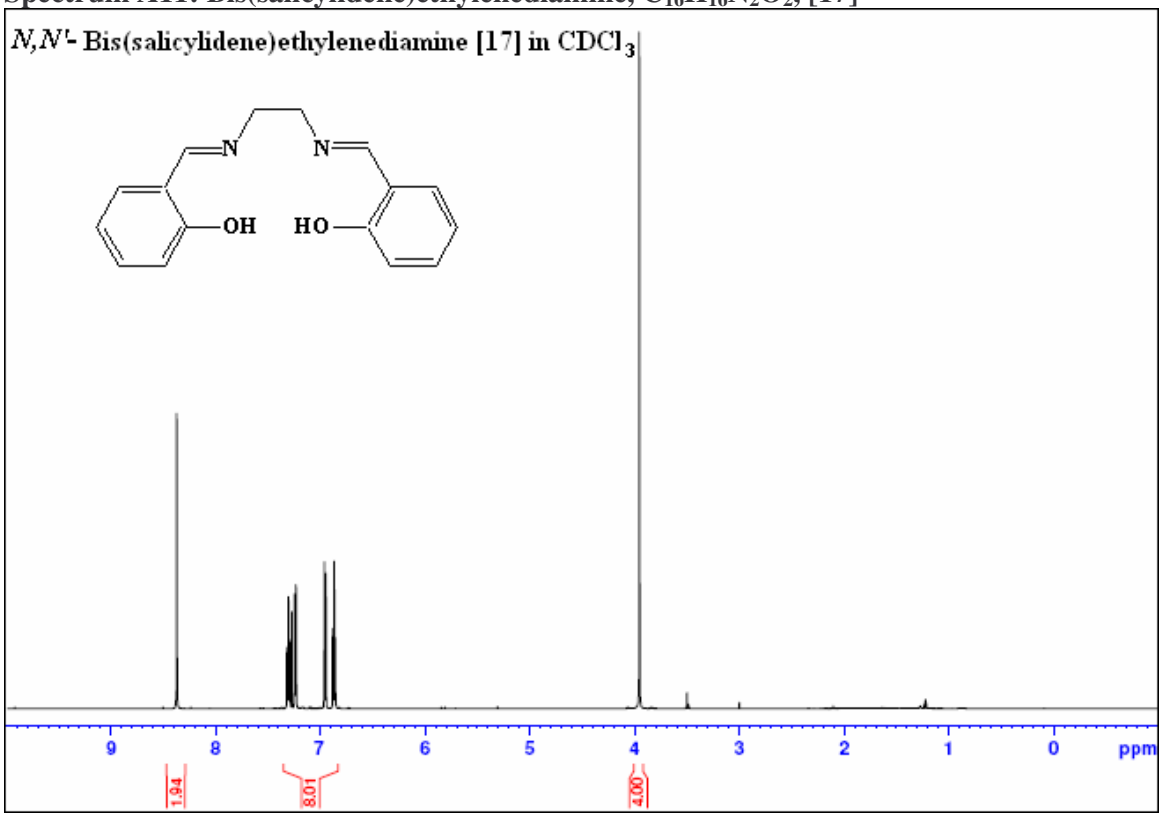

Spectrum A12: *N,N'*-Bis(salicylidene)ethylenediaminomanganese(III) acetate, $C_{18}H_{17}N_2O_4Mn$, [18]

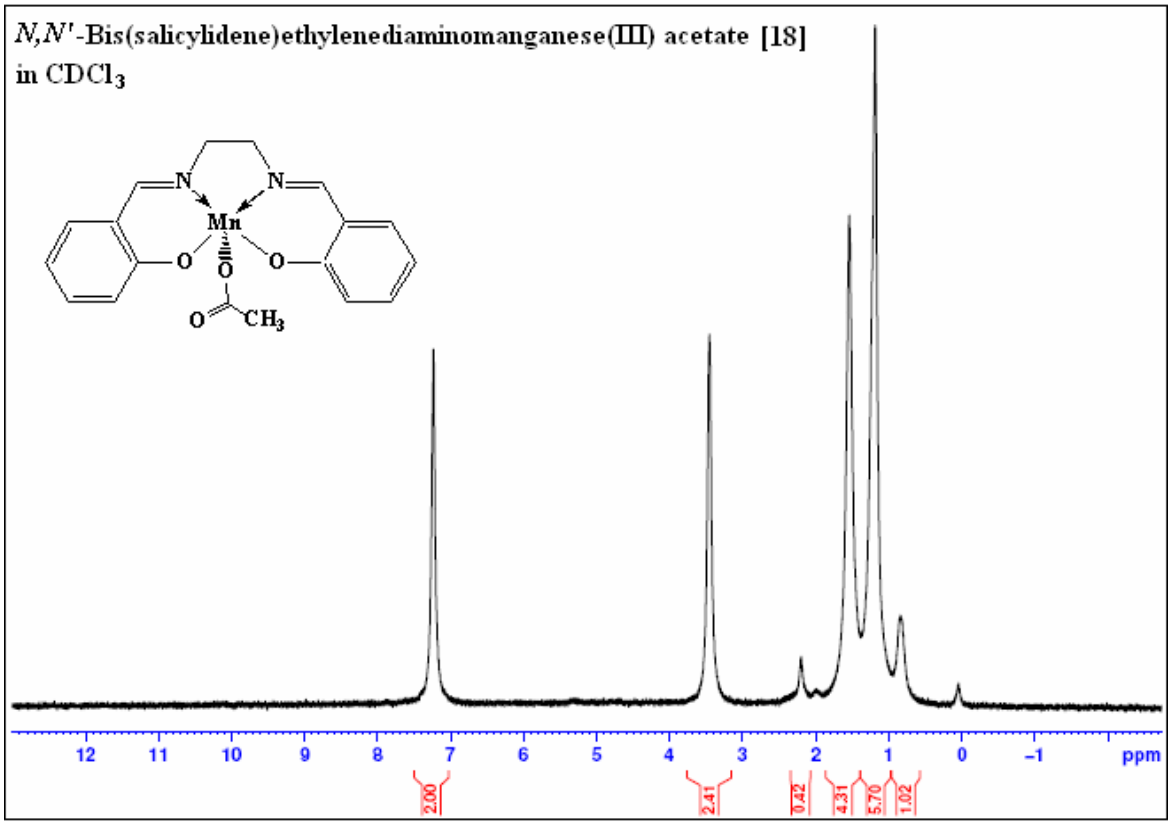

Spectrum A13: *N,N'*-Bis(salicylidene)ethylenediaminocobalt(II), $C_{16}H_{14}N_2O_2Co$, [19]

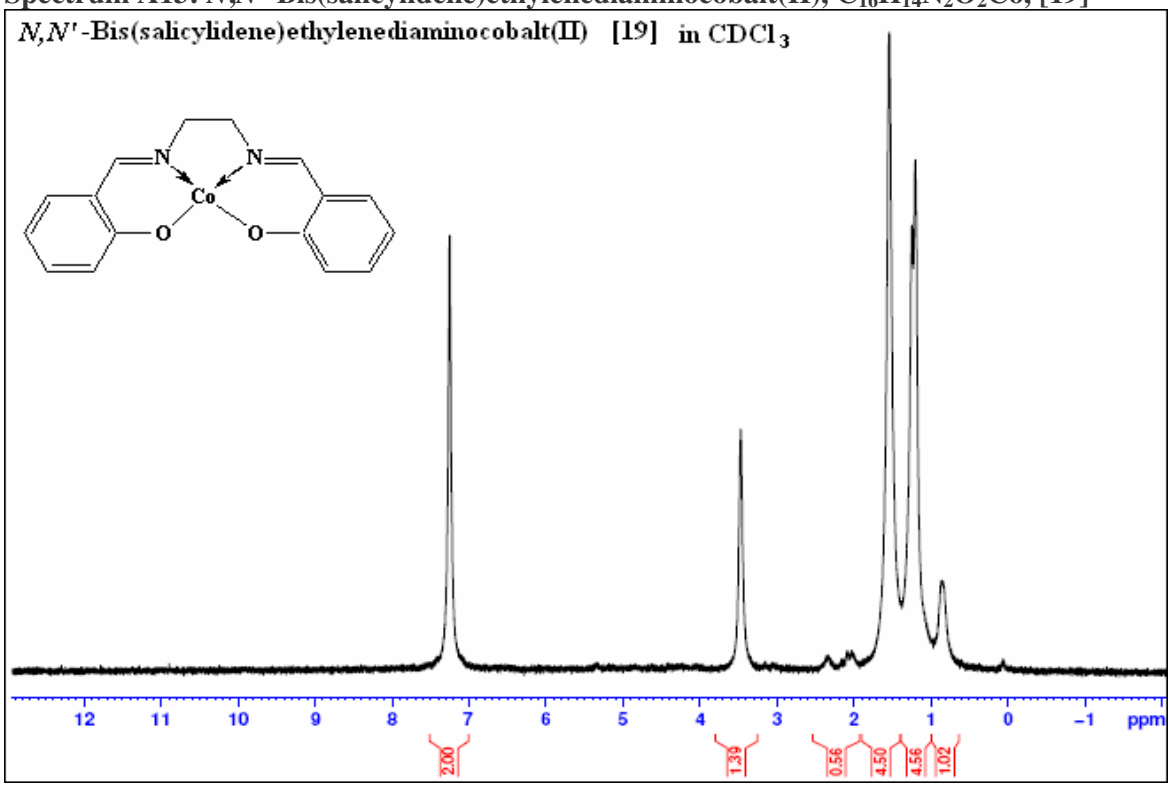

Spectrum A14: 2,5-Tridecylthiophene, $C_{30}H_{56}S$, [20]

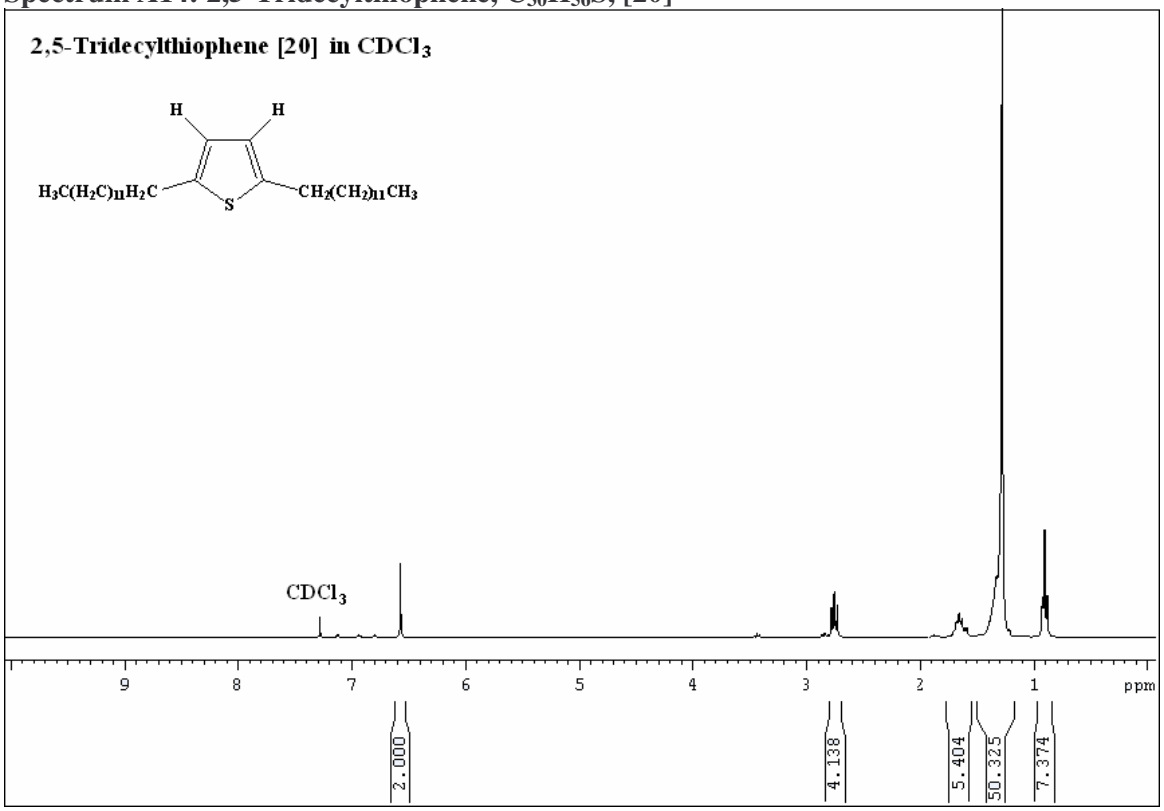

Spectrum A15: 2,5-Tridecylthiophenesulfone, $C_{30}H_{56}O_2S$, [21]

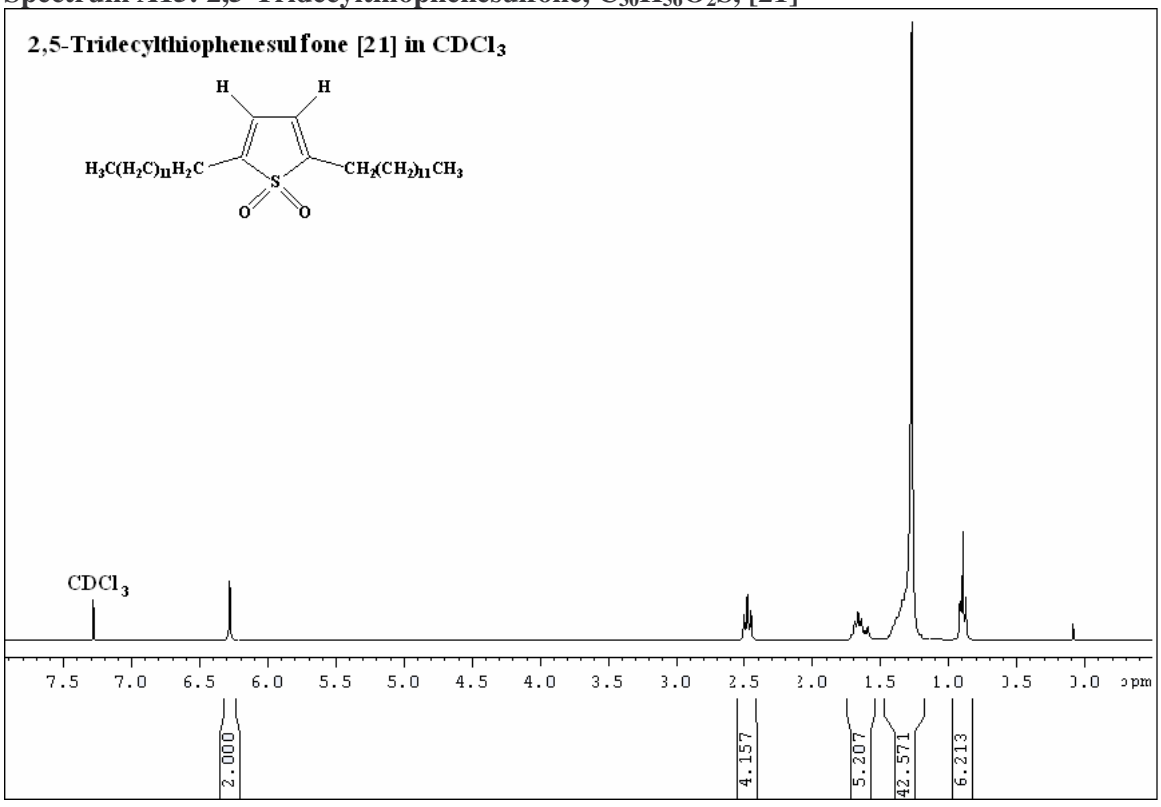

Spectrum A16: 3,6-Tridecylphthalonitrile, $C_{34}H_{56}N_2$, [22]

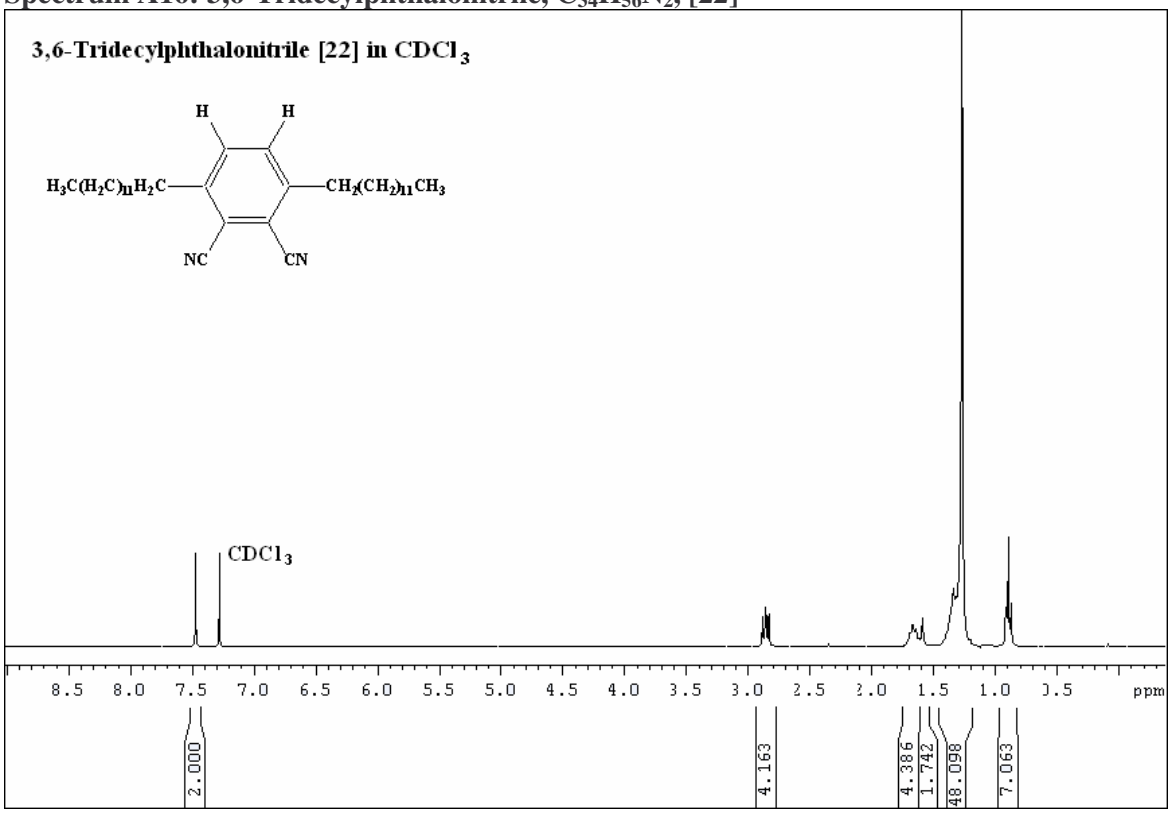

Spectrum A17: 1,4,8,11,15,18,22,25-Octatridecylphthalocyanine, $C_{136}H_{226}N_8$, [23]

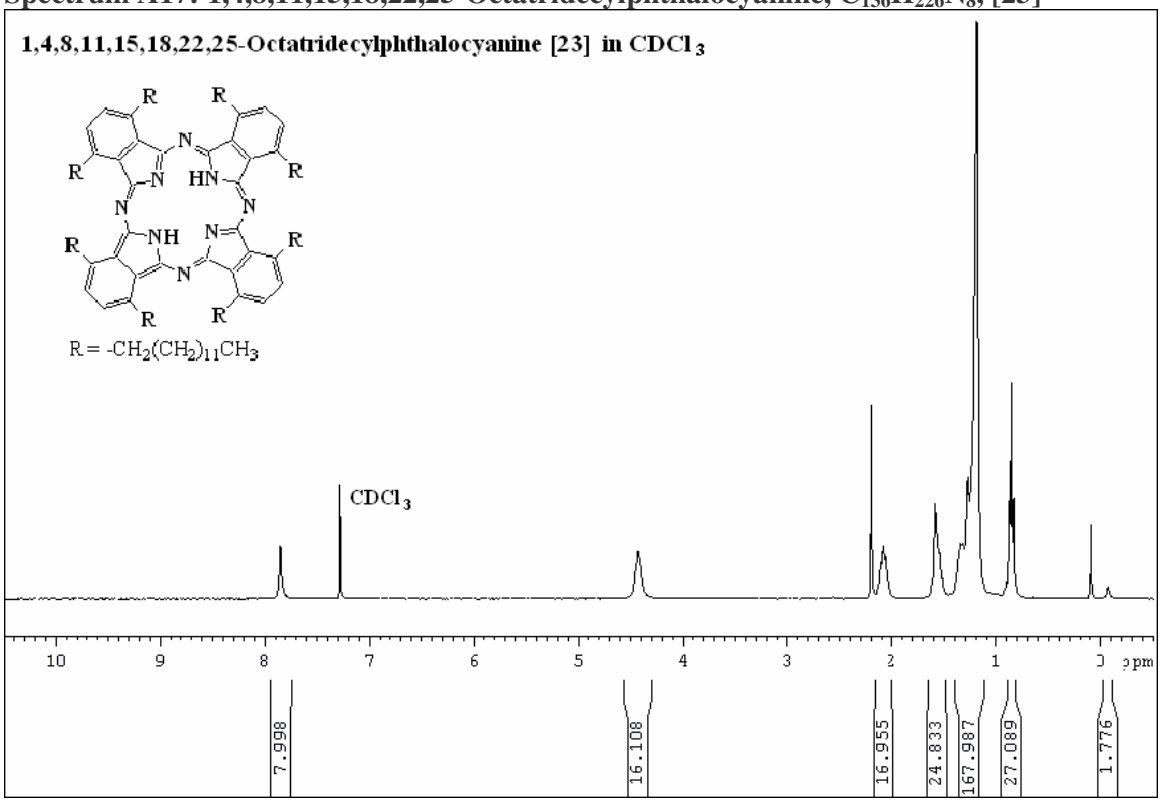

Spectrum A18: [1,4,8,11,15,18,22,25-Octatridecylphthalocyanatomanganese(III)] Chloride, 0.55:0.45 Mn(Cl)Pc($C_{13}H_{27}$)$_8$·5H_2O / Mn(OMe)Pc($C_{13}H_{27}$)$_8$·5H_2O, [24]

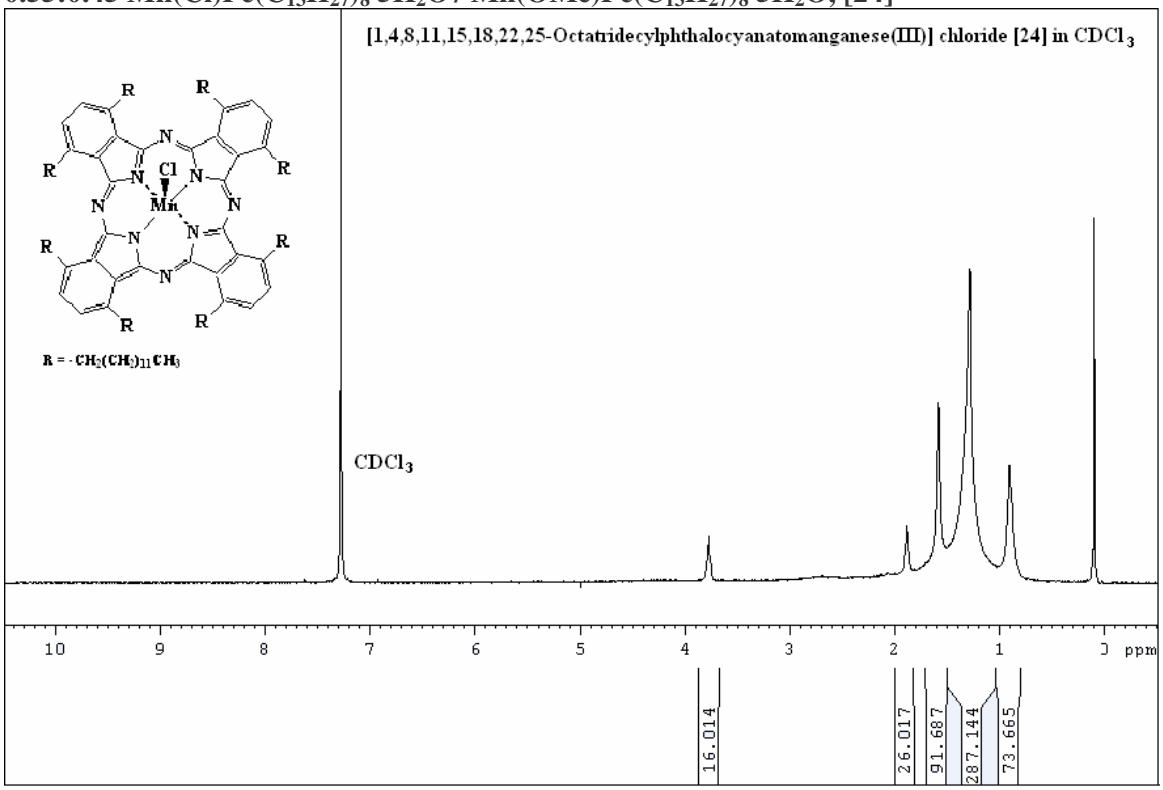

Spectrum A19: 1,4,8,11,15,18,22,25-Octatridecylphthalocyanatozinc(II), ZnPc($C_{13}H_{27}$)$_8$, [25]

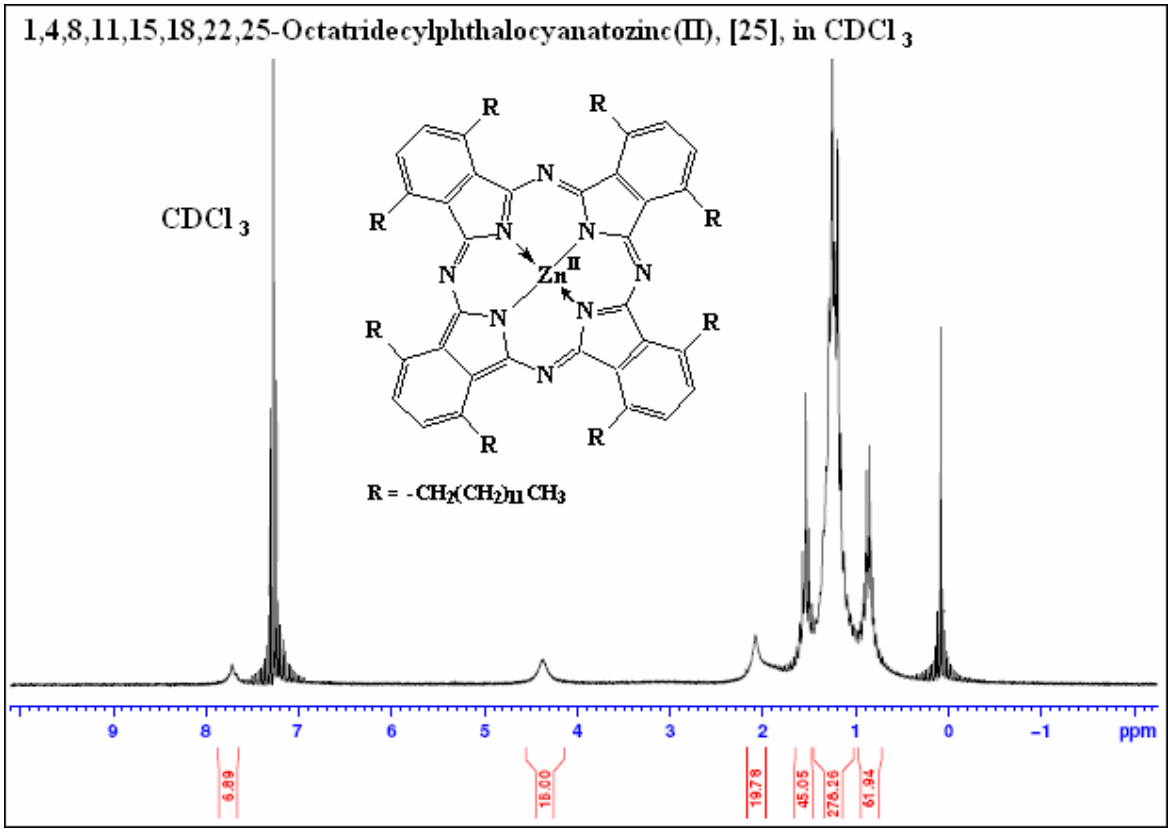

Spectrum A20: *trans*-Stilbene oxide

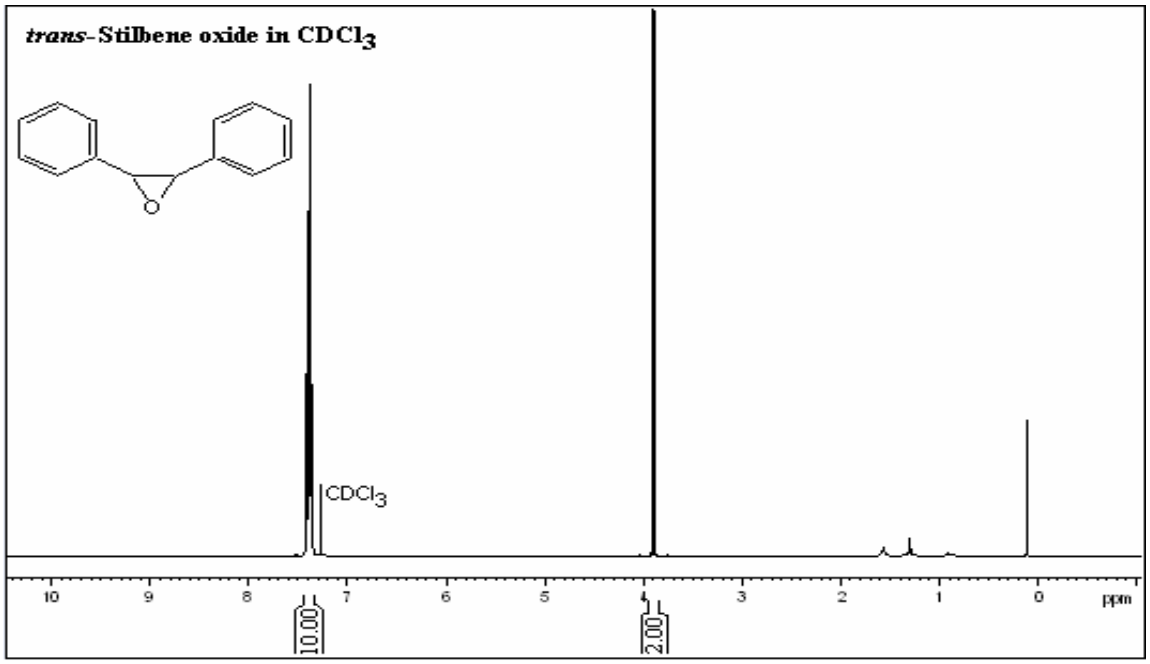

Appendix B

FT-IR Spectra

Infra-red spectra of synthesized compounds given as wavenumber (cm^{-1}), x, vs. transmittance, y.

Spectrum B1: Polysuccinimide, (PSI), [8]

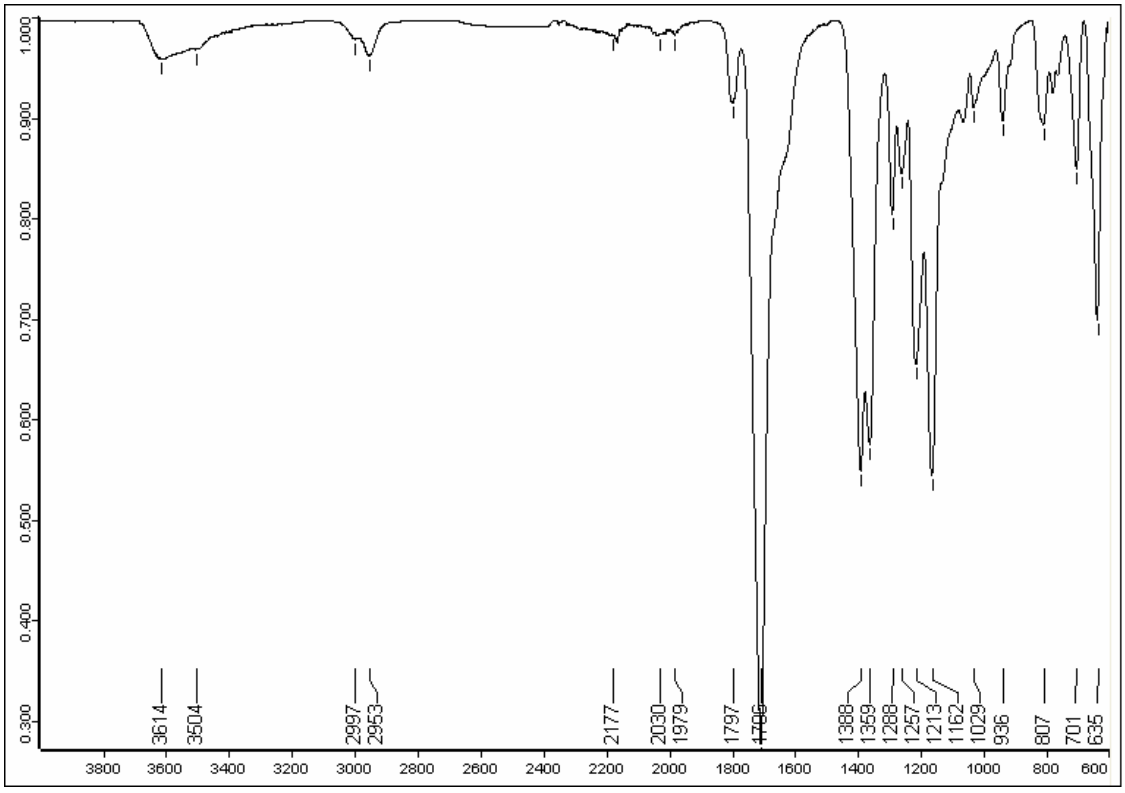

Spectrum B2: Poly-α,β-D,L-[N-(3-morpholinopropyl)]aspartamide, [10]

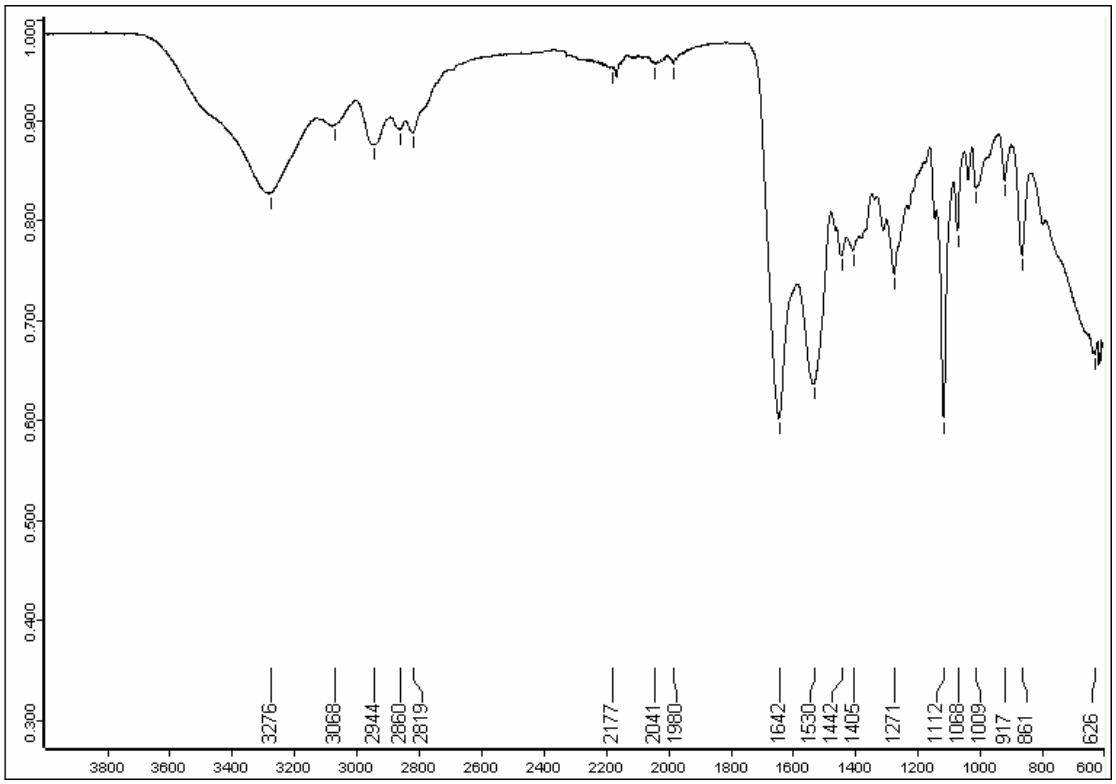

Spectrum B3: Poly-α,β-D,L-[N-(3-morpholinopropyl)-N-oxide]aspartamide, [13]

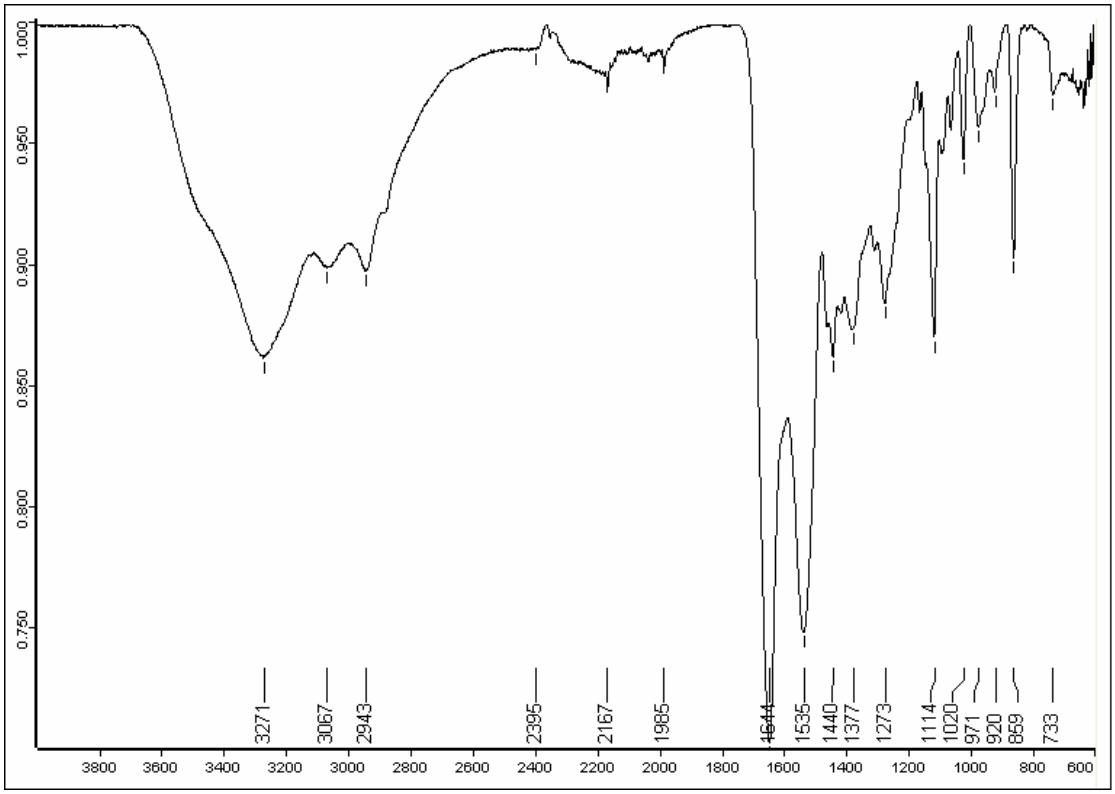

Spectrum B4: Polyepichlorohydrin, PECH [6]

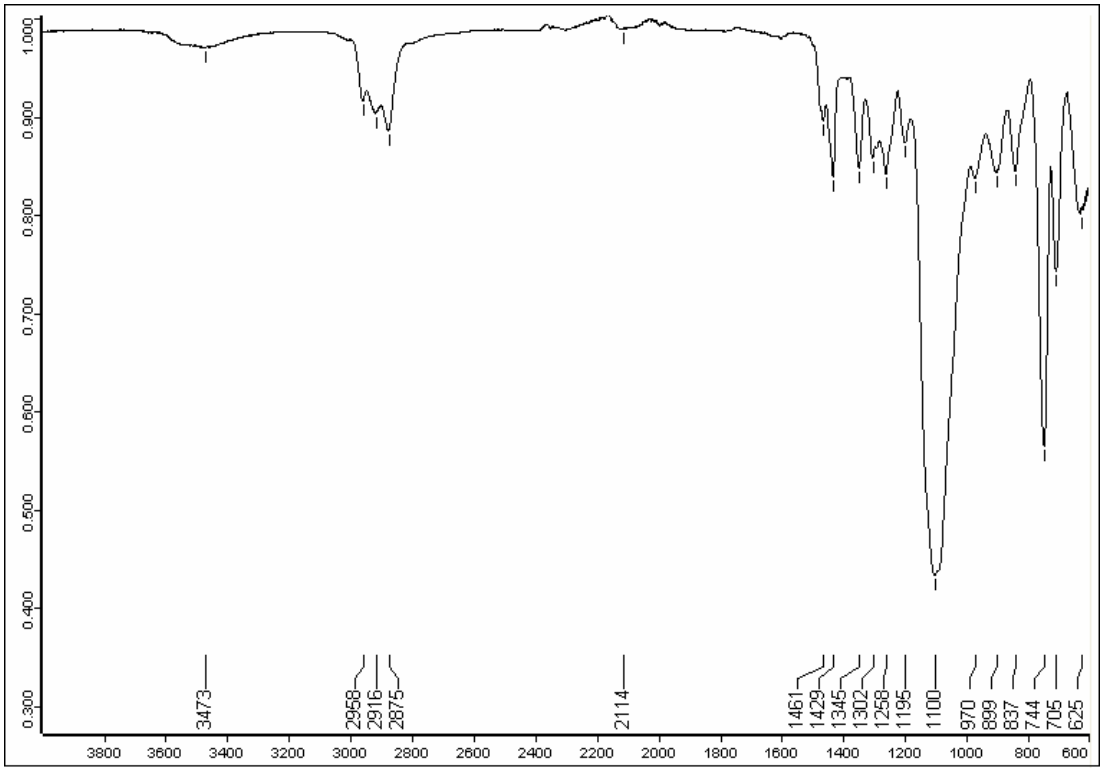

Spectrum B5: Poly[N-(morpholinomethylene)]ethylene oxide, [12] –Method 1

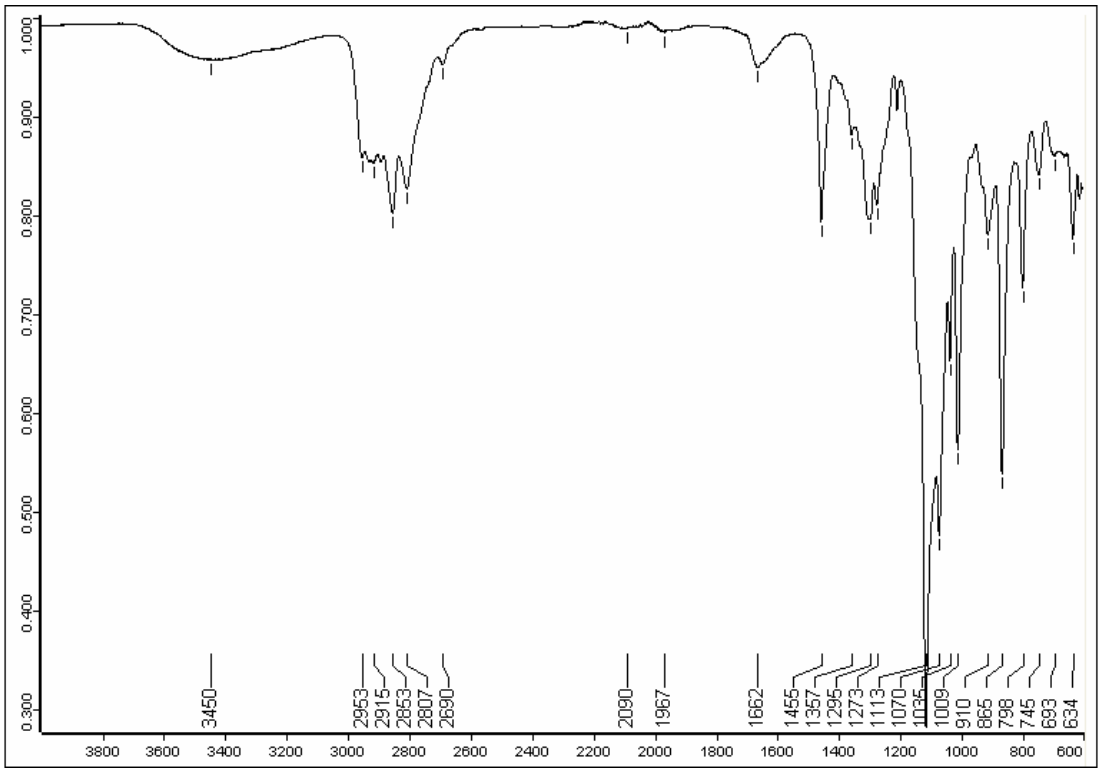

Spectrum B6: Poly[N-(morpholinomethylene)]ethylene oxide, [12] –Method 2

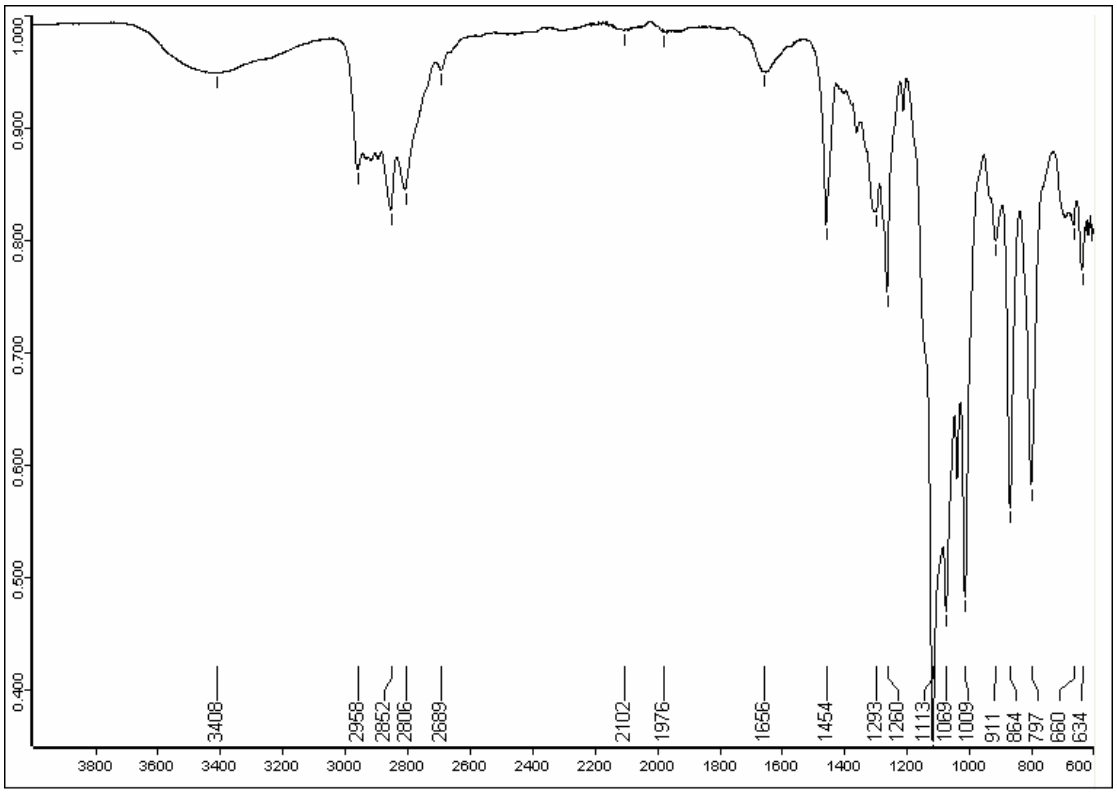

Spectrum B7: Poly[N-(morpholinomethylene)-N-oxide]ethylene oxide, [14], (incomplete oxidation).

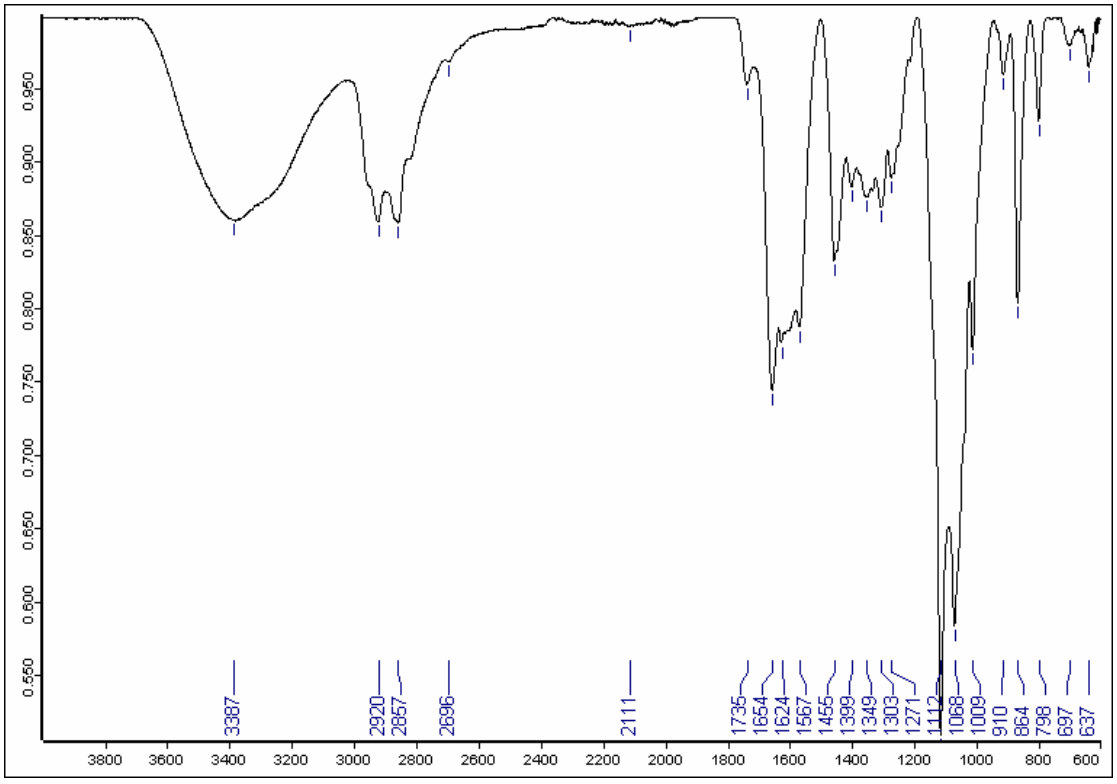

Spectrum B8: Poly[N-(morpholinomethylene)-N-oxide]ethylene oxide, [14], (complete oxidation).

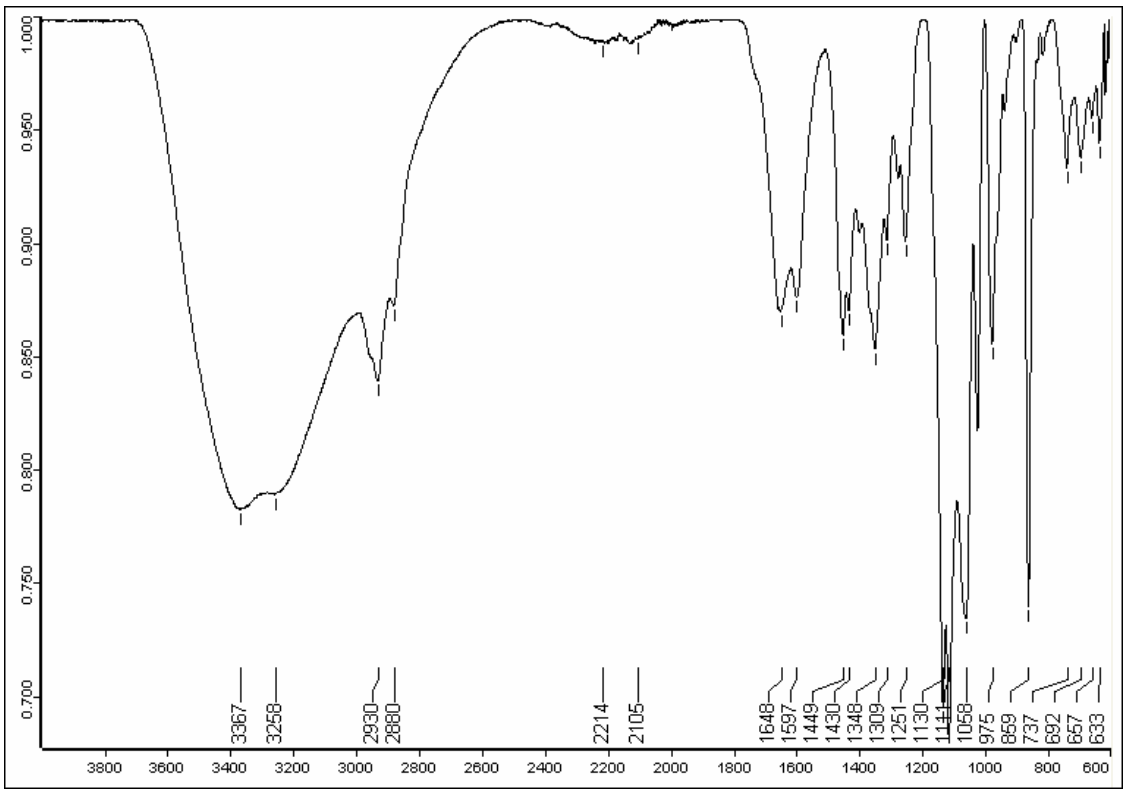

Spectrum B9: *meso*-Tetraphenylporphyrin, $C_{44}H_{30}N_4$, [15]

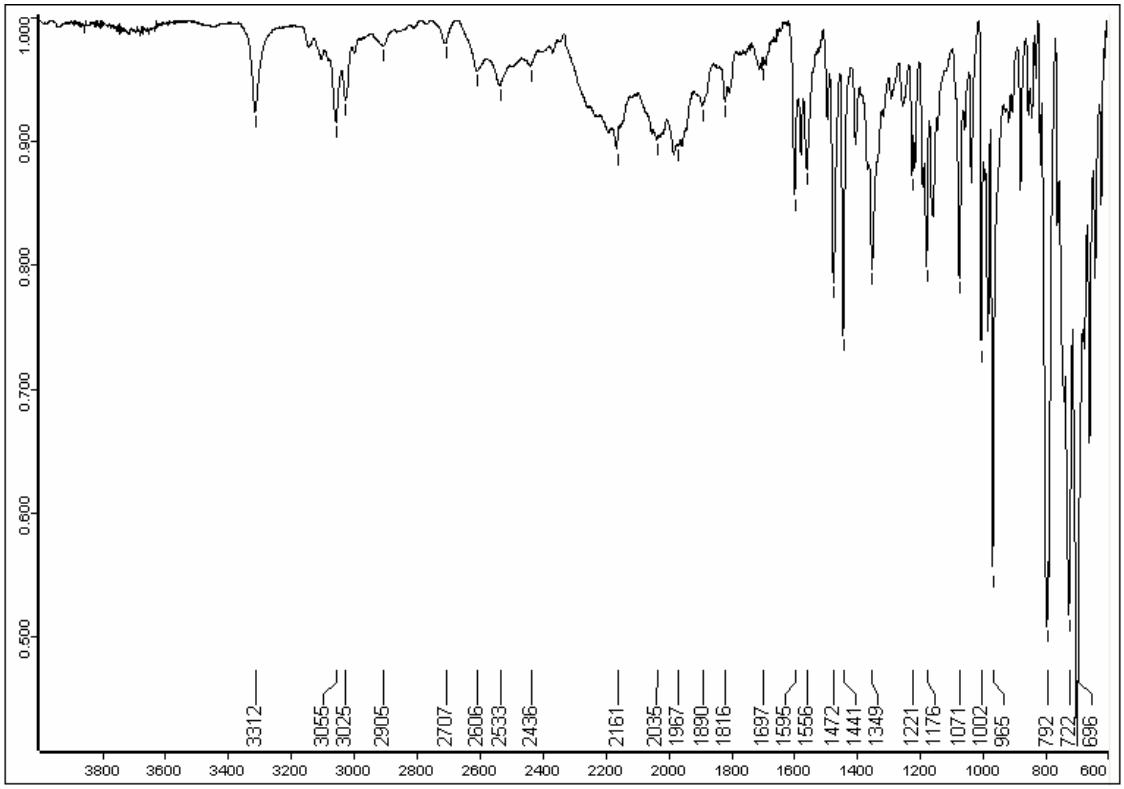

Spectrum B10: Tetraphenylporhyrinatocobalt(II), $C_{44}H_{28}N_4Co$, [16]

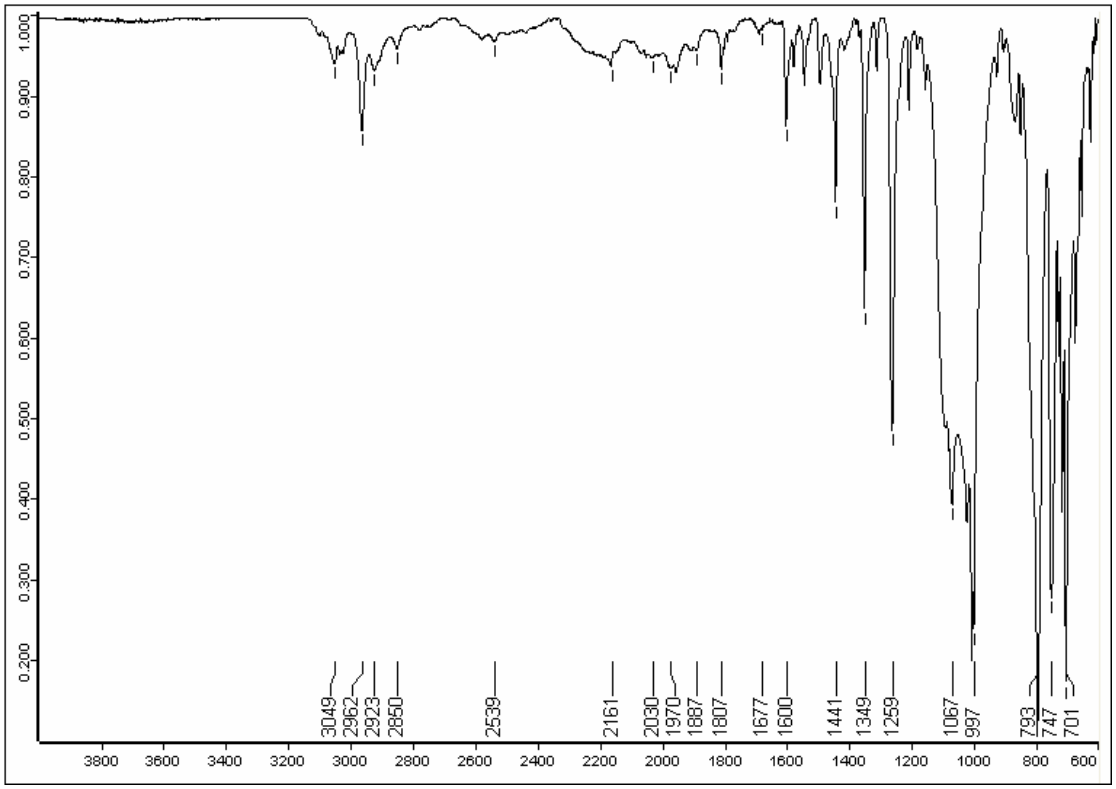

Spectrum B11: Bis(salicylidene)ethylenediamine, $C_{16}H_{16}N_2O_2$, [17]

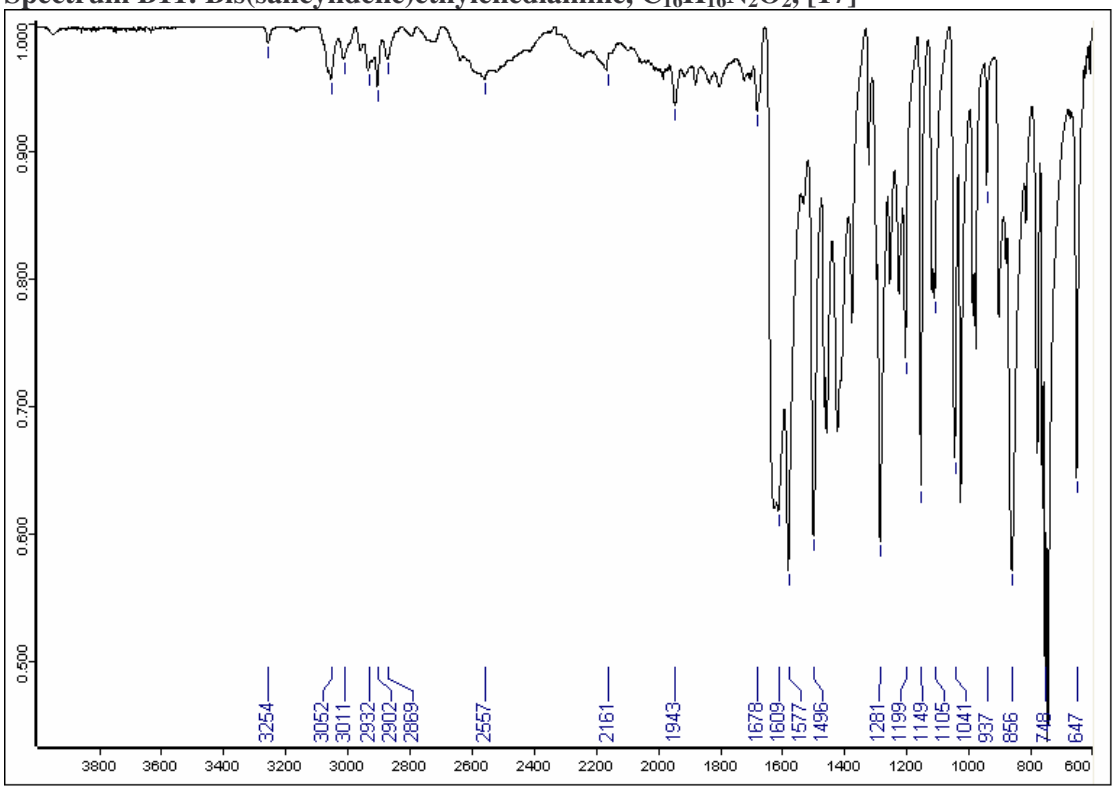

Spectrum B12: *N*,*N*'-Bis(salicylidene)ethylenediaminomanganese(III) acetate, $C_{18}H_{17}N_2O_4Mn$, [18]

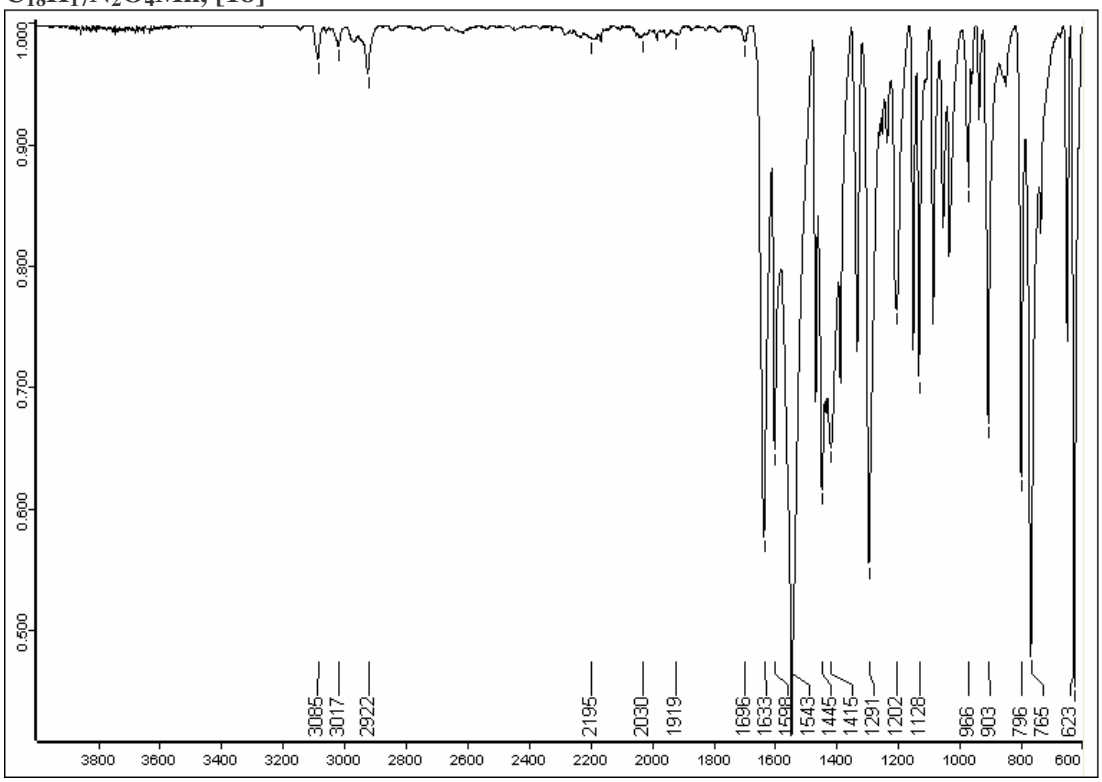

Spectrum B13: *N*,*N*'-Bis(salicylidene)ethylenediaminocobalt(II), $C_{16}H_{14}N_2O_2Co$, [19]

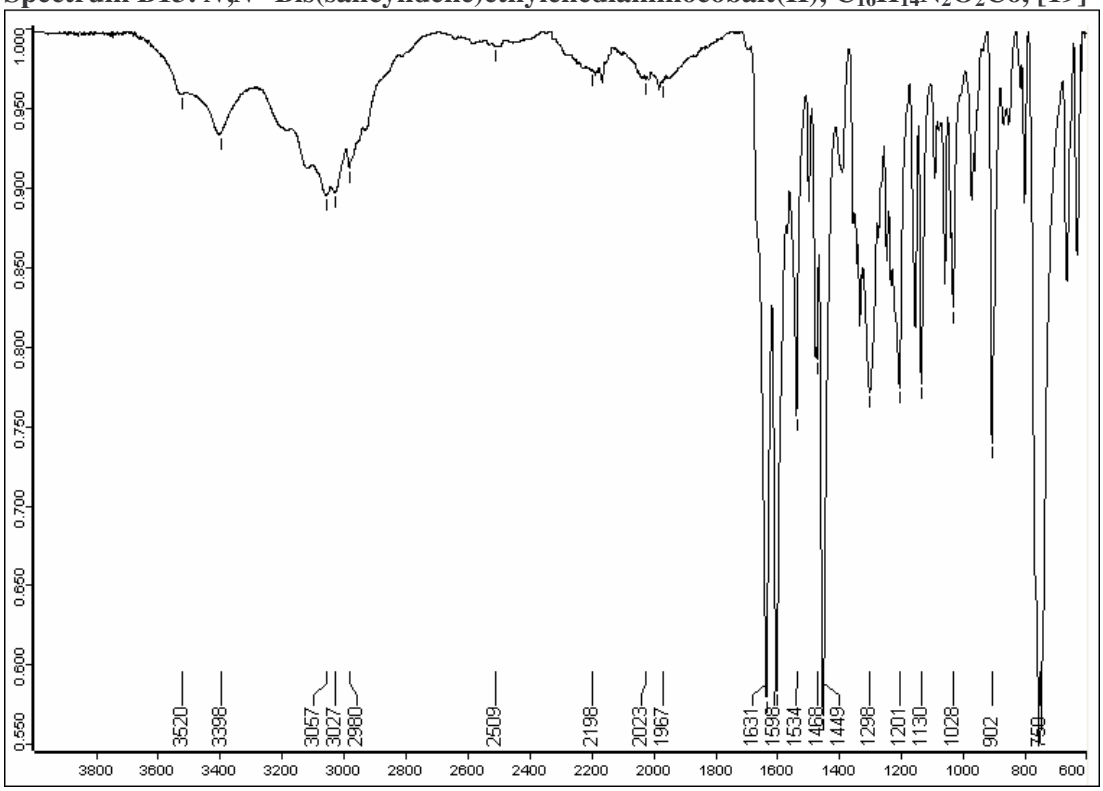

Spectrum B14: 2,5-Tridecylthiophene, $C_{30}H_{56}S$, [20]

Spectrum B15: 2,5-Tridecylthiophenesulfone, $C_{30}H_{56}O_2S$, [21]

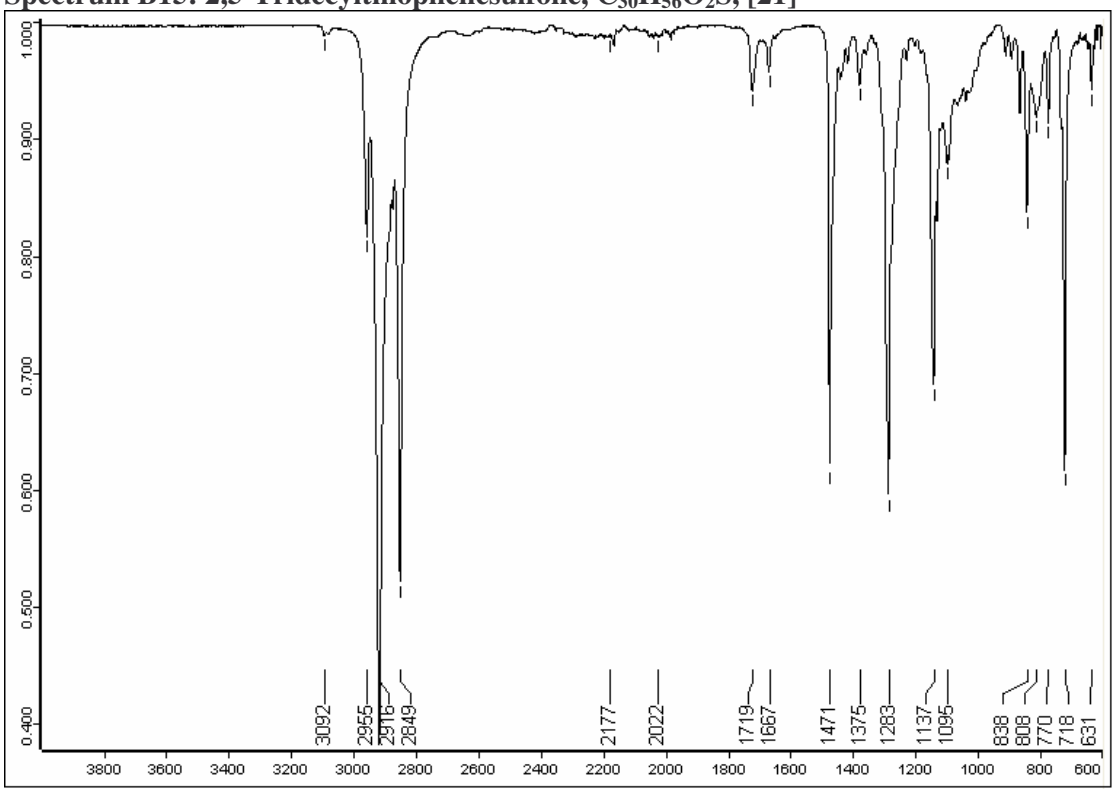

Spectrum B16: 3,6-Tridecylphthalonitrile, $C_{34}H_{56}N_2$, [22]

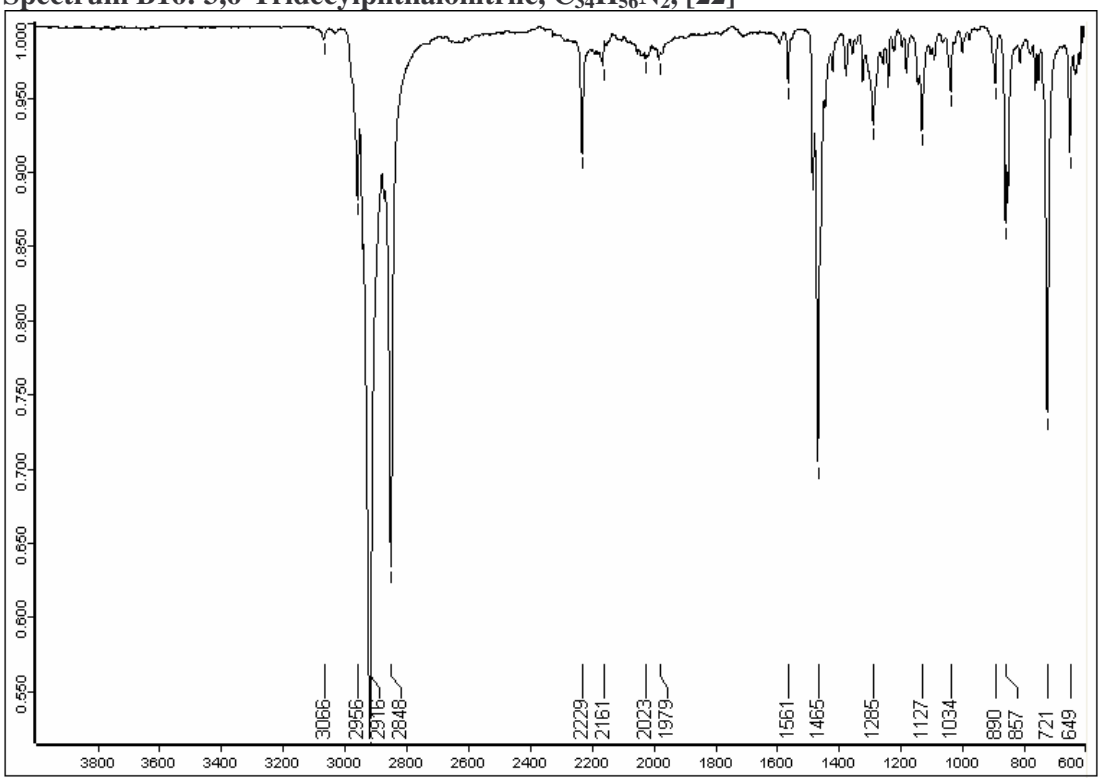

Spectrum B17: 1,4,8,11,15,18,22,25-Octatridecylphthalocyanine, $C_{136}H_{226}N_8$, [23]

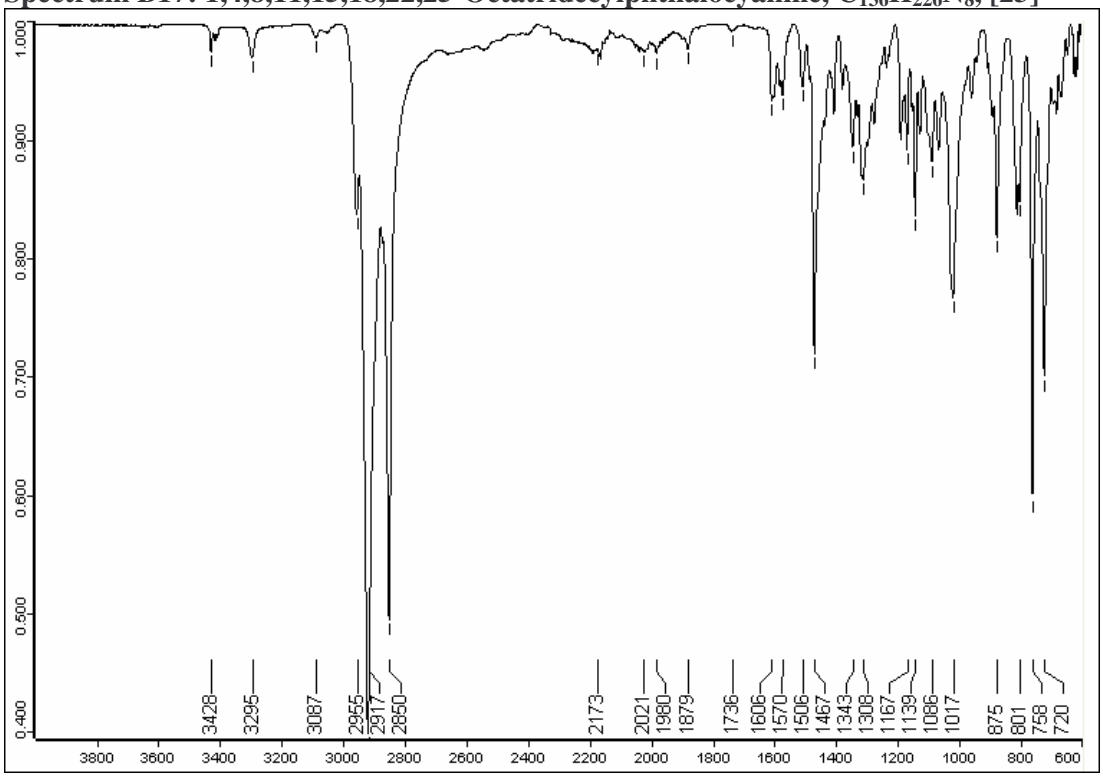

Spectrum B18: [1,4,8,11,15,18,22,25-Octatridecylphthalocyanatomanganese(III)] Chloride, 0.55:0.45 Mn(Cl)Pc($C_{13}H_{27}$)$_8$·5H_2O / Mn(OMe)Pc($C_{13}H_{27}$)$_8$·5H_2O, [24]

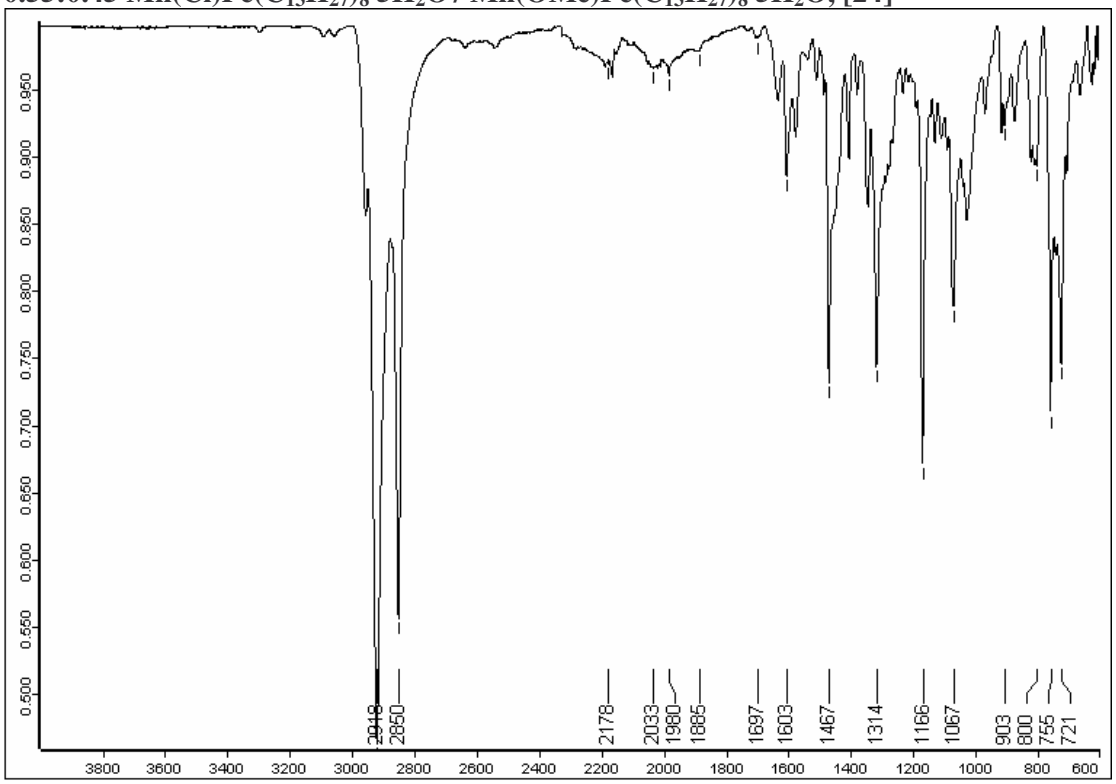

Spectrum B19: 1,4,8,11,15,18,22,25-Octatridecylphthalocyanatozinc(II), ZnPc($C_{13}H_{27}$)$_8$, [25]

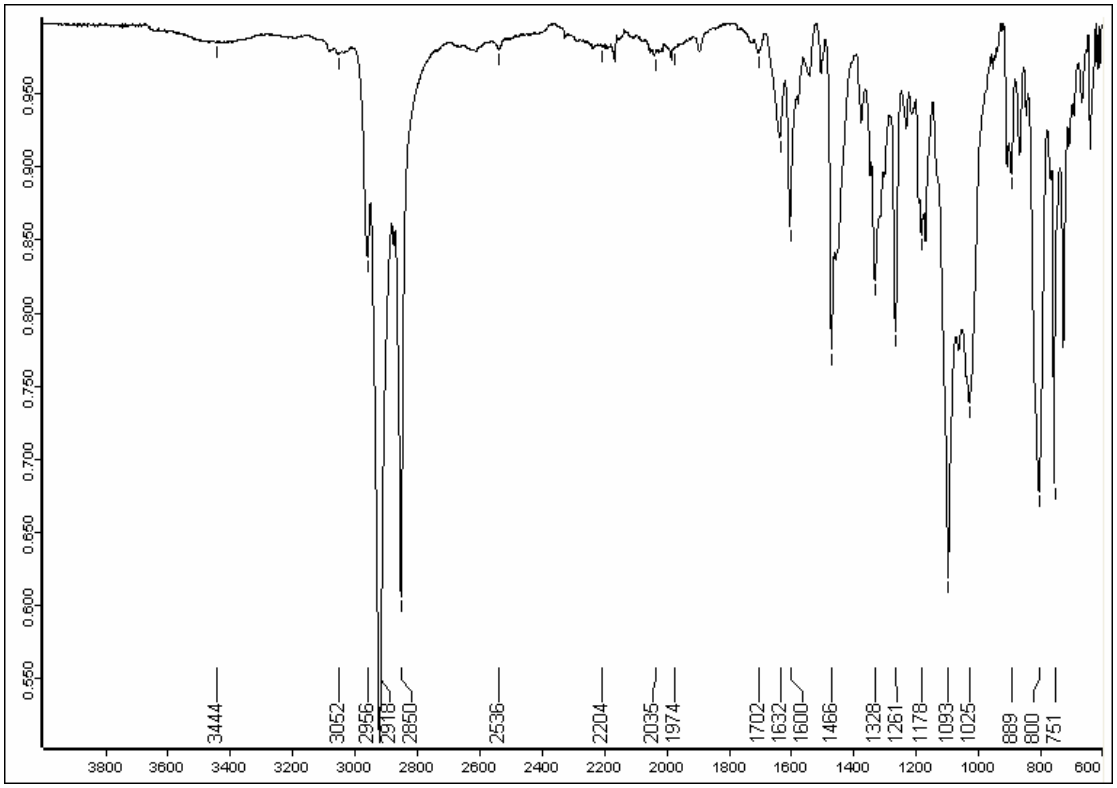

Spectrum B20: Tetraphenylporhyrinatomanganese(III) acetate, $C_{46}H_{31}N_4O_2Mn$, [32]

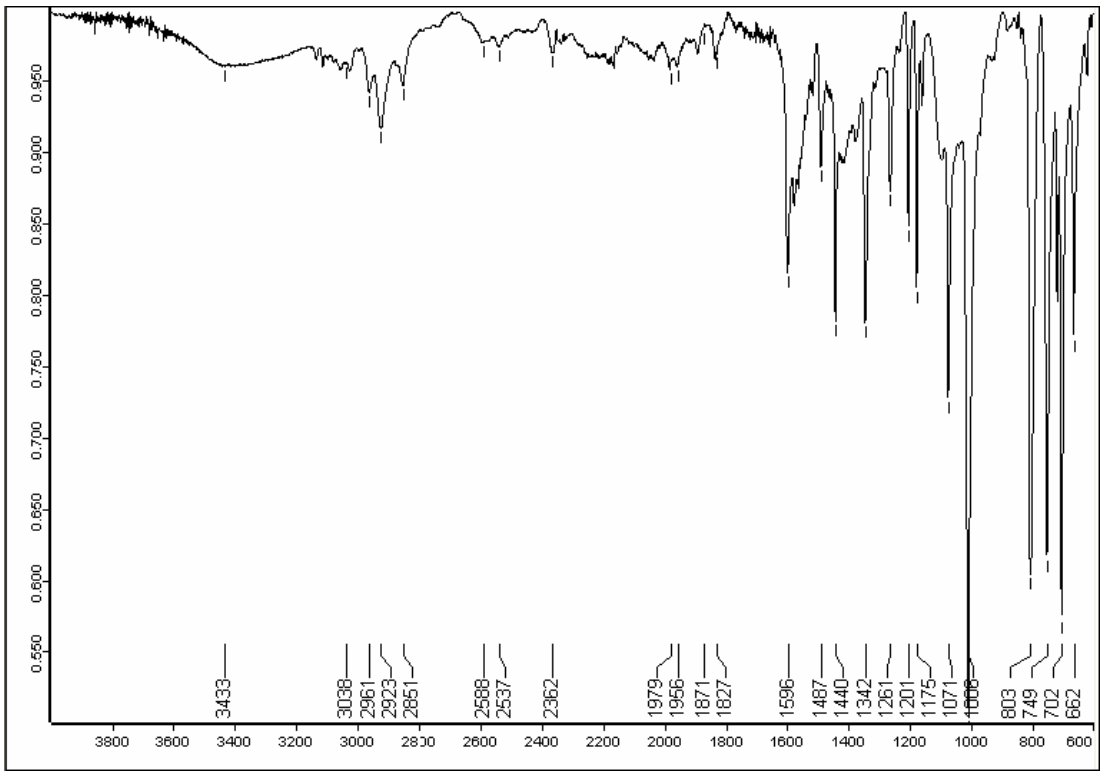

Spectrum B21: trans-Stilbene oxide